

ADVERTIMENT. La consulta d'aquesta tesi queda condicionada a l'acceptació de les següents condicions d'ús: La difusió d'aquesta tesi per mitjà del servei TDX (www.tesisenxarxa.net) ha estat autoritzada pels titulars dels drets de propietat intel·lectual únicament per a usos privats emmarcats en activitats d'investigació i docència. No s'autoritza la seva reproducció amb finalitats de lucre ni la seva difusió i posada a disposició des d'un lloc aliè al servei TDX. No s'autoritza la presentació del seu contingut en una finestra o marc aliè a TDX (framing). Aquesta reserva de drets afecta tant al resum de presentació de la tesi com als seus continguts. En la utilització o cita de parts de la tesi és obligat indicar el nom de la persona autora.

ADVERTENCIA. La consulta de esta tesis queda condicionada a la aceptación de las siguientes condiciones de uso: La difusión de esta tesis por medio del servicio TDR (www.tesisenred.net) ha sido autorizada por los titulares de los derechos de propiedad intelectual únicamente para usos privados enmarcados en actividades de investigación y docencia. No se autoriza su reproducción con finalidades de lucro ni su difusión y puesta a disposición desde un sitio ajeno al servicio TDR. No se autoriza la presentación de su contenido en una ventana o marco ajeno a TDR (framing). Esta reserva de derechos afecta tanto al resumen de presentación de la tesis como a sus contenidos. En la utilización o cita de partes de la tesis es obligado indicar el nombre de la persona autora.

WARNING. On having consulted this thesis you're accepting the following use conditions: Spreading this thesis by the TDX (www.tesisenxarxa.net) service has been authorized by the titular of the intellectual property rights only for private uses placed in investigation and teaching activities. Reproduction with lucrative aims is not authorized neither its spreading and availability from a site foreign to the TDX service. Introducing its content in a window or frame foreign to the TDX service is not authorized (framing). This rights affect to the presentation summary of the thesis as well as to its contents. In the using or citation of parts of the thesis it's obliged to indicate the name of the author

PhD Thesis
Doctoral program of Biomedical Engineering

**New approaches in calcium
phosphate cements and ceramics
for bone regeneration**

Sara Gallinetti

Supervised by:

Prof. Maria Pau Ginebra Molins

Dr. Cristina Canal Barnils

**Department of Materials Science and Metallurgical Engineering
Technical University of Catalonia**

September 2014



Acta de qualificació de tesi doctoral

Curs acadèmic:

Nom i cognoms

Programa de doctorat

Unitat estructural responsable del programa

Resolució del Tribunal

Reunit el Tribunal designat a l'efecte, el doctorand / la doctoranda exposa el tema de la seva tesi doctoral titulada

Acabada la lectura i després de donar resposta a les qüestions formulades pels membres titulars del tribunal, aquest atorga la qualificació:

NO APTE APROVAT NOTABLE EXCEL·LENT

(Nom, cognoms i signatura)		(Nom, cognoms i signatura)	
President/a		Secretari/ària	
(Nom, cognoms i signatura)	(Nom, cognoms i signatura)	(Nom, cognoms i signatura)	
Vocal	Vocal	Vocal	

_____, _____ d'/de _____ de _____

El resultat de l'escrutini dels vots emesos pels membres titulars del tribunal, efectuat per l'Escola de Doctorat, a instància de la Comissió de Doctorat de la UPC, atorga la MENCIÓ CUM LAUDE:

SÍ NO

(Nom, cognoms i signatura)	(Nom, cognoms i signatura)
President de la Comissió Permanent de l'Escola de Doctorat	Secretària de la Comissió Permanent de l'Escola de Doctorat

Barcelona, _____ d'/de _____ de _____

Alla mia mamma,

Al mio papà,

Al mio fratellone,

A Minnie,

A tutte le mie stelle fisse.

"Ever tried. Ever failed. No matter. Try again. Fail again. Fail better."

(S.Beckett)

Acknowledgments

The thesis is just the tip of the iceberg of what a PhD is. Regardless of how big it might appear, it is nothing compared to what is hidden below. Below, there is hard work, there is joy and pain, there are victories and falls, but above all the people who made it happen, each one in a different, special, way.

In primis I would like to thank my supervisors Prof. Maria Pau Ginebra and Dr. Cristina Canal. *Graciès* Pau por tu ejemplo, tu constancia, precisión y la calidad del trabajo, me enseñaste mucho y sobre todo aprendí a nunca parar de preguntar el porqué de las cosas. *Graciès* Cristina por tu paciencia, soporte y enseñanzas, nunca los olvidaré y siempre los llevaré conmigo. Además quería agradecer otra vez a Prof. Maria Pau Ginebra junto al Prof. Xavier Gil por haberme acogido en el grupo sin conocerme, ha sido un enorme placer.

I would like to thank to Prof. Farzaneh Arefi-Khonsari for hosting me in your lab in Paris and for the dedication you showed to me, and also Dr Sudhir Bhatt for having the patience of a stone in teaching me about plasma and for the fruitful discussions we had.

Tack to Prof. Håkan Engqvist and Prof. Cecilia Persson for welcoming me in your group in Uppsala and to Dr. Gemma Mestres for your guidance during the experiments. I have learnt a lot and it has been a pleasure collaborating with you.

Gracias a los técnicos del Crne, a Trifon por la ayuda y para transformar las sesiones de SEM en momentos tan agradables y a Montse por haber sido siempre tan disponible a resolver cualquier problema.

Acknowledgments

I would like to apologise in advance for the people I may forget or whom I won't be able to name, there are so many special people in my life, so thank you to everyone who has been a part of my life these past years.

Graciás a los colegas del departamento, sin vosotros no hubiera sido tan agradable ir al trabajo cada día. *Graciás* a los compañeros que acabaron antes por transmitir vuestra sabiduría, a quien se fue y a quien se quedó.

Primero gracias a “los cementos”: *Edgar*, maestro y amigo, me enseñaste los trucos de lo cementos, de las maquinas, nunca olvidaré nuestros buenos momentos y las canciones que me enseñaste. *Gemma*, amiga y compañera de despacho en las muchas horas de trabajo, gracias por haber sido a mi lado en todos momentos, por los consejos y las sonrisas! *Román*, nunca olvidaré la mano que me echaste, las enseñanzas, los chistes y mis abrazos diarios, *Graciás!* *Montse*, el ejemplo que eres en cuanto persona y investigadora no tiene palabras, tu humildad y dedicación son únicas, *Merci!* *Merci David*, llegamos al grupo al mismo tiempo y hemos vivido muchas cosas juntos, gracias por tu apoyo y amistad, y por sacarme de momentos de crisis! *Yassine*, compañero en los cementos y en el despacho! Solo los alpes nos dividieron pero ha sido un placer tenerte a mi lado, por el buen humor y las buenas conversaciones! *Merci a toi aussi!* *Annina cara*, que sería el día a día sin ti y tus abrazos, tan simpática cuanto humilde, siempre lista a ayudar y con una sonrisa, un buen discurso o un chiste, nunca olvidaré la gran persona que eres. *Thanks Zhitong and Jing* for answering all my curiosities about your culture, it was great to meet you! *Gracias a Maite*, hiciste que el principio fuera más fácil, nunca te olvidaré. *Gracias también a los nuevos componentes, Joanna y Priya*, enjoy the adventure. *Aprovecho para agradecer también a Malgo* por tu amistad, ayuda y dedición, nunca te olvidaré *Glu!*

Gracias a los metales también. A Carolina, compañera desde el principio hasta el final, nunca olvidaré nuestros discursos y tu visión de la vida, me siento muy afortunada a haber compartido contigo y con *Maria, corazón*, quien me va a cantar si no lo haces tú *Maria*, tan cabeza cuanto buena, gracias por las risas y las reuniones al final de las escaleras...sois lo mejor! *Marta*, nunca olvidaré el apoyo en mi primer congreso, he sido tan afortunada a tenerte a mi lado y tuve la fortuna de conocerte más a fondo, *moltès gracias per tot!* *Carles*, que puedo decir amigo, sabes

el cariño y la admiración que tengo por ti! Gracias por los abrazos, las sonrisas contagiosas y todo tipo de discursos, para que sean muchos más en futuro! *Romain*, no sabría cómo agradecer todos los abrazos y el apoyo en este último año y medio, eres un amigo y los has demostrado en todo momento, *merci beaucoup mon ami!* *Roberta*, grazie per tutti i bei momenti passati assieme, le lezioni di yoga e i bei discorsi, li porterò sempre con me! *Cris*, que fortuna que hayas venido al grupo, echaré de menos tus sonrisas, naturaleza y discursos en catalán...peró tendré que venir a visitar mi sobrinito/a! *Daniel*, ha sido un placer compartir y tener conversaciones interesantes contigo, graciès per tot! Gracias también a *José M, Nathy, Mireia y Maria Isabel*, aunque nos hemos cruzado poco, ha sido un placer compartir con vosotros! Gracias Judith por tus abrazos y por cuidar de Anna! Y como olvidar *Pablo y Marta G*, veros por los laboratorios siempre ha sido una alegría! Graciès al biòleg, el único y inimitable *Jordi*, por tu enseñanzas, alegría y tus “*allora*” que siempre han podido generar una sonrisa! *Txell*, no me olvido de ti y del grupo de empresas...gracias por tu eficiencia impecable, tu positividad y ayuda, no hubiera podido pedir técnico mejor, graciàs! *Monica*, los 5 minutos a las 8 de la mañana siempre me dieron la fuerza de enfrentar el dia con fuerza, *gracies per tot!* *Marquito!!* Me llevaré los discursos profundos a las 8 de la tarde y todas las risas también, no te preocupes, un día tomaremos café junto...;-) *Lluís*, tú y tus chistes, que gusto haberte tenido como compañero de despacho! *Miquel*, gracias por tu positividad en todo momento! *Noe*, tu siempre lista a ayudarme por cualquier cosa he necesitado, no sabes lo importante que has estado, *Gracies!*

Kim, crecí mirando Mc Giver a la TV y después ví que había alguien mucho mejor, gracias por las consultas técnicas y por tu risa tan auténtica!

Mari Angeles, en estos cuatro años encontré en ti mi mamá española, tu dedicación al trabajo y a los hijos (verdaderos o adoptivos como yo) es un ejemplo que siempre llevaré en mi corazón, gracias!

Gracias a los compañeros de despacho: *Erik*, amico autentico, capace di dirmi uno “scaprati fuori” al momento giusto, grazie per gli abbracci, le consulenze e tutti i momenti passati insieme, di sicuro sarebbe stata più dura senza di te! Graciès *José Maria* por tu buen humor constante, ha sido un placer llegar por la mañana y encontrar tu sonrisa! *Merci Quentin* por las historias y las canciones diarias! *Grazie Erica* per il sostegno in questi ultimi duri mesi di tesi. *Newsha*, so crazy and so nice,

Acknowledgments

it was amazing having you in the department and in my life! Tack *Lati*, I loved all our chats. Agradezco todos los miembros del grupo de fatiga y a Sandra, Pedro, Isaac y Casimir por haber compartido conmigo estos años.

Mis agradecimientos van a los otros amigos en Barcelona. Prima di tutto ai componenti di casa Vallirana... Grazie *Stefy*, per essere stata un'amica con cui ho sempre potuto condividere gioie e dolori, sei una persona fantastica e ti voglio davvero bene... Grazie *Umby*, il bullo, supergiovane, insomma la persona che ti può sempre risollevare la giornata e con cui una risata è d'obbligo...grazie davvero! Grazie anche a *Darío* e *Barby* che sono stati membri onorari...ci siete mancati! E grazie a *Vero* per lo svago giornaliero in questi mesi di tesi. Grazie *Fra*, per l'appoggio in questi anni, ho trovato in te un ottimo amico a vita. *Graciès Xenia*, como pueden las palabras explicar lo que tu has sido en estos años, excelente amiga, gran apoyo, siempre he podido contar contigo, Barcelona va a perder mucho sin ti. Gracias a *Mafe* y las compañeras de yoga, la luz en los días más duros...*Namasté!* Gracias también a todos los otros amigos de estos años, os quiero mucho.

Now my acknowledgments go to my friends spread across the world, far physically but close to my heart. *Kiaretta*, en ti encontré una hermana, una persona que echo de menos cada día que pero ha sabido ser apoyo diario, gracias por tu amistad y apoyo desde el principio hasta el final. *Lucertolina* piccola quanto forte, grazie di tutto! *Ema*, una forza della natura sempre in grado di strapparmi un sorriso! *Pisi*, grazie per essere un'amica fidata! *Sabri* e *Franco*, le amiche di sempre, che nonostante i cambi e la difficoltà nel vedersi sono sempre lì! *Giulio*, non so come avrei fatto senza la tua emoticon mattutina! Grazie *Anna*, *Silvano* e *Lorenzo* per essere un'altra parte della famiglia! *Alex*, always ready to support me during the good and the bad, ready to travel just to cheer me up! Thank you *Raghu*, incredible person, best party guy but at the same time really deep. Last but not least, thank you *Johnny* to support me beyond the distance, keeping me on track, making me smile in the worst moments, you know how much this means to me.

My stay in Paris would not have been the same without the special friends with whom I could share the experience: first of all *Jean*, my cornerstone, you took care

of me and made everything easier, it was great to spend time with you every day, *merci mon ami; Benoît*, new entry in my life, it was great to get to know you, I am always happy when I get to know great people like you; *Anne-Lo et Benoît*, spending time with you again was a blessing, merci! Y no me voy a olvidar de ti *Richi*, que bueno reirse contigo y con *Cris*, gracias por compartir conmigo y por la buena onda! Merci *Simon* for helping me every day in the lab and your constant smile! I cannot forget part of my skrapan family... especially thank you *Inge*, for coming to see me anywhere I was and for being patient even if I couldn't make it to South America with you. *Ilkka* for your support through skype. And *Aderfoula mou, s'agapo poly*, I missed spending time with you in person but I could always count on you and that gave me strength, *efkaristo poly*.

My stay in Uppsala wouldn't be so special without the people around me...*Shiuli Shiu*, such a great connection in such a short time, you are amazing, such a caring person, thanks for the support and for teaching me so much every day, you and *Michael* are the best! *Carol*, grazie per la tua amicizia e il tuo appoggio, le persone come te sono rare e sono felice che tu faccia parte della mia vita! Gracias *Ale* por los buenos momento y conversaciones. Tack *Nathalie*, I had the fortune of spending my days with such a great person, it was great laughing, cooking, chatting and learning with you every day! E poi grazie a te cara *Vale*, i tuoi principi e il tuo modo di essere non possono che vederci amiche, grazie davvero!

E infine i miei ringraziamenti vanno alle mie stelle fisse: quelle persone che non importa la distanza o cosa succeda...ci sono sempre state e sai che sempre ci saranno... siete la ragione del mio sorriso! *Enri*, presenza costante in grado di supportarmi in ogni passo della vita e del dottorato, non so come farei senza di te; *Lori*, sempre pronto a tendermi la mano ad ogni caduta e a gioire ad ogni vittoria, grazie anche per aver portato nella mia vita *Lu*, nuestra conexión ha sido inmediata, gracias por estar y por la persona que eres...*Niki*, ti voglio bene e per me sei un grande esempio... e nonostante a volte ci siano divergenze, sei il mio supporto! *Papà*, tu che hai vegliato su di me e mi hai protetta e aiutata nei momenti difficili...e infine grazie all'esempio più grande, colei che si è guadagnata questo dottorato tanto quanto me, la persona più forte, saggia e amorevole che conosca, a te, la migliore mamma che potessi mai desiderare... *grazie Mamma!*

Abstract

Bone is among the most frequently transplanted tissues in the body. In Europe, about one million patients encounter a surgical bone reconstruction annually. The worldwide market of bone replacement materials is currently estimated at 5 billion Euros, with a 10% growth due to the ageing of the population. Natural grafts present several drawbacks which pushed scientists to investigate synthetic biomaterials. Although most synthetic bone substitutes available possess some of the positive properties of autografts, none yet have all the benefits of one's own bone. Among the available biomaterials, Calcium Phosphates (CaPs) are of great interest. Nonetheless, these materials can still be improved in several respects.

The main aim of this PhD Thesis is to contribute to the improvement of the properties of CaPs for bone regeneration with primary regard to Calcium Phosphate Cements (CPCs). The Thesis is divided in three main parts: i) Biphasic Calcium Phosphates Cements (BCPCs) with modified solubility and ion release; ii) Fibre Reinforced Calcium Phosphate cements (FRCPCs) with improved mechanical properties; iii) Macroporous CaP scaffolds for simvastatin acid release.

In the first part novel biphasic CDHA/ β -TCP cements were obtained by mixing two Tricalcium Phosphate (TCP) polymorphs with different solubility (α -TCP and β -TCP). Upon mixing α -TCP/ β -TCP blends with an aqueous solution, only α -TCP completely hydrolysed to CDHA, whereas β -TCP remains unreacted and completely embedded in the CDHA matrix. Increasing amounts of the non-reacting β -TCP phase resulted in a linear decrease of the compressive strength, in association to the decreasing amount of precipitated CDHA crystals, which are responsible for the mechanical consolidation of apatitic cements. Ca^{2+} release and degradation in acidic medium was similar in all the BCPCs within the timeframe studied, although differences might be expected in longer term studies once β -TCP, the more soluble phase, is exposed to the surrounding media.

In the second part of this manuscript, new FRCPCs were fabricated with a focus on improving the adhesion fibres/matrix, in order to enhance the load transfer and, thus, the toughness of the material. Different approaches were studied. The first approach was to increase the chemical affinity of the fibres towards the matrix, adding an element in the matrix with high affinity to the fibres. In the first approach, TryMethyl Chitosan (TMC) was introduced in the liquid phase of a matrix reinforced with chitosan fibres. The addition of TMC to the CPC matrix reverted in immediate cohesion but increased setting times and decreased SSA. The good compatibility between the fibres and the matrix with TMC in the new FRCPCs resulted in a continuous interface (observed by SEM) and improved mechanical properties compared to the FRCPCs without the additive in the matrix. In the same line, lactic acid (LA) was added in the liquid phase of cements reinforced with Poly-L-lactic acid (PLLA) yarns. Although the CDHA formation was not impaired by the addition of LA, the reaction was slower and the matrix weaker. Even if no significant differences were found among the different FRCPCs, the addition of the yarns improved the bending properties compared to pristine CPCs. Biological characterisation of FRCPCs with human osteoblastic-like cells MG63 suggested that the slightly acidic pH produced from LA may be harmful and that PLLA fibres may have a role in stimulating osteoblast differentiation. Lastly, the potential of low temperature plasma surface modification of PLLA yarns was evaluated for reinforcement of CPCs. Oxygen low pressure plasma was employed at different treatment times and the surface properties of the untreated and plasma-treated PLLA were evaluated. Plasma treatment of the PLLA yarns reduced the setting times of the PLLA-CPC composites and tended to improve their flexural properties.

The third part of this Thesis consisted in producing low temperature (CDHA) or high temperature (β -TCP) macroporous scaffolds as carriers for Simvastatin acid (SVA), an osteogenic and angiogenic promoter. The loading of the drug was dependent on SSA of the scaffold. In order to modulate the drug release beyond the intrinsic capacity of the material, plasma polymerisation with PCL:PEG copolymers was used to dry-coat the CaP scaffolds. This coating led to significant changes in surface topography, and in their physical and chemical properties. The drug release was

successfully modified by the plasma polymerisation treatment performed, opening new routes for the design of CaP matrices for controlled release applications.

Resumen

El hueso es uno de los tejidos más trasplantado del cuerpo. Sólo en Europa, se cuentan alrededor de un millón de cirugías de reconstrucción ósea anualmente. La estimación del mercado global de los sustitutos óseos es aproximadamente de cinco billones de Euros por año, con un 10% de crecimiento anual debido al envejecimiento de la población. Debido a los problemas asociados a los injertos biológicos, la investigación y el desarrollo de materiales sintéticos y biocompatibles (Biomateriales) ha experimentado un gran auge. Aunque la mayoría de sustitutos sintéticos disponibles poseen algunas de las características de los autoinjertos, hasta el momento ninguno reúne todos los beneficios del hueso del propio individuo. Dentro de los biomateriales para regeneración ósea, los fosfatos de calcio han sido de gran interés debido a su composición química similar a la del hueso. Sin embargo, estos materiales pueden ser mejorados en diferentes aspectos.

El objetivo principal de esta Tesis Doctoral es contribuir a la mejora de las propiedades de los fosfatos de calcio para la regeneración ósea, con un interés especial en los cementos. La Tesis investiga diferentes estrategias para el desarrollo de materiales para la sustitución ósea, novedosos y con propiedades mejoradas respecto a los actuales. La Tesis comprende tres partes principales: i) Cementos bifásicos de fosfato de calcio (BCPCs), constituidos por materiales con diferente solubilidad; ii) Fosfatos de calcio reforzados con fibras (FRCPCs), para la mejora de las propiedades mecánicas; iii) Andamios macroporosos para la liberación de una sal de simvastatina.

En la primera parte de la Tesis, se describe el desarrollo de BCPCs compuestos por hidroxiapatita deficiente en calcio (CDHA) y fosfato tricalcico β (β -TCP). Estos materiales derivan de la reacción de las mezclas de dos polimorfos de fosfato tricalcico (TCP) con diferente solubilidad (α -TCP y β -TCP). Cuando ambas fases son mezcladas con una fase acuosa, sólo el α -TCP se hidroliza completamente a CDHA,

mientras que el β -TCP permanece inalterado. Los tiempos de fraguado aumentan con la incorporación de la fase β -TCP, lo cual se puede asociar al hecho que el fraguado del cemento depende de la transformación de α -TCP a CDHA, mientras que el β -TCP no está involucrado en la reacción. La microestructura final de los BCPCs está constituida por partículas de β -TCP integradas en una matriz de CDHA. El aumento de β -TCP, provoca una disminución lineal de la resistencia a la compresión debido a una menor cantidad de cristales de CDHA precipitados, los cuales son los responsables de la consolidación de los cementos apatíticos. La liberación de iones de calcio y la degradación en medio ácido son similares en todos los BCPCs en el periodo de tiempo de medida; sin embargo se podrían esperar diferencias a tiempos más largos, cuando el β -TCP, la fase más soluble, sea expuesta al medio.

En la segunda parte, se han desarrollado nuevos FRCPCs con un enfoque particular hacia la mejora de la adhesión entre fibras y matriz, con el objetivo de mejorar la transferencia de carga entre ellos y consecuentemente las propiedades mecánicas del compuesto. Se han investigado distintas estrategias, la primera de ellas basada en la investigación de materiales con una fase común (o con alta afinidad química) entre las fibras y la fase líquida del cemento; de esta manera se quiere crear un enlace más fuerte entre las fibras y la matriz. En un primer material se incorporó un 1 w/v% de Trimetilo de quitosán (TMC) en la fase líquida del cemento que a su vez se reforzó con fibras de quitosán. La incorporación del TMC en la matriz, comportó la cohesión inmediata del cemento, mayores tiempos de fraguado y una disminución de la SSA. La buena compatibilidad entre fibras y matriz se observó en la continuidad de la interfaz (observada por MEB) y por el hecho que las propiedades mecánicas fueron mejoradas respecto al FRCPC sin TMC en la matriz. En un segundo grupo de materiales, se añadió un 10 v/v% de ácido láctico (LA) a la matriz del cemento junto con hilos discontinuos de ácido poliláctico (PLLA). Aunque la presencia de LA permitió obtener CDHA, la reacción se ralentizó llevando a una matriz más débil. Aunque no se obtuvieron diferencias significativas, la incorporación de las fibras de PLLA mejoró las propiedades mecánicas a flexión respecto a la matriz sin fibras (tanto con, como sin LA en la matriz). La caracterización biológica por medio de células osteoblásticas MG63 sugiere que el LA es perjudicial para las células y que la presencia de las fibras afecta a la

diferenciación celular. La segunda estrategia investigada en los FRCPCs se basa en la modificación superficial de las fibras de PLLA con plasma de baja temperatura con el fin de aumentar su mojabilidad. Las fibras se trataron con plasma de oxígeno de baja presión a diferentes tiempos. El tratamiento de plasma sobre las fibras, disminuyó los tiempos de fraguado de los FRCPCs y mejoró las propiedades a flexión.

La tercera parte consiste en el desarrollo de andamios macroporosos obtenidos a baja (CDHA) o alta (β -TCP) temperatura para ser utilizados como formas de liberación de una sal de simvastatina (SVA), con propiedades osteogénicas y angiogénicas. Se observó una dependencia en la absorción del fármaco con la SSA. Para conseguir modular la liberación del fármaco se hizo un recubrimiento con un copolímero de PCL:PEG mediante polimerización por plasma después de cargar el fármaco en el material. El tratamiento resultó en cambios tanto en la topografía superficial, como en las propiedades físico-químicas del material y en la liberación del fármaco. La posibilidad de modular la liberación de fármaco mediante polimerización por plasma abre nuevas vías al diseño de matrices de fosfatos de calcio con mejor control de la liberación.

Publications and conference participation

Peer reviewed

Gallinetti S, Canal C, Ginebra MP. Development and Characterization of Biphasic Hydroxyapatite/ β -TCP Cements. *Journal of the American Ceramic Society* 2014; 97(4): 1085-1073. DOI: 10.1111/jace.12861

Canal C, Gallinetti S, Ginebra MP. Low pressure plasma treatment of polylactide fibres for enhanced mechanical performance of fibre-reinforced calcium phosphate cements. *Plasma Processes and Polymers*. 2014; 11(7): 694-703. DOI: 10.1002/ppap.201400018

Publications derived from conferences

Gallinetti S, Canal C, Ginebra MP. Biphasic Calcium Phosphate Cements For Bone Regeneration. *Book of Abstracts 6th EEIGM International Conference Advanced Materials Research 7th and 8th November, 2011 - EEIGM, Nancy, France, p.20.*

Gallinetti S, Canal C, Ginebra MP. Synthesis and evaluation of new α -TCP and β -TCP biphasic calcium phosphate cements. *Book of Abstracts 4th IBEC Symposium on Bioengineering & Nanomedicine, 18th October, 2011, Barcelona, Spain, p.78.*

Gallinetti S, Canal C, Ginebra MP. Degradation and characterization of new biphasic calcium phosphate cements. *European Cells and Materials*. 2012; 23 (Suppl. 3): 6. ISSN 1473-2262.

Conference Participation

Gallinetti S, Canal C, Ginebra MP. Biphasic Calcium Phosphate Cements for Bone Regeneration. 6th EEIGM International Conference on Advanced Materials Research, Nancy, France, November 7th-8th, 2011. (Oral presentation).

Gallinetti S, Canal C, Ginebra MP. Synthesis and evaluation of new α -TCP/ β -TCP biphasic Calcium Phosphate Cements. IV IBEC Symposium on Bioengineering & Nanomedicine, Barcelona, Spain, October 18th, 2011. (Poster Presentation).

Gallinetti S, Canal C, Ginebra MP. Degradation and characterisation of new biphasic calcium phosphate cements. The 22th Interdisciplinary Research Conference on Injectable Osteoarticular Biomaterials and Bone Augmentation, Uppsala, Sweden, May 10th-12th, 2012. (Oral Presentation).

Gallinetti S, Pastorino D, Canal C, Ginebra MP. Simvastatin acid release from low-temperature Calcium Phosphate scaffolds. ESB 2013 - 25th European Conference on Biomaterials, Madrid, Spain, September 8th-12th, 2013. (Poster Presentation).

Canal C, Gallinetti S, Ginebra MP. Enhanced adhesion at the interface between PLA fibres and calcium phosphate cements by low temperature plasma improves their mechanical. 25th Symposium and Annual Meeting of the International Society for Ceramics in Medicine (BIOCERAMICS 25), Bucharest, Romania, November 7th-10th, 2013. (Oral Presentation).

Ginebra MP, Gallinetti S, Canal C. Improving mechanical properties of Calcium Phosphate Cement – Fiber composites: Strategies for enhanced interface bonding. XIII Congreso Nacional de Materiales. Barcelona, Spain, June 18th-20th, 2014. (Oral Presentation).

Gallinetti S, Mestres G, Persson C, Canal C, Ginebra MP. A new approach for fibre reinforced calcium phosphate cements. 26th Symposium and Annual Meeting of the International Society for Ceramics in Medicine (BIOCERAMICS 26), Barcelona, Spain, November 6th-9th, 2014. (Poster Presentation).

Table of contents

Acknowledgements	I
Abstract	VII
Resumen	XI
Publications and conference participation	XV
Table of contents	XVII
1. Objectives and structure of the thesis	1
1.1. The context	1
1.2. Objectives	2
1.3. Structure	4
References	6
2. State of the art	7
2.1. The bone	7
2.1.1. Macrostructure and functions	7
2.1.2. Bone remodelling	10
2.2. Bone grafting	12
2.3. Calcium phosphates in bone repair	16
2.3.1. Properties of calcium phosphate materials	20
2.3.2. Calcium phosphate cements	23
References	29
3. Biphasic Calcium Phosphate Cements	39
3.1. Introduction	39
3.1.1. Osteoinduction	39
3.1.2. Biphasic calcium phosphate materials	43
3.2. Objectives	45
3.3. Experimental	46
3.3.1. α -TCP and β -TCP preparation	46
3.3.2. Powder characterisation	48
3.3.3. Cement preparation and characterisation	49
3.3.4. Statistics	53
3.4. Results	53
3.4.1. Powder characterisation	53
3.4.2. Biphasic calcium phosphate cement characterisation	55
3.5. Discussion	64
3.6. Conclusions	69
References	71

4. Fibre reinforced calcium phosphate cements	79
4.1 Introduction	79
4.1.1 Bone: a strong composite material	80
4.1.2 Mechanical properties of fibre reinforced inorganic cements	83
4.1.3 Fibre reinforced calcium phosphate cements	90
4.1.4 Polymeric additives used in this Thesis	97
4.1.5 Low temperature plasma in fibre reinforced cements	101
4.2 Objectives	102
4.3 Calcium phosphate cements reinforced with fibres and polymeric additives	103
4.3.1 Introduction: Experimental design	103
4.3.2 Materials and methods	103
4.3.3 Results	110
4.3.4 Discussion	126
4.3.5 Conclusions	131
4.4 Calcium phosphate cements reinforced with plasma treated fibres	133
4.4.1 Introduction	133
4.4.2 Experimental	133
4.4.3 Results	136
4.4.4 Discussion	143
4.4.5 Conclusions	149
4.5 Biological characterisation	150
4.5.1 Introduction	150
4.5.2 Materials and methods	151
4.5.3 Results	155
4.5.4 Discussion	162
4.5.5 Conclusions	163
References	165
5 Macroporous calcium phosphate scaffolds for the delivery of simvastatin acid	179
5.1 Introduction	179
5.1.1 Calcium phosphate for drug delivery	179
5.1.2 Potential of plasma polymerisation on controlled drug release from calcium phosphates	180
5.1.3 Statins in bone regeneration	182
5.2 Objectives	185
5.3 Experimental design	186
5.4 Materials and Methods	186
5.5 Results	194

5.6	Discussion	205
5.7	Conclusions	210
5.8	Biological characterisation of the foams	212
5.8.1	Evaluation of β -CPF and human mesenchymal stem cells	212
5.8.2	Rabbit Mesenchymal Stem Cell and Endothelial Cell Response to β -TCP Scaffolds with Simvastatin Acid	212
	References	214
6	Conclusions and future perspectives	221
6.1	Conclusions	221
6.2	Future Perspectives	223
Annexes		
	Annex I - X-ray diffraction (Phase quantification)	A.I
	Annex II-Simvastatin acid stability studies and cement interference	A.V

Chapter 1

Objectives and structure of the thesis

1.1 The context

Bone is among the most frequently transplanted tissues in the body. In Europe, about one million patients encounter a surgical bone reconstruction annually. The worldwide market of bone replacement materials is currently estimated at 5 billion Euros with a 10% growth due to the ageing of the population.

The human skeleton produces bone up to approximately the age of 30, after which bone is gradually lost (**Sroujia & Livneb, 2005**). Bone remodelling and bone loss, as a function of age, are under the control of both endogenous hormonal changes and external mechanical loads originating from physical activity. These impart their effects through regulation of the relative activities of bone cells, in particular osteoblasts and osteoclasts, which control bone deposition and reabsorption, respectively (**Ettinger, 2003; Seeman, 2003**). Decreased bone formation is the pathophysiological mechanism responsible for bone loss associated with aging. The most common problem is Osteoporosis. Osteoporosis is a disease where there is a drastic bone loss resulting in osteopenia and that involves a high risk of fractures (**Strømsøe, 2004**). It has been estimated that only 31–36 % people over the age of 70 years have normal bone mass. The lifetime risk for hip fracture for women in their fifties is 18–25 % and the risk for men 6–7 %. However, aging is not the only problem related to bone. Critical size defects due to traumatic injury, osteomyelitis or bone tumour resection are as important as problems related to aging.

The gold standard in bone replacement is tissue grafted from the same patient (autograft). However, bone autograft is limited in quantity (about 20 cm³) and the harvesting process requires additional surgery, with the potential for pain and complications. Bone grafts from donors from the same (allografts) or different (xenografts) species are also very common, but entail laborious sterilisation treatment and may associate immunological rejection. Due to the problems of the natural grafts scientists have long searched for synthetic bio-compatible materials, also known as “biomaterials”. Although most synthetic bone substitutes available possess some of the positive properties of autografts, none yet have all the benefits of one’s own bone. Among the available biomaterials, Calcium Phosphate (CaP) materials, and more specifically calcium phosphate cements (CPCs), are of great interest. Although these materials present many advantages, they can still be improved in several respects.

1.2 Objectives

The main aim of this PhD Thesis is to contribute to the improvement of the properties of Calcium Phosphate (CaP) biomaterials for bone regeneration with major regard to CPCs.

The specific objectives can be defined as follows:

1. Design of new biphasic CPC (named BCPC) containing two phases with different solubility.
 - Development of self-setting Biphasic Calcium Phosphates (BCP), which would add to the benefits of osteoinductive BCP ceramics, the advantages associated to calcium phosphate cements.
 - Characterisation of the properties of the new BCPCs obtained from initial blends of powders with different α -TCP/ β -TCP ratios, paying special attention to the setting reaction, mechanical properties, degradation and ion release.

2. Development of new CPC-fibre composites with enhanced mechanical properties. In order to improve the mechanical strength, it is very important to find a composition where the two phases (CPC and fibres) are intimately mixed with adequate adhesion at the interface. In this Thesis different approaches are investigated, all focused on the improvement of the adhesion between the fibres and the matrix:

- Development of new Fibre Reinforced Calcium Phosphate Cements (FRCPCs) using polymeric additives in the liquid phase with high affinity to either chitosan or (Poly)-L-Lactic Acid (PLLA) fibres in order to create a good fibre/matrix contact, aiming to improve the composite toughness.
- Use of low temperature plasma treated PLLA fibres, in order to create functional groups on the surface of the fibres, improving in this way their wettability and enhancing CPC mechanical properties through better adhesion fibre-matrix.

3. Development of new macroporous CaP scaffolds to be used as Simvastatin Acid (SVA) carriers. It is intended to design scaffolds with similar macrostructure but different composition and microstructure, so different processing routes either by low temperature processes or by sintering are envisaged. The issues tackled in this part are:

- Design and physico-chemical characterisation of the new macroporous calcium phosphate materials.
- Modification of CaP surface through low pressure plasma polymerisation and characterisation of the so-obtained polymeric layer.
- Study of the loading and release of Simvastatin Acid (SVA) from the CaP macroporous scaffolds and the potential effect of plasma polymerisation coatings on the drug-loaded scaffolds as a possible way to control the release of the drug.

The interdisciplinary scope of this PhD thesis is reflected by the fact that it involves different materials (ceramics and polymers), their preparation and/or optimisation, their characterisation with the related physico-chemical techniques, as well as the biological studies on selected materials among all these synthesised.

1.3 Structure

Even if all materials designed in this PhD Thesis are calcium phosphate materials (mainly based on the cementitious reaction of α -TCP), due to the different final aims and for the sake of clarity, it has been decided to divide the Thesis in three parts in order to facilitate its reading. In Figure 1 the structure of this Thesis is represented schematically. In the beginning a general state of the art including bone and bone substitutes (particularly calcium phosphates) is presented (**Chapter 2**). **Chapter 3** presents the development of biphasic calcium phosphate cements (BCPCs); followed by **Chapter 4** which introduces three different strategies with two different approaches to design fibre reinforced calcium phosphate cements and **Chapter 5** presents the development of macroporous scaffolds calcium phosphate scaffolds and their release of simvastatin acid. Finally, general conclusions and final remarks are presented in **Chapter 6**.

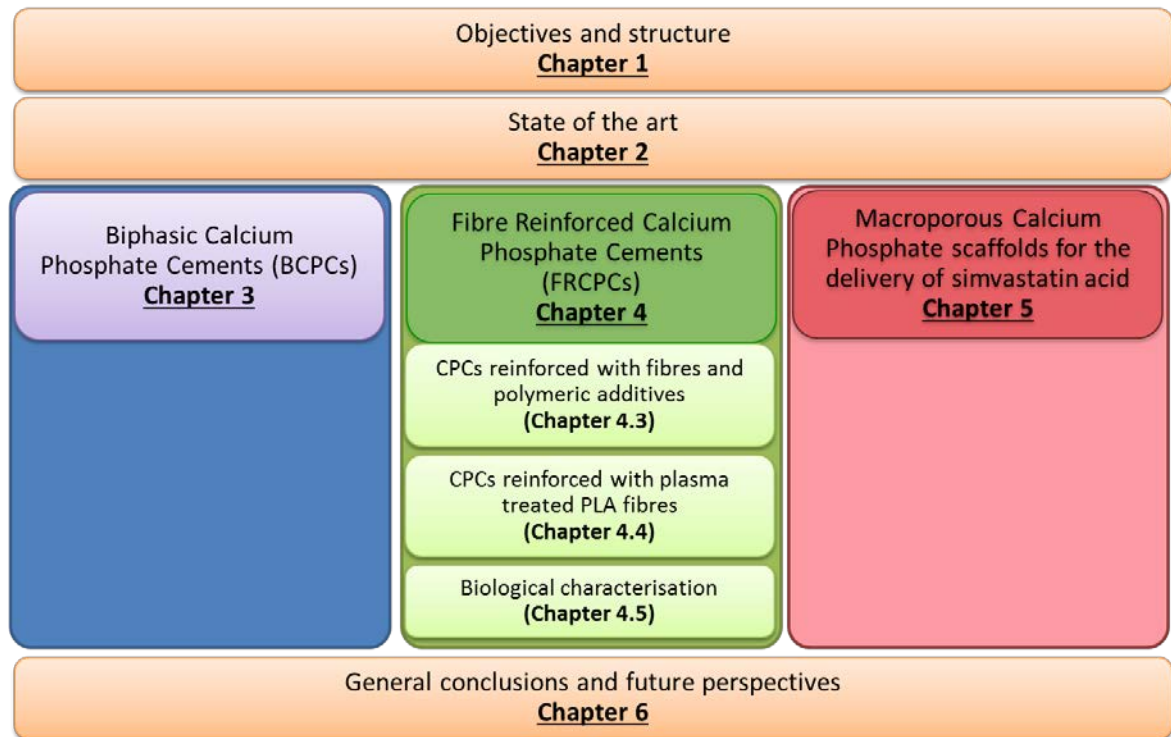


Figure 1- Scheme of the structure of the Thesis.

References

Ettinger MP. Aging bone and osteoporosis Strategies for preventing fractures in the elderly. *Arch Intern Med.* 2003; 163(18): 2237-2246.

Seeman E. Physiology of aging. Invited review: pathogenesis of osteoporosis. *J. Appl. Physiol* 2003; 95(5): 2142–2151.

Sroujia S, Livneb E. Bone marrow stem cells and biological scaffold for bone repair in aging and disease. *Mech Ageing Dev.* 2005; 126(2): 281-287.

Strømsøe K. Fracture fixation problems in osteoporosis. *Injury.* 2004; 35(2): 107-113.

Chapter 2

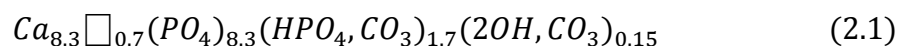
State of the art

2.1. The bone

Bone tissue, one of the hardest structures in the human body, is a type of dense connective tissue. Bones are rigid organs that constitute the vertebrate endoskeleton. Nevertheless, they possess a certain degree of toughness and elasticity **(Gray, 1918)**.

2.1.1. Macrostructure and functions

Bone is a dynamic, highly vascularised, composite material that contains two phases; a biopolymer consisting of matrix proteins, mostly collagen (type I), with some minor but important non-collagenous proteins (e.g. proteoglycans), minor amounts of lipids, and osteogenic factors **(LeGeros, 2008)**. And a biomineral or inorganic part, composed of carbonated hydroxyapatite (CHA) with a low crystallinity (250-500 x 30 Å) **(Dorozhkin, 2007)** described by the following general chemical formula **(Vallet-Regí, 2004)**:



Where \square represents a vacant.

This bone carbonated hydroxyapatite is non-stoichiometric and has a high specific surface area.

The inorganic to organic ratio is approximately 75 to 25 % by dry weight and about 65 to 35 % by volume. This ratio not only differs among animals but also among

bones in the same animal and over time in the same animal. A higher mineral to collagen ratio typically yields stronger but more brittle bones.

Bone is composed of a relatively dense outer layer (cortical or compact bone) covering an internal mesh-like structure (average porosity of 75 – 95%) of cancellous bone (also named: spongy or trabecular bone), the density of which is about 0.2 g/cm³. Bone is indeed a porous material with pore size ranges from 1 to 100 µm in normal cortical bone and 200 to 400 µm in trabecular bone. 55 to 70% of the pores in trabecular bone are interconnected (**Dorozhkin, 2009**). Furthermore, the two types of bone have different mechanical properties, which are reported in Table 2.1.

Table 2.1-Mechanical properties of cortical and trabecular bone tissue (Barinov, 2010).

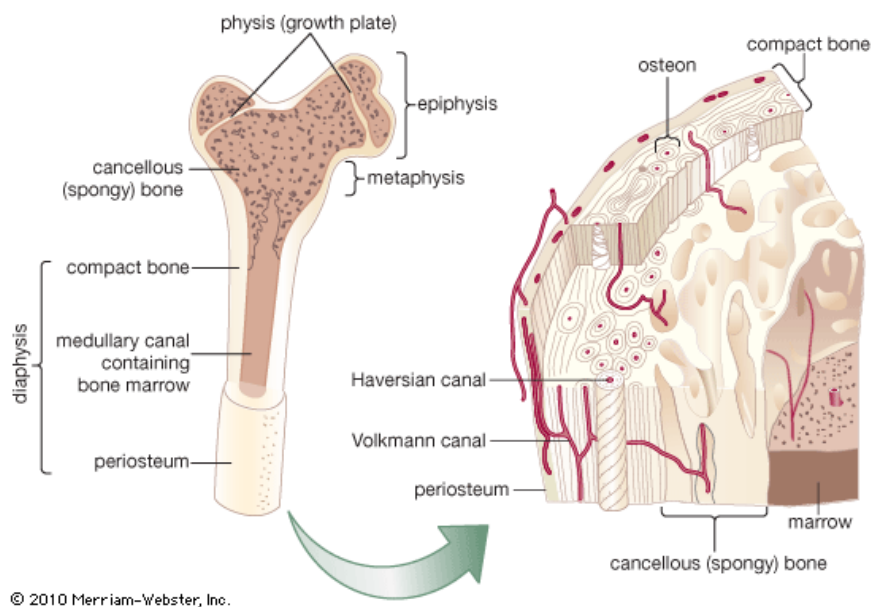
Property	Cortical bone tissue	Trabecular bone tissue
Compressive strength (MPa)	100-230	2-12
Bending and tensile strength (MPa)	50-150	10-20
Pre-failure deformation (%)	1-3	5-7
Crack resistance (MPa·m ^{1/2})	2-12	-
Young's modulus (GPa)	7-30	0.05-0.5

Bone is a very important organ due to the multiple functions it has to accomplish: mechanical, synthetic and metabolic (**Bilezikian, 2001**).

- **Mechanical functions**: protecting internal organs (for example the skull protects the brain and the ribs protect heart and lungs); giving a shape and keeping the body supported; permitting the movement through the interaction with muscles.
- **Synthetic function**: producing red and white blood cells in the inner part of the bone (bone marrow).
- **Metabolic function**: important source of minerals, such as calcium and phosphorous, growth factors (for instance Bone Morphogenetic Protein (BMP) and Transforming Growth Factor (TGF)) and fat (the yellow bone marrow acts as a storage reserve of fatty acids). Furthermore, bone buffers the blood against excessive pH changes by absorbing or releasing salts,

detoxifying the blood from heavy metals, storing them and avoiding their influence on other organs.

There are different types of bones in the human body with different functions. Bones come in a variety of shapes (long, short, plate, irregular and sesamoid) and have a complex internal and external structure. They are lightweight yet strong and hard, and serve multiple functions. Since the different types of bone are distinguished more by their external shape than by their basic structure, the bone structure is briefly described in the next paragraphs. Figure 2.1 shows the scheme of the structure of a long bone.



© 2010 Merriam-Webster, Inc.

Figure 2.1 - Structure of a long bone. Macroscopic structure (left) and transversal section of the bone (right) with its basic structure (Encyclopaedia Britannica).

The osteon, or Haversian system, is the fundamental functional unit of the compact bone. Osteons, roughly cylindrical structures, are typically several millimetres long and around 0.2 mm in diameter.

Each osteon consists of concentric layers, or lamella, of osseous tissue that surround a central canal, the Haversian canal. The Haversian canal contains the bone nerve and blood supplies. The boundary of an osteon is the cement line. Between adjoining osteons there are angular intervals that are occupied by interstitial lamellae. Near the surface of the compact bone, the lamellae are arranged parallel to the surface;

these are called circumferential lamellae. Osteons are connected to each other and to the periosteum by oblique vessels called Volkmann canals.

Vascularisation is really important in bone. In the diaphysis and metaphysis of long bones the vascularisation network is constituted by the nutrient artery, which passes through the cortex into the medullar cavity and then ramifies outward through Haversian and Volkmann canals to supply the cortex. Epiphyses are supplied by a separate arterial system.

2.1.2. Bone remodelling

Bone is a complex living organ composed by different types of cells and subject to continuous modifications (Figure 2.2), also known as bone remodelling (**Frost 1964**).

There are several types of bone cells with different functions:

- **Osteoprogenitors**: cells which are induced to differentiate to osteoblasts under the influence of growth factors, especially bone morphogenetic proteins (BMP).
- **Osteoblasts**: Mononucleated “bone-forming” cells found near the surface of bones. They are the cells responsible for bone production and mineralisation. They are responsible for making osteoid, which consists mainly of collagen. The osteoid becomes mineralised, thus forming bone.
- **Osteocytes**: osteoblast cells that become trapped in the matrix they secreted. These are osteoblasts that are no longer on the surface of bone, but are instead found in lacunae between the lamellae in bone. Osteocytes contact with the cytoplasm processes of their counterparts via a network of small canals, or canaliculi. This network facilitates the exchange of nutrient and metabolic waste and contributes to the homeostasis by maintaining the correct oxygen and mineral levels in the bone.

- **Osteoclasts**: Multinucleated cells that are responsible for bone resorption. They travel to specific sites on the surface of bone and secrete acid phosphatase, which resorbs the calcium in mineralised bone to break it down. Once osteoclasts have dissolved old bone, they disappear and die (Väänänen & Zhao, 1996).
- **Bone-lining cells**: quiescent osteoblasts covering the bone (Miller, 1987).

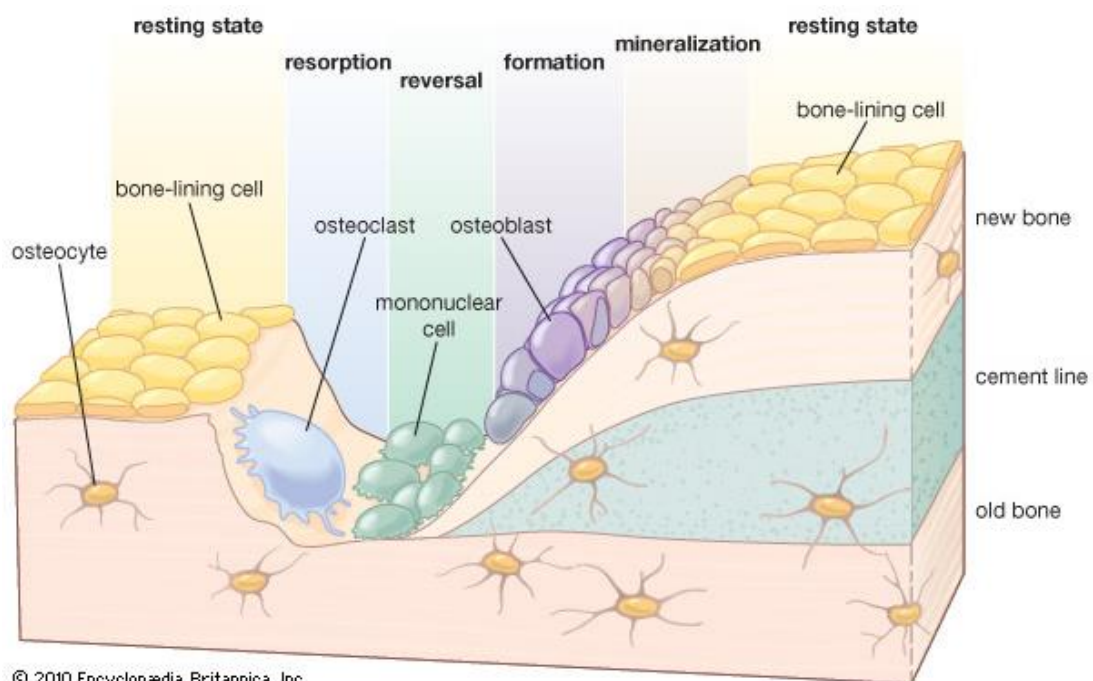


Figure 2.2- Bone cells and bone remodelling, from the resting state to new mineralization passing through resorption, bone formation and bone mineralisation (Encyclopaedia Britannica).

All these different kinds of cells are involved in bone remodelling (Frost 1964). This process occurs both in physiological as well as in pathological situations and controls the reshaping or replacement of bone during growth and following injuries such as fractures and micro-damages, which occur during normal activity.

Bone remodelling is a life-long process: osteoclasts, stimulated by mechanical or biochemical factors, start to resorb the bone while osteoblasts attach, proliferate and differentiate, and leading to the production of matrix proteins. These proteins include collagen (predominantly type I), osteocalcin (OSC) and BMPs. After mineral deposition occurs, new bone tissue is then formed through the process of

ossification. As a result, bone is added where needed and removed where it is not required.

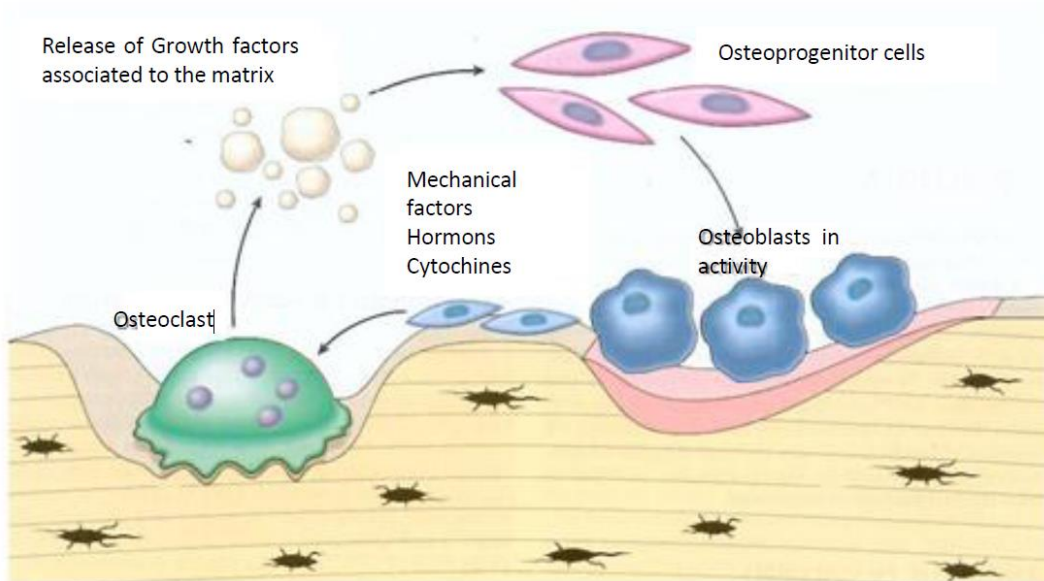


Figure 2.3- Bone remodelling. The cyclic process is shown: osteoclast cells are reabsorbing the mature bone, while osteoprogenitor cells are transformed into osteoblast cells producing new bone tissue; all these processes are regulated by mechanical and biochemical factors.

2.2. Bone grafting

A Graft is a tissue or an organ taken from a site of the same patient or from a different being and inserted into a new site or person. It is performed to repair a defect in structure. Bone grafting is widely used in hospitals to repair injured, aged or diseased skeletal tissue.

There are different types of grafts (Marsh, 2006):

- **Autologous bone graft or Autograft:** Tissue transplanted from one part of the body to another in the same individual. Traditionally, autologous bone is harvested from the iliac crest through a generous, open incision. This can result in significant pain (25-30%) and morbidity (up to 10%). In situations where rapid incorporation is required, autologous graft remains the treatment of choice in patients with poor vascularity, history of infection, failed attempts at non-union repair, fracture site gaps, unfavourable mechanical circumstances. There are different types of autografts depending

on the need. The harvest sites are first of all the iliac crest, fibula and occasionally the ribs.

- ***Allograft***: Transplant of an organ or tissue from one individual to another of the same species with a different genotype. A transplant from one person to another is an allograft. Allografts account for many human transplants, including those from cadaveric, living related, and living unrelated donors. It is also called allogeneic graft or homograft.

It is common to substitute bone with a derived-allograft product called demineralised bone matrix (DBM). In DBM the mineral phase of the bone tissue is extracted leaving behind only a matrix consisting of proteins, GFs, and collagen.

- ***Xenograft***: A surgical graft of tissue from one species to an unlike species (or genus or family). Xenograft bone is less common and, as allograft bone, has to be processed before implantation to avoid an immune reaction and consequent rejection of the implant.

Presently, bone autograft is the safest and most effective grafting procedure, since it contains patient's own bone growing cells and proteins, and it provides a framework for the new bone to grow into. However, bone autograft is limited in quantity (about 20 cm³), and its harvesting (e.g. from the iliac crest) represents an additional surgical intervention, with frequent subsequent pain and complications.

Allograft bone is also very common. It comes from tissue banks and it does not contain any living cells or matrix proteins since the tissue has been destroyed by virus-inactivation treatments and freezing processes. However allograft bone may transfer diseases or lead to immunological rejections (**Burchardt, 1987**).

Table 2.2 summarises the advantages and the drawbacks of the different kinds of grafts.

Table 2.2- Summary of the different grafts on the market with their advantages and drawbacks.

Type	Origin	Advantages	Drawbacks
Autograft	Same patient	<ul style="list-style-type: none"> ✓ Patient's growing cells and proteins 	<ul style="list-style-type: none"> ✗ Limited in quantity (about 20 cm³) ✗ Double intervention (pain, complications)
Allograft	Same species, different genotype	<ul style="list-style-type: none"> ✓ Structural function ✓ Abundant supply ✓ Lack of donor site morbidity 	<ul style="list-style-type: none"> ✗ Do not provide viable osteogenic cells ✗ Less effective than autografts ✗ Higher risk of infection ✗ Very small risk of disease transmission ✗ Risk of immunological rejections (Burchardt, 1987)
Demineralised bone matrix	Derived from allografts but without the mineral part	<ul style="list-style-type: none"> ✓ No risks of disease transmission ✓ Lack of donor site morbidity 	<ul style="list-style-type: none"> ✗ Does not provide viable osteogenic cells ✗ No structural support ✗ Less effective than autografts
Xenograft	Different species	<ul style="list-style-type: none"> ✓ Structural function ✓ Abundant supply ✓ Lack of donor site morbidity 	<ul style="list-style-type: none"> ✗ Do not provide viable osteogenic cells ✗ Less effective than autografts ✗ Higher risk of infection ✗ Very small risk of disease transmission ✗ Risk of immunological rejections (Burchardt, 1987)

Since autografts, allografts and xenografts have drawbacks, scientists have long searched for bio-compatible materials, coined as “biomaterials”. As defined by Williams: “*A biomaterial is a substance that has been engineered to take a form which, alone or as part of a complex system, is used to direct, by control of interactions with components of living systems, the course of any therapeutic or diagnostic procedure, in human or veterinary medicine*” (Williams, 2009). Although most synthetic bone substitutes available possess some of the positive properties of autograft, none yet have all the benefits of one’s own bone.

Current commercial substitute materials to replace or repair teeth and bones include metals, polymers (natural or synthetic), human bones (processed cadaver bones), animal bones (processed cow bones), corals and coral derived, synthetic ceramics (calcium phosphates, calcium carbonate, bioactive glasses), and composites (LeGeros, 2008). Depending on their ability to stimulate a response from the tissue, materials are classified into bioinert (e.g.: metals, some polymers, and some ceramics) and bioactive materials (including natural polymers, calcium phosphates, calcium carbonate, calcium sulphates and bioactive glasses, among others).

In 2006 Anderson presented the past, present and perspectives of the future of biomedical materials (Anderson, 2006), which is summarised below:

➤ **First Generation (1950 – 1975) → bioMATERIALS**

The development of these materials was due mainly to the need to find materials with a long- term integrity and non-toxic nature.

➤ **Second Generation (1975 – 2000) → BIOMATERIALS**

The biological interactions with biomaterials began to be more extensively investigated; advances in biological mechanisms knowledge led to a better understanding of interaction between biological systems and biomaterial surfaces; in these years the "biological" and the "material" parts were equally taken into account.

➤ **Third Generation (2000 - present) → BIOMaterials**

The advent and development of tissue engineering and regenerative medicine have given a heavy emphasis on the role of the biological interaction of biomaterials. The development of design criteria begins identifying the patient needs.

The capital letters emphasise the major direction of the research efforts in the complex subject of biomaterials.

Recently Holzapfel *et al.* (**Holzapfel, 2013**) analysed the past 50 years of research in biomaterials trying to reply from a clinical point of view to the question: “how smart do biomaterials need to be?” and pointed out the need to understand better how cells interact not only with the biomaterials but also with their own matrices. Thus, in the authors’ opinion, the immediate focus of biomaterials and tissue engineering research in the 21st century should contribute to elucidate the biology of the cell–extracellular matrix (ECM) interface and the scaffold/ECM/cell interface.

2.3. Calcium phosphates in bone repair

Calcium orthophosphates have been studied as bone repair materials for the last 80 years. The first in vivo test of calcium orthophosphates was performed in 1920, when researchers implanted tricalcium phosphate (TCP) into animals to test its efficacy as a bone substitute (**Albee & Morrison, 1920**). However, it was in 1951 when hydroxyapatite (HA) was implanted, for the first time, in rats and guinea pigs (**Ray, 1952**). In the 1970s other calcium orthophosphates were synthesised, characterised, investigated and evaluated in medicine. In 1971, Bhaskar published the first study concerning the preparation of biodegradable porous β -TCP scaffolds (**Bhaskar, 1971**) and the term “bioceramics” was introduced simultaneously. In 1973, the first study on preparation and implantation of resorbable and porous β -TCP bioceramics was published (**Driskell, 1973**). The following year, porous scaffolds consisting of hydroxyapatite and of whitlockite were prepared by employing exchange reactions at elevated temperatures and pressures (**Roy, 1974**). The modern dental application of calcium orthophosphates began in 1975: β -TCP was applied in surgically created periodontal defects (**Nery, 1975**); followed, in 1979, by a study in which dense HA cylinders were used for tooth root replacement (**Denissen & de Groot, 1979**). The first applications of calcium orthophosphate

coatings, films and layers started in 1976 (**Sudo, 1976**), while the first biocomposites and hybrid biomaterials containing calcium orthophosphate are dated back to 1981 (**Bonfield, 1981; Bonfield, 1981b**). In the 1980s an extensive commercialisation of the dental and surgical applications of calcium orthophosphate bioceramics was initiated, mainly due to the pioneering efforts by Jarcho (**Jarcho, 1976; Jarcho, 1977; Jarcho, 1979; Jarcho, 1981**) in the USA, de Groot (**Peelen, 1977; Rejda, 1977; de Groot, 1980; de Groot, 1983**) in Europe and Aoki (**Aoki, 1977; Kato, 1979; Akao, 1981; Akao, 1982**) in Japan.

The first publication on drug-loaded calcium orthophosphate bioceramics was issued in 1985 (**Randzio, 1985**). In the same year, works concerning biphasic, triphasic and multiphasic calcium orthophosphates were published (**Anuta & Richardson, 1985; Moore, 1985**). Finally yet importantly, the first paper on calcium orthophosphates used as scaffolds was published in 1994 (**Norman, 1994**), while applications of calcium orthophosphates in tissue engineering began in 1998 (**Dekker, 1998; Friedman, 1998**).

In the ternary system $\text{Ca}(\text{OH})_2\text{-H}_3\text{PO}_4\text{-H}_2\text{O}$ there are eleven known non-ion-substituted calcium orthophosphates with the Ca/P molar ratio within 0.5 and 2.0 (Table 2.3) (**Elliot, 1994**). Some of them are obtained by precipitation at room temperature while others by thermal decomposition or thermal synthesis. Important parameters in these materials are the molar Ca/P ratio, basicity/acidity and solubility. These parameters strongly correlate with the solution pH during synthesis. The lower the Ca/P molar ratio is, the more acidic and water-soluble the calcium orthophosphate is (**LeGeros, 1991; Elliot, 1994; Amjad, 1997**).

Table 2.3-Properties of the biologically relevant calcium orthophosphates (Bohner, 2000; Dorozhkin 2007).

Ca/P molar ratio	Compound	Formula	Solubility at 25°C, -log(Ks)	Solubility at 37°C, -log(Ks)	pH stability range in aqueous solutions at 25°C
Obtained by PRECIPITATION at ROOM TEMPERATURE					
0.5	Monocalcium phosphate monohydrate (MCPM)	Ca(H ₂ PO ₄) ₂ · H ₂ O	1.14	Data not found	0.0-2.0
1.0	Dicalcium phosphate dihydrate (DCPD), mineral brushite	CaH ₂ PO ₄ · 2H ₂ O	6.59	6.63	2.0-6.0
1.0	Dicalcium phosphate anhydrous (DCPA), mineral monetite	CaH ₂ PO ₄	6.90	7.02	a
1.33	Octacalcium phosphate (OCP)	Ca ₈ (HPO ₄) ₂ (PO ₄) ₄ · 5H ₂ O	96.6	95.9	5.5-7.0
1.5-1.67	Calcium-deficient hydroxyapatite (CDHA)	Ca _{10-x} (HPO ₄) _x (PO ₄) _{6-x} (OH) _{2-x} (0 < x < 1)	~85.1	~85.1	6.5-9.5
1.67	Precipitated Hydroxyapatite (PHA)	Ca ₁₀ (PO ₄) ₆ (OH) ₂	116.8	117.2	9.5-12
1.2-2-2	Amorphous calcium phosphate (ACP)	Ca _x H _y (PO ₄) _z · nH ₂ O, n = 3-4.5; 15-20% H ₂ O	b	b	~5-12 ^c
Obtained by THERMAL DECOMPOSITION or THERMAL SYNTHESIS					
0.5	Monocalcium phosphate anhydrous (MCPA)	Ca(H ₂ PO ₄) ₂	1.14	Data not found	a
1.5	α-Tricalcium phosphate (α-TCP)	α-Ca ₃ (PO ₄) ₂	25.5	25.5	d
1.5	β-Tricalcium phosphate (β-TCP)	β-Ca ₃ (PO ₄) ₂	28.9	29.5	d
1.67	Hydroxyapatite (HA or OHAp)	Ca ₁₀ (PO ₄) ₆ (OH) ₂	116.8	117.2	9.5-12
1.67	Fluorapatite (FA or FAp)	Ca ₁₀ (PO ₄) ₆ F ₂	120.0	119.2	7-12
2.0	Tetracalcium phosphate (TTCP or TetCP), mineral hilgenstockite	Ca ₁₀ (PO ₄) ₂ O	38-44	37-42	d

The solubility is given as the logarithm of the ion product of the given formulae (excluding hydrate water) with concentrations in mol/l

a) Stable at temperatures above 100 °C, b) Cannot be measured precisely. However, the following values were found: 25.7 ± 0.1 (pH = 7.40), 29.9 ± 0.1 (pH = 6.00), 32.7 ± 0.1 (pH = 5.28). The comparative extent of dissolution in acidic buffer is: ACP >> a-TCP >> b-TCP > CDHA >> HA > FA; c) Always metastable; d) These compounds cannot be precipitated from aqueous solutions

In low temperature synthesis of CaPs, due to the triprotic equilibrium that exists within orthophosphate-containing solutions, variations in pH alter the relative concentrations of the four polymorphs of orthophosphoric acid (Figure 2.4) and thus both the chemical composition and the amount of the calcium orthophosphates that forms by direct precipitation. (Lynn & Bonfield, 2005).

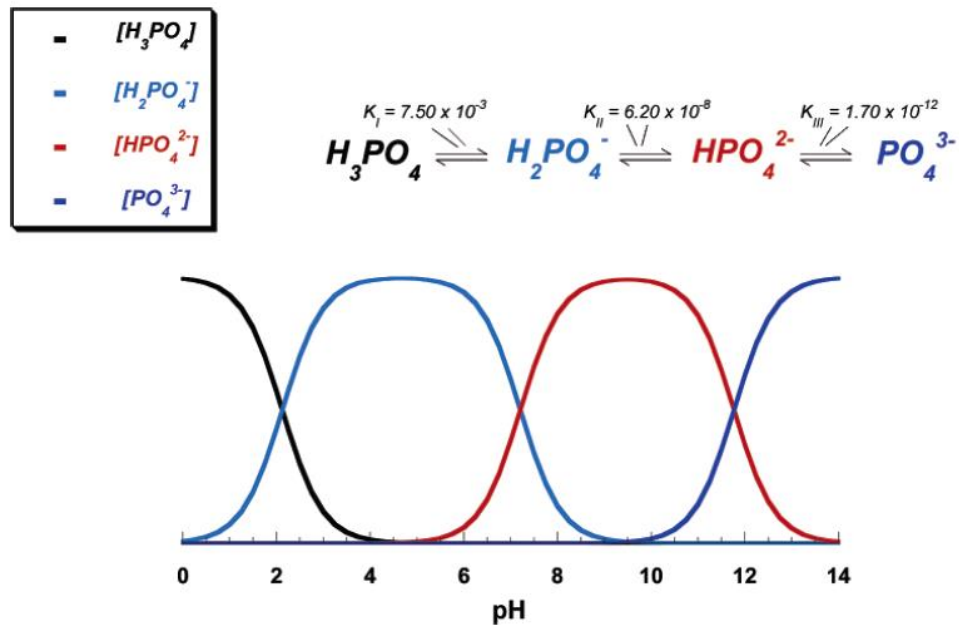


Figure 2.4- pH variation of ionic concentration in triprotic equilibrium for phosphoric acid solutions. (Lynn & Bonfield, 2005).

The pH is also important to predict the dissolution of the reaction products. Figure 2.5 shows the solubility phase diagrams of calcium orthophosphates at different pH.

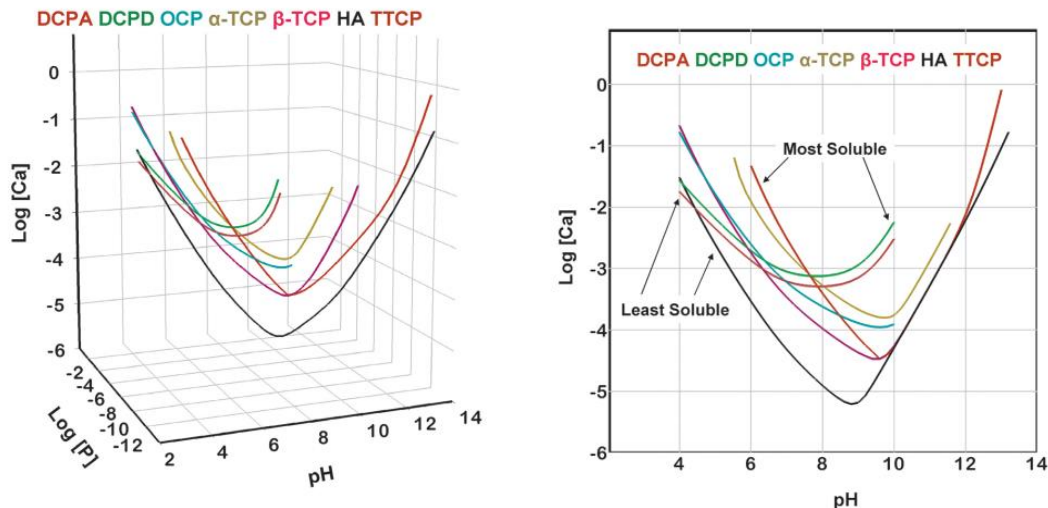


Figure 2.5 - Solubility phase diagram for the ternary system $\text{Ca}(\text{OH})_2\text{-H}_3\text{PO}_4\text{-H}_2\text{O}$, at 37 °C: (a) isotherms describing the solubility of a salt, expressed as the logarithm of the total calcium ($\log[\text{Ca}]$) and total phosphate ($\log[\text{P}]$) concentrations of the saturated solution as a function of pH; (b) solubility isotherms in a two dimensional graph showing $\log[\text{Ca}]$ and pH of the solutions (Chow & Takagi, 1996).

2.3.1. Properties of calcium phosphate materials

Depending on the synthesis method and composition, Calcium Phosphate (CaP) ceramics may present the following characteristics:

- Bioactivity
- Biodegradability
- Osteoconductivity
- Osteotransductivity

These concepts are further described subsequently.

a) Bioactivity

In the context of bone substitutes, bioactivity can be defined as the property of the material to develop a direct, adherent and strong bonding with bone (**Dorozhkin, 2007**).

In vitro bioactivity (assumed to predict *in vivo* bioactivity but as matter of fact just an approximation) has been associated with the formation of a bone-like apatite (carbonated hydroxyapatite) on the surface of the biomaterial when exposed to

metastable calcium phosphate solutions or to Simulated Body Fluid (SBF) with electrolyte composition similar to that of serum **(Kokubo, 1996)**.

In vivo bioactivity is evaluated after implantation in osseous sites **(LeGeros, 2003)**.

b) Biodegradability

A material is defined as biodegradable if all of its components are subject to decomposition through biological activity. Degradation can occur by two different mechanisms: simple dissolution (“passive”) or after osteoclastic bone remodelling (“active”).

In ceramic materials, “passive” *in vitro* resorption is measured by incubating the cement samples in a solution which simulates the body fluids, as for instance cell culture medium **(Grossardt, 2010)** and monitoring Ca²⁺ release or weight loss, whereas “active” *in vitro* resorption is determined through cell cultures of osteoclastic cells **(Grossardt, 2010)**. “Active” *in vitro* biodegradation can be simulated by immersing the material in an acidic buffer and monitoring the release of Ca²⁺ ions or weight loss with time **(Hankermeyer, 2003)**. The acidic buffer, to some extent, mimics the acidic environment during osteoclastic bone resorption activity **(Baron, 1985)**.

In vitro or *in vivo* degradation of CaPs depends on many features, among them their composition, particle size, crystallinity, porosity, and preparation conditions.

c) Osteoconductivity

Osteoconductivity, when referring to biomaterials, is the ability to serve as scaffold or template to guide formation of the newly forming bone along their surfaces **(Jarcho 1981; Davies & Hosseini, 2000)**. Osteoconduction is essential for stable long-term orthopaedic and dental implants. All bioactive materials are also osteoconductive.

There are three important features affecting the osteoconductivity of biomaterials:

- Surface chemistry → surface chemistry can be modified in order to obtain osteoconductive materials **(Kokubo, 2009)**.
- Surface topography → It has been shown that bone cells are sensitive both to micro- and nano- surface topography. On one hand, microgrooved HA surfaces have an influence on osteoblastic guidance **(Lu & Leng, 2003)**. On the other hand, nano-patterns seem to affect the focal adhesion of osteogenic cells **(Cassidy, 2014)**, and nano-topography has an effect on osteoclastic activity **(Geblinger, 2010)**.
- Architectural geometry → porous materials allow a better bone growth; the optimum pore size for bone ingrowth is 100-400 μm **(Tsuruga, 1997; Karageorgiou, 2005)**.

d) Osteotransductivity

The term osteotransductivity has been introduced to describe the “*in vivo*” behaviour of materials such as β -tricalcium phosphate (β -TCP), rhenanite (CaNaPO_4) and certain apatitic calcium phosphate cements (CPCs) **(Driessens, 1993)**. Upon implantation in bone these materials show a fast osteointegration, but later they are slowly resorbed and simultaneously and gradually replaced by new bone tissue without the formation of a gap between material and bone and, thus, probably without loss of mechanical stability during the transformation **(Driessens, 1998)**.

2.3.2. Calcium phosphate cements

A “cement” is a mixture of a solid and a liquid phase that sets and hardens independently and can bind other materials together (Figure 2.6).

A Calcium Phosphate Cement (CPC) is a bioactive and biodegradable graft, capable of self-setting to a solid body, in which the solid phase is a CaP powder and the liquid phase is water or an aqueous solution.

The possibility of obtaining monolithic calcium orthophosphate ceramics at ambient or body temperature via a cementitious reaction was put forward by LeGeros *et al.* (LeGeros, 1982) and Brown and Chow (Brown & Chow, 1983; Brown & Chow, 1985; Brown & Chow, 1986; Gruninger, 1984) in the early 1980s.

CPCs have been extensively investigated due to their excellent biological properties, potential resorbability, moulding capabilities, and easy manipulation.

A number of CPC formulations are currently available. Either hydroxyapatite (CDHA: $\text{Ca}_{10-x}(\text{HPO}_4)_x(\text{PO}_4)_{6-x}(\text{OH})_{2-x}$, with $0 < x < 1$ or PHA: $\text{Ca}_{10}(\text{PO}_4)_6(\text{OH})_2$) or brushite (DCPD: $\text{CaHPO}_4 \cdot 2\text{H}_2\text{O}$) can be formed in the cement setting reaction. The former are named apatitic cements and the latter brushitic cements. Their main advantages and disadvantages of the cement-type materials are listed in Table 2.4.

Table 2.4- Summary of the advantages and drawbacks of Calcium Phosphate Cements (Ginebra, 2006a; Ginebra, 2006b; Ambard, 2006; Ginebra, 2008).

Advantages	Drawbacks
<ol style="list-style-type: none"> 1. Self-setting ability in vivo. 2. Good osteoconductivity and occasional osteoinductivity. 3. Osteotransductivity. 4. Mouldability: perfect fitting to the implant site, which assures good bone-material contact, even in geometrically complex defects. 5. Potential injectability that allows cement implantation by minimally invasive surgical techniques. 6. Excellent biocompatibility and bioactivity. 7. No toxicity. 8. Low cost. 9. Ease of preparation and handling. 10. Setting at body temperature. 11. Form chemical bonds to the host bone. 12. Clinically safe materials in their powder components. 13. Can be used to deliver antibiotics, anti-inflammatory drugs, growth factors, morphogenic proteins, etc. at local sites, which are able to stimulate certain biological responses. 	<ol style="list-style-type: none"> 1. Mechanical weakness: limited use due to potential collapse of material followed by soft tissue formation instead of bone formation (loaded areas). Until cements with adequate shear strength are available, most complex fractures that can be repaired with cement will also require metal supports. 2. Can be washed out from surgical defect in excess of blood. 3. Lack of macroporosity, especially interconnected pores, which prevents fast bone ingrowth and the cements degrade layer-by-layer from the outside to the inside only. 4. The in vivo biodegradation of many formulations is slower than the growth rate of a newly forming bone.

Although some literature reports suggest that developments of CPCs stemmed from existing knowledge of calcium silicate or calcium sulfate cements, the discovery of the first CPC (**Brown & Chow, 1986**) was in fact a result of decades of basic studies on calcium phosphate solubility behaviours (**Chow & Takagi, 2001**) based on solubility phase diagrams (Figure 2.5) (**Brown, 1973**).

The mixture of the liquid and the solid phases is made in a tailored ratio that allows obtaining a mouldable paste that upon setting and hardening, after a certain time (depending on the formulation), transforms into a solid body that cannot be mould anymore (Figure 2.6).

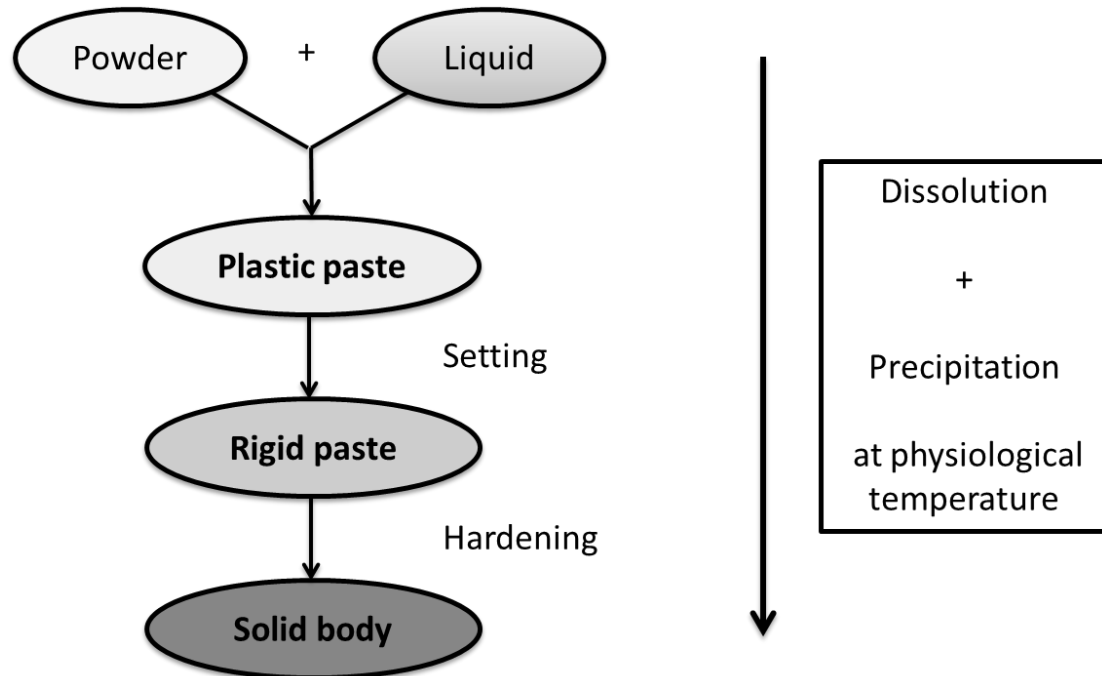


Figure 2.6 - Cementitious reaction of calcium phosphate cements.

The relevant parameters in the setting process are shown in Figure 2.7, and can be defined as follows:

- ***Cohesion time (C-T)*** is the time at which a CPC presents cohesion. Cohesion can be defined as the capacity of a CPC to set in a fluid without disintegrating (Ginebra, 2008). After the C-T is reached, the CPC in contact with blood or body fluids does not wash-out and can therefore be implanted.
- ***Initial setting time (I-T)*** is the time which indicates the end of mouldability of a CPC. The surgeon has the range of time between the C-T and I-T for introducing the CPC into the operated site.
- ***Final setting time (F-T)*** is the time after which it is not possible to mould the cement without causing serious structure damages to the CPC structure.

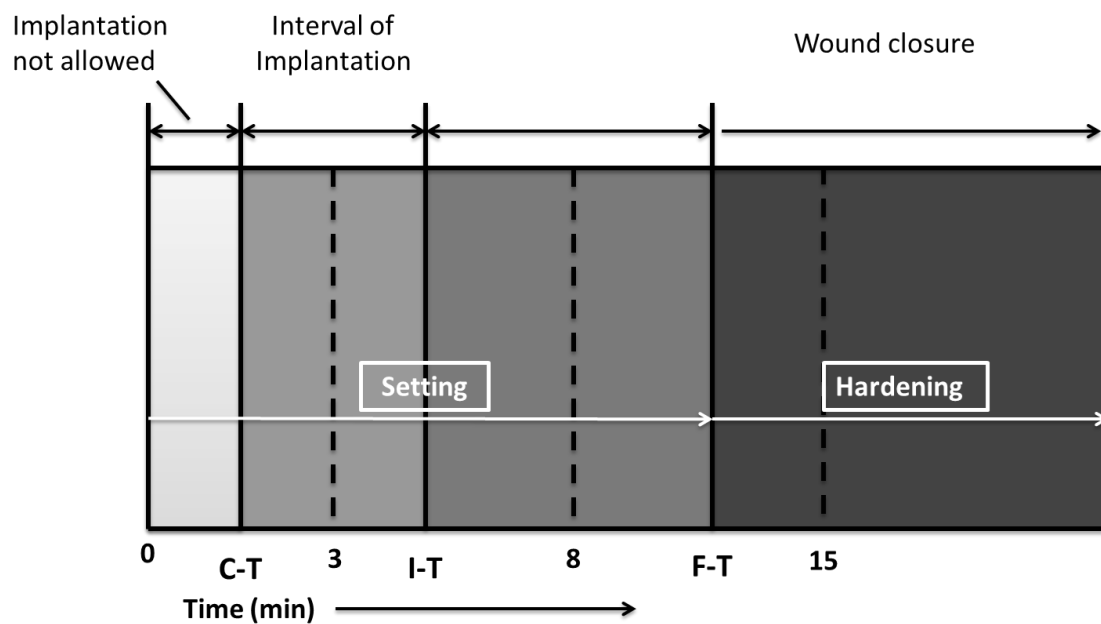


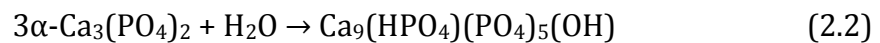
Figure 2.7 – Diagram of the setting parameters relevant for a calcium phosphate cement. (CT, Cohesion Time; I-T, Initial Setting Time; F-T, Final Setting Time). Figure revisited from (Driessens, 1998).

As far as the clinical application is concerned, adequate working ranges as proposed by Driessens *et al.* in 1998 (Driessens, 1998) were $0 \text{ min} < \text{C-T} < 3 \text{ min}$ for the cohesion time, $4 \text{ min} < \text{I-T} < 8 \text{ min}$ and $10 \text{ min} < \text{F-T} < 15 \text{ min}$ for the initial and final setting times, respectively. Apatitic cements, in general, present longer times than the ones proposed. These features for apatitic cements can be changed by:

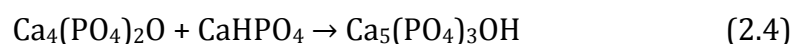
1. The reduction of the liquid to powder ratio (L/P).
2. The reduction of particle size.
3. The addition of calcium phosphate ions either pre-dissolved in the liquid phase or as highly soluble salt (common ion effect: the higher the concentration, the shorter the setting time).
4. The addition of seed materials, which act as crystal nuclei (the greater the number of nuclei, the shorter the setting time).

Apatitic CPCs, in other words those CPCs leading to the formation of PHA or CDHA as the reaction products, can be classified in three groups in (Ginebra 2008), taking into account the number and type of calcium phosphates used in the powder mixture:

1. Monocomponent CPCs, in which a single calcium phosphate compound hydrolyses to form PHA or CDHA. Since hydroxyapatite is the least soluble phase at pH > 4.2, this means that any other calcium phosphate present in an aqueous solution at that pH range will tend to dissolve, tending to precipitate to PHA at the equilibrium. As a result, H₃PO₄ or CaOH₂ are released into the solution. However, in most cases the formation of PHA is kinetically very slow, due to a decrease of the super-saturation level, as the reaction proceeds. The only cement system belonging to this category was first reported by Monma *et al.* (**Monma, 1976; Monma 1984**) and was further optimised and characterised by Ginebra *et al.* (**Ginebra, 1994; Ginebra, 1995; Ginebra 1997; Ginebra, 1999; Ginebra, 2004**). This system is based on the hydrolysis of α-TCP to CDHA according to equation (2.2):



2. CPCs formed by two calcium phosphates, one acidic and the other one basic, which set following an acid–base reaction. The basic component is normally TTCP (the only calcium phosphate having a Ca/P ratio higher than PHA). TTCP can be combined with one or more calcium phosphates with lower Ca/P ratio to obtain either PHA or CDHA. From a theoretical point of view, any calcium phosphate more acidic than PHA is able to react directly with TTCP to form PHA or CDHA. The most widely studied combinations are: i) TTCP + DCPD and ii) TTCP + DCPA blends, which were first developed by Brown and Chow (**Brown & Chow, 1983; Brown & Chow, 1985**) and have been the object of extensive research in the 1990s (**Brown & Fulmer, 1991; Xie & Monroe, 1990; Chow, 1991; Ishikawa, 1994; Fukase, 1990; Tenhuisen, 1996**). These blends produce cements that set at body temperature in a pH range around neutral, according to equations (2.3) and (2.4).



3. Systems formed by more than two compounds, including calcium phosphates, and other salts. An example of this group of CPCs is the product developed by Norian Corporation (Norian SRSTM, Skeletal Repair System) **(Constantz, 1995)**, where blends of calcium phosphates with a Ca/P ratio lower than PHA are used and CaCO₃ is added as an additional source of calcium ions.

This PhD thesis is focused on the modification of apatitic cements belonging to the first group, namely, based on the hydrolysis of α -TCP to CDHA, with the aim of improving their mechanical properties and in vivo performance.

References

Akao M, Aoki H, Kato K, Mechanical properties of sintered hydroxyapatite for prosthetic applications. *J. Mater. Sci.* 1981; 16(3): 809–812.

Akao M, Aoki H, Kato K, Sato A. Dense polycrystalline β -tricalcium phosphate for prosthetic applications. *J. Mater. Sci.* 1982; 17(2): 343–346.

Albee F, Morrison H. Studies in bone growth. *Ann. Surg.* 1920; 71(1): 32-38.

Ambard AJ, Mueninghoff L. Calcium Phosphate Cement: Review of Mechanical and Biological Properties. *J. Prosthodont.* 2006; 15(5): 321-328.

Amjad Z. Calcium phosphates in biological and industrial systems. Ed: Springer, 1997: pp 529

Anderson JM. The future of biomedical materials, *J. Mater. Sci. Mater. Med.* 2006; 17(11): 1025-1028.

Anuta DA, Richardson D. Biphasic Hydroxyapatite/Beta-tricalcium Phosphate Granules Bound in Polymerized Methyl Methacrylate: Bone Substitute Studies, Transactions of the Annual Meeting of the Society for Biomaterials in Conjunction with the Interna. 1985; 8: 62.

Aoki H, Kato KM, Ogiso M, Tabata T. Synthesis of Hydroxyapatite under Hydrothermal conditions. *J. Dent. Eng.* 1977; 18: 86–89.

Barinov SM. Calcium phosphate-based ceramic and composite materials for medicine. *Russ. Chem. Rev.* 2010; 79 (1): 13-29.

Baron B, Net L, Lourvard D, Couroy B. Cell-mediated extracellular acidification and bone resorption: evidence for a low pH in resorbing lacunae and localization of a 100 kD-lysosomal membrane protein at the osteoclast ruffled border. *J. Cell Biol.* 1985; 101(6): 2210-22.

Bhaskar SN, Brady JM, Getter L, Grower MF, Driskell T. Biodegradable ceramic implants in bone. Electron and light microscopic analysis. *Oral Surg. Oral Med. Oral Pathol.* 1971; 32(2):336-346.

Bilezikian JP, Raisz CG, Rodan GA. Principles of bone biology. Academic Press., San Diego, 2001.

Bohner M. Calcium orthophosphates in medicine: from ceramics to calcium phosphate cements. *Injury.* 2000; 31 (Suppl 4):37-47.

Bonfield W, Bowman J, Gryn timer MD. Composite Material for Use in Orthopaedics. UK Patent 8032647, 1981b.

Bonfield W, Gryn timer MD, Tully AE, Bowman J, Abram J. Hydroxyapatite reinforced polyethylene - A mechanically compatible implant. *Biomaterials* 1981; 2(3): 185-189.

Brown PW, Fulmer M. Kinetics of hydroxyapatite formation at low temperature. *J. Am. Ceram. Soc.* 1991; 74: 934-940.

Brown WE, Chow LC. A new calcium phosphate setting cement. *J. Dent. Res.* 1983; 62: 672.

Brown WE, Chow LC. A new calcium phosphate water setting cement. In *Cements Research Progress*; Brown, P.W., Ed.; American Ceramic Society: Westerville, OH, USA, 1986; 352-379.

Brown WE, Chow LC. Dental restorative cement pastes. US Patent No. 4518430, 1985.

Brown, WE. Environmental Phosphorus Handbook. John Wiley & Sons; New York: 1973.

Burchardt H. Biology of bone transplantation. Orthop. Clin. North Am. 1987; 18(2): 187-196.

Cassidy JW, Roberts JN, Smith C-A, Robertson M, White K, Biggs MJ, Oreffo ROC, Dalby MJ. Osteogenic lineage restriction by osteoprogenitors cultured on nanometric grooved surfaces: The role of focal adhesion maturation. Acta Biomater. 2014; 10(2): 651–660.

Chow LC, Takagi S, Costantino PD, Friedman CD. Self-setting calcium phosphate cements. Mat. Res. Soc. Symp. Proc. 1991; 179: 3–24.

Chow LC, Takagi S. A natural bone cement - A laboratory novelty led to the development of revolutionary new biomaterials. J. Res. Natl. Inst. Stand. Technol. 2001; 106: 1029–1033.

Chow LC, Takagi S. Self-setting calcium phosphate cements and methods for preparing and using them, patent number: US 5525148 A; June 11th, 1996.

Constantz BR, Ison IC, Fulmer MT, Poser RD, Smith ST, Vanwagoner M, Ross J, Goldstein SA, Jupiter JB, Rosenthal DI. Skeletal repair by in situ formation of the mineral phase of bone. Science. 1995; 267(5205): 1796–1799.

Davies JE, Hosseini MM. Histodynamics of endosseous wound healing. In: Davies JE, editor. Bone Engineering. 1st edition. Toronto, ON: Em squared inc; 2000. pp. 1–14.

de Groot K. Bioceramics consisting of calcium phosphate salts. Biomaterials 1980; 1(1): 47–50.

de Groot K. Ed. Bioceramics of Calcium Phosphate, CRC Press, Inc. Boca Raton, FL, USA, CRC Press. 1983; pp. 146.

Dekker RJ, de Bruijn JD, van den Brink I, Bovell YP, Layrolle P, van Blitterswijk CA, Bone tissue engineering on calcium phosphate-coated titanium plates utilizing cultured rat bone marrow cells: a preliminary study. *J. Mater. Sci. Mater. Med.* 1998; 9(12): 859–863.

Denissen HW, de Groot K. Immediate dental root implants from synthetic dense calcium hydroxyapatite. *J. Prosthet. Dent.* 1979; 42(5): 551–556.

Dorozhkin SV. Calcium orthophosphates in Nature, Biology and Medicine. *Materials.* 2009; 2(2): 399-498.

Dorozhkin SV. Calcium orthophosphates. *J. Mater. Sci.: Mater. Med.* 2007; 42(4): 1061-1095.

Driessens FCM, Boltong MG, Planell JA, Bermudez O, Ginebra MP, Fernandez E. A new apatitic calcium phosphate bone cement: preliminary results. *Bioceramics.* 1993; 6: 469–473.

Driessens FCM, Planell JA, Boltong MG, Khairoun I, Ginebra MP. Osteotransductive bone cements. *Proc. Inst. Mech. Eng. H.* 1998; 212 (6): 427-435.

Driskell T, Hassler C, Tennery V, McCoy L, Clark W. Calcium phosphate resorbable ceramics: a potential alternative to bone grafting. *J. Dent. Res.* 1973; 52:123-127.

Elliot JC. Structure and chemistry of the apatites and other calcium orthophosphates. Elsevier, Amsterdam, 1994.

Encyclopaedia Britannica 2010:

<http://global.britannica.com/EBchecked/topic/684133/bone-remodeling>.

Friedman CD, Costantino PD, Takagi S, Chow LC. BoneSource™ hydroxyapatite cement: A novel biomaterial for craniofacial skeletal tissue engineering and reconstruction. *J. Biomed. Mater. Res.* 1998; 43(4): 428–432.

Frost HM. Bone remodelling dynamics. *Plast. Reconstr. Surg.* 1964; 33(2): 196.

Fukase Y, Eanes ED, Takagi S, Chow LC, Brown WE. Setting reactions and compressive strengths of calcium phosphate cements. *J. Dent. Res.* 1990 69(12): 1852–1856.

Geblinger D, Addadi L, Geiger B. Nano-topography sensing by osteoclasts. *J. Cell. Sci.* 2010; 123(9): 1503-1510.

Ginebra MP, Driessens FCM, Planell JA. Effect of the particle size on the micro and nanostructural features of a calcium phosphate cement: a kinetic analysis. *Biomaterials* 2004; 25(17): 3453–3462.

Ginebra MP, Fernández E, Boltong MG, Planell JA, Bermúdez O, Driessens FCM. Compliance of an apatitic calcium phosphate cements with some short-term clinical requirements in bone surgery, orthopaedics and dentistry. *Clin. Mater.* 1994; 17(2): 99–104.

Ginebra MP, Fernández E, Driessens FCM, Planell JA. Modeling of the hydrolysis of a-tricalcium phosphate. *J. Am. Ceram. Soc.* 1999; 82(10): 2808–2812.

Ginebra MP, Traykova T, Planell JA. Calcium phosphate cements: competitive drug carriers for the musculoskeletal system? *Biomaterials* 2006b; 27(10): 2171-2177.

Ginebra MP, Traykova T, Planell, JA. Calcium phosphate cements as bone drug delivery systems: A review. *J. Controlled Release* 2006a; 113(2): 102–110.

Ginebra MP, Boltong MG, Fernández E, Planell JA, Driessens FCM. Effect of various additives and temperature on some properties of an apatitic calcium phosphate cement. *J. Mater. Sci.: Mater. Med.* 1995; 6(10): 612-616.

Ginebra MP, Fernández E, De Maeyer EA, Verbeeck RM, Boltong MG, Ginebra J, Driessens FCM, Planell JA. Setting reaction and hardening of an apatitic calcium phosphate cement. *J. Dent. Res.* 1997; 76 (4): 905-912.

Ginebra MP. Calcium phosphate bone cements, in: Deb S, ed. *Orthopaedic bone cements*. Woodhead Publishing Ltd., Cambridge, 206-230 (2008).

Gray's Anatomy of the Human Body–20thed. W.H. Philadelphia: Lea & Febiger, 1918.

Grossardt C, Ewald A, Grover LM, Barralet JE, Gbureck U. Passive and active in vitro resorption of calcium and magnesium phosphate cements by osteoclastic cells. *Tissue Eng. Part A.* 2010; 16(12): 3687-3695.

Gruninger SE, Siew C, Chow LC, O'Young A, Tsao NK, Brown WE. Evaluation of the biocompatibility of a new calcium phosphate setting cement. *J. Dent. Res.* 1984; 63: 200.

Hankermeyer CR, Ohashi KL, Delaney DC, Ross J, Constantz BR. Dissolution rates of carbonated hydroxyapatite in hydrochloric acid. *Biomaterials* 2002; 23 (3): 743-750.

Holzapfel BM, Reichert JC, Schantz JT, Gbureck U, Rackwitz L, Nöth U, Jakob F, Rudert M, Groll J, Hutmacher DW. How smart do biomaterials need to be? A translational science and clinical point of view. *Adv. Drug Deliv. Rev.* 2013; 65(4): 581–603.

Ishikawa K, Takagi S, Chow LC, Ishikawa Y, Eanes ED, Asaoka K. Behaviour of a calcium phosphate cement in simulated blood plasma in vitro. *Dent. Mater.* 1994; 10(1): 26–32.

Jarcho M , Bolen CH, Thomas MB, Bobick J, Kay JF, Doremus RH. Hydroxyapatite Synthesis and Characterization in Dense Polycrystalline Form. *J. Mater. Sci.* 1976; 11: 2027-2035.

Jarcho M, O'Connor JR, Paris DA. Ceramic hydroxylapatite as a plaque growth and drug screening substrate. *J. Dent. Res.* 1977; 56: 151–156.

Jarcho M, Salsbury RL, Thomas MB, Doremus RH. Synthesis and fabrication of β -tricalcium phosphate (whitlockite) ceramics for potential prosthetic applications. *J. Mater. Sci.* 1979; 14(1): 142–150.

Jarcho M. Calcium phosphate ceramics as hard tissue prosthetics. *Clin Orthopaed Rel Res* 1981; 157: 259-278.

Karageorgiou V, Kaplan D. Porosity of 3D biomaterial scaffolds and osteogenesis. *Biomaterials.* 2005; 26(27): 5474-5491.

Kato K, Aoki H, Tabata T, Ogiso M. Biocompatibility of Apatite Ceramics in Mandibles. *Biomater. Med. Devices. Artif. Organs.* 1979; 7(2): 291–297.

Kokubo T, Matsushita T, Takadama H, Kizuki T. Development of bioactive materials based on surface chemistry. *J. Eu. Ceram. Soc.* 2009; 29(7), 1267-1274.

Kokubo T. Formation of biologically active bone-like apatite on metals and polymers by a biomimetic process. *Thermochimica Acta.* 1996; 280-281: 479-490.

LeGeros R, Lin S, Rohanizadeh R, Mijares D, LeGeros J. Biphasic calcium phosphate bioceramics: preparation, properties and applications. *J. Mater. Sci. Mater. Med.* 2003; 14(3): 201-209.

LeGeros R.Z., Calcium phosphate-based Osteoinductive Materials. *Chem. Rev.* 2008; 108(11): 4742-4753.

LeGeros RG. Calcium Phosphates in Oral Biology and Medicine. Monographs in oral science; Myers, H, Ed: Karger AG, Basel, Switzerland, 1991, Vol.15, pp 1-201 (pp 27).

LeGeros RZ, Chohayeb A, Shulman A. Apatitic calcium phosphates: possible dental restorative materials. *J. Dent. Res.* 1982; 61: 343.

Lu X, Leng Y. Quantitative analysis of osteoblast behavior on microgrooved hydroxyapatite and titanium substrata. *J. Biomed. Mater. Res. A.* 2003; 66 (2):677-87

Lynn AK, Bonfield W. A novel method for the simultaneous, titrant-free control of pH and calcium phosphate mass yield. *Acc. Chem. Res.* 2005; 38(3): 202-207.

Marsh JL. Principles of Bone Grafting: Non-union, Delayed Union. *Surgery* 2006; 24(6): 207-210.

Miller SC, Jee WSS. The bone lining cell: A distinct phenotype? *Calcified Tissue Int.* 1987; 41(1): 1-5.

Monma H, Goto M, Komura T. Effect of additives on hydration and hardening tricalcium phosphate. *Gypsum Lime* 1984; 188: 11-16.

Monma H, Kanazawa T. The hydration of α -tricalcium phosphate. *J. Ceram. Soc. Jpn. (Yogo-kyokai-shi).* 1976; 84: 209-213.

Moore DC, Chapman MW, Manske DJ. Evaluation of a New Biphasic Calcium Phosphate Ceramic for Use in Grafting Long Bone Diaphyseal Defects, Transactions of the Annual Meeting of the Society for Biomaterials in Conjunction with the Interna. 1985; 8: 160.

Nery EB, Lynch KL, Hirthe WM, Mueller KH. Bioceramic implants in surgically produced infrabony defects. *J Periodontol.* 1975; 46(6): 328-347.

Norman ME, Elgendy HM, Shors EC, El-Amin SF, Laurencin CT. An in-vitro evaluation of coralline porous hydroxyapatite as a scaffold for osteoblast growth. *Clin. Mater.* 1994; 17(2): 85–91.

Peelen J, Rejda B, Vermeiden J, de Groot, K. Sintered tri-calcium orthophosphate as bioceramic. *Sci. Ceram.* 1977; 9: 226-236.

Randzio J, Thoma K, Alex R, Rhomberg B. Healing and pharmacokinetics of a beta-tricalcium phosphate-gentamycin combination in animal studies (preliminary report). *Dtsch. Zahnärztl. Z.* 1985; 40(6): 668–671.

Ray R, Degge J, Gloyd P, Mooney G. Bone regeneration. *J. Bone Joint Surg. Am.* 1952, 24-A-3: 638-647.

Rejda BV, Peelen JGJ, de Groot K. Tri-calcium phosphate as a bone substitute. *J. Bioeng.* 1977; 1(2): 93–97.

Roy D, Linnehan S. Hydroxyapatite formed from coral skeletal carbonate by hydrothermal exchange. *Nature.* 1974, 247(5428): 220-222.

Sudo SZ, Schotzko NK, Folke LEA. Use of hydroxyapatite-coated glass beads for preclinical testing of potential antiplaque agents. *Appl. Environ. Microbiol.* 1976; 32(3): 428–437.

Tenhuisen KS, Brown PW. The kinetics of calcium deficient and stoichiometric hydroxyapatite formation from $\text{CaHPO}_4 \cdot 2\text{H}_2\text{O}$ and $\text{Ca}_4(\text{PO}_4)_2\text{O}$. *J. Mater. Sci. Mater. Med.* 1996; 7(6): 309–316.

Tsuruga E, Takita H, Itoh H, Wakisaka Y, Kuboki Y. Pore size of porous hydroxyapatite as the cell-substratum controls BMP-induced osteogenesis. *J. Biochem.* 1997; 121 (2): 317-324.

Väänänen K, Zhao H. Principles of bone biology. Bilezikian JP, Raisz LG & Rodan GA (eds.), pp. 127 (1996).

Vallet-Regí M, González-Calbet JM. Calcium phosphates as substitution of bone tissues. *Prog. in Solid. State Chem.* 2004; 32(1-2): 1-31.

Williams DF. On the nature of biomaterials. *Biomaterials.* 2009; 30(30): 5897-5909.

Xie L, Monroe EA. Calcium phosphate and hydroxylapatite ceramics, in T Yamamuro, L Hench, J Wilson (Eds), *Handbook of Bioactive Ceramics, Vol. II.* CRC Press, Boca Raton Florida, 1990, pp. 29-37.

Chapter 3

Biphasic Calcium Phosphate Cements

In chapter 2 Calcium Phosphate Cements (CPCs) have already been introduced with their advantages and drawbacks. Due to their similar properties to those of bone they have been extensively studied in the last years. This thesis is centred on CPCs based on α -Tricalcium Phosphate (α -TCP) combined with different additives either ceramic, liquid polymers or polymer fibres. Specifically, in this chapter we investigate CPCs based on α -TCP incorporating β -TCP in order to form Biphasic Calcium Phosphates Cements (BCPCs).

3.1. Introduction

3.1.1. Osteoinduction

Osteoinduction is *“the induction of undifferentiated inducible osteoprogenitor cells that are not yet committed to the osteogenic lineage to form osteoprogenitor cells”* (**Friedenstein, 1968**). Even if this process was already observed in the first part of the past century, the milestone in this field was the identification by Urist of Bone Morphogenetic Proteins (BMPs) as inducers of heterotopic bone formation (**Urist, 1967; Urist & Strates, 1971**). Urist defined osteoinduction as *“the mechanism of cellular differentiation towards bone of one tissue due to the physicochemical effect or contact with another tissue”* (**Urist, 1967**). Later on, it was discovered that this property could be attributed to some biomaterials.

The osteoinduction mediated by biomaterials is their ability to induce bone formation when implanted at heterotopic sites (**Barradas, 2011**). Osteoinductive

biomaterials have great potential in bone regeneration, yet there is a lack of fundamental understanding of the biological mechanism underlying the phenomenon by which osteogenesis is induced. Both BMP-2 and BMP-7 have been successfully used in many applications due to their osteoinductive capacity **(Boakye, 2005; Vaccaro, 2004)**.

Osteoinductivity can be either caused by the addition of osteogenic factors to the material or be stimulated from the material itself. In the first case it is called “engineered” osteoinductivity while in the second case it is called “intrinsic” osteoinductivity.

a) Engineered or Programmed Osteoinductivity

Osteoinductivity can also be stimulated from the addition of osteogenic factors to the material. In the case of CaPs or CaP-based composite scaffolds, osteoinduction is caused by combining them with osteoprogenitor cells (stem cells, marrow cells, dental pulp cells, and chondrocytes) or bone growth factors (i.e. BMPs).

b) “Intrinsic” Osteoinductivity

In general, most CaP biomaterials are known to be osteoconductive but not osteoinductive **(Legeros, 1991)**. However, several CaP materials have been reported to have the ability to form bone in non-bony sites of different animals without addition of osteogenic factors. In particular, this has been observed in some porous synthetic HA **(Yamasaki & Sakai, 1992; Ripamonti, 1996)**, sintered β -TCP **(Toth, 1993)**, but especially in Biphasic Calcium Phosphate (BCP) ceramics composed of HA and β -TCP **(Yang, 1996; Le Nihouhannen, 2005; Gosain, 2002; Habibovic, 2005)**.

Since this osteoinductive property was observed in some CaP materials but not in others of similar composition, the aforementioned materials were described to have ‘intrinsic’ osteoinductivity.

This inductive phenomenon of some CaP materials was attributed to:

➤ **Physical properties:** Macro and micro-structure are really important.

In particular, the microstructure is believed to allow entrapment and concentration of circulating bone growth factors (BMPs) and osteoprogenitor cells imparting osteoinductive properties to the CaP materials (**Legeros, 2008**). Habibovic *et al.* claimed that to be osteoinductive, the materials need an appropriated macro and micro porosity (**Habibovic, 2005**). The macropores allow the bone ingrowth whilst the micropores accelerate the dissolution-precipitation process of CaP. To support this theory Yuan and co-workers found that the absence of micropores showed absence of bone induction (**Yuan, 1998**). This was further confirmed by Zhang *et al.* who found that, in mice, gene expression of osteocalcein (an osteoblastic specific marker) in tissue grown in HA or BCPs pores, was higher than in pure β -TCP (**Zhang, 2009**). Furthermore, they claimed complete differentiation of adipocytes (originated from mesenchymal stem cells). However Le Nihouhannen and coworkers affirmed that the pre-existence of macropores in the biomaterials is not essential for osteoinduction to occur (**Le Nihouhannen, 2005**). A recent paper (**Bianchi, 2014**) showed that the dimension of the concavities in a material has an effect on *in vitro* mineralisation. Small concavities ($\Phi = 0.4$ mm) showed a much higher mineralisation than large ones ($\Phi = 1.8$ mm), a 4-fold decrease in dimension increased 124-fold the mineralisation. They concluded that concavity size is an effective parameter to control position and extent of mineralisation *in vitro*. Furthermore, they found that this mineralisation starts preferentially within concavities and not planar surfaces suggesting that surface microstructure is really important. By controlling the surface morphology it seems possible to modulate the mineralisation.

➤ **Chemical properties:** Chemical composition is as important as the topography.

In 1998 Yuan supposed that osteoinductivity could be related to Calcium phosphates with specific chemical and structural characteristics (**Yuan,**

1998). Scientists have investigated what could be the role of Ca^{2+} and P_i ions in the environment on osteogenesis. In order to prove the importance of these ions, Chai and co-workers added Ca^{2+} and/or P_i to the cell media to see the effects on mesenchymal stem cells. They saw an increase of proliferation and, at longer times, an increase in osteogenic gene expression (**Chai, 2011**). The same group found that in vitro exogenous Ca^{2+} and P_i supplementation promote osteogenic differentiation of human periosteum-derived cells (osteoprogenitor cells) in vitro (**Chai, 2012**). Yet the exact role of the chemical properties is not clear.

The mechanisms of bone induction by CaP biomaterials involve many factors. They have not yet been elucidated and the debate about them is still open (**Daculsi & Layrolle, 2004; Barradas, 2011**). Several hypotheses have been proposed to explain this interesting biological property:

- de Groot proposed that some calcium phosphate ceramics can concentrate endogenous bone growth factors (e.g. BMPs) from body fluids which will trigger stem cells to form bone tissue (**de Groot, 1998**).
- Blood vessels might be a source of progenitor cells, which can differentiate into osteoblasts under the stimulation of the inflammatory cytokines released by macrophages and induced by CaP loose particles smaller than 5 μm (**Le Nihouhannen, 2008**).
- Some authors support the idea that the nanostructured rough surface or the surface charge of implants might cause the asymmetrical division of stem cells into osteoblasts (**Habibovic, 2005**).
- Mesenchymal cells may be triggered by the local high level of calcium ions and recognise the bone-like apatite layer formed in vivo by dissolution-precipitation of CaPs to differentiate into osteoblasts (**Daculsi & Layrolle, 2004**).
- Ripamonti *et al.* (**Ripamonti, 2009**) suggested that “active” biodegradation could have a role. When osteoclastic resorption of the osteoinductive

substrate occurs, calcium ions are released which, in turn, stimulate angiogenesis and osteogenic differentiation of stem cells.

All these hypotheses are based on the triggering of stem cells and osteogenic differentiation due to local CaP environments resulting from micro- and macro-porous structures of materials.

Finally yet importantly, the osteoinductivity of calcium phosphate biomaterials in animal models is a complicated matter, considering that osteoinduction is both material-dependent and animal-dependent (different times for bone formation and different amounts of bone induced by the same material in different animal models) **(Yuan, 1998)**. Gosain *et al.* tried to explain this difference claiming that it could be due to a difference in concentration of GFs in different animals **(Gosain, 2002)**. To date, the debate remains open.

3.1.2. Biphasic calcium phosphate materials

Biphasic Calcium Phosphates (BCPs) were introduced in the late 1980s **(Daculsi, 1989)** in an effort to design synthetic bone grafts with tunable resorption rate. They are composed of Hydroxyapatite (HA), the most stable calcium orthophosphate (solubility at 25 °C, $-\log(K_s) = 116.8$), and β -Tricalcium phosphate (β -TCP), a more soluble compound (solubility at 25 °C, $-\log(K_s) = 28.9$) **(Chow, 2009)**, with varying HA/ β -TCP ratios. The resorption and bioactivity of BCPs can be controlled by changing the HA/ β -TCP ratio and the crystallinity of the ceramic **(Legeros, 2003)**.

As mentioned in the previous section, in recent years it has been shown that, in addition to being osteoconductive (promoting bone ingrowth in direct contact with their surface), BCPs could be also osteoinductive, i.e., they are able to foster differentiation of stem cells to the osteogenic lineage, leading to bone induction even in a non-osseous environment. This capacity, that initially was associated to the action of some growth factors, such as bone morphogenetic proteins, can also be triggered by some materials with specific chemical and structural characteristics **(Yuan, 1998; Yuan, 2010; Le Nihouannen, 2005)**. This is the case of BCPs, where a proper combination of chemical composition, macroporosity and microporosity has

been shown to promote osteogenesis *in vivo* (**Habibovic, 2005; Barradas, 2011**), even without the addition of exogenous growth factors. In addition to specific microstructural features, the higher release of Ca^{2+} ions by BCPs compared to pure HA is proposed to be one of the parameters that explain the higher osteoinductive potential of this group of materials (**Barradas, 2011; Chai, 2011**).

BCPs are normally obtained by high-temperature sintering of calcium deficient apatites or other calcium phosphate precursors (**LeGeros, 2003**), with the limitations associated to this type of materials, e.g. they can be obtained only as preformed ceramics or granules.

The objective of this work is to obtain self-setting BCPs, which would add to the benefits of osteoinductive BCP ceramics the advantages associated to calcium phosphate cements like mouldability or injectability. Our hypothesis was that a biphasic HA/ β -TCP material could be obtained from a mixture of α -TCP and the less soluble polymorph β -TCP, upon reaction with an aqueous solution. It is known that α -tricalcium phosphate (α -TCP, solubility at 25 °C, $-\log(K_s) = 25.5$) hydrolyses to a calcium deficient HA (CDHA) upon setting (**Ginebra, 1997**). α -TriCalcium Phosphate ($\alpha\text{-Ca}_3\text{PO}_4$, α -TCP) and β -TriCalcium Phosphate ($\beta\text{-Ca}_3\text{PO}_4$, β -TCP) are two allotropic phases of the three possible (β , α and α') at Ca/P ratio of 1.5 (Figure 3.1).

The β -phase is stable at room temperatures up to 1180 °C, whereas the α -phase is stable at temperatures higher than 1180 °C. The last one (α') lacks practical interest because it only exists at temperatures >1430 °C and reverts almost instantaneously to α -TCP on cooling below the transition temperature.

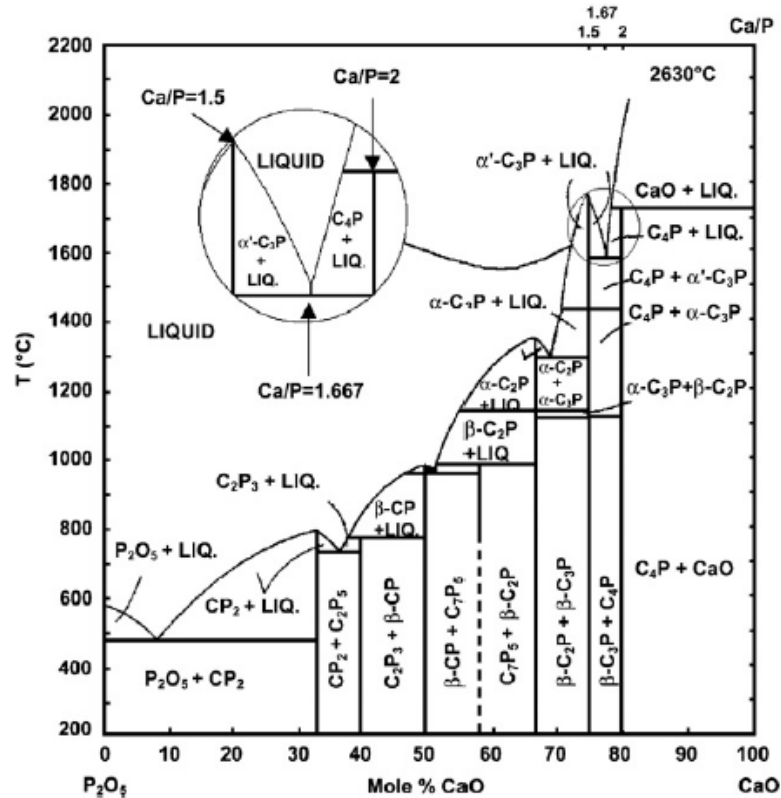


Figure 3.1- Phase diagram of the system CaO-P₂O₅ (C = CaO, P = P₂O₅) at high temperatures. Each line represents a phase boundary. Here C₇P₅ represents 7CaO·5P₂O₅; the other abbreviations can be written out in the same manner (Dorozhkin, SV, 2012).

In this study, the properties of new Biphasic Calcium Phosphate Cements (BCPCs) with different α -TCP/ β -TCP ratios are characterised, paying special attention to the setting reaction, mechanical properties, degradation and ion release.

3.2. Objectives

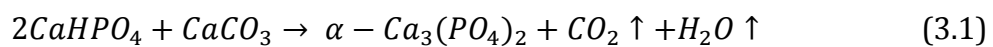
This work aims at designing new biphasic CPCs (herein named BCPCs) composed by CDHA and β -TCP, starting from blends of α -TCP and β -TCP at different α -TCP/ β -TCP ratios, and characterising them in terms of setting properties, mechanical properties, and degradation.

3.3. Experimental

3.3.1. α -TCP and β -TCP preparation

a) α -TCP synthesis

The powder phase of CPCs was obtained by sintering at 1400°C for 15 hours (Hobersal CNR-58) a mixture of calcium hydrogen phosphate (CaHPO_4 , Sigma-Aldrich C7263) and calcium carbonate (CaCO_3 , Sigma-Aldrich C4830) at a molar ratio of 2:1, according to equation:



The powder was homogenised for 15 minutes with a mechanical homogenizer (whip mix) and introduced into a Platinum-Rhodium crucible. The solid solution was sintered following the heating treatment in Figure 3.2.

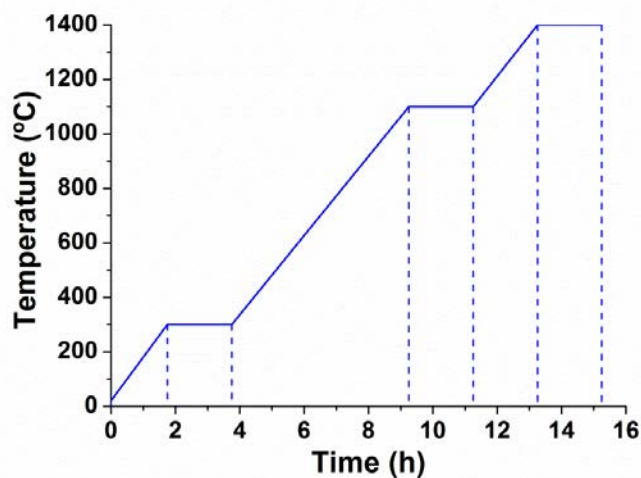
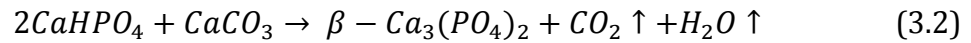


Figure 3.2 - α -TCP heating treatment

After sintering, the material was extracted from the furnace and quenched in air by crushing into small, homogeneous pieces to stabilise the α -TCP phase.

b) β -TCP synthesis

β -TCP was obtained by sintering at 1100°C for 5 hours a mixture of calcium hydrogen phosphate (CaHPO_4 , Sigma-Aldrich C7263) and calcium carbonate (CaCO_3 , Sigma-Aldrich C4830) at a molar ratio of 2:1, according to equation:



As in the case of α -TCP, the powder was homogenised for 15 minutes with a mechanical homogenizer (whip mix) and introduced into a Platinum-Rhodium crucible. The solid solution was sintered in a furnace (Hobersal PR/300 serie 8B) following the heating treatment reported in Figure 3.3.

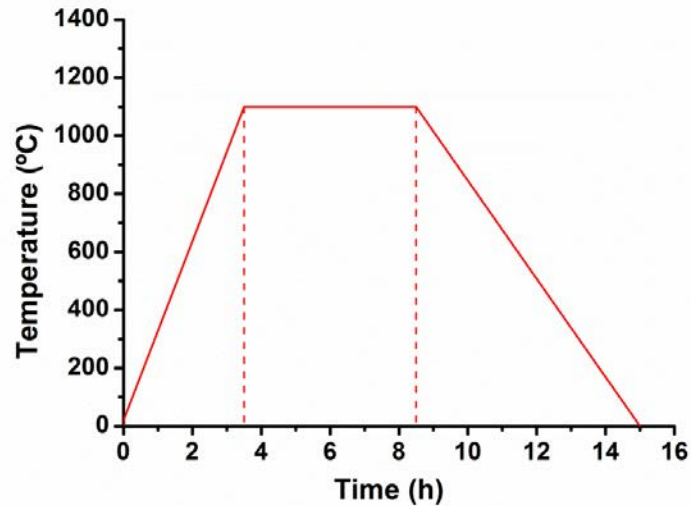


Figure 3.3 - β -TCP heating treatment

After sintering, the material was allowed to cool down in the furnace till room temperature.

c) Powder grinding

The milling of the reagents is an important step in the CPC fabrication process and a critical point that determines the final properties of the different CPCs. Milling was performed in a 500 ml volume agate jar (Pulverisette 6, Fritsch GmbH).

Regarding α -TCP, 145 g of material were milled, using the following parameters:

- $m_{\text{material}}/m_{\text{balls}} = 0.5$ (10 agate balls of 3 cm diameter);
- Rotation speed: 450 rpm;
- Time: 15 min.

In the case of β -TCP 50 g of material were milled using to the following parameters:

- $m_{\text{material}}/m_{\text{balls}} = 0.42$ (4 agate balls of 3 cm diameter);
- Rotation speed: 150 rpm;
- Time: 60 min.

3.3.2. Powder characterisation

a) Particle size distribution

The particle size distribution of the powder was measured by laser diffraction (LS 13 320 Beckman Coulter). The powder was previously dispersed in ethanol in an ultrasonic bath to avoid the presence of agglomerates during measurement. The circuit was rinsed between each sample. Three measurements were taken for each composition in order to avoid errors due to possible surviving aggregates.

b) Specific surface area

Specific Surface Area (SSA) was determined by Nitrogen Adsorption at 77 K following the Brunnauer–Emmet–Teller method (BET) in an ASAP 2020 (Micromeritics).

c) Phase quantification

Phase composition of α -TCP and β -TCP powders was assessed by X-ray powder diffraction (XRD, PANalytical, X'Pert PRO Alpha-1) by scanning in Bragg-Brentano geometry using $\text{CuK}\alpha$ radiation ($\lambda=1.5406 \text{ \AA}$). The experimental conditions used were: 1.3 h of scan time with 2θ scan step of 0.017° and scan range between 4° and 100° , with measuring time of 50 s per step. X-ray generator parameters: voltage 45 kV and intensity 40 mA. The diffraction patterns were compared with the Joint Committee on Powder Diffraction Standards for α -TCP (JCPDS No. 9–348), β -TCP (JCPDS No. 9–169) and HA (JCPDS No. 9–432) (**JCPDS, 1991**). Rietveld refinements were carried out in order to quantify the phases present. The Inorganic Crystal Structure Database was used, including structural models for α -TCP (ICSD No. 923), β -TCP (ICSD No. 6191) and HA (ICSD No. 151414) (**ICDS, 1998**).

3.3.3. Cement preparation and characterisation

a) Cement preparation

Biphasic Calcium Phosphate Cements (BCPCs) were prepared by mixing the powder, consisting in combinations of α -TCP and β -TCP in various proportions, with the liquid phase (water or an aqueous solution of 2 wt % Na_2HPO_4 (Panreac) at a Liquid to Powder ratio (L/P) of 0.35 ml/g. Subsequently, the cement paste was put in Teflon moulds and immersed in Ringer's solution at 37°C for 7 days to allow the reaction of the cement. Hereafter, the BCPCs will be named according to the amount of β -TCP (0, 20, 40, 60, 80, and 100 wt% β -TCP).

b) Phase quantification

Phase composition of BCPCs was assessed by X-ray powder diffraction as described in section 3.3.2c). The cement phase composition was studied by a semi-quantitative analysis performed on base of the patterns ((**Chung, 1974**); see Annex I) since Rietvelt refinements were not adequate due to low crystallinity.

c) Initial and final setting time and cohesion

The initial and final setting times of the cement pastes were determined with Gillmore needles according to the **ASTM-C266-89 (ASTM-C266-89-Standard Test Method for time of setting of hydraulic cement paste by Gillmore needles)**. The cohesion time was determined by visual inspection after immersion of the samples in deionised water at 37°C (**Fernandez, 1996**). Thus, the samples were checked up to a reasonable period of time (6-8 hours) to verify if the cement was releasing particles with time.

d) Compressive strength testing

The compressive strength was evaluated in cylindrical specimens (12mm height x 6mm diameter) at a cross-head speed of 1 mm/min using a Servohydraulic Testing Machine MTS BIONIX 358 equipped with a 2.5 kN load cell. At least six replicates

were prepared for each cement formulation. The material was tested wet and the specimens were previously manual polished in order to obtain parallel surfaces and assure a full contact of the specimen surface with the piston surface.

e) Microstructure analysis

To ascertain the microstructure of the BCPCs, the fracture surfaces were investigated by Field Emission Scanning Electron Microscopy (FE-SEM, Hitachi H-4100FE or FIB, Zeiss Neon40). The samples were mounted on the sample holder with carbon tape and a thin layer of colloidal silver (Electron Microscopy Sciences, 12630) was applied on the side walls to improve conductivity, and the surface of samples was coated with Au/Pd by mean of Emitech K950X metal evaporator and then investigated.

f) Specific surface area

The SSA of the BCPCs was measured by Nitrogen adsorption (ASAP 2020, Micromeritics) at 77 K according to the BET method. The sample holder was filled with around 6-8 samples of BCPCs.

g) Focus ion beam sectioning

To ascertain the bulk microstructure of 0% and 80% β -TCP cements, Focus Ion Beam tomography (FIB, Zeiss Neon40) was performed. The preparation of the sample was the same as for microstructure analysis (section 3.3.3e). A 30 x 30 x 25 μm parallelepiped (preparation shown in Figure 3.4), was coated with Au-Pd (in order to protect the surface) and cut in slices and FE-SEM pictures were taken in order to reconstruct the 3D material structure (Smart3D, Carl Zeiss).

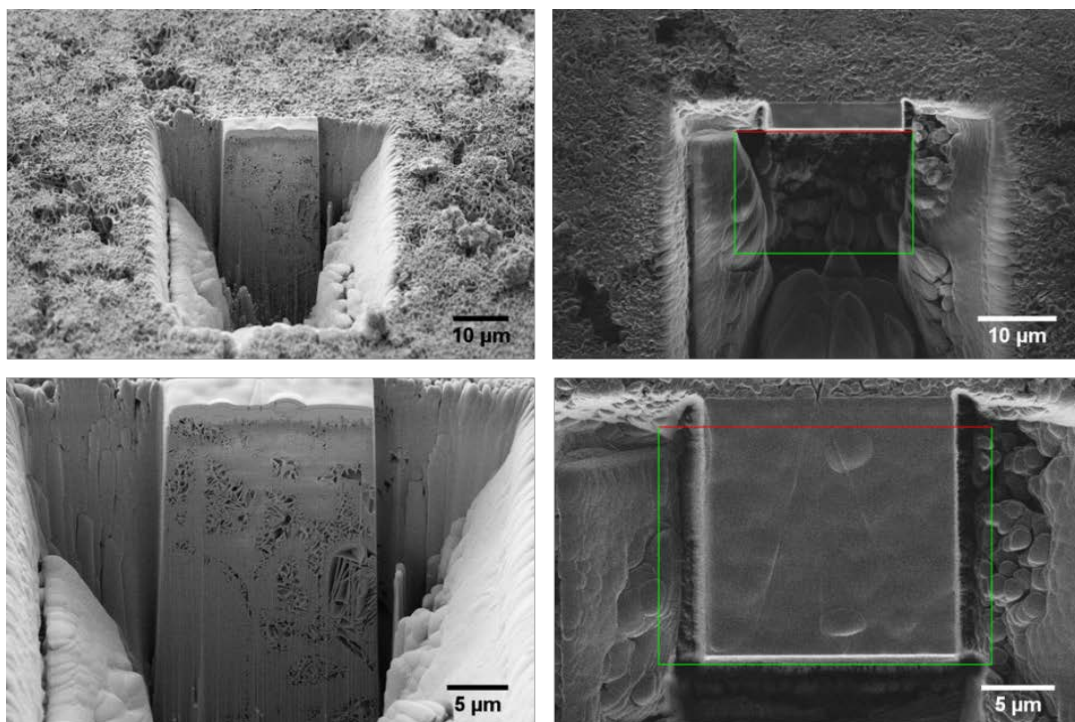


Figure 3.4 - FIB cross sectioning sample preparation.

h) Mercury Intrusion Porosimetry

The porosity and pore entrance size distribution were measured by Mercury Intrusion Porosimetry (MIP, Autopore IV 9500, Micromeritics), using 5-6 samples (12 mm height x 6mm diameter).

i) Ion release in water

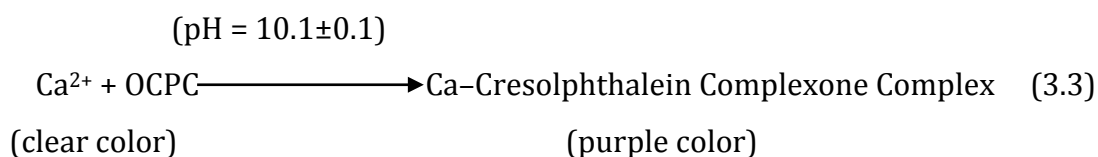
To measure Ca^{2+} release in water, set BCPC discs (2 mm height x 15 mm diameter) were prepared and introduced in 1.5 mL of MilliQ water. At different time points of 2, 6, 10, 24, 48, and 72 h the samples were removed and the Calcium concentration in the media was analysed with an Ion-selective electrode (ILyte Na/K/Ca/pH, Instrumentation Laboratory). Three replicates of each formulation were prepared and measured at each time point.

j) Accelerated in vitro degradation test

In vitro degradation of BCPCs was evaluated under accelerated conditions in acidic solution during 8 h (**Hankermeyer, 2002; Sariibrahimoglu, 2012**). Set discs (2 mm height x 15 mm diameter, which accounts for an apparent surface of 447 mm²) were prepared and dried in an oven at 120°C until constant weight. A control consisting of 100% β-TCP compacted discs was also evaluated, with the aim of assessing if the fact of using as-milled powders instead of hydrated ones had some effect on the dissolution rate of pure β-TCP. The compacted discs (2.7 mm height x 9 mm diameter) were prepared by compressing β-TCP powders (0.5 g) at 10 kN, for 10 s. To maintain a total apparent surface similar to the BCPC samples, two β-TCP compacted discs were used for each experiment (accounting for an apparent surface of 407 mm²).

Each sample was introduced in 50 mL of a pH 2 aqueous solution (0.01M HCl and 0.14M NaCl) at 37°C. The medium was refreshed every hour and the specimens were weighted after carefully removing remaining droplets on the surface using a wet paper. The assay was performed in triplicate for 8 h. After the assay, samples were dried in the oven at 120°C until constant weight to calculate the weight loss.

Given the low pH of the solutions, the ion-selective electrode could not be used, and the concentration of calcium at each time point was obtained by reaction with ortho-cresolphthalein complexone (OCPC, Sigma-Aldrich) in alkaline solution to obtain a purple coloured solution (**Sariibrahimoglu, 2012**):



The Ca²⁺ concentration was measured by absorbance in a UV-VIS spectrometer at λ_{max} = 570 nm (Infinite M200 Pro Microplate Reader, TECAN).

The values were normalised to the initial sample weight.

3.3.4. Statistics

Statistical differences were determined using one-way ANOVA with Tukey’s post-hoc test (95%) using Minitab software (Minitab Inc). Statistical significance was noted when $p < 0.05$.

3.4. Results

3.4.1. Powder characterisation

a) Powder phase quantification

The X-ray diffraction patterns of α -TCP and β -TCP powders are reported in Figure 3.5. It can be noticed that there are small impurities both in α -TCP and β -TCP. In the β -TCP pattern, the α -TCP peak is not visible in the figure due to the proximity of the main peaks of α -TCP and β -TCP (Figure 3.5b). However, it was possible quantify it by Rietveld refinements, as reported in Table 3.1.

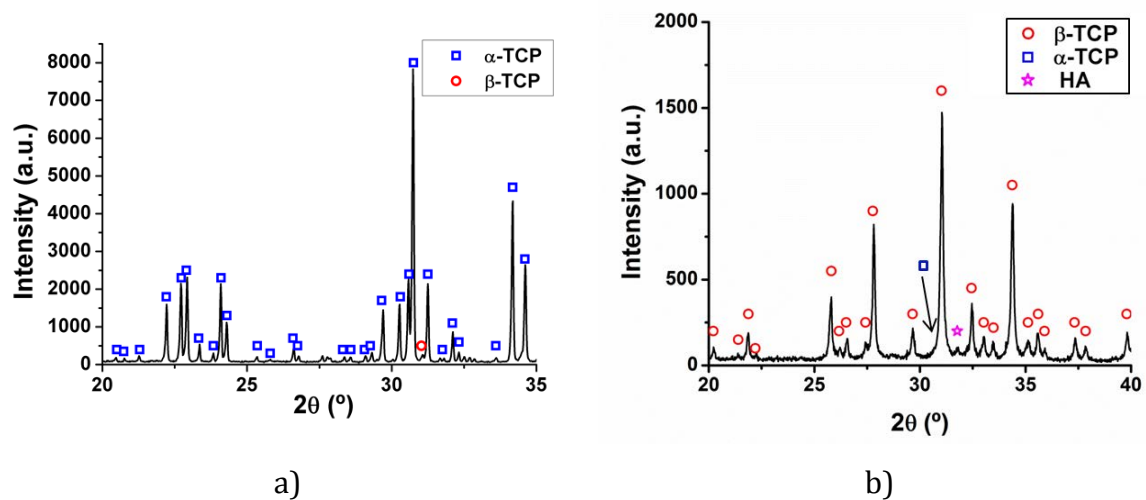


Figure 3.5- X-Ray diffraction pattern of a) α -TCP and b) β -TCP.

Table 3.1- XRD data of the raw α -TCP and β -TCP powders.

Phase Material	% α -TCP	% β -TCP	% HA
α -TCP	95	3	2
β -TCP	2.4	97.5	0.1

However, in both reagents prepared (α -TCP and β -TCP) the amount of impurities was low and acceptable for subsequent work.

b) Particle size distribution and specific surface area

The particle size distributions of α -TCP and β -TCP are reported in Figure 3.6, and their main volume features, together with SSA, another important parameter of the reactant powders, are summarised in Table 3.2.

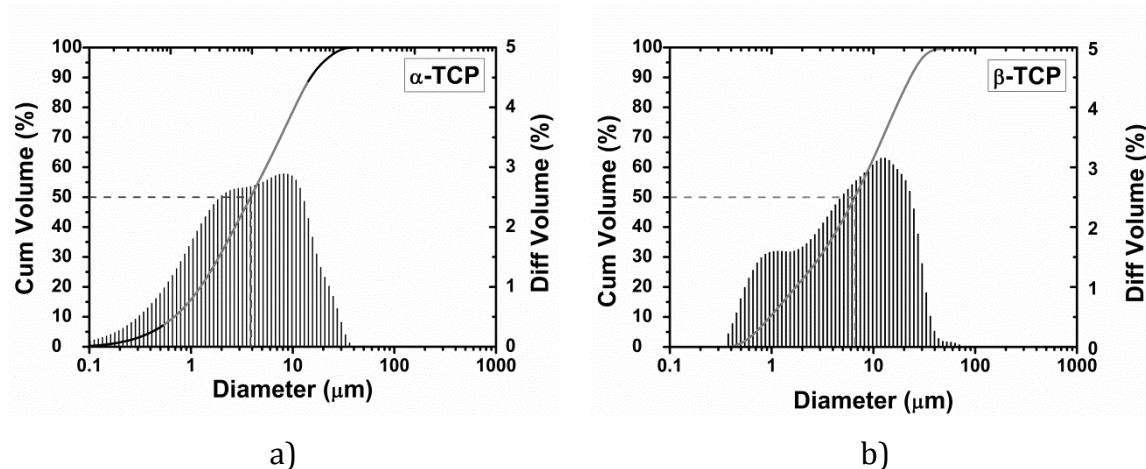


Figure 3.6 -Particle size distribution of: a) α -TCP and b) β -TCP.

Table 3.2- Particle size distribution parameters in volume and Specific Surface Area of α -TCP and β -TCP reactant powders are showed. D_{10} means 10% of the powder particles are smaller than this value. D_{90} means 90% of the powder particles are smaller than this value.

Material	D_{10} (μm)	Median Size, D_{50} (μm)	D_{90} (μm)	Specific Surface Area SSA(m^2/g)
α -TCP	0.684	3.855	15.05	0.975 ± 0.006
β -TCP	0.963	6.561	23.04	0.739 ± 0.003

3.4.2. Biphasic calcium phosphate cement characterisation

a) Cohesion and setting times

The results obtained for the cohesion time, initial setting time and final setting time of BCPCs are given in Figure 3.7. All cements presented cohesion in water after a few minutes and, as shown in Figure 3.7, cohesion time increased by adding β -TCP, irrespective of the amount. The addition of a second phase (β -TCP) did not alter much the initial setting time but did substantially increase the final setting time. The 100% β -TCP cement showed faster cohesion than the BCPCs but the final setting time was significantly higher.

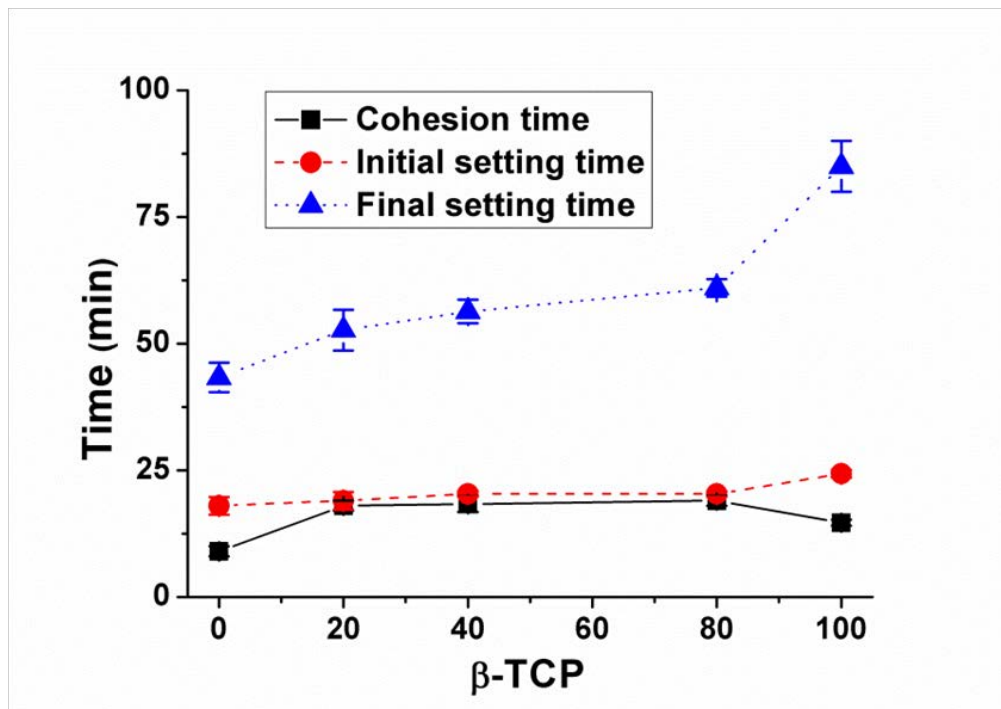


Figure 3.7- Cohesion time, initial setting time and final setting time of BCPCs composed of α -TCP and β -TCP at different ratios at a L/P = 0.35 ml/g.

b) Phase quantification in the BCPCs

The XRD patterns of the starting BCPC powders and of the set cements after 7 days in Ringer's solution at 37°C are shown in Figure 3.8 a) and b), respectively.

The evolution by the addition of β -TCP is reported. The addition of a second phase showed clearly the growth of the corresponding peaks. In the setting cements (Figure 3.8a) the α -TCP peaks are substituted by CDHA ones, reflecting the transformation process.

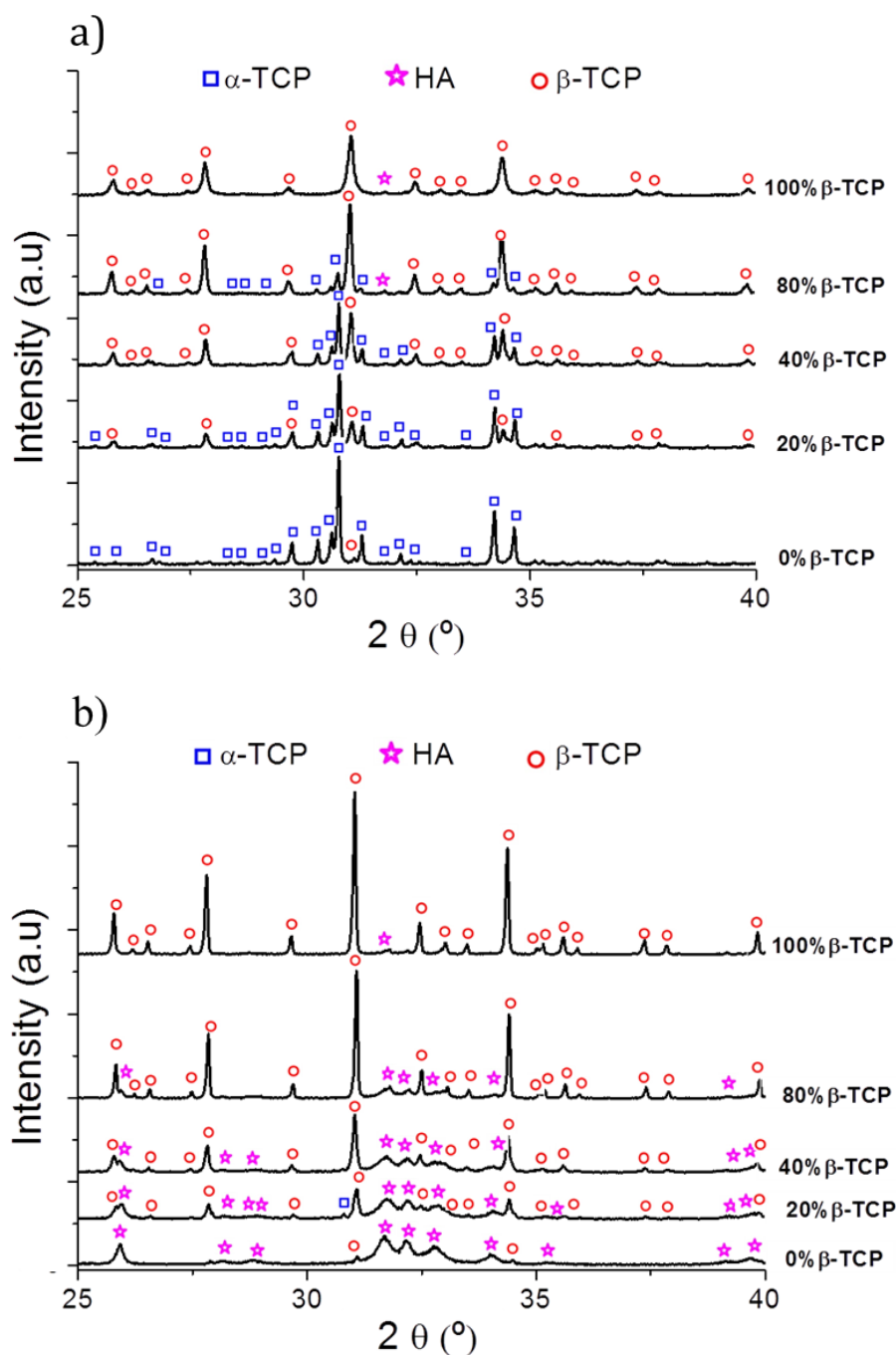


Figure 3.8- X-ray diffraction patterns of the starting powders (a) and the set cements (b) for the different BCPCs, with increasing contents of β -TCP. The set cements were obtained after 7 days reaction in Ringer's solution at 37°C.

The phase composition of the powder mixtures as determined by Rietveld refinement and of the BCPCs after setting, determined by the intensity of the peaks is summarised in Table 3.3. It can be observed that α -TCP was completely hydrolysed to an apatitic phase, more specifically a calcium deficient HA (CDHA) (Ginebra, 1997), whereas the amount of β -TCP remained nearly unchanged.

Table 3.3 - Phase composition of the reactants and set cements. The measured composition was determined by Rietveld refinement of the XRD patterns.

	Nominal composition		Initial powders			Set cements		
			Measured composition (XRD/Rietveld refinement) *			Measured composition (XRD/peak area method)		
Material	% α -TCP	% β -TCP	% α -TCP	% β -TCP	% HA	% α -TCP	% β -TCP	% HA
0% β	100	0	94.9	2.9	2.2	0	3.7	96.3
20% β	80	20	76.7	22.8	0.5	0	21.4	78.6
40% β	60	40	54.8	44.6	0.6	1.5	37.4	61.1
80% β	20	80	17.4	82.1	0.5	0	77.8	22.2
100% β	0	100	2.4	97.5	0.1	0	99.5	0.5

*Error $\pm 1\%$

c) Mechanical properties

The compressive strength of the different BCPCs is shown in Figure 3.9. A linear decrease can be observed in the compressive strength of the BCPC with the increase in β -TCP amount.

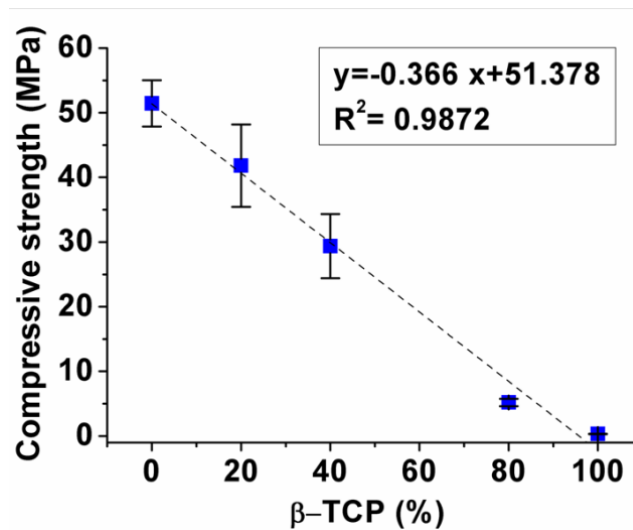


Figure 3.9 - Compressive strength of BCPCs with different β -TCP %.

d) Total porosity and pore entrance size distribution

The total porosity of BCPCs measured by mercury intrusion porosimetry (shown in Figure 3.10) slightly increased with growing amount of β -TCP.

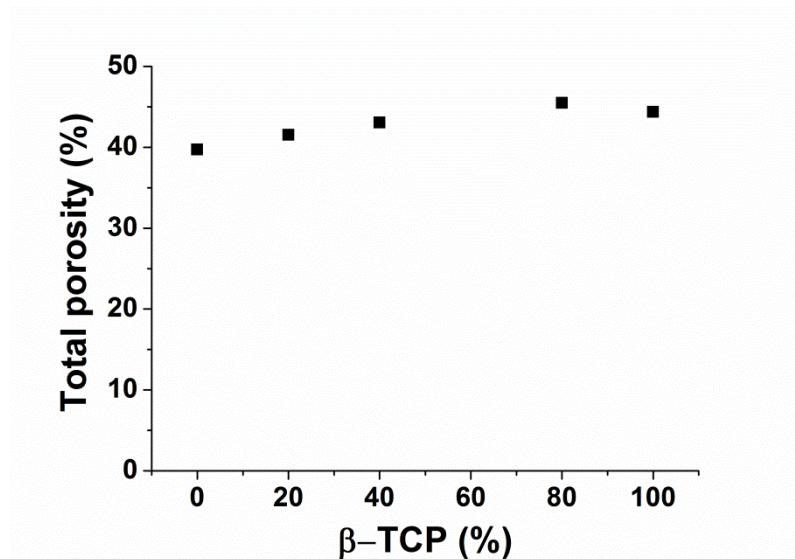


Figure 3.10 - Total porosity of BCPCs measured by mercury intrusion porosimetry.

The pore size distribution of the BCPCs (Figure 3.11) was broad (between 6 nm – lower limit of the technique – and 3 mm for the 100% β -TCP composition). The 0% β -TCP showed a broad peak centred at around 0.01 μm , with a shoulder around 0.06 μm . Incorporation and progressive percentage increase of β -TCP led to a displacement of the main peak to higher values (0.02 and 0.04 μm for 20% and 40% β -TCP respectively) with an intensification of the shoulder around 0.1 μm . 80% β -TCP showed a bimodal pore size distribution with maxima at 0.1 and 0.6 μm . The first peak was still present in the 100% β -TCP although with a lower population of pores, together with a sharper peak around 2 μm .

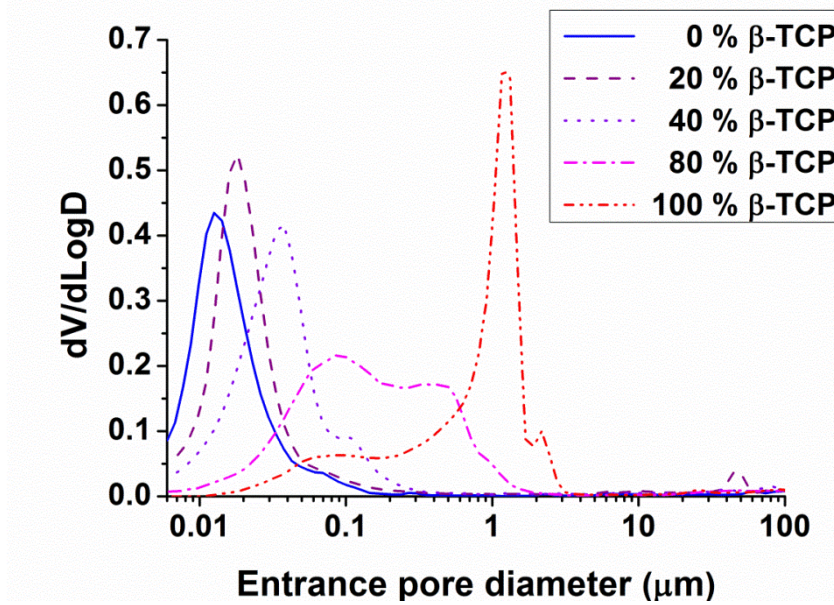


Figure 3.11- Entrance pore diameter of BCPCs measured by mercury intrusion porosimetry.

e) Scanning electron microscopy and Specific Surface Area

The surface morphology of the various BCPCs observed by FE-SEM is shown in Figure 3.12. The β -TCP particles were not exposed in any of the BCPCs, even those containing large amount (80%) of β -TCP (Figure 3.12e), as they were completely covered with CDHA precipitated crystals. However, a change in morphology of the crystals was observed. On the surface of BCPCs containing low amounts of β -TCP (up to 40%), predominantly plate-like crystals were found (Figure 3.12 a-c), some acicular crystals were found in the 60% β -TCP (Figure 3.12d), and most extensively in the 80% β -TCP (Figure 3.12e), where much smaller needle-like crystals were formed. In the 100% β -TCP sample (Figure 3.12f), the shape of the initial β -TCP particles was visible, although partially covered with small crystals.

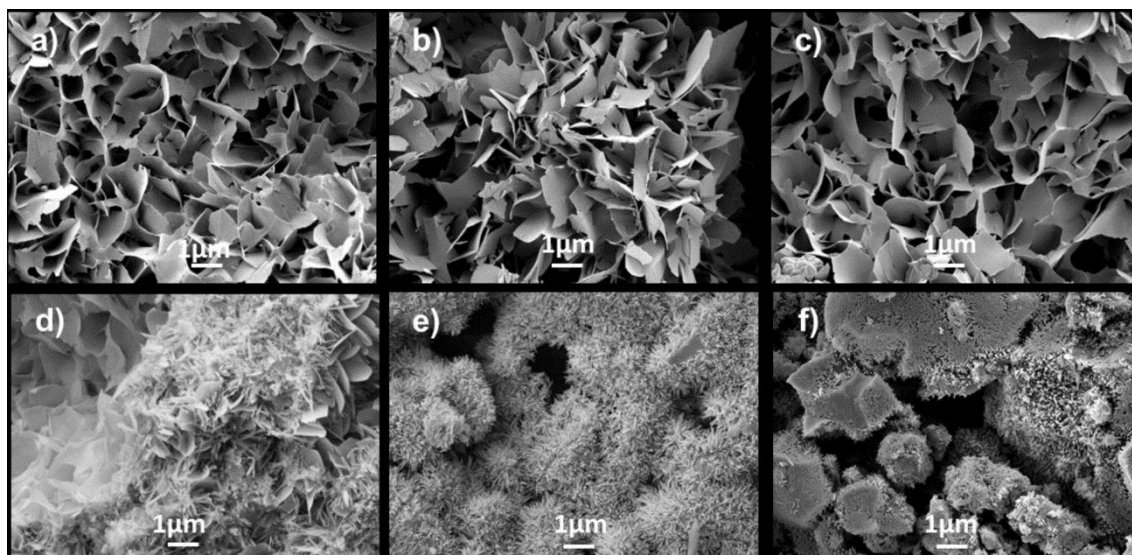


Figure 3.12- Surface microstructure of BCPCs set for 7 days in Ringer's solution: a) 0% β -TCP, b) 20% β -TCP, c) 40% β -TCP, d) 60%, e) 80% β -TCP, f) 100% β -TCP.

The addition of β -TCP resulted in a decrease of the SSA of the set cements (Figure 3.13), since it results from the contribution of both CDHA and β -TCP. This decrease was as a direct consequence of the lower SSA of the β -TCP particles compared to the precipitated CDHA crystals. This is compatible with the lower size of the CDHA crystals observed in Figure 3.12f.

Figure 3.13 reports the SSA both as measured and as calculated with the rule of mixtures. The data reveal that there was a drastic increase of the measured SSA of CDHA for the sample with 80% β -TCP, which was in accordance with the SEM images that showed an evolution of the microstructure from plate-like to needle-like crystals (Figure 3.12).

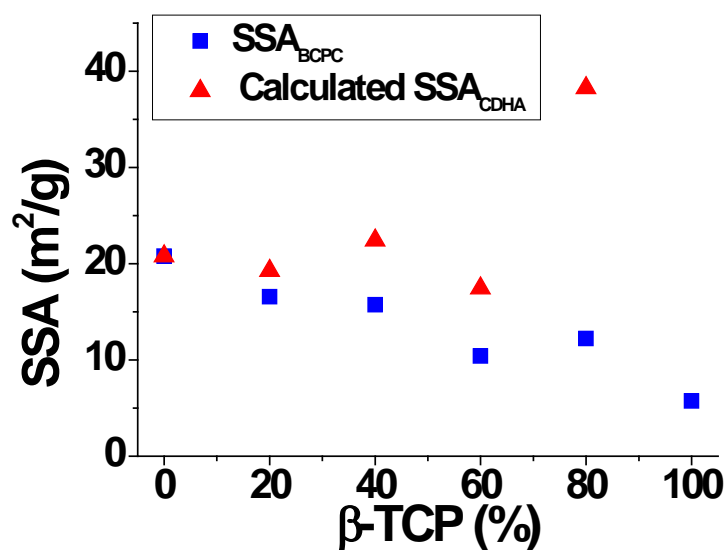


Figure 3.13 – Specific Surface Area of BCPCs with different β -TCP

SSA of 100% β -TCP (Figure 3.13) is five times higher than the powder before setting (Table 3.2). This could be explained by Figure 3.14, where scanning electron micrographs of β -TCP powder (Figure 3.14a) and 100% β -TCP sample (Figure 3.14b) surface morphology are shown. The presence of small precipitated crystals on the surface of β -TCP, after 7 days immersion in Ringer's, is consistent with the five-fold increase in SSA.

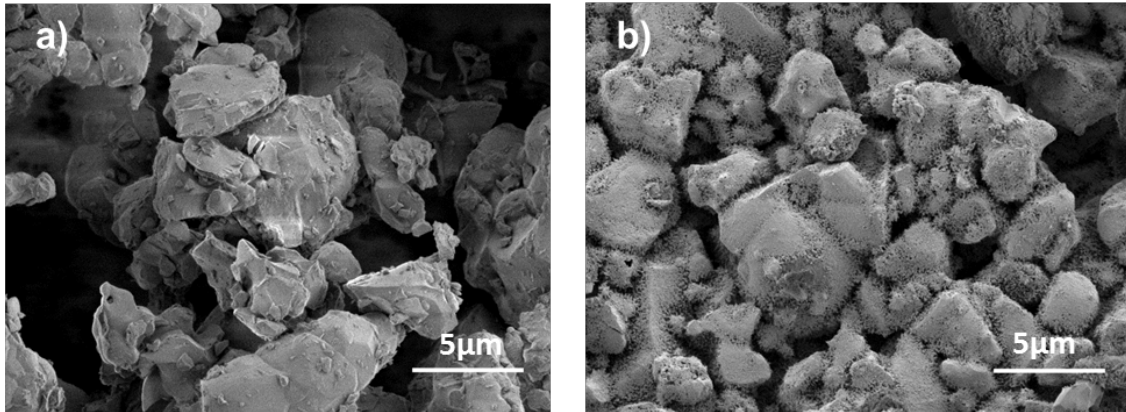


Figure 3.14 - Surface microstructure of a) β -TCP powder and b) 100% β -TCP sample, immersed for 7 days in Ringer's solution.

Ω FIB cross-sectioning

The cross-sections obtained by FIB tomography provided relevant information (Figure 3.15). In the 80% β -TCP sample (Figure 3.15a and b), CDHA crystals were observed to grow on the surface of the β -TCP particles, which were fully embedded in the cement matrix. In the 0% β -TCP no particles were observed (Figure 3.15c). Instead, dense shells with loosely packed cores were found, that reproduced the shape of the original α -TCP particles, as highlighted in Figure 3.15d.

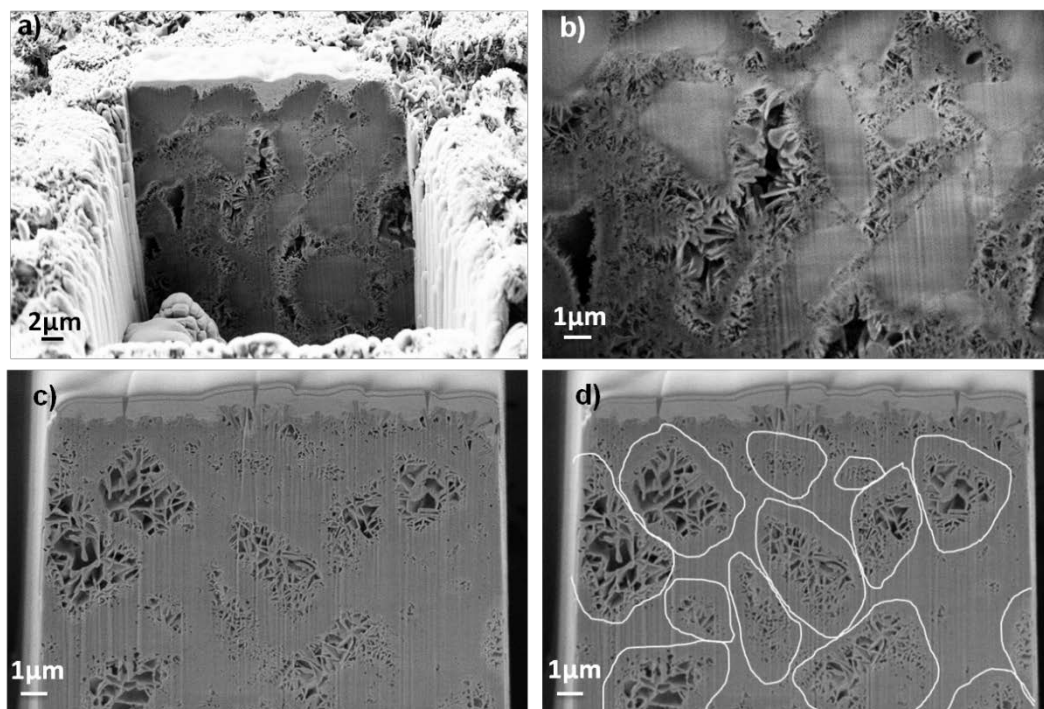


Figure 3.15- a) General view of a the FIB tomography of the 80% β -TCP cement; b) detail of the same specimen showing the β -TCP particles embedded in the CDHA crystals. c) FIB tomography of the 0% β -TCP cement; d) the same image highlighting the Hadley grains formed after hydrolysis of the initial α -TCP particles, with a dense shell and a core with bigger and loose crystals, where the size and morphology of the original particles can be estimated. All specimens were previously set for 7 days in Ringer's solution.

g) Ion release in water

The release of calcium in deionised water by the different set BCPC formulations is represented in Figure 3.16. Despite the highest solubility of β -TCP compared to CDHA, Ca^{2+} release decreased when the amount of β -TCP in BCPCs increased.

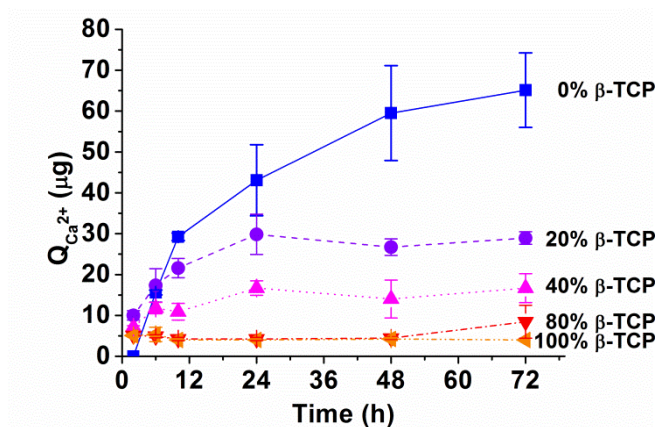


Figure 3.16 - Calcium release of different set BCPCs immersed in deionised water over 72 hours. The BCPCs were previously set for 7 days in Ringer's solution at 37°C.

h) Accelerated in vitro degradation

Accelerated acidic degradation was performed at pH = 2. Figure 3.17a shows the weight loss of the different BCPCs. Cements with no or low amount of β -TCP showed similar weight losses, while the 80% β -TCP had the lowest loss. The greatest weight loss was recorded for the cement containing 100% β -TCP and for the 100% β -TCP compacted discs. The related calcium release in acidic media (Figure 3.17 b) showed that all formulations released calcium, the concentration increasing linearly with time, and no significant differences were found among the various cements. Significantly higher amounts of Ca^{2+} release were registered only for the 100% β -TCP compacted discs.

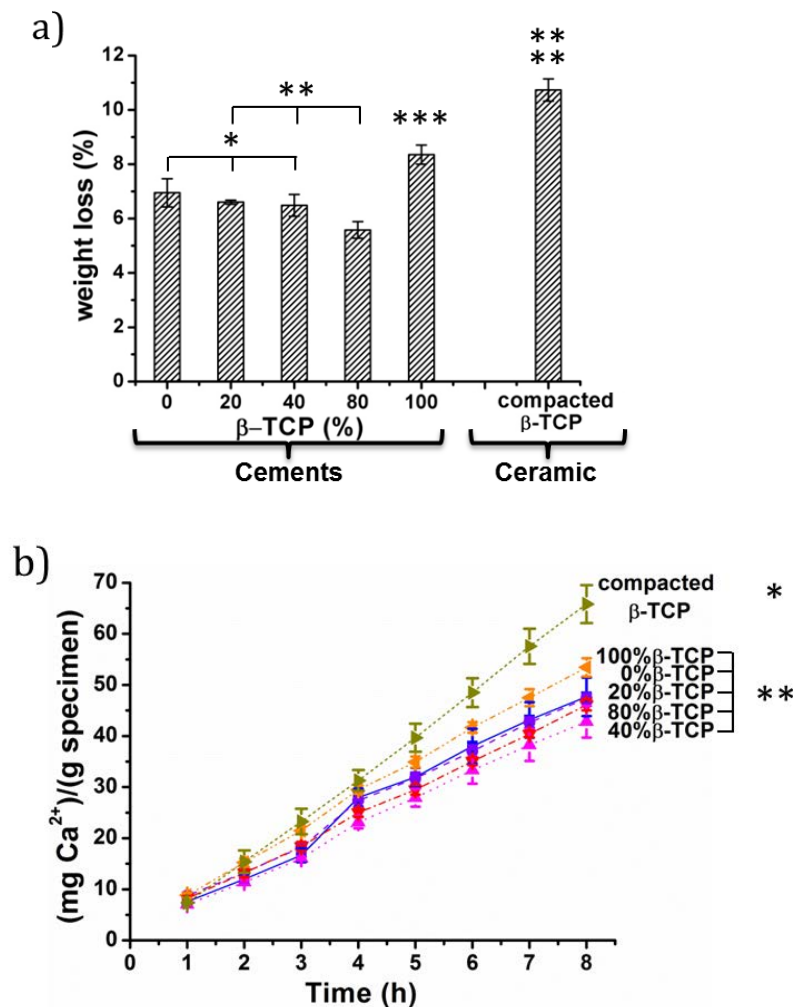
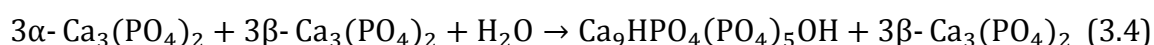


Figure 3.17- Acid degradation assay (8h, pH=2): a) Weight loss b) Ca^{2+} release normalised to the sample weight. BCPCs with different amounts of β -TCP, ranging from 0 to 100%, and a compacted β -TCP powder were analysed. The BCPCs were previously set for 7 days in Ringer's solution at 37°C. Differences were considered statistically significant at $p < 0.05$. Series with statistically significant differences are marked with different number of asterisks.

3.5. Discussion

In this work biphasic CDHA/ β -TCP cements were obtained by mixing two Tricalcium Phosphate (TCP) polymorphs with different solubility. The structure of α -TCP is less densely packed than β -TCP, and this difference in packing densities is consistent with thermodynamic considerations and with their stability temperature ranges. This provokes, in a physiological environment, the faster dissolution and degradation of α -TCP compared to β -TCP (**Carrodeguas, 2011**). In this Thesis α -TCP and β -TCP powders were mixed in different proportions and allowed to set. In spite of the small differences in solubility (**Chow, 2009**), for the reason above mentioned, when the two polymorphs were mixed with an aqueous solution, only α -TCP was completely hydrolysed to CDHA, whereas β -TCP remained unreacted (Figure 3.8, Table 3.3). This is probably due to the setting of these biphasic cements based on α -TCP and β -TCP follows, therefore, the following reaction.



It was shown that β -TCP particles acted as nucleation points, and they became embedded in the CDHA matrix as the reaction progressed, as represented in Figure 3.18.

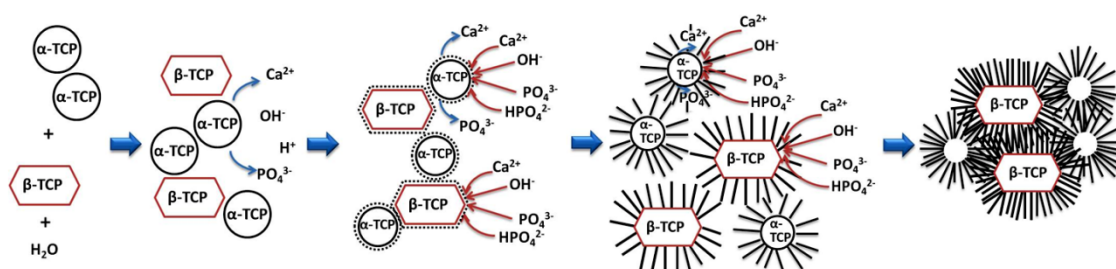


Figure 3.18 - Proposed dissolution-precipitation mechanisms involved in BCPCs cements prepared with α -TCP and β -TCP. In contact with water, only α -TCP starts dissolving, followed by CDHA precipitation around both α -TCP and β -TCP and subsequent crystal growth.

When α -TCP and β -TCP are mixed with water or an aqueous solution, ions start to dissolve. Subsequently, they start to precipitate both on α -TCP and β -TCP particles and form crystals on their surface. Depending on the reaction speed and on the number of nucleation points, the microstructure obtained was either prevalently plate-like or needle-like. Therefore, this mechanism would explain the presence of smaller needle-like crystals in the composition containing 80% β -TCP (Figure

3.12e), since the higher amount of β -TCP provided a greater surface for heterogenic nucleation. After complete reaction, the β -TCP phase remained hidden in the structure, as evidenced by the FIB tomography for the 80% β -TCP sample (Figure 3.15a and b). In the 0% β -TCP the FIB tomography evidenced the presence of shell-like structures formed during the hydration of the α -TCP particles (Figure 3.15c and d) **(Ginebra, 1999; Espanol, 2010)**, which are analogous to the Hadley grains produced during hydration of Portland cement **(Hadley, 1972; Kjellsen, 1996)**.

The presence of small precipitated crystals observed by SEM in the 100% β -TCP sample (Figure 3.14b and f), consistent with the five-fold increase in SSA (Figure 3.13), which can be attributed to the hydrolysis of the small percentage of α -TCP in the initial powder (Table 3.3), and probably also to the dissolution and reprecipitation of the more external layer of the β -TCP particles, that were subjected to an amorphisation due to the milling, understood not in the sense of a new phase, but to the introduction of defects and dislocations in the crystal network, which increase their reactivity, as previously reported **(Gbureck, 2003; Zhang, 1991; Lopez-Heredia, 2011; Montufar, 2013; Bohner, 2009)**. In fact, although the formation of CDHA was not detected by XRD, presumably due to its small amount and low crystallinity, a narrowing and higher intensity of the β -TCP peaks was observed after 7 days immersion in Ringer's solution (Figure 3.8), which can be attributed to the dissolution of the partially amorphised surface of the β -TCP particles, as reported in previous works **(Montufar, 2013)**.

The addition of a non-reacting phase (β -TCP) modified significantly various cement parameters, albeit to different extents. In particular, initial setting times and cohesion were not greatly modified. However, the final setting times clearly increased with the addition of β -TCP, which was consistent with the limited reactivity of this phase. The fact that the 100% β -TCP cement showed also cohesion and an apparent setting, can be explained by the powder activation produced by ball milling, as discussed in the previous paragraph **(Gbureck, 2003; Zhang, 1991; Lopez-Heredia, 2011; Montufar, 2013; Bohner, 2009)**, together with the presence of small amounts of α -TCP, which led to the partial dissolution of the particles, although limited to the most external surface.

The hardening mechanism of α -TCP-based cements is due to the entanglement of the precipitated CDHA crystals. Previous studies by Ginebra *et al.* (**Ginebra, 1997**) demonstrated a direct correlation between compressive strength and % of precipitated CDHA. Thus, the progressive reduction of compressive strength with higher β -TCP percentages in the BCPC (Figure 3.9a) can be related to the decreasing amount of CDHA with increasing β -TCP amounts, and therefore it can be concluded that the β -TCP particles embedded in the cements, rather than reinforcing the material, had a weakening effect.

These results were obtained using small β -TCP particles, with the idea of favouring β -TCP dissolution. The properties of the non-reacting phase, like particle size, shape and surface texture are expected to have an effect on the properties of both freshly mixed and hardened cements, although this was beyond the scope of this study. This in fact has been extensively studied in the case of concrete, where a non-reactive phase (i.e. the aggregate), is embedded in the reacting matrix (i.e. the cement). Aggregate properties are known to affect workability and rheological properties of the paste and also the mechanical performance of the hardened paste (**Illston, 1979**). Thus, the use of particles with different sizes has been shown to be more effective than monodisperse particles because of a higher packing efficiency. Bigger aggregate sizes result in higher fracture energy (**Issa, 2000**), and rough-textured, angular, and elongated particles require more water to produce workable pastes than smooth, rounded particles, this affecting also the final mechanical properties of the material (**Illston, 1979; Issa, 2000**).

The addition of β -TCP also led to a decrease of SSA of the BCPCs, as a direct consequence of the lower SSA of the β -TCP particles compared to the precipitated CDHA crystals. This is compatible with the lower size of the CDHA crystals observed in Figure 3.12f. In fact, the total SSA of the material results from the contribution of two different phases, CDHA and β -TCP, following the rule of mixtures:

$$SSA_{BCPC} = X_{CDHA} \cdot SSA_{CDHA} + X_{\beta-TCP} \cdot SSA_{\beta-TCP} \quad (3.5)$$

where X is weight fraction of each of the components. Assuming that the cement was formed just by the two phases:

$$X_{\text{CDHA}} + X_{\beta\text{-TCP}} = 1 \quad (3.6)$$

If we assume that SSA of β -TCP is constant during the whole process (it suffers only a very limited surface dissolution), then we can estimate a calculated SSA of the CDHA:

$$\text{SSA}_{\text{CDHA}} = (\text{SSA}_{\text{BCPC}} - X_{\beta\text{-TCP}} \cdot \text{SSA}_{\beta\text{-TCP}}) / (1 - X_{\beta\text{-TCP}}) \quad (3.7)$$

As shown in Figure 3.13, there is a drastic increase of the estimated SSA of CDHA for the sample with 80% β -TCP, which is in accordance with the SEM images that show an evolution of the microstructure from plate-like to needle-like crystals (Figure 3.12).

The porosity of BCPCs increased with growing amounts of β -TCP, as well as the entrance pore size (Figure 3.10 and Figure 3.11). Interestingly, a significant change in the MIP curves was found in the group with 80% β -TCP, which can be explained by the fact that in this material the reacting phase, which accounted for only 20% of the total, was unable to fill the large voids between the β -TCP particles, as shown in Figure 3.15a and b.

The dissolution behaviour of the biphasic materials, which is relevant not only when considering the resorption behaviour of the material *in vivo*, but also the ion exchange patterns, which have been shown to affect several signalling pathways relevant for osteogenesis. In fact, it has been shown recently that Ca^{2+} plays an essential role in bone remodelling processes. High Ca^{2+} concentrations are shown to stimulate pre-osteoblast chemotaxis to the site of bone resorption, and their maturation into cells that produce new bone (**Chai, 2011; Yamada, 1997**). This has been hypothesised to be behind the osteoinductive properties of some BCP ceramics. Therefore, the effect of varying amounts of β -TCP on the release profile of calcium from the BCPCs was studied. After the setting reaction, biphasic CDHA/ β -TCP materials were obtained. CDHA is more soluble than stoichiometric HA

(solubility at 25 °C, $-\log(K_s) \approx 85.1$ as compared to 116.8 for HA) and less than β -TCP (solubility at 25 °C, $-\log(K_s) = 28.9$) (**Chow, 2009**).

Surprisingly, Ca^{2+} release in water was higher in the set 0% β -TCP cement, consisting in pure CDHA, and decreased with increasing amounts of β -TCP in the material, i.e., when the CDHA/ β -TCP ratio decreased (Figure 3.16). This result could seem to be in contradiction with the fact that CDHA is less soluble than β -TCP, and also with the behaviour found in BCP ceramics composed of HA/ β -TCP, where the higher the ratio, the lower was the extent of dissolution (**Legeros, 2003**). This behaviour can be explained by two factors: i) β -TCP remained hidden within the CDHA matrix, which impaired the contact with surrounding media (Figure 3.15b, Figure 3.18), and ii) the decreasing SSA of the BCPC with increasing β -TCP content, due to the lower SSA of β -TCP compared to CDHA.

In general the solubility of calcium phosphates is strongly affected by pH, being more soluble in acidic environment (**Yamada, 1997**). This mechanism is exploited by osteoclasts, which trigger bone resorption by dissolving the hydroxyapatite contained in bone through the acidification of the extracellular fluids. In fact, Silver *et al.* found that a pH decrease of about 1 unit/min takes place in the sealed regions under the osteoclasts known as resorption lacunae (**Silver, 1988**). Following the model proposed by Hankermeyer *et al.*, in here, the accelerated degradation of BCPCs was studied at pH = 2 (**Hankermeyer, 2002**). The Ca^{2+} release in acidic medium was similar for all BCPCs, in spite of the different compositions (Figure 3.17). Again, even in acidic conditions the microstructure and the textural properties were more determining factors than the solubility of the different phases present in the material, as no differences were observed between the different BCPCs, and a higher weight loss was found only for the 100% β -TCP cement. Interestingly, even though the apparent surface was slightly smaller, significantly higher values of weight loss and Ca^{2+} release were recorded for the as-milled compacted β -TCP discs than for the 100% β -TCP cement. This can be associated to two different phenomena: i) the increase in powder reactivity in the as-milled powder, due to some degree of amorphisation of the surface of the particles produced during milling, understood not as the formation of a distinct amorphous phase, but to the introduction of defects in the crystal structure, which makes the particles more

reactive, as observed in previous (Gbureck, 2003; Zhang, 1991; Lopez-Heredia, 2011; Montufar, 2013; Bohner, 2009); ii) the loss of reactivity of the β -TCP powder after being mixed with water, which induces dissolution of the amorphous fraction of the mechanically activated surface of the particles and subsequent reprecipitation, leading to the formation of a CDHA layer on the surface of the particles of the 100% β -TCP cement (Figure 3.14b). This layer, although very thin, hinders further dissolution of the particles (Bohner, 1997).

Lopez-Heredia *et al.* (Lopez-Heredia, 2011) obtained calcium phosphate cements, containing α and β -TCP phases in dual form in the same granule. To this end, various thermal treatments were applied to α -TCP to obtain different degrees of conversion to β -TCP, so particles containing both polymorphs in different ratios were used as powder phase for the preparation of cements. Although their cement formulations were far more complex than the ones analysed in this study, since they contained other phases in addition to TCPs, such as anhydrous dicalcium phosphate and precipitated hydroxyapatite, similar trends were found in terms of the reduction of SSA and compressive strength with increasing content of β -TCP. No differences were found after 8 weeks in the *in vivo* behaviour when multiphasic cements containing either dual TCP phases or only α -TCP were implanted in tibial intramedullary cavities in guinea pigs. Although only one time-point was analysed that can be considered relatively short, these results are in good agreement with the lack of significant differences in the *in vitro* degradation or Ca^{2+} release among BCPC formulations found in the present study. However, a higher dissolution and Ca^{2+} release from the BCPCs *in vitro*, and a higher resorption rate *in vivo*, should not be excluded in longer-term studies, once the more soluble phase is exposed to the surrounding media.

3.6. Conclusions

Novel biphasic CDHA/ β -TCP self-setting cements with a precise control of phase composition were successfully prepared by hydrolysis of a combination of α -TCP and β -TCP. Setting times increased by the addition of β -TCP, which was associated to the fact that the setting of the cement was caused by the transformation of α -TCP to

CDHA, whereas β -TCP remained unaltered. The final microstructure consisted of β -TCP particles embedded in the CDHA matrix. This complex microstructure, together with the decreasing SSA with increasing β -TCP content explains the fact that Ca^{2+} release and weight loss were unaffected by the increasing amounts of β -TCP in the timeframe evaluated. However, higher dissolution and Ca^{2+} release from the BCPCs should not be ruled out in longer-term studies, once the more soluble phase is exposed to the surrounding media.

References

Barradas AM, Yuan H, van Blitterswijk CA, Habibovic P. Osteoinductive biomaterials: current knowledge of properties, experimental models and biological mechanisms. *Eur. Cell Mater.* 2011; 21: 407-429.

Bianchi M, Edreira ER, Wolke JGC, Birgani ZT, Habibovic P, Jansen JA, Tampieri A, Marcacci M, Leeuwenburgh SCG, Beucken JJ. Substrate geometry directs the in vitro mineralization of calcium phosphate ceramics. *Acta Biomater.* 2014; 10(2): 661-669.

Boakye M, Mummaneni PV, Garrett M, Rodts G, Haid R. Anterior cervical discectomy and fusion involving a polyetheretherketone spacer and bone morphogenetic protein. *J. Neurosurg. Spine* 2005; 2(5): 521-525.

Bohner M, Lemaitre J, Ring TA. Kinetics of dissolution of β -Tricalcium Phosphate. *J. Colloid. Interface Sci.* 1997; 190(1): 37-48.

Bohner M, Luginbühl R, Reber C, Doebelin N, Baroud G, Conforto E. A physical approach to modify the hydraulic reactivity of alpha-tricalcium phosphate powder. *Acta Biomater.* 2009; 5(9): 3524–3535.

Carrodeguas RG, De Aza S. α -Tricalcium phosphate: synthesis, properties and biomedical applications. *Acta Biomater.* 2011; 7(10): 3536–3546.

Chai YC, Roberts SJ, Desmet E, Kerckhofs G, van Gastel N, Geris L, Carmeliet G, Schrooten J, Luyten FP. Mechanisms of ectopic bone formation by human

osteoprogenitor cells on CaP biomaterial carriers. *Biomaterials* 2012; 33(11): 3127-3142.

Chai YC, Roberts SJ, Schrooten J, Luyten FP. Probing the osteoinductive effect of Calcium Phosphate by Using An In-Vitro Biomimetic Model. *Tissue Eng. Part. A.* 2011; 17(7-8): 1083-1097.

Chow LC. Next generation calcium phosphate-based biomaterials. *Dent. Mater.* 2009; 28 (1): 1-10.

Chung FH. Quantitative interpretation of x-ray diffraction patterns mixtures. II. Adiabatic Principle of X-ray Diffraction Analysis of Mixtures. *J. Appl. Cryst.* 1974; 7(6): 526-531.

Daculsi G, Layrolle P. Osteoinductive properties of micro and macroporous Biphasic Calcium phosphate bioceramics. *Key Eng. Mater.* 2004; 254-256: 1005-1008.

Daculsi G, Legeros RZ, Nery E, Lynch K, Kerebe B. Transformation of biphasic calcium phosphate ceramics in vivo: ultrastructural and physicochemical characterization. *J. Biomed. Mat. Res.* 1989; 23 (8): 883-894.

De Groot K. Carriers that concentrate native bone morphogenetic proteins in vivo. *Tiss. Eng.* 1998; 4(4): 337-341.

Dorozhkin SV. Biphasic, triphasic and multiphasic calcium orthophosphates. *Acta Biomater.* 2012; 8(3): 963-977.

Español M, Perez RA, Montufar EB, Marichal C, Sacco A, Ginebra MP. Intrinsic porosity of calcium phosphate cements and its significance for drug delivery and tissue engineering applications. *Acta Biomater.* 2010; 5(7): 2752-2762.

Fernandez E, Boltong MG, Ginebra MP, Driessens FCM, Bermúdez O, Planell JA. Development of a method to measure the period of swelling of calcium phosphate cements. *J. Mater. Sci. Lett.* 1996; 15 (11): 1004–1005.

Friedenstein AY. Induction of bone tissue by transitional epithelium. *Clin. Orthop. Relat. Res.* 1968; 59: 21-37.

Gbureck U, Grolms O, Barralet JE, Grover LM, Thull R. Mechanical activation and cement formation of beta-tricalcium phosphate. *Biomaterials* 2003; 24 (23): 4123-4131.

Ginebra MP, Fernández E, Driessens FCM, Planell JA. Modeling of the hydrolysis of α -tricalcium phosphate. *J. Am. Ceram. Soc.* 1999; 82(10): 2808–2812.

Ginebra MP, Fernández E, De Maeyer EA, Verbeeck RM, Boltong MG, Ginebra J, Driessens FCM, Planell JA. Setting reaction and hardening of an apatitic calcium phosphate cement. *J. Dent. Res.* 1997; 76 (4): 905-912.

Gosain AR, Song L, Riordan P, Amarante T, Nagy PG, Wilson CR, Toth JM, Ricci JL. A 1-year study of osteoinduction in hydroxyapatite-derived biomaterials in an adult sheep model: part I. *Plast. Reconstr. Surg.* 2002; 109(2): 619-630.

Habibovic P, Yuan H, van der Valk CM, Meijer G, van Blitterswijk CA, de Groot K. 3D microenvironment as essential element for osteoinduction *Biomaterials* 2005; 26(17): 3565-3575.

Hadley D. The nature of the paste–aggregate interface, Ph.D. Thesis, Purdue University, 173 (1972).

Hankermeyer CR, Ohashi KL, Delaney DC, Ross J, Constantz BR. Dissolution rates of carbonated hydroxyapatite in hydrochloric acid. *Biomaterials* 2002; 23 (3): 743-750.

Illston JM, Dinwoodie JM, Smith AA. Concrete, timber, and metals: the nature and behaviour of structural materials. Van Nostrand Reinhold, Co Ltd; New York (1979).

Issa MA, Issa MA, Islam MS, Chudnovsky A. Size effects in concrete fracture: Part I, experimental setup and observations. *Int. J. Fracture* 2000; 102(1): 1–24.

Joint Committee for Powder Diffraction Studies [JCPDS] –International Center for Diffraction Data, and American Society for Testing and Materials. Powder Diffraction File. Swarthmore, PA: Joint Committee for Powder Diffraction Studies; 1991.

Kjellsen KO, Jennings HM, Lagerblad B. Evidence of hollow shells in the microstructure of cement paste. *Cem. Concr. Res.* 1996; 26(4): 593–599.

Le Nihouannen D, Saffarzadeh A, Gauthier O, Moreau F, Pilet P, Spaethe R, Layrolle P, Daculsi G. Bone tissue formation in sheep muscles induced by a biphasic calcium phosphate ceramic and fibrin glue composite. *J. Mater. Sci. Mater. Med.* 2008; 19(2): 667-675.

Le Nihouhannen D, Daculsi G, Gauthier O, Saffarzadeh A, Delplace S, Pilet P, Layrolle P. Ectopic bone formation by microporous calcium phosphate ceramic, *Bone* 2005, 36(6): 1086-1093.

Legeros RZ, Lin S, Rohanizadeh R, Mijares D, Legeros JP. Biphasic calcium phosphate bioceramics: preparation, properties and applications. *J. Mater. Sci.: Mater. Med.* 2003; 14 (3): 201-209.

Legeros RZ. Calcium phosphate-based Osteoinductive Materials. *Chem. Rev.* 2008; 108(11): 4742-4753.

Legeros RZ. Calcium Phosphates in Oral Biology and Medicine. *Monographs in Oral Sciences*; Myers, H., Ed.; Karger: Basel, 1991; Vol. 15.

Leibniz Institute for Information Infrastructure. Inorganic Crystal Structure Database (ICSD). Karlsruhe, Germany: Leibniz Institute for Information Infrastructure; 1998

Lopez-Heredia MA, Bohner M, Zhou W, Winnubst AJ, Wolke JG, Jansen JA. The effect of ball milling grinding pathways on the bulk and reactivity properties of calcium phosphate cements. *J. Biomed. Mater. Res. B.: Appl. Biomater.* 2011; 98(1): 68–79.

Montufar EB, Maazouz Y, Ginebra MP. Relevance of the setting reaction to the injectability of tricalcium phosphate pastes. *Acta Biomater.* 2013; 9(4), 6188–6198.

Ripamonti U, Crooks J, Khoali L, Roden L. The induction of bone formation by coral-derived calcium carbonate/hydroxyapatite constructs. *Biomaterials* 2009; 30(7): 1428-1439.

Ripamonti U. Osteoinduction in porous hydroxyapatite implanted in heterotopic sites of different animal models. *Biomaterials* 1996; 17(1): 31-35.

Sariibrahimoglu K, Leeuwenburgh SC, Wolke JG, Yubao L, Jansen JA. Effect of calcium carbonate on hardening, physicochemical properties, and in vitro degradation of injectable calcium phosphate cements. *J. Biomed. Mater. Res. A.* 2012; 100 (3): 712-719.

Silver IA, Murrills RJ, Etherington DJ. Microelectrode studies on the acid microenvironment beneath adherent macrophages and osteoclasts. *Exp. Cell. Res.* 1988; 175(2): 266-276.

Standard Test Method for time of setting of hydraulic cement paste by Gillmore needles. ASTM C266-89. In: Annual book of ASTM standards, vol. 04.01. Cement, lime, Gypsum. Philadelphia, PA: ASTM, 189–91 (1993).

Toth JM, Lynch KL, Hackbart DA. Ceramic-induced osteogenesis following subcutaneous implantation of calcium phosphates in Bioceramics P. Ducheyne and D. Christiansen, Editors 1993, Butterworth-Heinemann Philadelphia, pp. 9-14.

Urist MR, Silverman BF, Buring K, Dubuc FL, Rosenberg JM. The bone induction principle. Clin. Orthop. 1967; 53: 243-283.

Urist MR, Strates BS. Bone morphogenetic protein. J. Dent. Res. 1971; 50: 1392-1406.

Vaccaro AR, Patel T, Fischgrund J, Anderson DG, Truumees E, Herkowitz HN, Phillips F, Hilibrand A, Albert TJ, Wetzel T, McCulloch JA. A pilot study evaluating the safety and Efficacy of OP-1 Putty (RHBMP-7) as a replacement for iliac crest autograft in posterolateral lumbar arthrodesis for degenerative spondylolisthesis. Spine 2004; 29 (17): 1885-1892.

Yamada S, Heymann D, Bouler JM, Daculsi G. Osteoclastic resorption of calcium phosphate ceramics with different hydroxyapatite/ β -tricalcium phosphate ratios. Biomaterials 1997; 18(15): 1037-1041.

Yamasaki H, Sakai H. Osteogenic response to porous hydroxyapatite ceramics under the skin of dogs. Biomaterials 1992; 13(5): 308-312.

Yang Z, Yuan H, Tong W, Zou P, Chen W, Zhang X. Osteogenesis in extraskeletally implanted porous calcium phosphate ceramics: Variability among different kinds of animals. Biomaterials 1996; 17: 2131-2137.

Yuan H, Fernandes H, Habibovic P, de Boer J, Barradas AMC, de Ruitter A, Walsh WR, van Blitterswijk CA, de Bruijn JD. Osteoinductive ceramics as synthetic alternative to autologous bone grafting. Proc. Nat. Acad. Sci. USA 2010; 107(31): 13614-13620.

Yuan H, Yang Z, Li Y, Zhang X, De Bruijn J, De Groot K. Osteoinduction by calcium phosphate biomaterials. *J. Mater. Sci. Mater. Med.* 1998, 9(12), 723-726.

Zhang J, Nancollas GH. *Advances in Industrial Crystallization*. Garside J, Davey RJ, Jones AG (Eds.), p. 47. Butterworth-Heinemann, London, 1991.

Zhang L, Hanagata N , Maeda M, Minowa T, Ikoma T, Fan H, Zhang X. Porous hydroxyapatite and biphasic calcium phosphate ceramics promote ectopic osteoblast differentiation from mesenchymal stem cells. *Sci. Technol. Adv. Mater.* 2009; 10(2): 9pp.

Chapter 4

Fibre reinforced calcium phosphate cements

4.1 Introduction

One of the major constraints of the mechanical performance of CPCs arises from the intrinsic brittleness derived from their composition and microstructure. CPC are in fact intrinsically porous ceramics, with porosities that vary between 20 and 50 % depending on the liquid to powder ratio used in their preparation.

With respect to the toughness of the material, the values reported in literature of the work of fracture of pristine CPCs are usually between 0.010 and 0.050 kJ/m² **(Canal & Ginebra, 2011)**, far below the work of fracture of the bone which is in the range between 1.5 and 15 kJ/m² **(Currey & Butler, 1975)**. Although the bending strength values reported for CPCs, typically in the range of 5-15 MPa **(Martin & Brown 1995; Ginebra, 2001)**, are in the range of trabecular bone (estimated between 10 and 20 MPa, **Barinov, 2010**), they are well below those of cortical bone, which Currey and Butler reported to be close to 200 MPa **(Currey & Butler, 1975)** and Barinov in the range between 50 and 150 MPa **(Barinov, 2010)**. A successful improvement of the mechanical properties would significantly extend the applicability of calcium phosphates. This improvement can be achieved by forming composite materials. In the past ten/fifteen years scientists tried to ameliorate mechanical properties by adding fibres to the CPC matrix and forming in this way fibre reinforced calcium phosphate cements (FRCPCs) **(Canal & Ginebra, 2011; Krüger, 2012)**.

In cements intended for medical applications, specific requirements arise; on one hand, the fibres must be biocompatible. On the other hand, if the fibres are biodegradable, they can be used not only as reinforcement for the cement matrix but also as pore-generating agents. The rationale of such approach is to provide temporary reinforcement at the implant site and, subsequently to fibre degradation, to allow bone ingrowth into the macropores. Although CPCs are intrinsically porous, their inherent porosity is of submicron to a few microns of size, being too small for cell infiltration. The addition of fibres with faster resorption rate than the CPC matrix and with large diameter, would allow creating macropores to favour cell colonisation and blood vessel infiltration, and eventually fostering bone regeneration. Ideally, the loss of strength produced by fibre degradation should be compensated by the formation of new bone **(Xu, 2001a; Xu, 2001b; Xu, 2002; Xu, 2004)**.

Furthermore it is known that the behaviour of the interface fibres-matrix is the one which determines the first crack strength of the composite **(Nelson, 2002)**. Thus, in most cases adhesion between the fibres and the CPC matrix is one of the main factors hampering an optimum mechanical reinforcement **(Canal, 2011)**. A good adhesion would improve the mechanical properties of the composite.

4.1.1 Bone: a strong composite material

Most biological materials with predominantly mechanical function have a hierarchical structure consisting of several levels. In this way, tough materials are designed by nature, based on extremely different base materials. For example bone is a composite based on polymer-ceramic. From a mechanical viewpoint, bone contains defects ranging in size from micrometres to millimetres as, for example, cavities for blood vessels (Havers and Volkmann channels) and a network of canaliculi connecting osteocytes. As a consequence, bone tissue must be flaw-insensitive not only at the nanoscopic but also the microscopic level **(Peterlik, 2006)**. A robust material design requires the abovementioned characteristic of being defect-insensitive both at nanoscopic and microscopic level. When the local strain energy exceeds a certain critical level it has to be effectively transferred into a large macroscopic volume, as micrometre-sized channels or lacunae are acting as

stress concentrators. The toughening mechanisms identified in bone during the past years are several (Figure 4.1) and can be compared to similar phenomena in technical materials (such as ceramics, polymers or gels).

Bone mineral is a ceramic material and exhibits normal Hookean elastic behaviour (i.e. a linear stress-strain relationship). In contrast, collagen is a polymer that shows a J-shaped stress-strain curve where molecular uncoiling occurs with considerable deformation under low stress (**Meyers, 2013**). Thus, in the bone composite, the resulting behaviour is not Hookean.

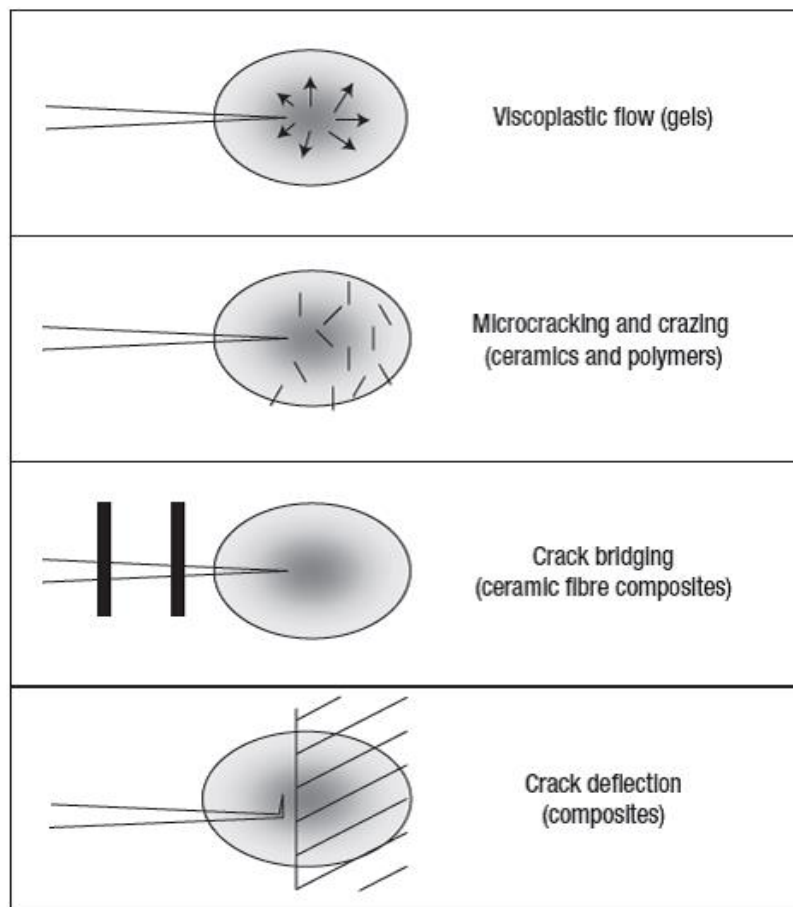


Figure 4.1 - The toughening mechanisms in bone. Different toughening mechanisms such as viscoplastic flow, microcracking, crack bridging and crack deflection were identified in bone. The shaded area visualises the highly stressed region in the vicinity of the crack tip (Peterlik, 2006).

As shown in Figure 4.1, different toughening mechanisms are involved in bone mechanics. As in polymers, the dissipation of energy to keep bone from fracture was attributed to *viscoplastic flow*, with “sacrificial bonds” in collagen needing time to re-form after pulling, which was correlated to the time needed for bone to recover its toughness (**Peterlik, 2006**). Deformation energy is dissipated by shearing of the thin “glue” layer between mineral-reinforced collagen fibrils

(Gupta, 2005). The *formation of microcracks* in the vicinity of the main crack due to stress concentrations ahead of the crack tip was observed by laser scanning confocal microscopy in the frontal process zone (Vashishth, 2003). Furthermore, *Crack deflection* at weak interfaces, a toughening mechanism well known from composites, was attributed to the interlamellar boundaries and the cement lines (Liu, 1999). Finally, *Crack bridging* (a mechanism well known in ceramic fibre composites) by collagen fibres, was proposed to play a dominant role in enhancing the fracture properties of bone. It was shown that the crack-tip driving force was reduced by uncracked ligaments which span the crack wake (Nalla, 2004). These toughening mechanisms are strongly dependent on the orientation of the crack propagation: the fracture toughness of long bones is considerably lower if the crack propagates along the long axis of the bone rather than perpendicular to it. This strong anisotropy affects the fracture properties (Behiri, 1989) as well as the elastic moduli (Table 4.1) which, in compression, was found to decrease of more than 50% when tested transversally to collagen fibres direction instead of parallel to them (Bonfield, 1971). In effect, in long bones, anisotropy is a consequence of the preferential alignment of collagen fibrils together with platelet-shaped mineral crystals aligned along their axis (Martin, 1989).

Table 4.1- Young's moduli of the principal constituents of bone and of bone both in longitudinal and transverse direction.

Material	Young's Modulus, E (GPa)
Collagen (dry)	6
Bone mineral (Hydroxyapatite)	80
Cortical bone, longitudinal	11-21
Cortical bone, transverse	5-13

Peterlik *et al.* (Peterlik, 2006) correlated the energy required to propagate the crack with the collagen fibre angle orientation, the main origin of the anisotropy, as shown in Figure 4.2. They found that when the main crack propagated along the fibrils and the lamellae, the crack path was straight, typical of brittle fracture; on the contrary, as the main fracture crossed the collagen fibrils, the structure appeared heavily distorted, which is characteristic of the quasi-ductile fracture. Furthermore, they found that transition from brittle to quasi-ductile was at around

50°. They found that the lamellar morphology of cortical bone seems a perfect design for a tough material, and the variation of fibril angles across the bone tissue increased the crack-extension energy per area, transported energy to a higher volume and led to more ductile fracture behaviour of bone tissue.

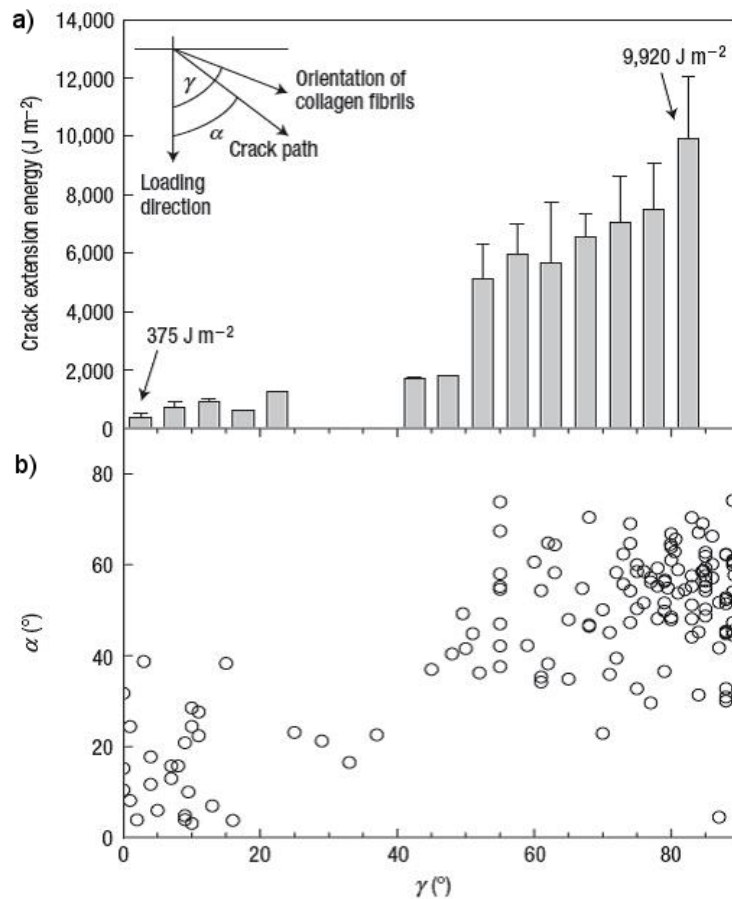


Figure 4.2- Crack extension as a function of the collagen angle γ . a) The energy required for crack extension and b), the standard deviation of the crack path angle α . A significant jump for both parameters is observed at approximately 50°. The authors calculated the standard deviation from the distribution of the crack path angles (obtained from digitised scanning electron microscopy images with a resolution of about 1 μm), which were overlaid with the digitised images from polarisation light microscopy, on which the ranges of constant collagen angles were identified (which are typically in the range of about 10 μm , but significantly larger, up to 100 μm , for specimens cut out in the longitudinal direction). Thus, a distribution of crack-path angles was obtained within each interval of approximately constant collagen angle, from which mean values and a standard deviation could be calculated (Peterlik, 2006).

4.1.2 Mechanical properties of fibre reinforced inorganic cements

Inorganic cements are brittle materials characterised by a sudden fracture without any significant preceding plastic deformation. Therefore, fracture deformation is small and the work necessary to induce failure is low. The addition of fibres to

form composites has the consequence that a brittle material can be used in structural applications (**Kelly, 1970**).

a) *Fracture behaviour of fibre reinforced cements*

The mechanical behaviour of fibre reinforced cements (FRCs) is a result of the complex interaction between both the matrix and the fibres which compound the composite and the constituents' features. Contributions to the macroscopic behaviour come from the fibre strength and stiffness, the cementitious matrix toughness (which can be modified by additives, generally polymeric) and the mechanical interaction between fibres and matrix.

Apart from material strength, two aspects are important in which the material classes show different behaviours: strain to failure and the area under the curves of load versus displacement, the latter being a measure for the energy necessary to yield material failure.

The materials can be classified depending on the failure mode (**Krüger, 2012**), and both the strain to failure and the fracture energy increase with the following order: *brittle* < *tension softening (quasi-brittle materials)* < *strain hardening (strictly pseudo strain hardening; highly ductile materials)*. Typical curves are reported in Figure 4.3.

In contrast to pure *brittle* failure where the material has an immediate fracture into two or more pieces, fibre reinforced cementitious composites display a high amount of energy absorbed during fracture and the strain to failure is higher. *Quasi-brittle* composites show *tension softening* behaviour. Their peak load is associated with fracture of the matrix but fibre bridging in the single opening crack dissipates fracture energy and delays the fracture into pieces. Yet, when the peak load is reached, the composite can no longer carry substantial load. The highest ductility and therefore the most desirable behaviour for fibre reinforced composites is achieved with *(pseudo) strain-hardening* behaviour. After initial matrix cracking still more load can be borne and strain at peak load and strain to failure can be up to several percent. Substantial amount energy is dissipated in the fracture process due to the development of a network of multiple cracks (**Aveston, 1971; Li, 1995**).

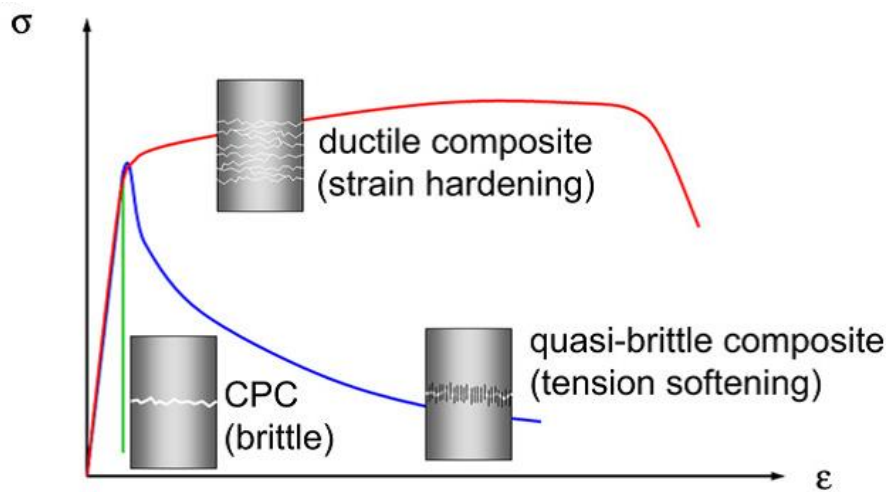


Figure 4.3 - Fracture of cement and composites. a) Typical stress-strain curves for brittle behaving CPC and FRPCPC composites showing either quasi-brittle tension softening or strain hardening behaviour (Krüger, 2012).

The mechanisms underlying the fracture behaviours aforementioned are different. Upon applying flexural load on a *brittle* solid, stress increases until its intensity reaches a critical value leading to failure. Thus, in monolithic cements, there is a fast single crack propagation which causes catastrophic failure (Callister, 2009). In fibre reinforced cements with *quasi-brittle* behaviour, the linear elastic region ends with the first cracking of the matrix. What determines this first crack strength is the behaviour at the frontal process zone of the composite (Nelson, 2002). As the crack propagates, the material presents a softening. In the wake zone of a crack, interface debonding, frictional sliding (pull-out) and inclined angle effects for fibres that are not orthogonal to the crack plane lead to energy absorption (Li, 1995; Li, 1996). On the other hand, in *ductile composites*, after the elastic region a loss of stiffness is observed but the composite can still carry substantial load. Multiple microcracks are formed whose number and density increase with increasing load until it reaches a saturation level which leads to failure. Indeed, strain hardening is preferred to tension softening. For this, it is necessary to have stiff fibres and appropriate interface matrix-fibres strength.

b) Effect of fibres on the elastic properties and strength of fibre reinforced cements

The two main components of the FRCs are the matrix and the fibres. Different properties of the fibres affect the final performance of the composite, like their mechanical properties (Young's modulus, strength and elongation to fracture), length and diameter (important for the aspect ratio), chemical composition, cytotoxicity, degradability and surface properties (functional groups, roughness).

The aspect ratio of the fibres (diameter/length) determines, for the same amount of fibres, the total surface of the fibre in contact with the matrix, and this is important because the higher the surface in contact, the greater the load transfer.

Although there are different possible disposition of fibres in the matrix, most biomedical composites are reinforced by discontinuous fibres. In the case of randomly distributed fibres, Young modulus E_c (Equation 4.1) and stress σ_c (Equation 4.2) of the composite can be described by the following equations:

$$E_c = \phi_i \cdot E_f \cdot V_f + E_m \cdot V_m \quad (4.1)$$

And:

$$\sigma_c = \phi_i \cdot \sigma_f \cdot V_f + \sigma_m \cdot V_m \quad (4.2)$$

Where V_f and V_m are volume fractions of the fibres and the matrix, respectively. Elastic moduli of fibres and matrix are denoted by E_f and E_m respectively, and σ_f and σ_m are the corresponding tensile strengths. The composite efficiency factor (ϕ_i) accounts for the reduction in composite mechanical property values due to such factors as fibre length, orientation, defects and fibre-fibre interaction. If the fibres are continuous, aligned, and parallel to the direction of the applied load, $\phi_i = 1$ (**Beaudoin, 1990**).

As aforementioned, for strengthening purposes, it is important to have a good load transfer from the matrix to the fibres, through their interface. The load is transferred at the lateral surface of the fibres while the transfer via the end faces is

negligible (Callister, 2009). This means that for fibres of an insufficient length, the lateral surface is so small that the transferable load is below the strength of the fibre. Thus, pull-out occurs before the fibre fracture and the strengthening capability of the fibre is not fully utilised (Rösler, 2006).

In order to maximise the reinforcement given by the fibres, the parameter which can help selecting the length of the fibres is the critical length (l_c). It is remarkable that the critical length depends on the diameter of the fibre (d_f):

$$l_c = \frac{d_f \sigma_{f,B}}{2\tau_i} \quad (4.3)$$

Where $\sigma_{f,B}$ is the fracture strength of the fibre, while τ_i is the shear stress at the interface.

If the fibre is shorter than l_c , the fibre is pulled out without rupture and without reaching the maximum stress bearable (Figure 4.4). For aligned fibre-reinforced composite systems, it has been reported that the optimal fibre length should be close but not more than twice the critical fibre length to ensure that all fibres are pulled out with the maximum amount of frictional work and yet not rupture (Li VC, 1991).

Figure 4.4 reports the stress distribution along the fibre in the cases of: $l < l_c$, $l = l_c$ and $l > l_c$.

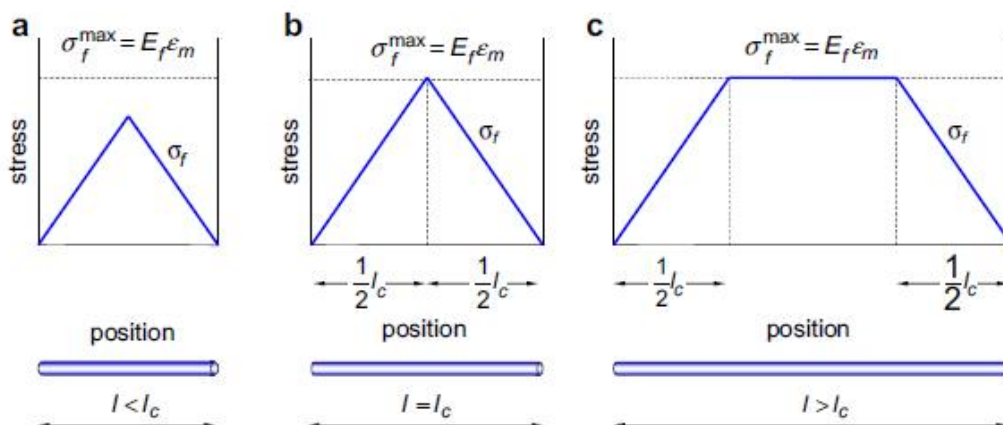


Figure 4.4 -Stress distribution in the fibre along its axis for fibres a) shorter, b) equal and c) longer than the critical length l_c (Krüger, 2012)

As bone, composite materials show anisotropy; in random distributed fibres the orientation distribution of the fibres is likely to be biased, and not in an ideal

random or aligned state, due, for example, to handling factors (i.e: mixing or moulding of the paste). The final orientation of the fibres determines the toughness of the material **(Jain, 1992)**.

Another important factor is the amount of fibres in the composite. In civil engineering materials the amount is usually low, due to the fact that fibre contents greater than 2-3 v/v % result in poor workability and more aggregation of the fibres in the material **(Li, 2003; Li 1997)**. Regarding the biomedical field, many studies use higher amounts of fibres. Moderate load transfer due to non-optimised interface strength and low modulus of the fibres require a higher volume fraction of fibres **(Krüger, 2012)**.

c) Evaluation of mechanical properties

In order to characterise the mechanical properties of composites, different tests have been performed over the years. These methods include uniaxial compression, diametral compression, three- and four- points bending and biaxial flexure (ring-on-ring).

Compression seems to be not the most appropriate method to characterise the mechanical properties of composite materials. The same is valid for diametral compression testing; this test would apply only to a perfectly brittle material **(Krüger, 2012)** and evidently FRPCs do not belong to this type of materials. Thus, bending testing is a common testing method which seems to be appropriated. Bending tests can be performed by either three- or four- point bending depending on the number of pins where the load is applied. Figure 4.5 represents schematically the two set-ups and how the load is distributed in the case of three-point (Figure 4.5a) or four-point (Figure 4.5b) bending tests.

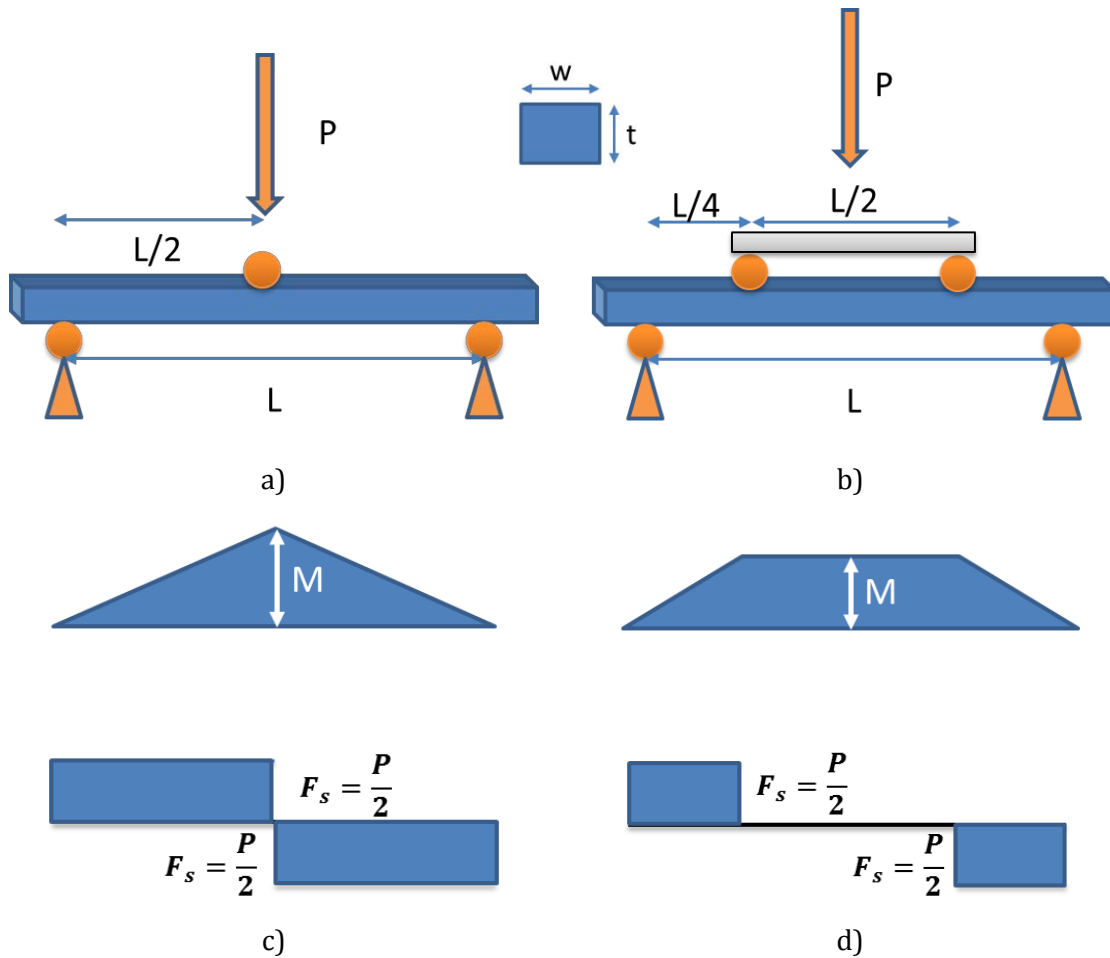


Figure 4.5 - Schematic representation of a) three-point and b) four-point bending test set-ups. Bending moment (M) and Shear force (F_s) diagrams in c) three-point and d) four-point bending test.

In this thesis, three-point bending tests were employed. The elastic modulus (E), bending strength (BS) and the work of fracture (WOF) of the new composites for three-point bending tests were calculated using the following formulae (**ASTM C1161 - 02c(reapproved 2008)**):

$$E = \frac{PL^3}{4wt^3y} \quad (4.4)$$

$$BS = \frac{3PL}{2wt^2} \quad (4.5)$$

$$WOF = \frac{\text{Area curve load vs displacement}}{2wt} \quad (4.6)$$

Where P = load, L = span, w = width of the sample, t = thickness of the sample and y= deflection at the load point.

The area under the load-displacement curve divided by twice the sample section, called “work of fracture” (**Tattersall & Tappin, 1966**), is an appropriate term for defining the toughness of a brittle or quasi-brittle material (**Krüger, 2012**). Notwithstanding, it is important to take into account that it is difficult to compare data with the literature for different reasons:

- 1) Different arbitrary deflection values are in use (generally ranging between 2 and 3.5 mm) and at this deflection point samples are usually not yet broken apart.
- 2) Elastic deformation energy interferes with the work of fracture.
- 3) In the case of branched cracks the fracture area is greater than the nominal sample cross section and is not known.
- 4) Some people notch the samples before testing. In such cases the work of fracture may differ by a factor of four (**Guinea, 1992**).

Therefore, the assumptions done are several, which make difficult the comparison of the different data.

4.1.3 Fibre reinforced calcium phosphate cements

In the past few years different materials have been used as reinforcement of CPCs, forming the so-called fibre reinforced CPCs (FRCPCs). FRCPCs can be classified depending on different features. One classification is related to the biodegradability of the fibres. In this respect, the materials can be distinguished between composites reinforced with non-resorbable or resorbable fibres (**Canal, 2011**). Belonging to the first category there are the cements reinforced with several polyamides and ceramic fibres, while in the second category FRCPCs evaluated contained mainly different polyesters (such as poly lactic acid (PLA), poly glycolic acid (PGA), their mixtures (PLGA) and poly caprolactone (PCL)).

Another possible classification is related to the way the fibres are embedded in the CPC matrix (which is also relevant for the contribution to the mechanical properties). In the literature regarding FRCPCs, fibres have been mixed within the cements using different structures of the fibrous materials, which are reported in Figure 4.6 (**Canal, 2011**). The fibres can be either randomly distributed (Figure

4.6a, 4.6b, 4.6c) or aligned (Figure 4.6e), or can be knitted or woven in meshes (Figure 4.6d).

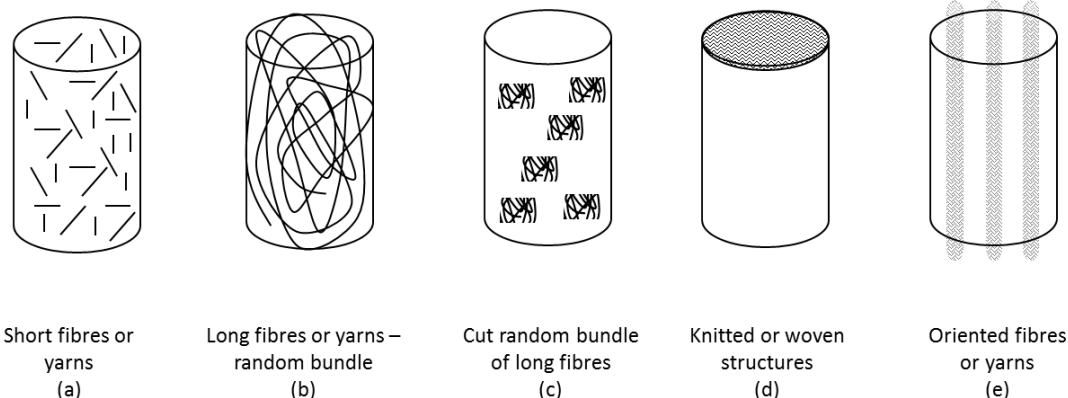


Figure 4.6 - Possible disposition of fibrous materials in calcium phosphate cement composites: a) short fibres or yarns randomly distributed, b) long fibres or yarns as random bundle, c) cut random bundle of long fibres, d) knitted structures as for instance meshes, e) oriented yarns (Canal, 2011).

As summarised in Table 4.2, many FRCPCs have been developed in the past 15 years. Nevertheless, the matrices of FRCPCs are mainly based on apatitic cements obtained by mixing cement blends with water or aqueous solutions; an apatitic pre-mixed cement has been used (Xu, 2007a) as well as a brushitic cement (Gorst, 2006).

Non resorbable fibres with diameters ranging from the nanoscale (Wang, 2007; Low, 2011; Chew, 2011) to the microscale have been used (Xu, 2000; Xu, 2001a; Xu, 2001b), and generally caused an increase (Xu, 2000) or maintained the elastic modulus but improved both the flexural strength and WOF (in the studies where it was measured (Xu, 2001b)).

Investigation on resorbable fibres and yarns has been robust. Many works have dealt with randomly distributed PLGA yarns of 322 µm diameter. Their length varied between 3 and 75 mm, with 8 mm as the most used (Xu & Quinn, 2002; Xu & Simon, 2004, Burguera, 2005) and volume percentages varying between 1.9 and 60 v/v % (Canal & Ginebra, 2011). An increase of the fibre amount reverted in an increase of the WOF, up to a certain amount. In fact it was found that a too high amount of fibres caused a decrease of elastic modulus and bending strength (Xu, 2000; Pan, 2007; Zuo, 2010). This means that the amount of fibres should

be optimised since a high amount of fibres not only impairs good workability of the paste but also reverts in poorer mechanical properties.

The addition of additives in the cement matrix such as chitosan lactate caused an increase of both bending strength and WOF (**Zhang & Xu, 2005**). The further addition of mannitol (a porogen) allowed obtaining macroporous FRPCs (**Xu, 2006; Xu, 2007a; Xu, 2007b**).

Furthermore, in literature there are some works focusing on the reinforcement of CPCs with more complex structures such as meshes (**Xu, 2004; Weir, 2006**).

Table 4.2 - Summary of the main FRPCs in the state of the art (modified from Canal, 2011).

Fibre polymer	Fibre (wt %)	Fibre length (mm)	Fibre diameter (μm)	Additives	Cement composition	Liquid phase	L/P	WOF (kJ/m^2)	Flexural Strength (MPa)		Elastic modulus (GPa)	Ref
									Pristine CPC	Fibre-CPC		
CPC composites with non-resorbable fibers												
PA66	0.2-1.6	3	100		α -TCP, 5% Organic monomers 2% PHA	2.5% NaHPO ₄	0.55	-	9.5 ^d	↑12.5-9.8 ^d	-	dos Santos, 2000
Aramid	1.9-3.8	75	15±2	-	DCPA:TTCP	H ₂ O	0.33	↑5-10	13	↑25-65	↑4-6.5	Xu, 2000
Aramid	6 ^a	75	15±2	Mannitol (10-40%)	DCPA:TTCP	H ₂ O	0.33	↑6.5-1	15-2	↑44-4	=6.5-1	Xu, 2001b
C	1.9-9.5 ^a	3-200			DCPA:TTCP	H ₂ O	0.33	↑3.5-6.5	13	↑32-59	↑4-7	Xu, 2000
CNTs	0.2-0.5	unknown	60-100 nm	CNTs mineralised with HA	nano DCPA:PCCP	H ₂ O	0.45	-	26 ^d	↑55 ^d	-	Wang, 2007
CNTs	0.2-0.5	30 nm	20-30nm	MWCNTs, MWCNT-OH, MWCNTs-COOH, BSA	β -TCP:DCPA	H ₂ O	0.27	-	-	2-14 ^d	-	Low, 2011
e-glass	1.9-9.5 ^a	3-200	16±2	-	DCPA:TTCP	H ₂ O	0.33	↑2-4.5	13	↑20-35	↑4-5	Xu, 2000
Bioactive glass	5-25	unknown	<20	-	DCPD:TTCP	6% NaHPO ₄	0.33	↑0.2-0.5 ^d	0.6 ^d	↑1.5-3.7 ^d	-	Nezafati, 2010

Fibre polymer	Fibre (wt %)	Fibre length (mm)	Fibre diameter (μm)	Additives	Cement composition	Liquid phase	L/P	WOF (kJ/m^2)	Flexural Strength (MPa)		Elastic modulus (GPa)	Ref
									Pristine CPC	Fibre-CPC		
CPC composites with resorbable/biodegradable fibers												
PLLA	1-7	0.2x3 ^b	1-2	-	α -TCP, CaH ₂ PO ₄ , CaCO ₃ , PHA	1% NaH ₂ PO ₄	0.33	\uparrow 0.1-0.25	7	\downarrow 4-2.6	\downarrow 32-15	Zuo, 2010
PGA/PLA fibres-CPCs												
PGA/PLA	1.9-9.5 ^a	3-75	198 \pm 64 ^c	-	DCPA:TTCP	H ₂ O	0.33	\uparrow 2.5-5	13	\uparrow 15-25	\uparrow 2.2-4.5	Xu, 2000
PGA/PLA	25 ^a	8	322 ^c	-	DCPA:TTCP	H ₂ O	0.5-0.33	\uparrow 1.6-3.3	5-10	\uparrow 14-25	5.5-2.2	Xu & Quinn, 2002
PGA/PLA	25 ^a	8	322 ^c	-	DCPD:TTCP / DCPA:TTCP	H ₂ O	0.33	\uparrow 3.5	8	\uparrow 17	\downarrow 2.7	Burguera, 2005
PGA/PLA	15-60 ^a	8	322 ^c	-	DCPA:TTCP	H ₂ O	0.5	\uparrow 0.6-1.7	4	\uparrow 4.2-13	\downarrow 1.5-2.0	Xu & Simon, 2004
PGA/PLA	24 ^a	5	322 ^c	-	β -TCP	3.5M H ₃ PO ₄	0.33	-	12.8 ^e -2.8	\downarrow 7.4 ^e - \uparrow 5.1	\downarrow 6.5 ^e -2.5	Gorst, 2006
PGA/PLA	12// fibres	∞	322 ^c	-	β -TCP	3.5M H ₃ PO ₄	0.33	-	12.8 ^e -2.8	\uparrow 19.8 ^e -7.8	\downarrow 7.6 ^e -1.0	Gorst, 2006
PGA/PLA fibres-CPCs with other additives												
PGA/PLA	45 ^a	8	322 ^c	Chitosan	DCPA:TTCP	15% Chitosan lactate sol.	0.5	\uparrow 11	2.5	\uparrow 40.5	\uparrow 3.2	Zhang & Xu, 2005
PGA/PLA	20 ^a	8	322 ^c	Chitosan	DCPA:TTCP	15% Chitosan lactate sol.	0.33	-	10	\uparrow 25	\uparrow 7	Zhao, 2010a

Fibre polymer	Fibre (wt %)	Fibre length (mm)	Fibre diameter (μm)	Additives	Cement composition	Liquid phase	L/P	WOF (kJ/m^2)	Flexural Strength		Elastic modulus (GPa)	Ref
									Pristine CPC	Fibre-CPC		
PGA/PLA	5-20 ^a	8	322 ^c	Chitosan, Alginate beads, hUCMSC	DCPA:TTCP	15% Chitosan lactate sol.	0.33	\uparrow 0.7-1.5	3.5	\uparrow 7-11	\uparrow 1-2	Zhao, 2010b
PGA/PLA	20 ^a	8	322 ^c	Chitosan, Alginate hydrogel beads, hBMSC,	DCPA:TTCP	15% Chitosan lactate sol.	0.33	\uparrow 1.7	2.3	\uparrow 11.7	\uparrow 2	Weir & Xu, 2010
PGA/PLA	30 ^a	8	322 ^c	Mannitol, Chitosan (Bilayer)	DCPA:TTCP	15% Chitosan lactate sol.	0.5	-	10-2	\uparrow 10-25	0.8-3	Xu, 2007b
PGA/PLA	2.5-7.5 ^a	5	322 ^c	Mannitol, HPMC	DCPD:TTCP	0.2mol/L NaH_2PO_4	0.5	\uparrow 0.3	1.1	\uparrow 1-3.2	1.2-1.5	Xu, 2006
PGA/PLA	25 ^a	8	322 ^c	Glycerol, HPMC, MCPM, Mannitol	DCPA:TTCP	15% Chitosan lactate sol.	0.25	-	0.7-6.6	\uparrow 1.8-11.7	\downarrow 0.37-1.58	Xu, 2007a
PGA/PLA	20 ^a	3-6-10	322c	Chitosan, Alginate beads (0, 20, 30, 50, 60, 70%)	DCPA:TTCP	15% Chitosan lactate sol.	0.33	\uparrow up to 20 fold	1.8	1.5-8.4	\downarrow 0.4-0.5	Zhou, 2011
PGA/PLA laminar structures-CPCs with other additives												
PGA/PLA	1 layer	Mesh	-	-	DCPA:TTCP	H_2O	0.25	122.65 $\text{N}\cdot\text{cm}^f$	-	-	-	Von Gonten, 2000

Fibre polymer	Fibre (wt %)	Fibre length (mm)	Fibre diameter (μm)	Additives	Cement composition	Liquid phase	L/P	WOF (kJ/m^2)	Flexural Strength		Elastic modulus (GPa)	Ref
									Pristine CPC	Fibre-CPC		
PGA/PLA	13 layer	Mesh	-	Alginate hydrogel beads, MC3T3-E1, Chitosan	DCPA:TTCP	15% Chitosan lactate sol.	0.33	\uparrow 0.5-2	2.5	\uparrow 4-10	\uparrow 1.5-2.5	Weir, 2006
PGA/PLA	13 layers	Mesh	140-200 (node thickness)	Chitosan	DCPA:TTCP	H ₂ O or 15% Chitosan lactate sol.	0.5	\uparrow 9	3.5-12.5	\uparrow 22-42	\uparrow 2.6	Xu, 2004
PCL-CPC composites												
PCL	1-7	0.2x3 ^b	1-2	-	α -TCP, CaHPO ₄ , CaCO ₃ , PHA	1%	0.33	\uparrow 0.1-0.5	7	\downarrow 3.5-6.9	\downarrow 15-47	Zuo, 2010
Chitosan-CPC composites												
Chitosan	10-30 ^a	6-8	-	Gelatin	DCPA:TTCP	5% gelatin sol.	0.5	-	6.1	\uparrow 8.1-9.0	-	Pan, 2007

\uparrow or \downarrow indicate higher or lower mechanical property of the fiber-CPC composite with respect to the pristine CPC.

^a Fiber volume fraction % . ^b Fibre bundle. ^c Yarn diameter. ^dCompression strength / compressive tests. ^eMechanical compaction. ^fRing on ring biaxial test.

4.1.4 Polymeric additives used in this Thesis

Polymeric additives have been used in CPCs for several years (**Dorozhkin SV, 2009; Neumann, 2006; Low, 2010, Perez, 2012**). These polymers in most cases present biodegradability. They can be used both in the matrix (solubilised in the liquid phase) or as particles and fibres. The first strategy to increase the mechanical properties of CPCs and develop FRCPCs consists in using a common polymer in the matrix (as additive in the liquid phase) and in the fibres. A critical parameter that controls the reinforcing efficiency of fibre-reinforced composites is the interfacial bonding between the fibre and the matrix (**Krüger, 2012**). However, little attention has been paid to this issue in fibre-reinforced calcium phosphate cements. The hypothesis is that the common element should enhance the bonding.

The additives used in this thesis are following described.

a) Chitosan, its derivatives and β -Glycerol Phosphate

Chitosan is a linear aminopolysaccharide of glucosamine and N-acetylglucosamine units (reported in Figure 4.7) and it is obtained by partial alkaline deacetylation of chitin, the first polysaccharide identified by man (**Braconnot, 1811**). Chitin is extracted from the exoskeleton of crustaceans such as shrimps and crabs, as well from the cell walls of some fungi (**No, 1997**). The following major characteristics of chitosan make this polymer advantageous for numerous applications (**Badawy, 2011**): i) it has a defined chemical structure; ii) it can be modified both chemically and enzymatically; iii) it is functional both physically and biologically; iv) it is biodegradable and biocompatible; v) it can be processed into several products including flakes, fine powders, beads, membranes, sponges, fibres, and gels.

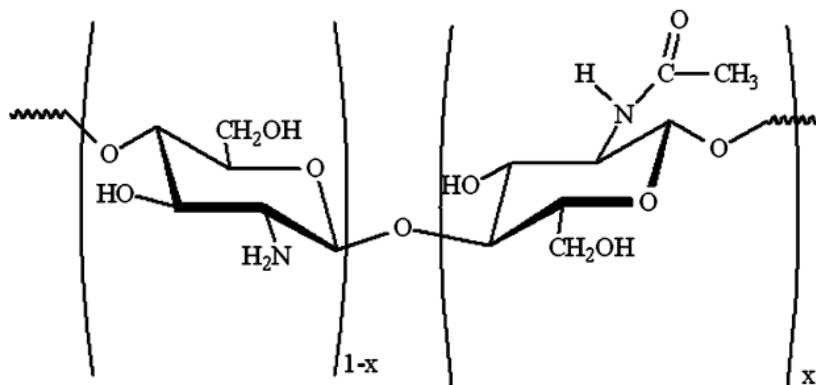


Figure 4.7- Chitosan chemical structure (da Silva, 2010).

Owing to its high biodegradability, low toxicity, and antimicrobial properties, chitosan is widely-used as an antimicrobial agent either alone or blended with other natural polymers. Furthermore, chitosan has shown an excellent combination of properties and it has been demonstrated that it is a suitable biomaterial for the development of scaffolds for bone tissue engineering (**Costa-Pinto, 2008**). In this thesis chitosan fibres are used as reinforcing agents, and TriMethyl Chitosan (TMC) an additive in the liquid phase.

Figure 4.8 shows the chemical formula of TMC, which is the product of the quaternisation of chitosan and becomes a gel when mixed with water. TMC's synthesis is based on the method developed by Domard and coworkers (**Domard, 1986**). TMC has been shown to have mucoadhesive properties above a certain degree of quaternisation (**Thanou, 2001**). The quaternisation process decreases the cytotoxicity, improves both aqueous solubility at physiological pH and positive charge (**Handbook of chitosan research and applications**). Cytotoxicity seems to be dependent on the molecular weight of the TMC: the higher the molecular weight, the higher the cytotoxicity.

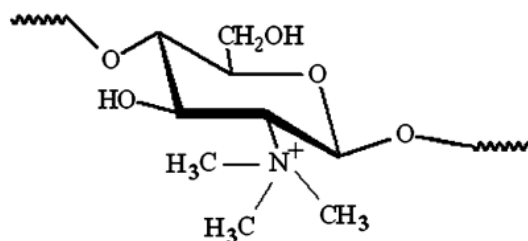


Figure 4.8- TryMethyl Chitosan chemical structure (da Silva, 2010).

Another additive investigated in this chapter, due to its ability to crosslink chitosan, is β -Glycerol phosphate (GP, chemical formula reported in Figure 4.9). GP has already been used as additive in calcium phosphate cements with a totally different rationale: to improve paste injectability (**Leroux, 1999**).

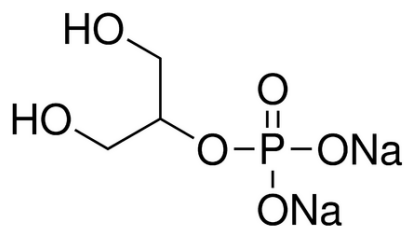


Figure 4.9- β -Glycerol phosphate chemical structure.

This molecule is of interest in this work, because it is a salt that, when mixed in solution with chitosan, is able to transform a simple solution into a reversible hydrogel upon pH and/or temperature variation (**Chenite, 2001**). Figure 4.10 shows a schematic image of TMC/GP hydrogel formation via electrostatic crosslinking between amine cationic groups of the TMC chains and the phosphate anionic groups of the GP.

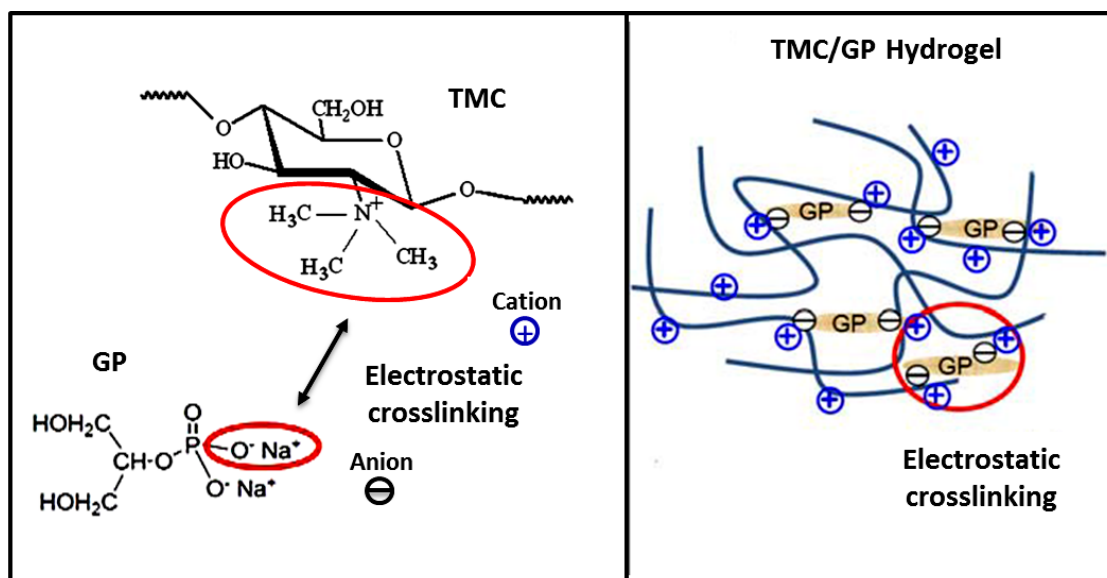


Figure 4.10 -Schematic image of TMC/GP hydrogel formation via electrostatic crosslinking between amine cationic groups of the TMC chains and the phosphate anionic groups of GP.

Chitosan and chitosan derivatives have been used in CPCs to improve their properties. As previously mentioned, chitosan lactate (a water-soluble chitosan salt containing the lactate counter-ion) has been widely used as additive in the liquid phase of CPC (**Zhang & Xu, 2005; Zhao, 2010a, Zhao, 2010b; Weir & Xu, 2010; Xu, 2007b**), improving rheological and biological properties of the cement paste. It is important to specify that all these works have employed chitosan lactate instead of pure chitosan (**Dash, 2011**), while the fibres used as reinforcement in such composites were always Vicryl[®] suture yarns, a PLA-PGA copolymer which

maintains its mechanical properties for around 4 weeks and shows complete reabsorption in 56-70 days and (Xu & Quinn, 2004).

To our knowledge there is just one group who has worked with chitosan fibres for reinforcing CPCs (work described in section 4.1.3). Recently the same group prepared FRCPCs based on TTCP:DCPA and reinforced with chitosan fibres either plain or RGD-functionalised aiming at improving both mechanical properties and cellular response (Wu, 2014).

b) Lactic acid and poly(lactic acid)

Lactic acid (LA, CH₃-CHOH-COOH) is a natural compound involved in cell metabolism. In animals, lactic acid is a metabolic compound produced by proliferating cells and during anaerobic conditions such as strenuous exercise. There are two enantiomers of LA (L-LA and D-LA) depending on the stereometry of the methyl group. Furthermore, LA is the monomer of the polymer called Poly-lactic acid (PLA). The chemical formulae of both compounds are illustrated in Figure 4.11.

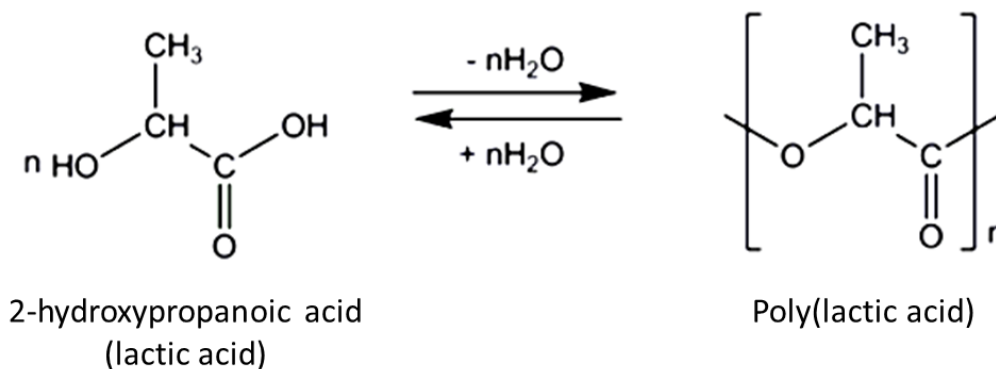


Figure 4.11- Chemical formulae of (left) the monomer Lactic acid and (right) its polymer, Poly (lactic acid).

Poly-L-lactic acid (PLLA) has a semi crystalline structure which reverts in high tensile strength, elongation, and modulus, properties that make it more suitable for load bearing applications (Sabir, 2009) than Poly-D-lactic acid (PDLA). Moreover PLLA was FDA approved in 1971 for the development of an improved suture over the ones already on the market marketed as, i.e. DEXONs (Thomas, 2013). The biodegradability of PLLA depends on its molecular weight, and it has been reported

that high molecular weight PLLA can take between 2 and 5.6 years for total resorption in vivo (**Middleton & Tipton, 2000; Bergsma, 1995**).

To our knowledge, LA was used as additive of CPC (**Leroux, 1999**), with the aim of improving the injectability. After temporary transformation of the Cementek¹ initial powders to brushite, the cement transformed into HA. As reflected in Table 4.2, extensive work has been performed regarding the use of PLA/PGA copolymer, which is more resorbable and has lower mechanical properties than PLLA. Electrospun PLLA was used as reinforcing agents in apatitic cements (**Zuo, 2010**).

4.1.5 Low temperature plasma in fibre reinforced cements

Another strategy that is explored in this thesis to improve the interfacial fibre/matrix strength in FRPCs is the modification of the fibre surface by low temperature plasma, hereinafter plasma. Plasma can be defined as a particular state of a gas or mixture of gases containing a mixture of ions, free radicals, electrons, excited molecules, UV and visible radiation that preserves electrical neutrality. This reactive medium can modify the first nanometres of the surface of the material without altering its bulk properties. Roughly, the three main effects of plasmas on the surface of a material are: i) functionalisation or grafting (covalent bonding of new chemical species); ii) etching (removal of surface material); and iii) thin film deposition (deposition of thin layers). In the past decade, the use of non-thermal plasmas for selective surface modification of biodegradable polymers has been a rapidly growing research field, with many works concerning the treatment of PLA films (**Morent, 2010**). Plasmas allow selection of the treatment gas and have the advantage of controlled conditions leading to highly reproducible results.

In the literature there are few examples of successful surface plasma modification of fibre reinforced concrete (**Li, 1996**), that show that plasma treatment of the fibres can be used as a method to modify the chemical and frictional bonds between the PLLA fibres and the cement matrix. Up to now, limited efforts have been made towards improving wettability of the fibres in fibre-reinforced CPCs. It is expected

¹ Cementek is a commercial blend of α -TCP, Tetra calcium phosphate and sodium glycerol Phosphate.

that, given that the matrix is a hydraulic paste, improving the wettability of the fibres will have an effect on the matrix/fibre contact, and therefore in the final performance of the composite; in particular by improving the elastic modulus, flexural strength and work of fracture with respect to untreated PLLA-CPC composites.

4.2 Objectives

The objective of this chapter is the development of FRCPCs with enhanced mechanical properties. Two strategies are proposed:

1. Addition of polymeric additives in the liquid phase of the cement with high affinity to the fibres used as reinforcement. The aim is to create better chemical interactions which would revert in higher toughness.
2. Use of plasma to modify Poly-Lactic acid (PLLA) yarns surface, increasing their wettability in order to generate stronger fibre-matrix adhesion and obtaining tougher FRCPCs.

4.3 Calcium phosphate cements reinforced with fibres and polymeric additives

4.3.1 Introduction: Experimental design

In this section the strategy adopted consists in dissolving in the liquid phase either the polymer or the monomer of the fibres selected for reinforcement in order to increase the adhesion between the fibre and the matrix. Two strategies are undertaken: i) Chitosan fibres and TMC in the liquid phase of the cement, and ii) PLLA fibres and LA in the liquid phase of the cement. The liquid to powder ratio (L/P), fibre amount and length of the fibres were optimised in each formulation studied, to ensure a good workability of the paste.

4.3.2 Materials and methods

a) Materials

a.1. Solid and liquid phases

α -TCP powders were obtained as described in section 3.3.1. 2 wt% of precipitated hydroxyapatite (Alco) was added as a seed in the powder.

➤ Chitosan - reinforced cements

Three liquid phases were explored for the cements containing chitosan. Aqueous solutions based on TMC (Kytzyme, Belgium) and β -Glycerol Phosphate (GP, Sigma Aldrich) were used as follows:

Solution 1: water

Solution 2: TMC: 1 w/v % TMC in water.

Solution 3: TMC-GP: 1 ml of solution 2 (1 w/v % of TMC) mixed with 0.714 ml of 60 w/v% GP aqueous solution, with pH adjustment down to 7.5 (according to Kitozyme, Belgium).

➤ **PLLA - reinforced cements**

The liquid phase for cements containing PLLA fibres was an aqueous solution containing 10 v/v% Eur Ph approved LA (Fluka; MW = 90.08 g/mol). Water was used as control.

a.2. Fibres

The characteristics of the fibres used are summarised in Table 4.3 and Figure 4.12. 100% highly purified chitosan microfibrils and films were used β -sterilised (11 kGy) (Medovent GmbH, Mainz, Germany). Their degree of acetylation was 2%. The diameter of chitosan fibres used as reinforcement in CPCs was $200 \mu\text{m} \pm 10 \mu\text{m}$. Fibres were cut to 8 mm length prior to mixing with the powder phase of the cements. Chitosan films (thickness: 0.05 mm) were used as a model flat surface for characterising the contact angle.

Partially oriented PLA multifilament of 213.9 dtex/68, false-twist textured at 150°C and 29% crystallinity (kindly supplied by ANTEX, Spain) (as characterised in **(Manich, 2010)**) was employed as resorbable reinforcing agent. The polymer used is polylactide for fibres with a proportion of D/L lactide 1.4/98.6 (hereinafter named PLLA). The yarns have a breaking stress $\sigma_B = 795 \text{ MPa}$ and a strain at break is $\varepsilon_B = 35.73\%$ **(Manich, 2011)**.

Before use, the fibres were accurately washed according to ISO 105-C06 using ECE colour detergent (Testgewebe GmbH, 88030) in a concentration of 5 g/l and then rinsed 5 times with distilled water.

PLLA films (Goodfellow, UK), biaxially oriented, with 37% crystallinity and thickness of 0.05 mm, were employed as model surface for the determination of contact angle.

Table 4.3 - Fibres or yarns characteristics.

Type of fibres or yarns	Composition	Features	Diameter	Tension breaking stress
Chitosan fibres	acetylation degree 2%	Cylindrical smooth	$(200 \pm 10) \mu\text{m}$	$471 \pm 13 \text{ MPa}$
PLLA yarns	98% PLLA	68 false-twist fibres (fibre diameter $\approx 17 \mu\text{m}$)	$(287 \pm 18) \mu\text{m}$	795 MPa

b) **Cement preparation**

Calcium phosphate cements (CPCs) reinforced with chitosan fibres, were prepared by mixing the α -TCP powder, with the liquid phase at L/P = 0.35 ml/g.

The optimised FRCPCs containing PLLA fibres were produced with 10 % LA at L/P = 0.40 ml/g.

Fibre Reinforced CPCs (FRCPCs) were produced in the same way of pristine cements but with the addition of different amounts (4, 8 and 12 wt%) of staple chitosan 8 mm long fibres in the case of TMC or 2 wt% of PLLA yarns cut either 4 mm or 8 mm long in the case of LA. In both cases the reinforcing agents were previously randomly mixed in the powder phase in order to obtain the configuration reported in Figure 4.12.

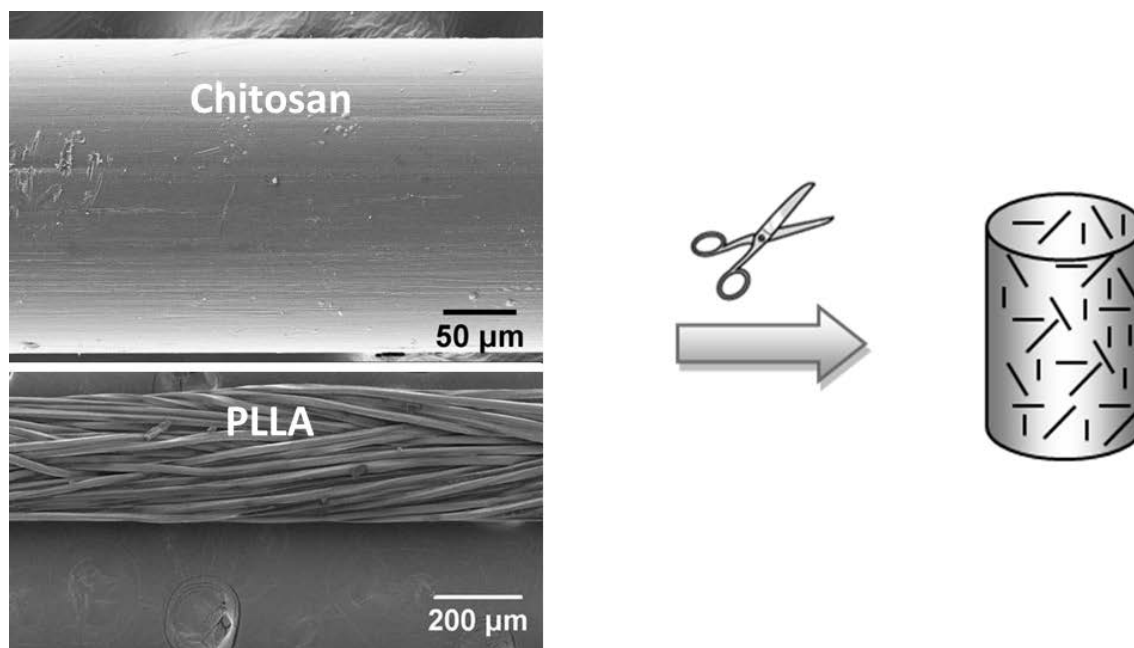


Figure 4.12- Scanning Electron Micrograph of a chitosan fibre (top-left) and a PLLA yarn (bottom-left) with representation of the random distribution of the fibres or yarns in the CPC composite.

Subsequently, the cement paste was put in Teflon moulds and immersed in Ringer' s solution (0.15 M sodium chloride solution) at 37°C for 7 days to allow the reaction of the cement. The different samples evaluated in this section are reported in Table 4.4.

Table 4.4 – Samples tested: the samples are given a reference depending on the liquid phase, fibre content and “s” (short) is specified for shorter fibres. All cements are based on 98% α -TCP+ 2% pHA.

	Reference	Liquid phase	L/P (ml/g)	Fibres (wt %)	Fibre length (mm)
TMC	C35	H ₂ O	0.35	-	-
	TMC	1 wt% TMC in H ₂ O	0.35	-	-
	TMC-GP	TMC-GP solution	0.35	-	-
	C-f8	H ₂ O	0.35	8	8
	TMC-f4	1 wt% TMC in H ₂ O	0.35	4	8
	TMC-f8	1 wt% TMC in H ₂ O	0.35	8	8
	TMC-f12	1 wt% TMC in H ₂ O	0.35	12	8
LA	C40	H ₂ O	0.40	0	-
	LA	10 v/v% LA in H ₂ O	0.40	0	-
	C-f2	H ₂ O	0.40	2	8
	C-f2s	H ₂ O	0.40	2	4
	LA-f2	10 v/v% LA in H ₂ O	0.40	2	8
	LA-f2s	10 v/v% LA in H ₂ O	0.40	2	4

c) Cement characterisation

In this section the different characterisation techniques used on calcium phosphate cements are described.

c.1. Phase quantification

Phase composition of TMC cements was measured by X-ray powder diffraction (XRD) as in section 3.3.2.c). Phase composition of LA cements was assessed by XRD (Bruker D8 Advance) by scanning in Bragg-Brentano geometry using CuK α 1 radiation ($\lambda=1.5406 \text{ \AA}$), with detector PSD Lynx-eye. The experimental conditions used were: 2θ scan step of 0.017° and scan range between 5° and 75° . X-ray generator parameters: voltage 40 kV and intensity 40 mA. The diffraction patterns were compared with the Joint Committee on Powder Diffraction Standards for α -TCP (JCPDS No. 9–348), β -TCP (JCPDS No. 9–169) and HA (JCPDS No. 9–432) (JCPDS, 1991). The cement phase was calculated with a semi-quantitative analysis,

performed on base of the patterns' relative heights and of their I/I_c values^{4.2} (method described in annex I, introduced by **(Chung, 1974)**).

c.2. Cohesion, initial and final setting time

The cohesion, initial and final setting times were determined as described in section 3.3.3.c).

c.3. Specific surface area

The SSA was measured by Nitrogen adsorption at 77 K according to the BET method. The sample holder was filled with the maximum number of samples (5-6 cylinders 6mm Φ x 12 mm height). The degasification of CPCs was performed at 60 °C in order to avoid polymer degradation which would have affected the final result.

c.4. Setting pH

Setting pH of the mixture of α -TCP powders with MilliQ water or 1% TMC solution, was measured by means of a multimeter (Multimeter Crison MM41, software ComLab EASY v 1.0) for 72 hours, at 37°C and at a L/P ratio of 200 ml/g **(Ginebra, 1996)**. In the case of 10 v/v% LA solution, pH was recorded for 3 hours (due to fast equilibrium reached) and both at L/P = 200 ml/g and L/P = 20 ml/g. The data were taken at a rate of 20 points/min for the first 10 minutes and 6 points/h for the following hours.

c.5. Contact angle

The contact angle was determined in chitosan and PLLA films with an Oca15+ contact angle meter (Dataphysics) connected to a CCD. In the case of pure chitosan films using either water or 1 % TMC aqueous solution as wetting liquid; in the case of PLLA films, using either water or 10 v/v% LA solution . Five replicates of each sample were measured and contact angles were calculated using the software SCA20.

^{4.2} I/I_c = peak intensity referenced to a single standard (corundum (α -alumina) in this case)

c.6. Compression test

The compressive strength of the samples was evaluated in cylindrical specimens (12mm height x 6mm diameter) at a cross-head speed of 1 mm/min using a Servohydraulic Testing Machine MTS BIONIX 358. At least six replicates were tested for each cement formulation. The material was tested in wet conditions and the specimens were previously flattened through manual polishing in order to obtain parallel surfaces and assure a full contact of the specimen surface with the piston surface. A 2.5 kN load cell was used for the experiment.

c.7. Three-point bending test

Three-point bending tests were performed using sample bars (Length x width x height: 50 x 4 x 3 mm³, span 40 mm, Figure 4.13) following the ASTM c1161-02c (**ASTM C1161 - 02c (2008)**) using Universal Servohydraulic Testing Machine BIONIX 358 MTS equipped with a load cell of 2.5 kN.

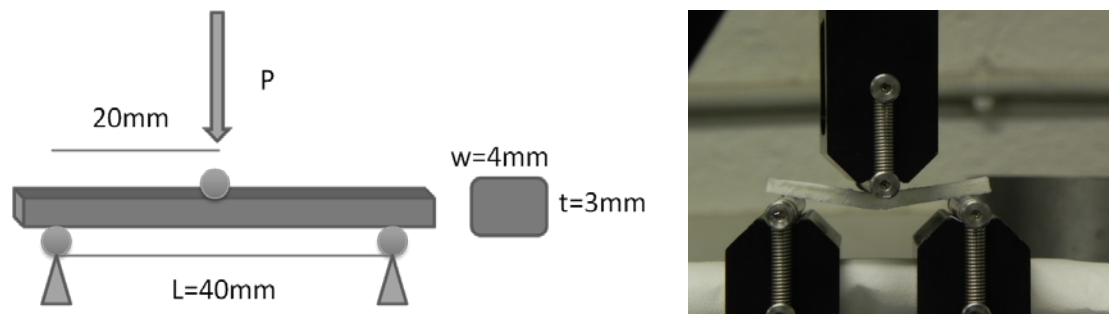


Figure 4.13- Three-point bending test scheme and test.

The elastic modulus (E), bending strength (BS) and the work of fracture (WOF) of the new composites were evaluated. The properties were calculated following the equations (4.4), (4.5), (4.6) which have been previously presented (paragraph 4.1.2c) and are reported below for the sake of clarity:

$$E = \frac{PL^3}{4wt^3y} \quad (4.4)$$

$$BS = \frac{3PL}{2wt^2} \quad (4.5)$$

$$WOF = \frac{\text{Area curve load vs deflection}}{2wt} \quad (4.6)$$

Where P = load, L = span, w = width of the sample, t = thickness of the sample and y= deflection at the load point.

The deflection considered for calculating the WOF was 3mm.

c.8. Scanning Electron Microscopy

To ascertain the microstructure in the fracture surface of the CPC matrices or of FRCPCs, the materials were imaged by Field Emission Scanning Electron Microscopy (FE-SEM, Hitachi H-4100FE or FIB, Zeiss Neon40). Prior to observation the samples were stuck with carbon tape to the sample holder and a thin layer of colloidal silver (Electron Microscopy Sciences, 12630) was put on the side walls to improve conductivity, which is low in ceramic materials. Finally, the surface of samples was coated with Au/Pd by means of Emitech K950X metal evaporator and then investigated.

c.9. Statistics

Statistical differences were determined using one-way ANOVA at 95% confidence with Tukey's post-tests using Minitab 16 software (Minitab, Inc., State College, PA). Statistical significance was noted when $p < 0.05$.

4.3.3 Results

a) Effects of polymer additives to the matrix of CPCs

In a first stage the matrix composition was optimised. Different CPCs were prepared containing either TMC or TMC-GP hydrogels and properties were characterised.

a.1. Setting pH

The solution used as liquid phase in the preparation of CPCs affects the reaction of α -TCP. In order to follow the evolution in the first setting hours, the pH was recorded for the control cement with water (C), the TMC cement (TMC) and the cement with lactic acid (LA) (the latter at two different L/P). Figure 4.14a shows that in C, the pH increased immediately after the addition of α -TCP to water up to a value around 9.2 and then gradually decreased until it stabilises at a pH around 7 after 36 h (blue curve). Differently, the pH of TMC increased gradually (orange curve) up to a pH around 7, when it stabilised.

Figure 4.14b shows again the evolution of pH of α -TCP mixed with water^{4.3} or that of LA during the first hours of setting. Setting pH was measured at a L/P = 200 ml/g, up to 3 hours. In case of 10% LA, due to the low pH of the initial solution (around 1.3) and the high L/P, α -TCP was immediately dissolved as shown by the clear solution (Figure 4.14c) and the increase in pH was minimum (Figure 4.14b). Thus, the L/P was increased 10 fold (L/P = 20 ml/mg) for 10% LA and the pH of the liquid phase rapidly increased up to pH = 3 when α -TCP was added.

It can thus be expected that the pH during setting of the cements at L/P = 0.40 ml/g is higher but still in the acidic range.

^{4.3} Note that the both the pH scale and the time-scale are different.

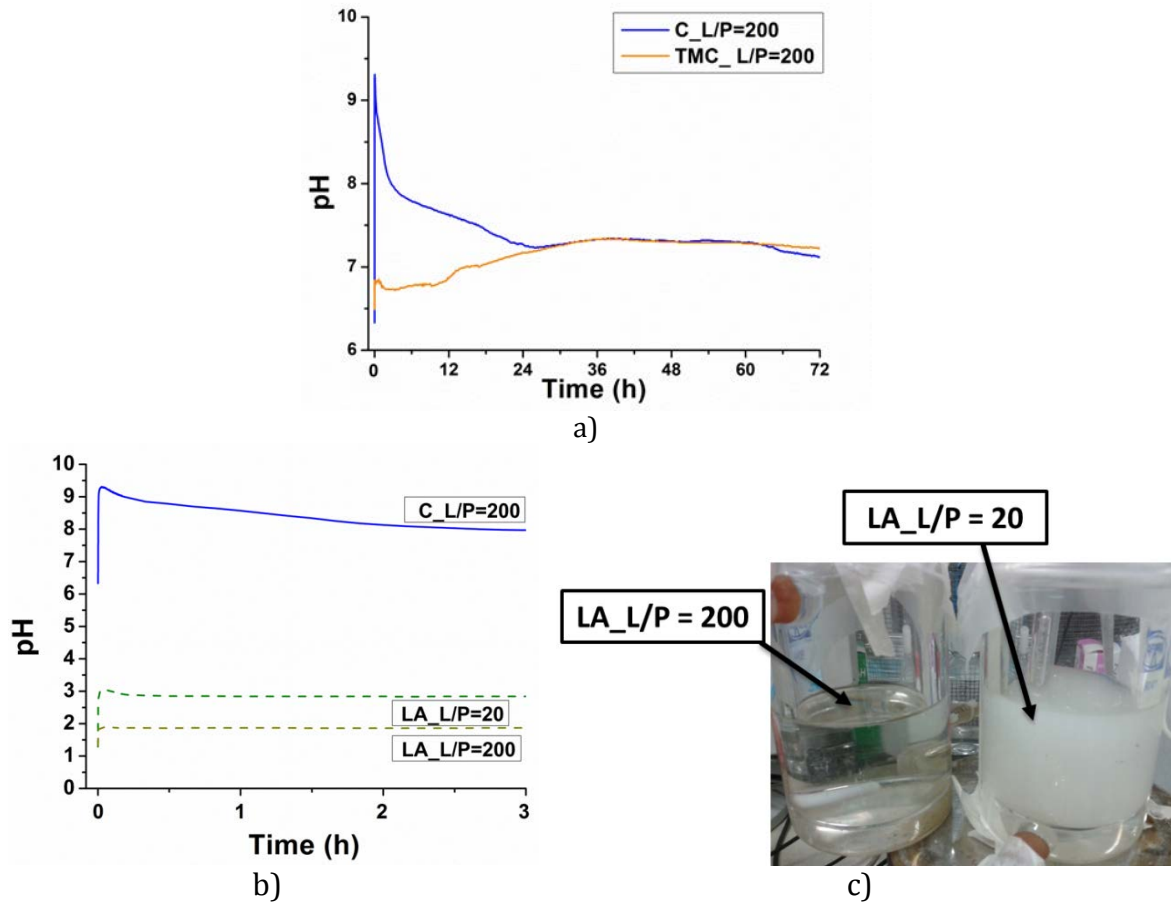


Figure 4.14 - a) Setting pH of α -TCP mixed with water or 1 wt% TMC solution (TMC) at a L/P = 200 for 72h; b) setting pH of α -TCP mixed with water (C) at L/P=200 ml/g or with Lactic acid (LA) at L/P=200 ml/g or L/P=20 ml/g for 3 h; c) a picture of the solutions of α -TCP in 10% LA.

a.2. Cohesion, initial and final setting time

The handling of the cement paste at T_{amb} was easy in all the blends of α -TCP with the different liquid phases containing water, TMC, TMC-GP or LA. Figure 4.15 reports cohesion and setting times. As shown by the cohesion time (C-T), TMC in the liquid phase enhanced the cohesion of the cement paste which was immediate. Similarly, for LA, cohesion was adequate at very short time. However, both the polymer (TMC) and the monomer (LA) complicated the measurement of the initial (I-T) and final setting times (F-T) due to the fact that up to the time examined, a small mark was always visible. In the case of TMC this fact can probably be attributed to an effect of the polymer chains in the matrix. In any case, the addition of TMC, TMC-GP or LA increased F-T compared to the control (C35).

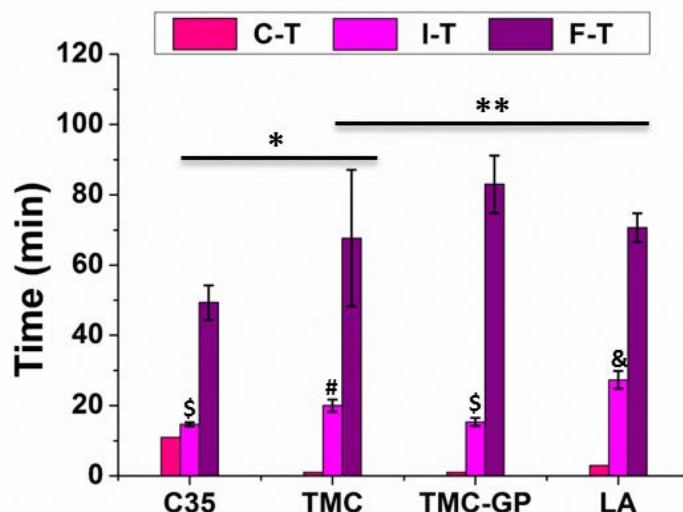


Figure 4.15- Cohesion time (C-T), initial setting time (I-T) and final setting time (F-T) of cements composed of α -TCP mixed with different liquid phases at L/P = 0.35 ml/g. Groups indicated with the same symbol do not have statistically significant differences (\$, #, & for I-T; *,** for F-T: $p > 0.05$).

a.3. Phase quantification

The XRD patterns of the starting powders and of the cements with 1 wt % TMC aqueous solution (TMC) as liquid phase at L/P = 0.35 ml/g or 10 v/v% LA in the liquid phase at L/P = 0.40 ml/g, after 7 days setting in Ringer's solution at 37°C are shown in Figure 4.16.

The quantification of the different phases is shown in Table 4.5, where it can be remarked that the conversion into CDHA after 7 days was incomplete both in TMC and in LA cements, differently from the control C35. However, the amount of CDHA is higher in TMC than in LA cements, where some β -TCP was detected. Although α -TCP in LA solution had a low pH (Figure 4.14b), no brushite was detected at day 7.

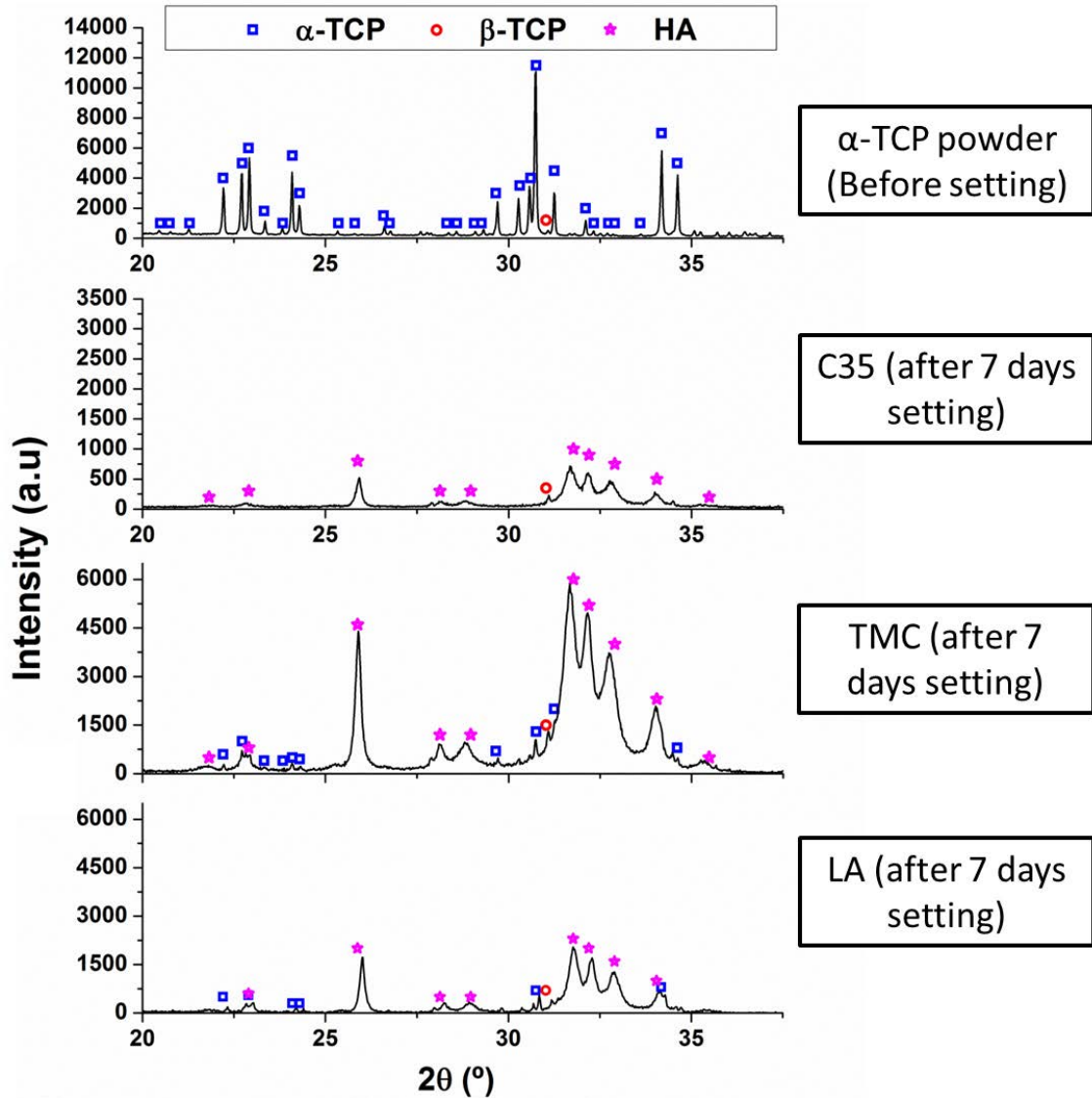


Figure 4.16- From top to bottom, DRX spectra of: the initial α -TCP powders; C35, the control cement at L/P = 0.35 ml/g; TMC, cement at L/P= 0.35 ml/g with TMC in the liquid phase and of the LA, cement at L/P = 0.40 ml/g; all cements were allowed to set for 7 days in Ringer's.

Table 4.5 - XRD data of the raw powder and of the material containing TMC in the liquid phase.

	Phase (%)				
	Material	% α -TCP	% β -TCP	% HA	
Initial powder	α -TCP	97	3	0	*
Set cements	C35	0	3.7	96.3	**
	TMC	6.2	1.8	92.0	**
	LA	6.9	6.4	86.7	**

Quantification method employed: *Rietveld, ** Peak area ratios

a.4. Specific surface area

The different liquid phases also led to changes in the microstructure, as revealed by changes in the SSA shown in Table 4.6. The C35 sample (control CPC with a L/P = 0.35 ml/g) had a SSA of 13.6 m²/g while when 1% TMC was introduced as liquid phase, the SSA decreased to 10.5 m²/g which could be partially due to the fact that around of 6 % of the sample did not convert into CDHA (Table 4.5). The addition of GP (TMC-GP) increased SSA up to 15.0 m²/g, which might be due to changes in rheology of the liquid phase at 37°C that could modify the dissolution-precipitation process. The SSA of a C40 is 13.24 m²/g, really close to the one of the homologues at L/P = 0.35 ml/g. When LA was added, SSA decreased down to 10.8 m²/g while. Decrease possibly due to the presence of unreacted α -TCP in the cement (Table 4.5).

Table 4.6- Surface area of α -TCP reactant powders and of the cements after 7 days setting in Ringer's.

	Material	Specific Surface Area SSA(m ² /g)
Initial powder	α -TCP	0.975
Set cements	C35	13.6
	TMC	10.5
	TMC-GP	15.0
	C40	13.24
	LA	10.8

a.5. Microstructure of the matrices

Figure 4.17 shows the fracture region of the different matrices. All the cements had similar crystal size. In the case of C35 (Figure 4.17a), it is possible to identify the typical plate-like structure of CDHA. Dissimilarly, the structure of the material with TMC (Figure 4.17b) or TMC-GP (Figure 4.17c) showed a mixture of plate- and needle-like structures around the Hadley cells. C40 (Figure 4.17d) displayed the typical plate-like CDHA structures, while LA appeared more compact showing unreacted α -TCP particles (Figure 4.17e), as confirmed also by XRD (Table 4.5).

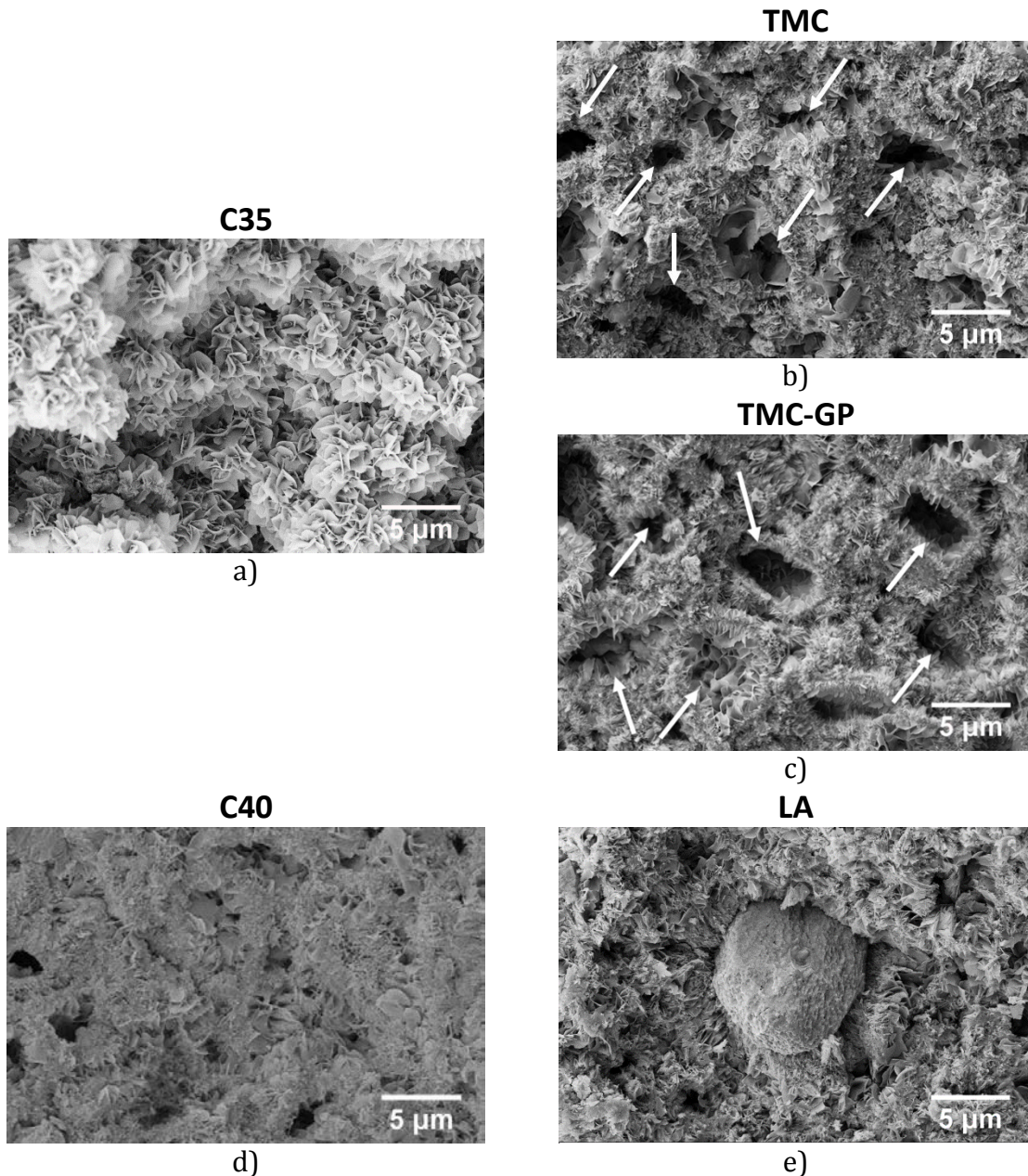


Figure 4.17 - SEM images of the microstructure of the different CPC matrices as obtained employing different liquid phases: a) control with water at L/P = 35 (C35), b) TMC (TMC), c) TMC-GP hydrogel (TMC-GP) as liquid phase, d) control with water at L/P = 40 (C40) in the matrix and e) 10 % LA (LA) as liquid phase. Hadley cells are highlighted in the figures by arrows.

a.6. Compression test

The presence of TMC in the liquid phase slightly increased the compressive strength with respect to the C sample, while GP addition decreased it (Figure 4.18a). The data for LA are not available.

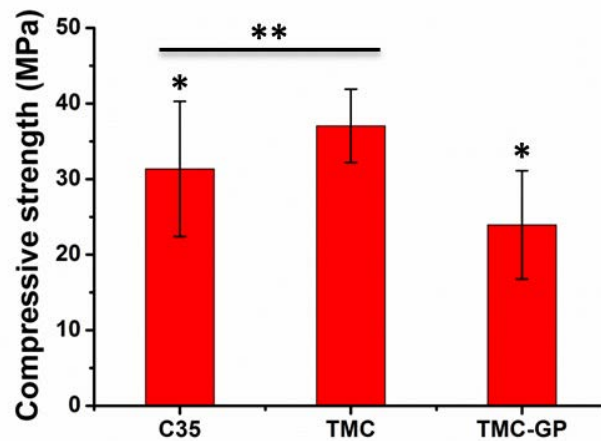


Figure 4.18- Compressive strength of CPCs with different liquid phases. Groups indicated with the same symbol do not have statistically significant differences ($p>0.05$).

a.7. Three-point bending test of the matrices

The bending elastic modulus (E), bending strength (BS) and work of fracture (WOF) of different matrices are reported in Figure 4.19. It can be noticed that no statistically significant differences were found between the matrices C35, TMC and TMC-GP, and just a slight increase in the modulus or bending strength was registered when TMC was introduced as liquid phase of the cement. Since the fracture of the different cement matrices is fragile, as the samples break following a typical brittle failure (Figure 4.19d), the WOF was very low for all of them (Figure 4.19c).

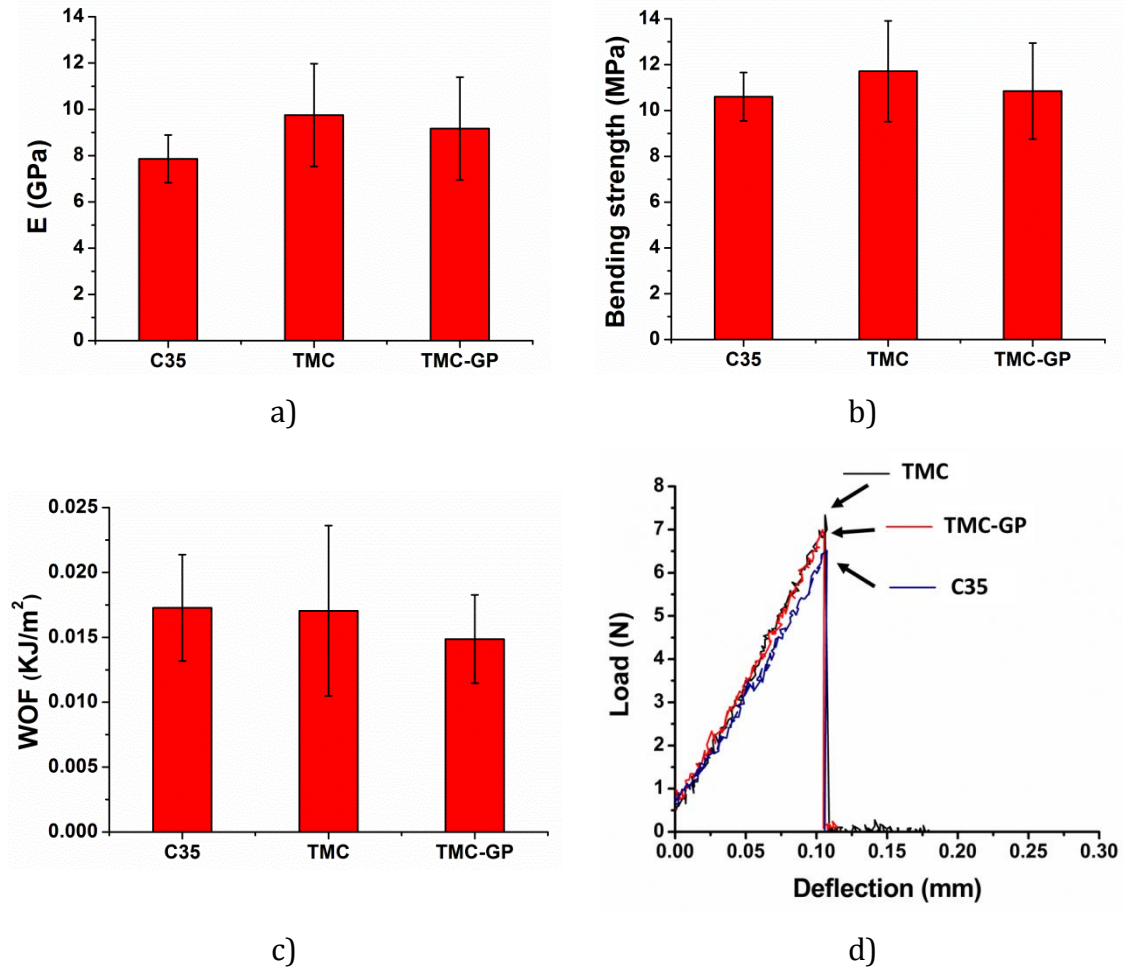


Figure 4.19- a) Young modulus (E), b) Bending strength (BS), c) Work of fracture (WOF) and d) example curves of matrices of CPCs. The samples are: the control which has water as liquid phase (C35), TMC based matrix (TMC) and TMC-GP based matrix (TMC-GP). No statistically significant differences were observed among the samples ($p>0.05$).

The crosslinking of TMC by adding GP in the liquid phase did not yield any benefits neither in mechanical properties (Figure 4.19) or notable changes in the matrix microstructure (Figure 4.17). Thus, for the preparation of FRCPCs, the matrix was based solely on TMC.

As shown in Figure 4.20, the matrices C40 and LA presented similar mechanical properties. The presence of LA in the matrix of CPCs tended to produce weaker materials (even if differences were not significant from the control C40), probably due to the lower transformation to CDHA (Table 4.5). As expected, since the L/P is higher (0.40 ml/mg instead of 0.35 ml/mg as in Figure 4.19), the mechanical properties of C40 are slightly lower than the one of C35.

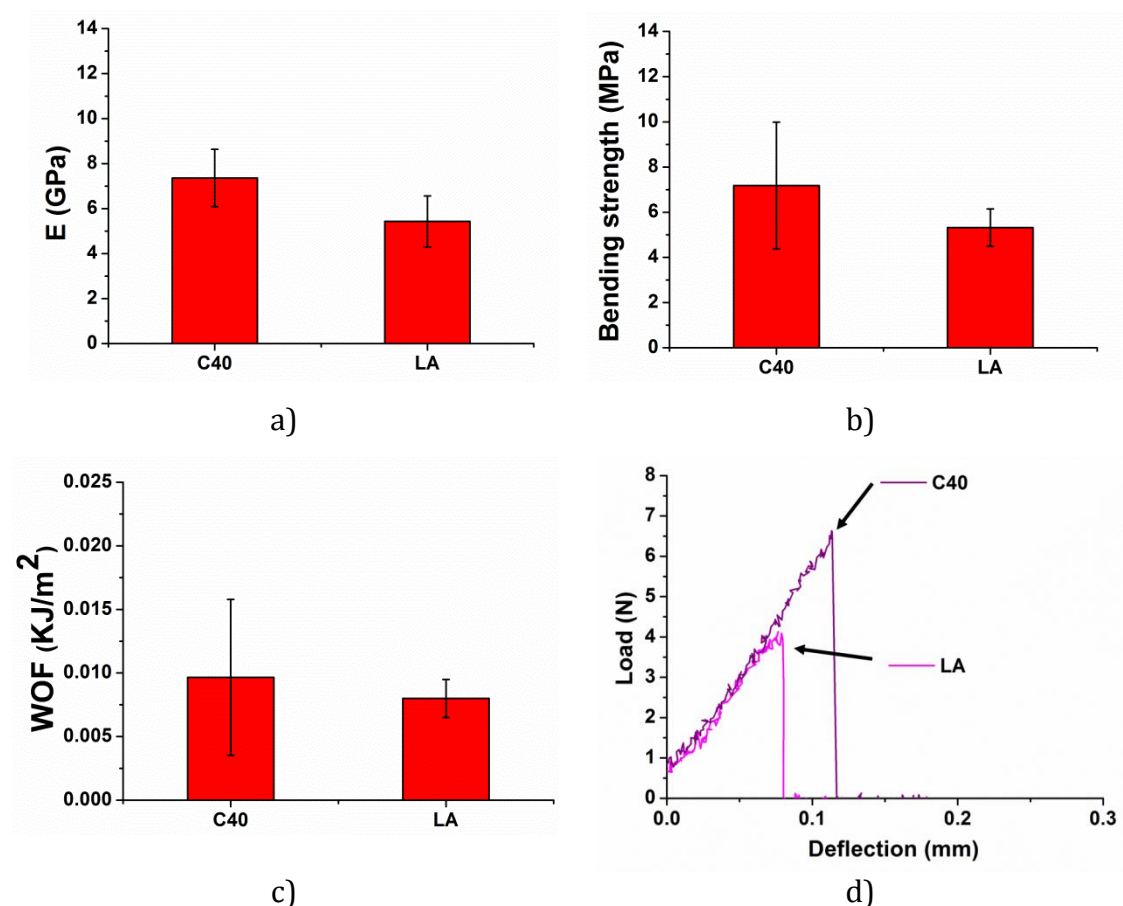


Figure 4.20- a) Young modulus (E), b) Bending strength (BS), c) Work of fracture (WOF) and d) example curves of pristine CPCs matrices with water in the liquid phase (C40) or with 10% LA in the matrix (LA). No statistically significant differences were observed among the samples ($p > 0.05$).

b) Contact angle

Figure 4.21 shows contact angles of the polymers used for reinforcement of CPCs with different wetting liquids. Comparing water contact angle of chitosan films with the one of PLLA films, it can be noticed that chitosan is more hydrophobic than PLLA. The contact angles of chitosan films using either water or 1 wt% TMC solution as wetting liquid is shown in Figure 4.21a. The contact angle of chitosan films with water was $95.9^\circ \pm 1.5^\circ$ while with TMC solution it decreased down to $80.7^\circ \pm 7.3^\circ$. This result indicates that chitosan is wetted better by the TMC solution than by water, and this may be relevant with regard to the adhesion between the chitosan fibres and the matrix in FRCPCs.

Similar behaviour was found in PLLA films. Figure 4.21b displays the contact angle of the PLLA film with water, which was $71.2^\circ \pm 3.1^\circ$, while with 10 v/v% LA it

decreased down to $61.5^\circ \pm 3.6^\circ$, reflecting an improved wettability of PLLA by LA, which is intended to be used here to produce stronger interface between fibres and matrix.

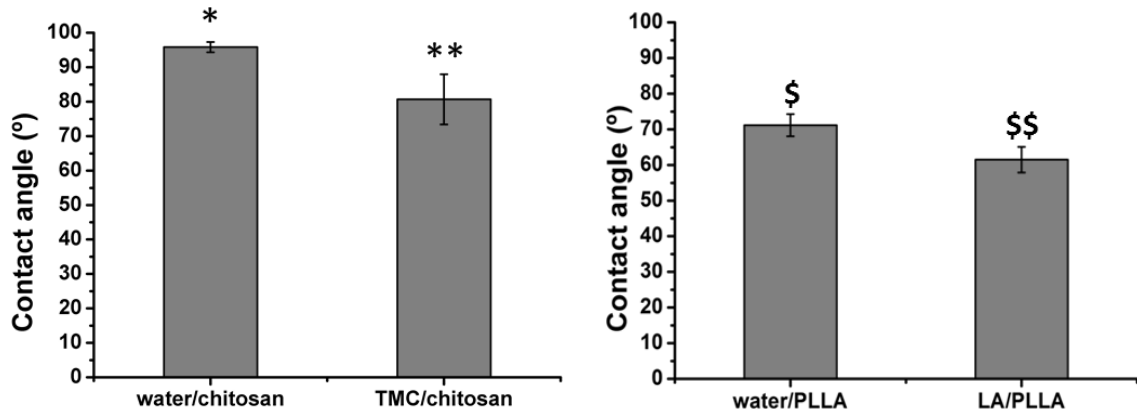


Figure 4.21 - Contact angle of a) water or TMC solution on chitosan film and b) water or LA solution on PLLA film. Groups indicated with the same symbol do not have statistically significant differences ($p > 0.05$).

c) Fibre Reinforced Calcium Phosphate Cements
c.1. Three-point bending test

Figure 4.22 shows the bending strength parameters of FRCPCs with different amounts of 8 mm long chitosan fibres (4, 8, 12 wt%). The addition of 8 wt% chitosan fibres to the control matrix (C35-f8) decreased significantly the Young modulus and bending strength with regard to its pristine counterpart (C35), probably due to low adhesion of the fibres to the matrix. In contrast, in the case of TMC matrix the addition of 8 wt% fibres did not result in a decrease of the elastic modulus and bending strength, and increased significantly the WOF. Other amounts of fibres led to worse results (TMC-f4 and TMC-f12) (Figure 4.22a). As it can be noticed in Figure 4.22b, bending strength of C35-f8 is lower than that of all the other samples, while the FRCPC specimens containing TMC and chitosan fibres tended to show lower (TMC-f4 and TMC-f12) or equal (TMC-f8) bending strength than their pristine counterpart (TMC). In terms of WOF (Figure 4.22c), all samples with fibres and TMC showed at least 10-fold improvement respect to pristine cement; TMC-f8 had the greatest WOF, significantly higher than C35-f8, the control matrix with the same amount of fibres (Figure 4.22c). A further increase of the fibre content (TMC-f12)

did not have a positive effect on the strength. The Load vs deflection curves (Figure 4.22d) showed a tension softening behaviour for all FRCPCs with TMC in the matrix and different chitosan fibre contents, while a negative action of the fibres was observed in the case of C35-f8. It is due to point out that even if the fibres were aimed to be randomly distributed, possibly the moulding process led to a partial alignment, as fibres of 8 mm were used and mould in 4 mm wide moulds.

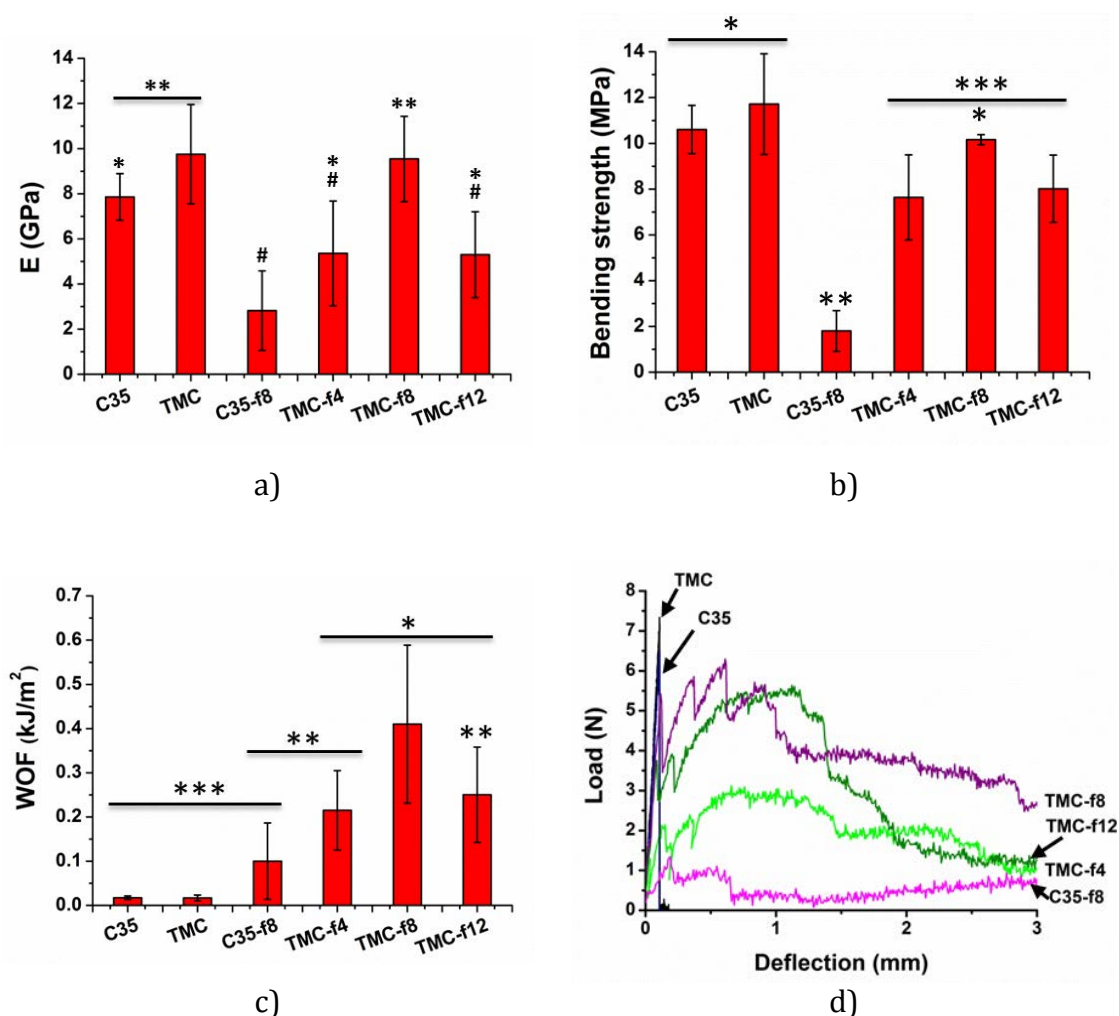


Figure 4.22 - Three-point bending tests: a) Young modulus (E), b) Bending strength (BS), c) Work of fracture (WOF) and d) example curves of FRCPCs: pristine control (C35), pristine cement containing TMC (TMC), control with 8 wt % chitosan fibres (C35-f8) and then the samples with TMC matrices and containing 4 wt% (TMC-f4), 8 wt% (TMC-f8) and 12 wt% (TMC-f12). Length of the fibres: 8 mm. Groups indicated with the same symbol do not have statistically significant differences ($p > 0.05$).

Figure 4.23 shows the bending properties of cements reinforced with PLLA yarns. Two different lengths were compared, 8 and 4 mm PLLA yarns were added at 2 wt% in the matrix containing either water or 10% LA. Samples were coded as f2 with 8 mm long yarns and those with 4 mm long yarns as f2s (for short fibres). As shown in Figure 4.23 the introduction of LA in the matrix reverted in a decrease (even if not

significant) of both Young modulus and bending strength. Comparing the control with water (C40) to the materials with the addition of PLLA fibres, it can be noticed that there was not significant improvement of Young modulus, but there was an improved bending strength of the material with shorter fibres (C40-f2s) compared to the pristine cement (C40). Concerning the materials containing LA, although the Young modulus was not modified by the addition of the monomer, the bending strength (Figure 4.23b) significantly increased by the addition of the PLLA yarns in the matrix, both in the case of long (LA-f2) and short (LA-f2s) yarns. However, the work of fracture was approximately the same in all FRCPCs (Figure 4.23c). Figure 4.23d shows bending curves: C40 and LA showed a brittle fracture, while the FRCPC samples showed a tension softening behaviour, which was faster in the case of shorter fibres (C40-f2s and LA-f2s), possibly due to a faster debonding and pull out. However, it is due to indicate that the dispersions among samples is really high.

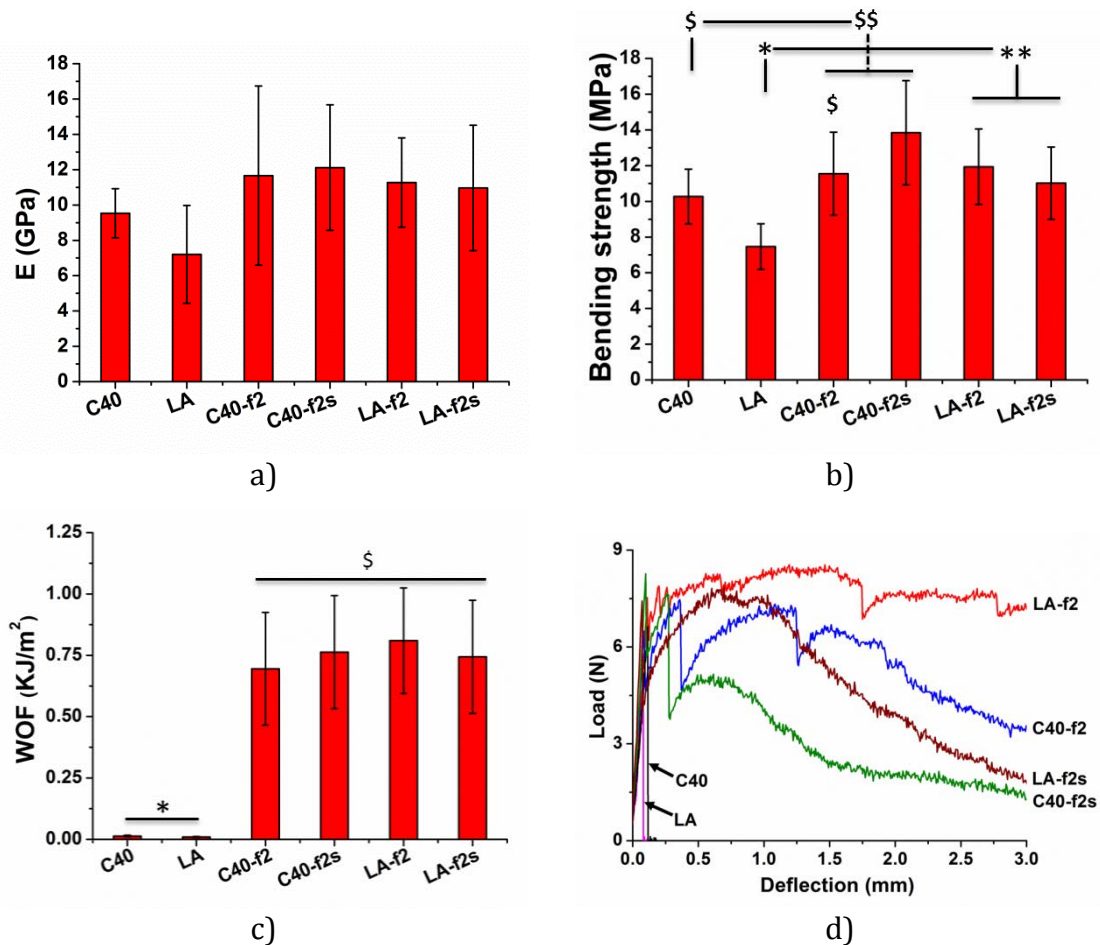


Figure 4.23- a) Young modulus (E), b) Bending strength, c) work of fracture (WOF) and d) example curves of FRCPCs. The samples are pristine cement (C40), cement with 10% LA in the matrix (LA) and their composite with 2 wt% of 8 mm long fibres (C40-f2, LA-f2) and with 2 wt% of 4 mm long fibres (C40-f2s, LA-f2s). Groups indicated with the same symbol do not have statistically significant differences. No statistically significant differences were observed among the elastic modulus of the samples ($p > 0.05$).

c.2. Scanning Electron Microscopy

Figure 4.24 shows that the randomly oriented fibres were not homogeneously distributed within the matrix but rather they concentrated in some areas, probably due to the manual pressure applied during the moulding process. Chitosan fibres generated macropores of the size of their diameter (200 μm , Figure 4.24b). Contrarily, the pores and fibres observed for PLLA yarn reinforced CPCs did not correspond to the $\approx 320 \mu\text{m}$ of yarn diameter (in Figure 4.24c and d) but were much smaller. It is possible that after cutting the yarns into 4 mm or 8 mm long segments, and then mixing them energetically with the cement, the yarn separated in its constituent fibres. Furthermore, important differences were noticed from sample to sample, due to the difficulties in the mixing and moulding processes to obtain high uniformity and reproducibility. This is reflected in the relatively high standard deviations associated to the different mechanical parameters obtained from the bending tests (section 4.3.3c.1).

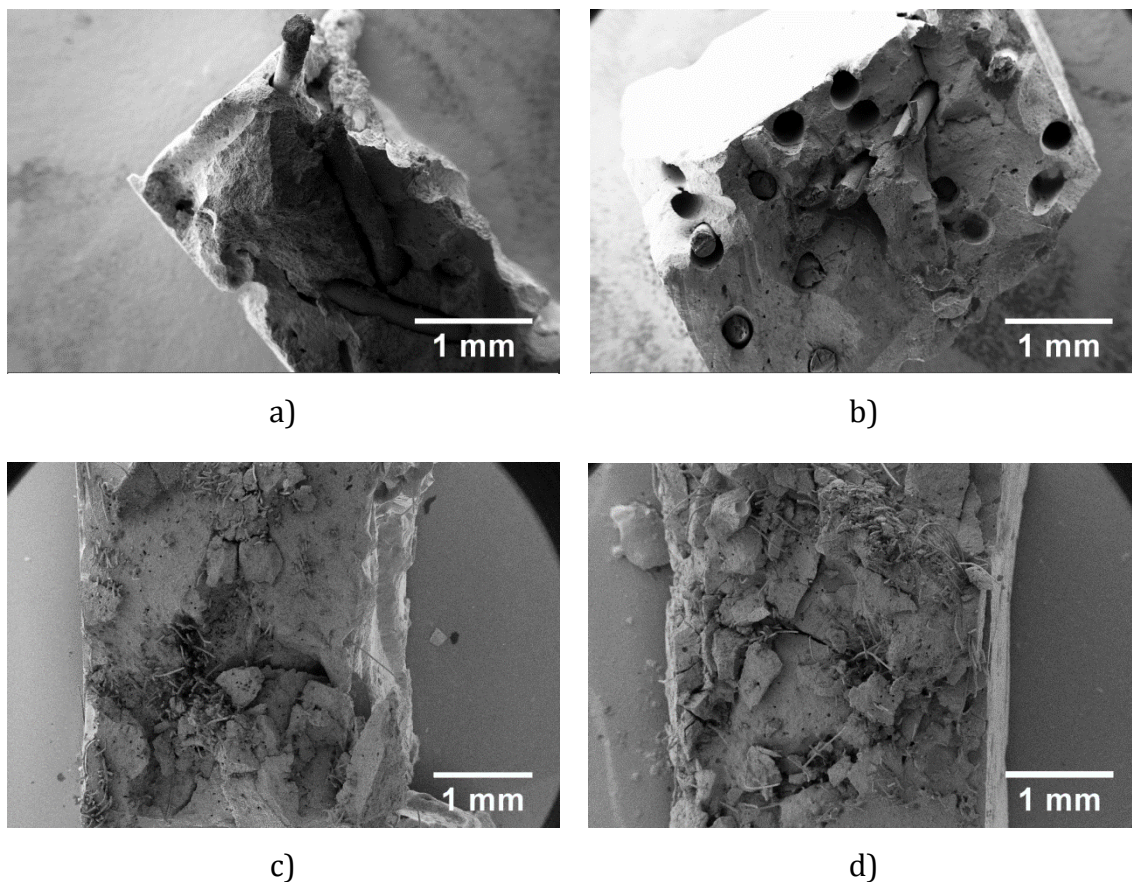


Figure 4.24 - SEM images representing a general view of different FRCPCs reinforced with chitosan fibres as a) C35-f8, b) TMC-f8, or with PLLA yarns c) C40-f2 and d) LA-f2.

Figure 4.25 shows scanning electron micrographs of the fibre/matrix interfaces of FRCPCs. Chitosan fibres seemed to show greater affinity to the matrix when it contained TMC, both for the fibres probably involved in the reinforcement of the matrix (Figure 4.25b versus a) and for the fibres embedded in the matrix which, due to their orientation, might have participated less in the mechanical reinforcement (Figure 4.25d versus c). As a matter of fact, it can be noticed that the gap fibre/matrix is smaller (or there is even continuity fibre-matrix) in TMC-f than C35-f8. Figure 4.25e shows the continuity fibre-matrix in TMC-f8 while Figure 4.25f displays the bridging of two chitosan fibres possibly by the TMC polymer.

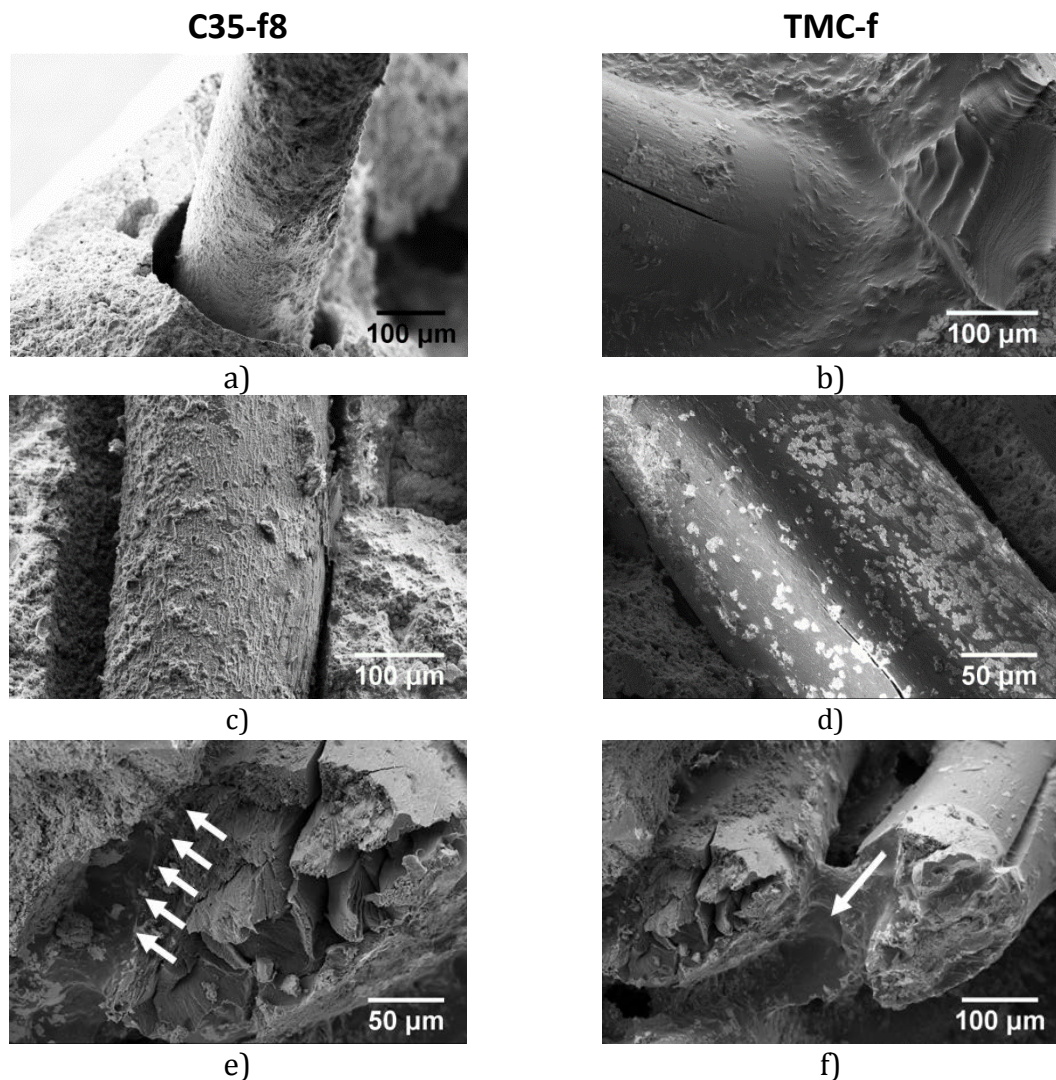


Figure 4.25- SEM images of fracture region after three-point bending tests of FRCPCs. a) chitosan fibre embedded in C35 (C35-f8), b) chitosan fibre embedded in TMC (TMC-f4), c) good adhesion of a fibre with the matrix in TMC-f8, d) TMC bridging two fibres in TMC-f8 (signalled by the arrow).

Figure 4.26 shows the interfacial transition zone (ITZ), which has been described in literature as the layer between fibre and matrix and it can be 5-100 μm thick (**Krüger, 2012**), of the materials which contain chitosan fibres. This layer can be either more porous and weaker or denser and stronger. In the case of the control (C35-f8) the matrix was a mixture of plate-like and small needle-like structures (Figure 4.26a and b). On the contrary, in TMC-f8 significant differences could be observed in the ITZ (Figure 4.26c), as it looked smooth revealing the presence of a layer of polymer in the ITZ (Figure 4.26d).

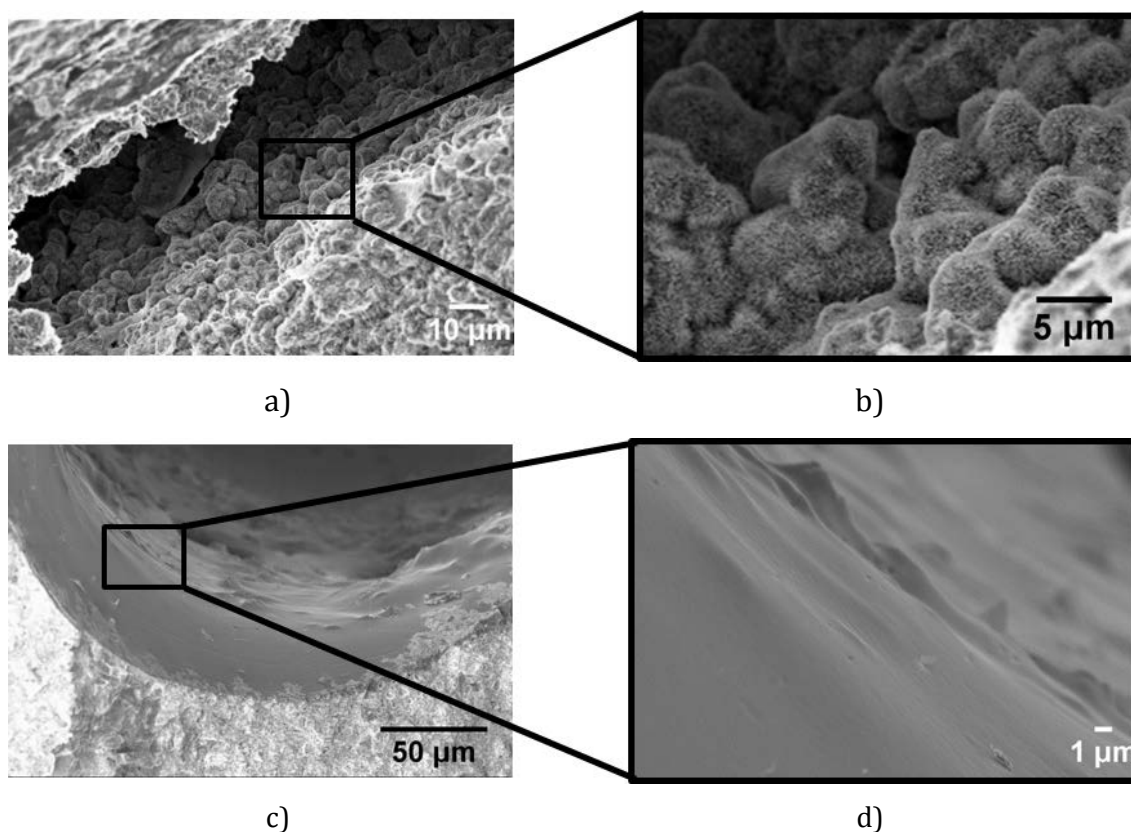


Figure 4.26- SEM images of the ITZ between chitosan fibres and control matrix C35, a) with a zoom of the microstructure of the selected area in b) and between chitosan fibres and TMC matrix, c) with zoom of the selected area in d).

As previously shown for chitosan fibres, the fracture zone of bending samples containing PLLA yarns was imaged by SEM with the aim to observe the interface fibre/matrix.

Figure 4.27 shows a gap fibre/matrix of the composites. In this case, the gap between the fibre and the matrix looked comparable in both C40-f2 and LA-f2.

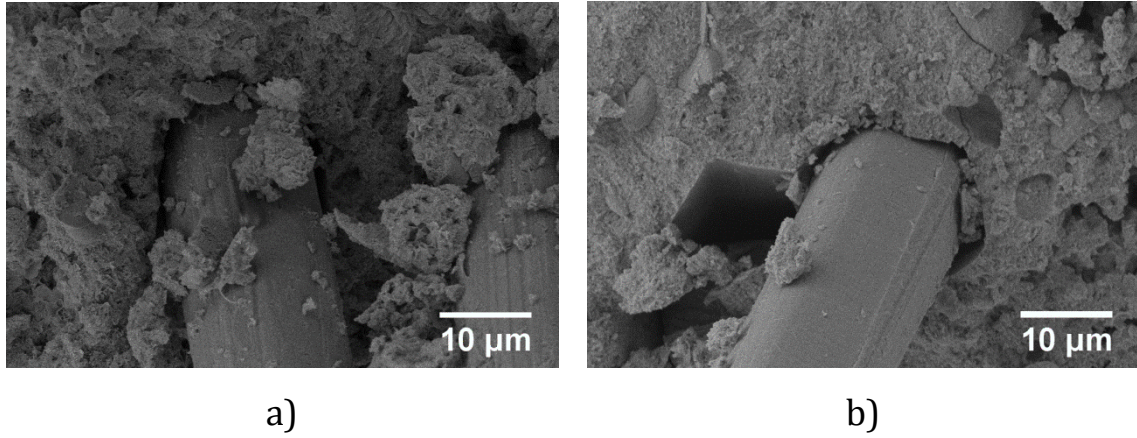


Figure 4.27- SEM images of the interface fibre/matrix a) C40-f2 and b) LA-f2.

4.3.4 Discussion

Calcium Phosphate Cements (CPCs) have shown many advantages (**Ginebra, 2010**). However, their poor mechanical properties limited their applicability to non-load-bearing applications. To this purpose, in the last 15 years, fibre reinforcement of CPCs has been widely investigated, with fibre types ranging from non-resorbable polymer or mineral fibres, to different resorbable polymer fibres (**Canal, 2011; Krüger, 2012**). In the last years the scientists' interest focused mainly on resorbable fibres as reinforcing agents. The strategy behind this choice is providing temporary mechanical support, and, after resorption of the fibres, allowing fluid and cell ingrowth (in the case of fibres or yarns with large diameters) in the CPC to enhance bone resorption of the implant and new bone formation. Since it is known that the behaviour of the interface fibres-matrix determines this first crack strength of the composite (**Nelson, 2002**), this work aimed at improving the strength at the interface.

Fibre Reinforced Calcium Phosphate Cements (FRCPCs) with improved adhesion matrix-fibre were obtained in this work by introducing a polymer with high affinity to the fibres used as reinforcing agent. Specifically, chitosan fibres were coupled with Trimethyl Chitosan (TMC) and PLLA yarns with LA (their forming monomer), in the form of randomly oriented distributed fibres. Each cement formulation was optimised in fibre concentration and/or length depending on both reinforcement and workability. In this work, amounts of chitosan fibres < 4 % were discarded because they were too low to provide any reinforcement, whereas in the case of PLLA yarns, amounts > 2 % were not used since they reverted in poorer mechanical properties as well as worse workability. This could be explained by the fact that in an excess of fibres, the contacts fibre/matrix would be replaced by contacts fibre/fibre since the yarns tend to aggregate (**Li, 2003**).

The introduction of the additives caused some changes in the cement matrix: the addition of Trimethyl Chitosan (TMC) to the liquid phase of CPCs remarkably modified the setting reaction, as it can be noticed through the pH evolution in Figure 4.14a. Instead of the fast basification (in the range of seconds) due to the α -TCP dissolution and then a slow decrease (due to the precipitation of CDHA) until pH

around 7 is reached, as it happened for α -TCP mixed with water, 1% TMC aqueous solution as liquid phase led to a gradual increase (from pH 6.5 up to pH around 7 in 29h). A similar behaviour was obtained when collagen was used as additive in liquid phase by Perez *et al.* (Perez, 2013a). This was probably the cause of a slowing down of the dissolution-precipitation process of α -TCP (Figure 4.16a) which led to slightly lower conversion to CDHA (6% of α -TCP was unreacted) and could possibly be related to the lower SSA measured. Differently, when the additive was TMC-GP, SSA increased, maybe due to the fact that the hydrogel could act as further nucleation point.

A different behaviour was observed when LA was present as liquid phase in the CPCs. The setting pH in the LA solution was different, as the low pH of 10 v/v% LA in the solution used as liquid phase led to a different kinetics of the dissolution. The low pH stimulated a fast dissolution rate at L/P = 200 ml/g (Figure 4.14b), as α -TCP was completely dissolved, while at L/P = 20 ml/g the solution was supersaturated (Figure 4.14c). Although the low pH, no brushitic phase was found in the final CPCs even if it is the most stable phase at pH lower than 4.5 (solubility diagrams reported in chapter 2, Figure 2.5). It can be speculated that possibly brushite temporary formed in the beginning of the reaction and progressively converted to HA during the 7 days setting, as previously described by Leroux *et al.* (Leroux, 1999). The lower SSA of the cement containing 10% LA compared to the one with water, agrees with the incomplete conversion of α -TCP to CDHA (87 %).

Initial and final setting times were difficult to measure due to the presence of the polymer (Figure 4.15), which was related to the Gillmore needles always producing a mark on the surface of CPCs in the timeframe studied (100 min). Notably, in cements containing TMC or TMC-GP, cohesion was immediate, possibly due to the higher viscosity of the solution and to the fact that the polymer chains in solution might act as nucleation points where α -TCP particles could start reacting. Similarly, cohesion time was really short for cements containing LA, but a slightly higher than the previous ones.

In this work, the addition of TMC to the liquid phase of the cement tended to improve compressive strength but did not affect it significantly (Figure 4.18).

Differently, Xu and co-workers (**Xu, 2004**) found that the compressive strength of a pristine apatitic matrix was significantly increased when a chitosan derivative was introduced in the liquid phase (15% chitosan lactate, a chitosan salt containing the lactate counter-ion); the higher concentration they employed together with the different structure of the molecule and the different pH of their liquid phase could influence the setting reaction and, thus, the strength of the final material. The addition of GP to TMC to form a hydrogel reverted in a slight decrease of the mechanical properties in compression (Figure 4.18). For this reason, the final FRCPCs were based simply on TMC matrix in combination with chitosan fibres of 8 mm length and 200 μm diameters.

In order to estimate how the fibres would behave in contact with the wetting liquid, static contact angles were performed on flat polymer films used as models for the surface.

The water contact angle of chitosan films was similar to values found in literature for this material (**Bumgardner, 2003**), it was above 90° corresponding to a hydrophobic material. The wettability of chitosan with TMC solution (Figure 4.21a) was better than with water, which reverted into an improved adhesion fibre/matrix (Figure 4.25). Similarly, the contact angle of LA solution as wetting solution and PLLA films as substrate was lower than water contact angle on PLLA films, indicating an improved wettability. Creating a stronger chemical bond between fibres and matrix could be the keystone to improve mechanical properties. However, the expectation that the better wettability could revert into better adhesion fibre-matrix and thus higher toughness, was only partially accomplished.

Each type of composite was used to investigate different effects. Cements containing chitosan fibres were used to investigate the effect of different amounts of fibres, while FRCPCs with PLLA yarns were used to study two different lengths.

The addition of chitosan fibres or PLLA yarns affected differently the cements. First of all, it has to be reminded that chitosan fibres have worse mechanical properties than PLLA yarns (as shown in Table 4.3). Thus, the theoretical values for the FRCPCs (corresponding to eq. 4.2 and 4.3) are lower in the former than in the latter case. Blending of chitosan fibres in the CPC control matrix (C35-f8) caused a really low

Young modulus as well as low bending strength, probably due to low adhesion fibre/matrix, also confirmed by SEM images (Figure 4.25). This could be due to the fact that the fibres are smooth, so pull out may take place quite quickly due to poor interactions. Differently, PLLA yarns slightly improved (even if not significantly) both Young modulus and bending strength of CPC matrices, possibly due to better interlocking of the fibres of the partially separated yarn. No differences between the two fibre lengths (C40-f2 and C40-f2s) were found. In the case of addition of chitosan fibres the WOF was not improved (Figure 4.22c), the low values and the high error bar did not allow concluding that C35-f8 sample was significantly tougher than pristine cements (C35). In the case of the addition of PLLA fibres the improvement in WOF was remarkable (Figure 4.23c). Some studies reported the use of chitosan fibres with large diameters implanted in vivo (**Lian, 2008; Lian, 2009**) finding an improvement in compression. However, in those studies fibres were coated with collagen, while in our case there is no coating. Xu *et al.*, widely studied the addition of PLGA yarns to CPCs and, similarly to us, they found an increase of the mechanical properties by the fibre addition (**Xu & Quinn, 2002; Burguera, 2005; Xu & Simon, 2004**).

The addition of TMC in the matrix improved mechanical properties. Similarly to compressive strength, the Young modulus in bending of TMC pristine cements was higher than the cement with water possibly due to the plasticizer effect of the polymer. This increase was maintained for the cement with 8 wt% of fibres (TMC-f8) but decreased for lower (TMC-f4) and higher (TMC-f12) fibre quantities. The decrease itself was similar to other works (**Xu, 2000; Xu, 2002; Xu, 2004a; Xu, 2004b; Gorst, 2006**) where the addition of fibres or meshes caused a decrease of the Young modulus with respect to the pristine sample. The decrease obtained with a too high amount of fibres agrees with previous works in the literature (**Xu, 2000; Pan, 2007; Zuo, 2010**) and confirms the need for adjusting the optimal fibre amount for each kind of fibre. Bending strength followed the same trend of the Young moduli. The addition of chitosan fibres decreased the values compared to the pristine cement with TMC, either slightly (TMC-f8) or significantly (TMC-f4, TMC-f12). Contrarily to TMC, the addition of LA caused a decrease of the mechanical properties of the pristine cement, possibly due to the lower conversion ($\approx 10\%$ less)

of α -TCP to CDHA (Table 4.5). However, the mechanical properties lost with the addition of LA were recovered with the addition of PLLA yarns. Furthermore, the addition of PLLA yarns reverted in significantly higher bending strength in the case of LA-f2 and LA-f2s compared to LA cements. As in the control matrix, no differences were found between the different lengths.

Comparing the elastic moduli of the CPCs reinforced with PLLA ($11 \div 12$ GPa) and of the one containing 8 wt% fibres and TMC (TMC-f8, 10 ± 2 GPa) with those of cortical bone ($13 \div 15$ GPa (**Ziopus & Currey, 1998**)), it can be concluded that the values are quite close. Notwithstanding, bending strength displayed values which were much lower than the one of cortical bone, which has been estimated between 50 and 200 MPa (**Barinov, 2010; Currey, 1988**). Regarding WOF, the FRCPCs containing chitosan fibres and TMC showed a remarkable increase of the WOF (Figure 4.22c), especially TMC-f8 where the WOF was the highest. Even if differences among FRCPCs reinforced with PLLA yarns were not significant, LA-f2 had the highest WOF, as the value found was 0.81 ± 0.22 kJ/m², which was closer to the lower limit of cortical bone (which has been reported to range between 1.5 and 15 kJ/m² (**Currey, 1975**)), being much higher compared to the one of pristine cements C40 (50-fold lower) or LA (80-fold lower).

The causes of the differences in mechanical properties, especially in the work of fracture (WOF), can be attributed to the different parameters: first of all the different morphology of chitosan fibres and PLLA yarns (Figure 4.12). The former are smooth cylinders, while the latter are yarns formed by 68 false twist fibres, feature which probably increased friction work prior to debonding and pull out. However, as it was observed that the yarns partially separated into the individual fibres during the cement preparation, other factors have to be considered. For instance, the higher tensile breaking stress of the PLLA yarns, and their higher surface area ratio can justify their better performance compared to chitosan fibres.

By comparing the curves reported in Figure 4.22d or Figure 4.23d, different behaviours could be observed: in fact, upon applying bending load on pristine CPCs (Figure 4.19), either prepared with water (C35, C40) or additives in the liquid phase (TMC and LA), stress increased until its intensity reached a critical value (at a fault

in the microstructure) typical of brittle solids. When this happens in a monolithic CPC, due to fast propagation from the initial crack, catastrophic failure occurs (**Callister, 2009**). In FRCPCs, the linear elastic region ended with the first cracking of the matrix but the fracture is not catastrophic. In this specific case, the behaviour seemed to be between tension softening and, in some curves, tending to strain hardening. The material underwent multiple cracking, leading to a non-catastrophic failure. However the dispersion between samples is quite high.

In the materials reinforced with chitosan, the best result was obtained in one case by TMC-f8, since a further increase of fibre amount reverted in decreased mechanical properties. The addition of TMC in the matrix enhanced significantly the mechanical properties compared to C35-f8, due to improved adhesion shown by the SEM images (Figure 4.25 and Figure 4.26). However the enhancement was limited. Higher mechanical properties were obtained by adding PLLA yarns to CPCs. In this case the additive to the liquid phase (LA) initially caused a decrease of the mechanical properties, which was recovered by the addition of the reinforcing agent with no differences between the two yarn lengths. Nonetheless this recovery was not enough to obtain better results than the control materials with fibres (C40-f2 and C40-f2s).

4.3.5 Conclusions

In this work it has been shown that it was possible to obtain FRCPCs with good interface fibre-matrix, using additives in the matrix together with polymeric fibres with great affinity for each other. Chemical similarity between chitosan fibres and TMC (a chitosan derivative) in the liquid phase resulted in good interfacial adhesion, as revealed by SEM. As result, the bending strength of the material was maintained when the fibres were added, together with a significant improvement of the WOF compared to FRCPCs without TMC in the liquid phase or the pristine cement. However, the good adhesion did not revert in sufficient improvement, compared to the bone, probably due to the smoothness of the fibres, so further investigations will need to be performed in this line. Although SEM images proved a good integration of the PLLA yarns in the matrix due to the improved wettability of PLLA fibres from LA,

there was not a significant improvement of the mechanical properties compared to the cements containing water.

4.4 Calcium phosphate cements reinforced with plasma treated fibres

4.4.1 Introduction

In the line of the previous chapters, in the present section the focus is put on enhancing the adhesion at the interface between fibres and matrix in FRCPCs. The strategy in this case relies on surface modification of the fibres with non-thermal low pressure plasma. In the present work the surface effects of low pressure oxygen plasma treatments on PLLA multifilaments are evaluated. The plasma-treated multifilaments are then incorporated to a CPC matrix as a reinforcing phase. The influence of the surface modification of the PLLA multifilaments on different processing parameters of relevance in CPCs, as well as on the mechanical performance of FRCPCs is investigated.

4.4.2 Experimental

a) Preparation of liquid and solid phase

α -TCP powders were obtained as described in section 3.3.1. 2 wt% of precipitated hydroxyapatite (Alco) was added as a seed in the powder. The same PLLA yarns and PLLA films described in 4.3.2a.2 were used in this work.

The liquid phase employed consisted of a 2 wt% solution of Na_2HPO_4 in MilliQ water.

b) Preparation of fibre-reinforced cements

For the preparation of fibre-reinforced CPCs, PLLA multifilaments were cut into 4 mm length. 1.8 wt% of staple multifilaments were blended with the solid phase of the cement prior to the addition of the liquid phase to obtain a random distribution of fibres in the matrix (Figure 4.28).

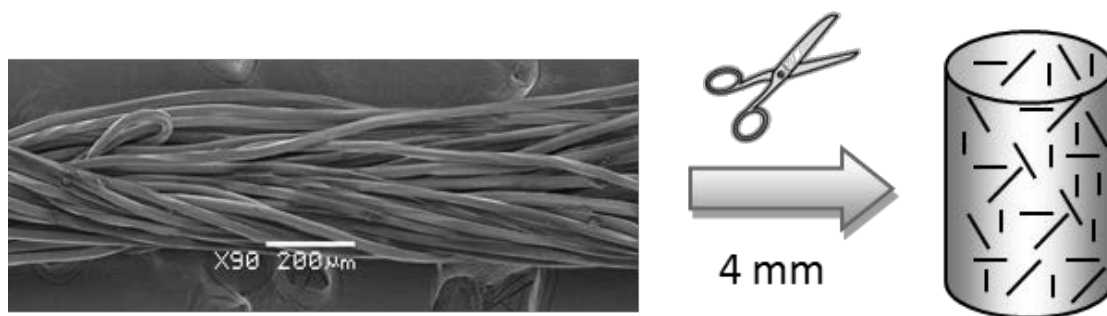


Figure 4.28- Scanning Electron Micrograph of the PLA yarns with representation of the random distribution of PLLA yarns in the CPC composite.

Cements were prepared by mixing the powder phase with the liquid phase at L/P ratio of 0.35 in a mortar for 1 min. Samples devoted to characterisation were allowed to set in Ringer’s solution in 6 mm diameter x 12 mm height cylindrical moulds for 7 days at 37°C. Samples devoted to bending tests were cast onto rectangular moulds of 3 x 4 x 50 mm³ and allowed to set in the same conditions.

c) Low Pressure Plasma treatment

PLLA multifilaments were treated with low pressure plasma in a Diener Femto reactor composed of a quartz chamber of 2 l. Multifilaments were laid horizontally on a quartz tray (Figure 4.29) and treated with O₂ plasma at 100 W and 0.40 mbar for either 30 s or 5 min. The treatment conditions employed were selected according to a previous screening performed with different plasma treatment times, powers and pressures by using contact angle measurements and SEM imaging.

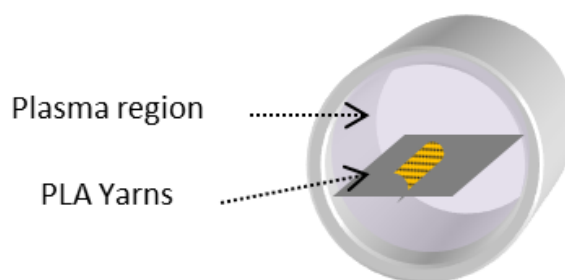


Figure 4.29- Scheme of the low pressure plasma reactor employed for the treatment of the yarns

To avoid ageing of the plasma-treated samples all characterisation and the fabrication of the cements was performed immediately after treatment (Canal, 2004).

d) **Contact angle**

The contact angle of untreated and plasma-treated PLLA films was determined as in 4.3.2c.5.

e) **X-Ray Photoelectron Spectroscopy**

The chemical composition of the PLLA films was analysed by XPS with a SPECS (Germany) using an Al non monochromated source XR50 (200 W and 14 kV) with an analyser Phoibos 150 MCD-9 with pass energy of 25eV, high resolution steps of 0.1eV, chamber pressure of 5.109 mbar and using a Flood gun FG15/40. Peak deconvolution was performed with CasaXPS software.

f) **Scanning Electron Microscopy**

Topography of untreated and plasma treated PLLA fibres and also of the cements' microstructure and of their fracture region was studied by Field-Emission Scanning Electron Microscopy using a *Jeol JSM-5000/5610* SEM. Samples were Au-coated before SEM observation. Observations were carried out at 10 kV working voltage.

g) **Cement's characterisation**

g.1. **Initial and final setting time**

Initial and final setting times of the CPC pastes and of PLLA-CPC composite pastes were measured as in 3.3.3.c.

g.2. **Specific surface area and porosity**

The specific surface area (SSA) of set cements and composites' was measured by Nitrogen adsorption according to the BET method (ASAP 2020 Micromeritics), and their porosity and pore size distribution were determined by Mercury Intrusion Porosimetry (MIP, Micromeritics Autopore IV 9500). In both cases, composite samples were evaluated after setting and also after thermal treatment at 250°C for 2h to eliminate the PLLA fibres. For each N₂ adsorption and MIP experiment, 5-6 cylindrical samples (6 mm diameter x 12 mm height) were measured.

g.3. Three-point bending tests

The flexural strength was measured by three-point bending using the same parameters described in 4.3.2c.7. A minimum of 8 specimens were tested in flexion for each kind of treatment.

h) Statistics

Statistical differences were determined using one-way ANOVA at 95% confidence with Tukey's post-tests using Minitab 16 software (Minitab, Inc., State College, PA). Statistical significance was noted when $p < 0.05$.

4.4.3 Results

a) Surface effects of plasma on PLLA filaments

Chemical modifications on the surface of PLLA by the O₂ low pressure plasma treatment performed were investigated by evaluating the surface chemistry by X-ray Photoelectron Spectroscopy as well as the Wettability by static contact angle measurements (Table 4.7).

Table 4.7- X-ray photoelectron spectroscopy and contact angle of PLLA films used as model surface.

PLLA films				
Reference	Atomic percentage			θ_s (°)
	C1s	O1s	O/C	
UT PLLA	61.15	38.85	0.63	70.0 ± 0.7
0.5min O ₂ Plasma PLLA	58.23	41.77	0.72	61.9 ± 0.9
5min O ₂ Plasma PLLA	58.93	41.97	0.71	62.5 ± 1.3

The chemical composition on the surface of untreated (UT) PLLA agrees with its theoretical composition (C₃H₄O₂)_n, with 60% C and 40% O. After O₂ low pressure plasma treatment either for 0.5 or 5 min similar increase in the oxygen contents was obtained, with a simultaneous decrease of the carbon contents. Interestingly, the O/C ratio of PLLA showed very good linear correlation with the contact angle (Figure 4.30), which exhibited a decrease of nearly 8°, increasing the hydrophilicity of the fibres.

The untreated PLLA fibre surface shows smooth topography typical for synthetic fibres (Figure 4.30). The topographical effects of O₂ low pressure plasma on the multifilaments were mild at 0.5 min of treatment, which had slightly lower contact angle and slightly higher O/C ratio. In contrast, clear topographic modifications, following a regular pattern perpendicular to the fibre axis, which can be possibly attributed to preferential etching on the amorphous regions of the polymer, were observed for 5 min low pressure plasma treated PLLA fibres.

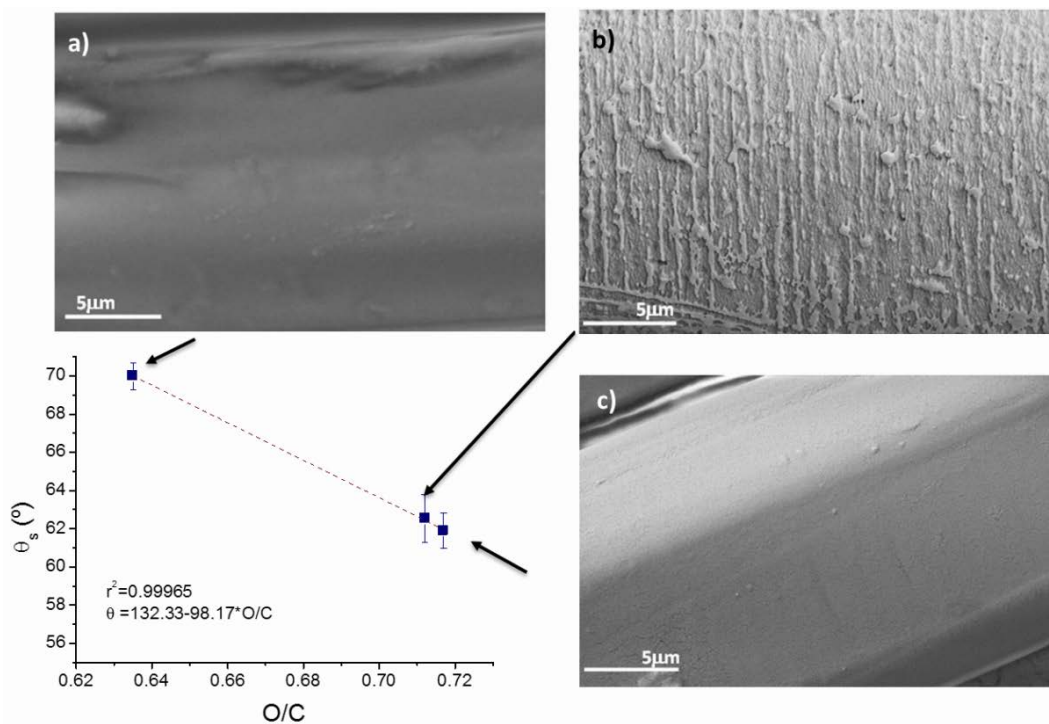


Figure 4.30- Static contact angle of untreated or plasma-treated PLLA with respect to their O/C ratio and scanning electron micrographs of the PLLA fibre surface (a) Untreated, and treated with low pressure O₂ plasma for (b) 0.5 min and (c) 5 min.

b) Effects of fibre addition to the cements

After surface modification of the multifilaments with low pressure plasma, they were introduced randomly as short staple fibres in the Calcium Phosphate Cements. Different parameters are relevant when evaluating the processability of CPCs, as, for instance the setting time. As shown in Table 4.8, the initial setting time of the pristine CPC (C) is of 10 min, while the final setting time is around 30 minutes. Introduction of untreated PLLA multifilaments (C + UT PLLA) reduced the initial setting time to 6 minutes, while the final setting time remained unchanged. The plasma treatment on the PLLA multifilaments led to a significant reduction (of 66%)

in the final setting time of the CPC composites, with no recordable differences among the low pressure plasma treated PLLA multifilament composites.

Table 4.8- Initial and final setting times of the CPC-PLLA fibre composites

Reference	$t_{\text{initial}}^{\text{setting}}$ (min)	$t_{\text{final}}^{\text{setting}}$ (min)
C	10	30
C + UT PLLA	6	31
C + 0.5min Plasma PLLA	4	10
C + 5min Plasma PLLA	4	10

As shown in Figure 4.31, pristine CPCs presented a pore entrance size distribution with a main peak at 0.01 μm , corresponding to hydroxyapatite intercrystallite spaces. To simulate the voids that would be left by the multifilaments after resorption, PLLA-CPC composites where the fibres have been eliminated by burn out are shown, revealing a new peak centred at 10 μm , which corresponds to the diameter of the individual fibres and not the multifilament. The total porosity of the materials was around 32 % and slightly increased in the PLLA-CPC composites after burn-out of the fibres. As shown by the SEM micrographs in Figure 4.31a, during blending of the CPC paste, the fibres in the 4 mm staple multifilaments were separated, confirming that the final distribution in the CPC-PLLA composites was as random individual fibres.

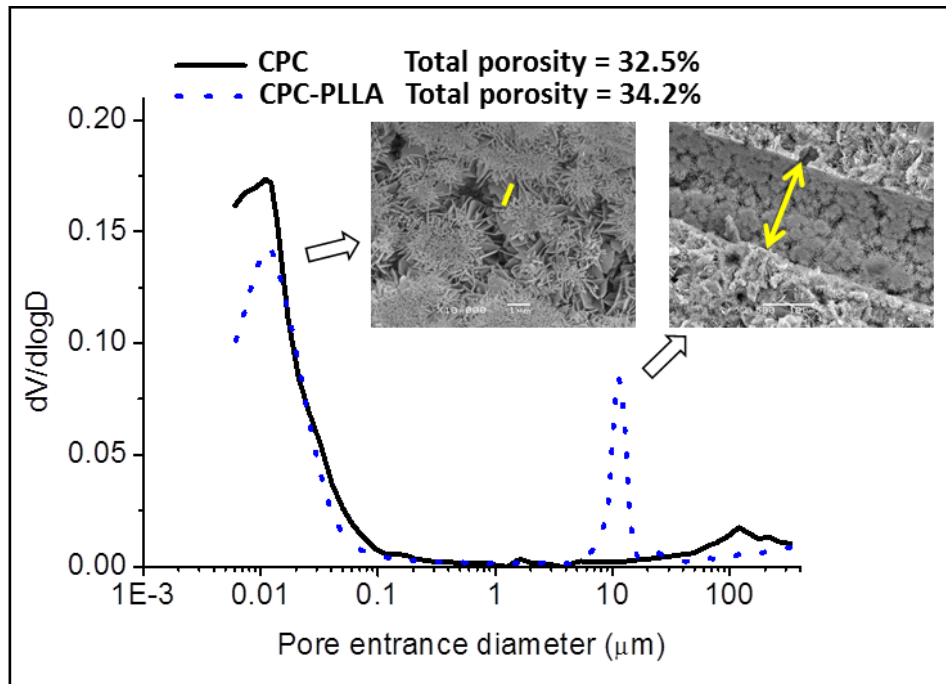


Figure 4.31- Entrance pore size distribution of CPCs, and of PLLA-CPC composites after burn-out of PLLA. The lines in the SEM images indicate the intercrystallite distance corresponding to the peak, and the void in the CPC corresponding to the diameter of a single PLLA fibre.

Both when using untreated PLLA multifilaments or plasma-treated ones, the fibres were apparently well integrated in the calcium-deficient hydroxyapatite (CDHA) crystal network, according to the different images of Figure 4.32. The set CPC-PLLA composites were constituted by a network of plate-like CDHA plates grew normally disregard of the presence of the PLLA fibres, so there was good contact between the fibres and the CPC matrix.

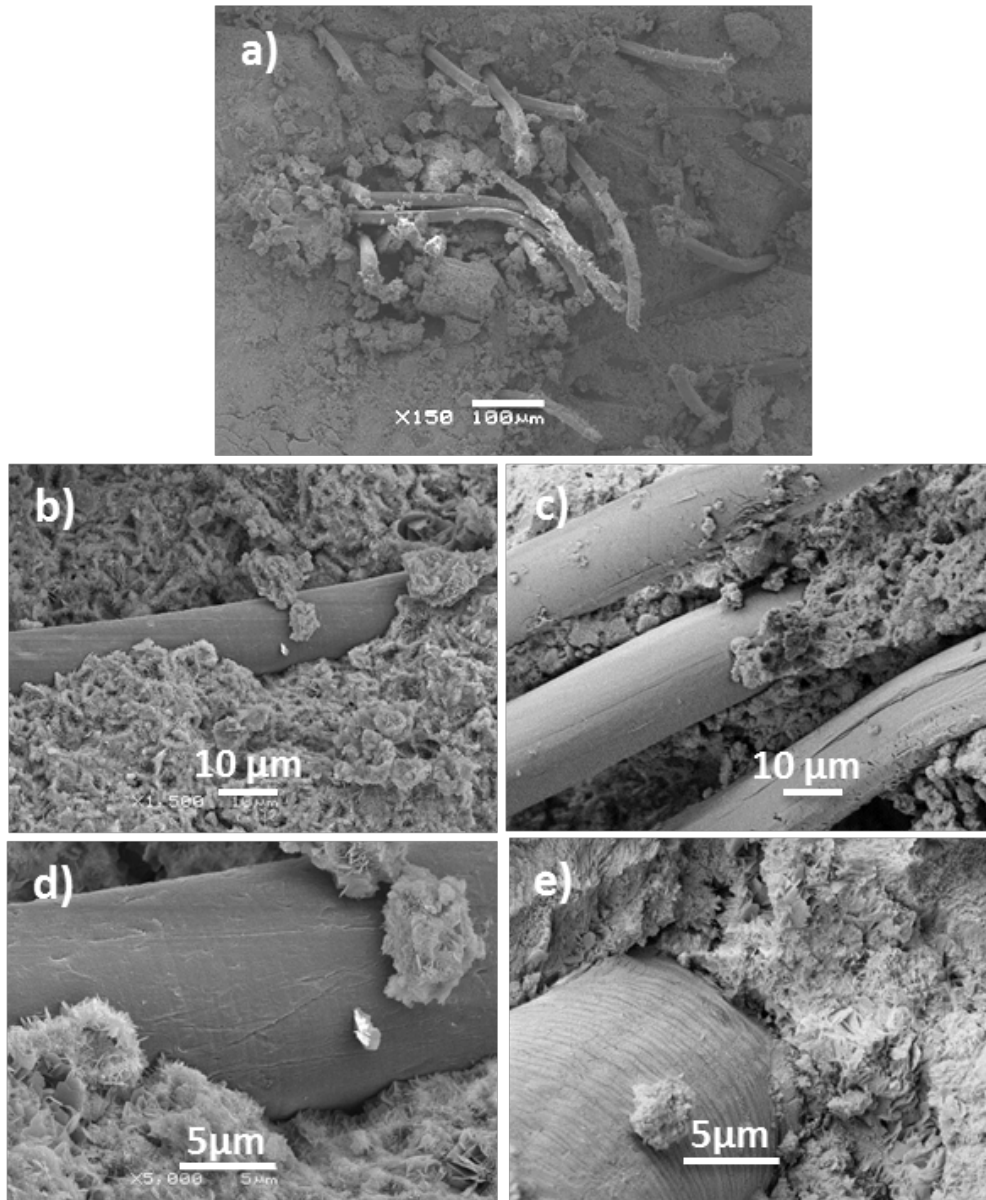


Figure 4.32- Scanning electron micrographs of PLLA-CPC composites (a, b, d) Untreated, and (c, e) treated with O₂ low pressure plasma for 5 min at different magnifications.

The mechanical properties recorded in the 3-point bending tests of the CPC-PLLA composites, either untreated or plasma treated, are shown in Figure 4.33. In fact, the elastic modulus and the bending strength decreased with the introduction of untreated PLLA fibres in the CPCs, while as expected, the work of fracture increased. Low pressure plasma treatment of the PLLA yarns led to an improvement in the mechanical properties, as bending strength and elastic modulus recovered up to values close of those of pristine CPC while work of fracture was nearly doubled with respect to the rest of CPC-PLLA composites.

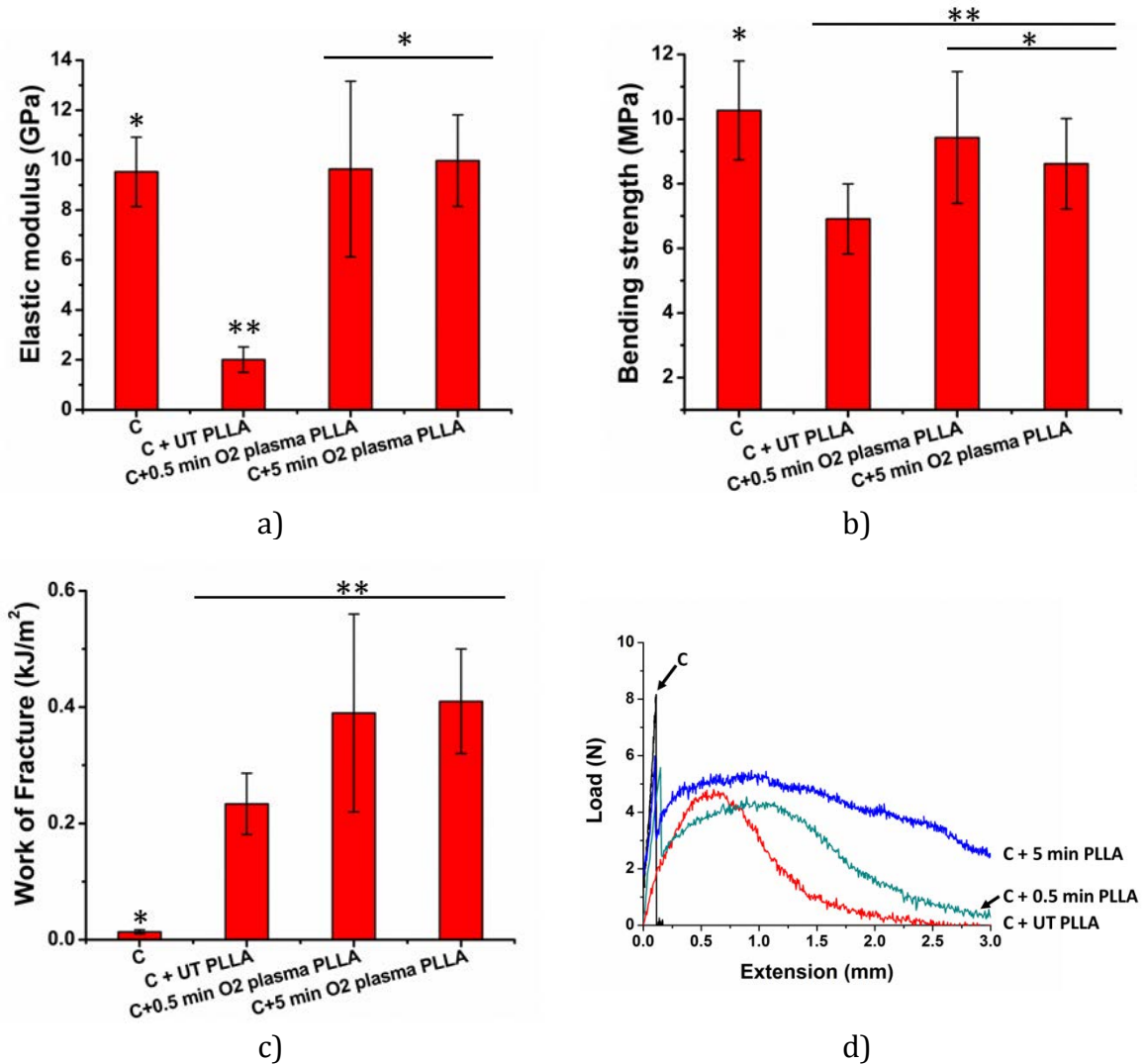


Figure 4.33- Flexural properties obtained from three-point bending tests (a) Elastic modulus, (b) Bending strength and (c) Work of Fracture of the different Calcium Phosphate Cement-based materials tested. Groups indicated with the same symbol do not have statistically significant differences ($p>0.05$).

Analysis of the load-deflection curves during the bending tests (Figure 4.34) showed different failure behaviour; pristine CPC underwent critical fracture, while the reinforced CPCs with untreated PLLA fibres displayed a decrease in the peak load associated with the fracture of the matrix, followed by a more ductile post-peak evolution. In contrast, plasma-treated fibres led to PLLA-CPC composites with sustained load carrying capacity. Close observation of the fracture surface of the CPC-PLLA composites after the bending test (Figure 4.34) confirmed that the adhesion at the interface fibre-CDHA was different in the different composites. Those prepared from untreated PLLA fibres showed a space between the matrix and the fibre, while plasma-treated fibres presented no discontinuity between the matrix and the fibre surface after the flexural tests.

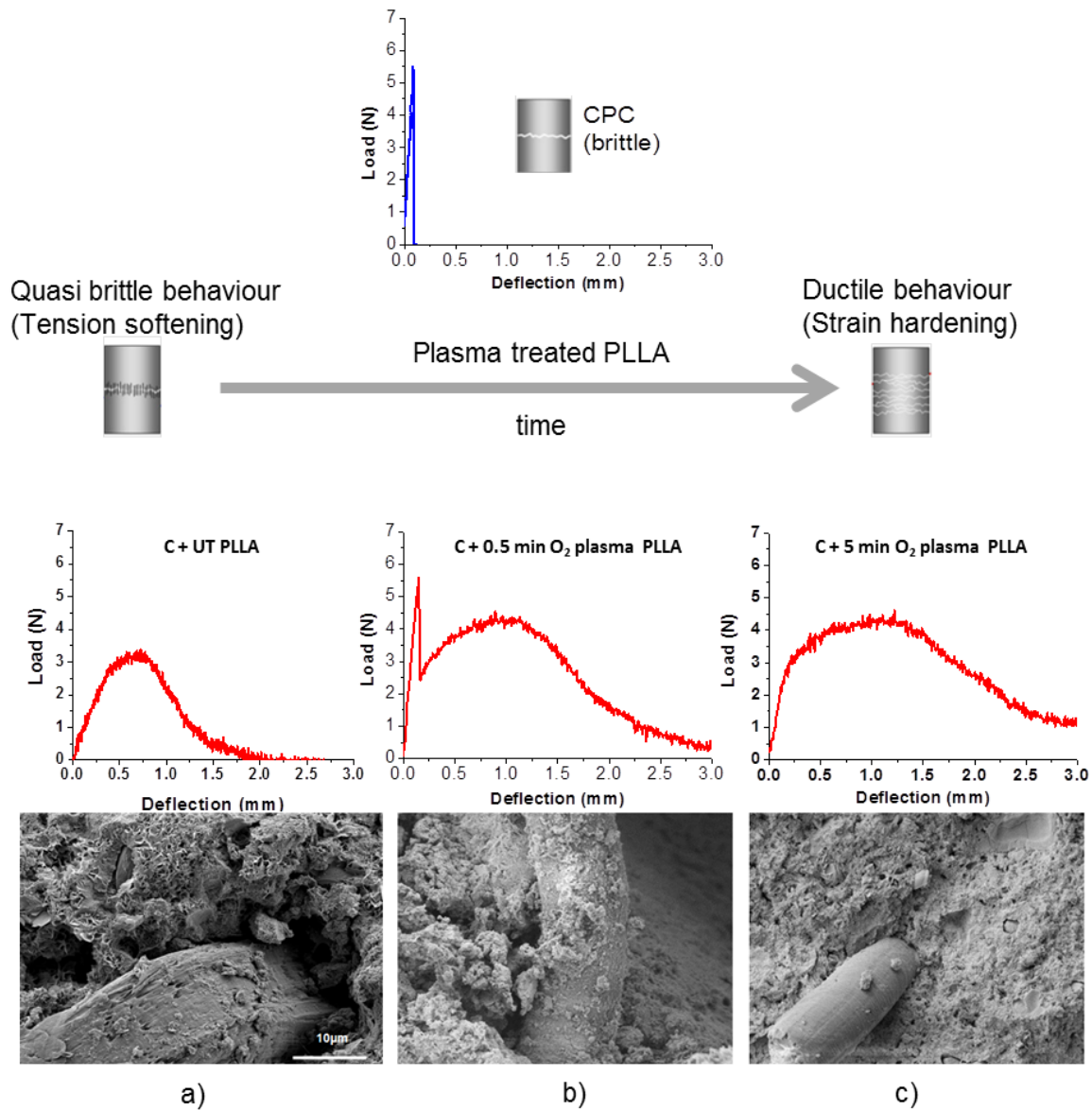


Figure 4.34- Load-deflection curves of CPCs (top) and of PLLA-CPC composites with either untreated (UT PLLA-CPC) or plasma-treated fibres (from left to right). Scanning electron micrographs of the fracture region of the CPC-PLLA composites after bending test untreated (a), and treated with low pressure plasma for either 0.5min (b) or 5 min (c).

4.4.4 Discussion

One of the main drawbacks of calcium phosphate cements (CPCs) is their poor mechanical performance which has limited their applicability to non-stress-bearing applications. Although fibre reinforcement of CPCs improved the toughness of these materials and the adhesion fibre-matrix is really important for the composite strength (**Nelson, 2002**), it has not been object of studies (**Canal, 2011**).

The medical applications of PLA rest upon its biodegradability and the compatibility of its degradation products with the human body, so it has many emerging applications (**Gupta, 2007**). PLA has been approved by the Food and Drug Administration (FDA, USA) for use as a suture material because of features that offer crucial advantages (**Benicewicz, 1990; Davis, 1996**). In physiological conditions the polymer may take from 10 months to 4 years to degrade, depending on microstructural factors such as chemical composition, porosity and crystallinity that may influence tensile strength for specific uses (**Vainionpaa, 1989**). Concerning bone substitution applications, it has been shown that due to their low solubility, apatite cements are mostly resorbed by the local action of macrophages and osteoclasts (**Frankenburg, 1998; Wenisch, 2003**). It has thus been estimated their resorption time to be slow, and varying a lot depending on the experimental conditions, and can be estimated to be in the frame of years. Therefore, PLA fibers could provide reinforcement to CPCs for a significantly long timeframe before being degraded.

The present work investigates the effects of O₂ low temperature plasma treatments on PLLA multifilaments prior to mixing with CPCs to yield CPC-PLLA fibre-reinforced composites to improve the adhesion at the interface between matrix and reinforcing agent.

In the first place, the effects of different treatment times with low pressure plasma on the surface properties of PLLA were analysed. We have recorded surface functionalisation by oxygenated moieties with a linear relationship between the increasing O/C ratio as determined by XPS with the decreasing contact angle (and thus improved wettability) – Figure 4.30. Different authors have investigated the

surface modification of PLLA by low temperature plasmas, most studies having focused on PLA films. Hirotsu *et al.* treated PLA fabrics with low pressure radiofrequency (RF) glow discharge in pure oxygen or nitrogen and found that weight loss due to plasma etching which was more pronounced for oxygen plasmas than for nitrogen plasmas **(Hirotsu, 1997)**.

The oxygen low pressure plasma treatment evaluated here did not alter topography at 0.5 min, while at longer times of 5 min clear etching was produced on the surface, with a regular pattern perpendicular to the fibre axis (Figure 4.30). This kind of patterns was also observed in previous works for oxygen low pressure plasma treatments on PA6 microfibres **(Canal, 2005)**.

Different plasma treatments (low pressure, dielectric barrier discharge, etc.), with oxidizing gases used for the modification of PLA films **(Alves, 2008; De Geyter, 2010)**, found oxygen incorporation on the surface, with significant increases in the concentration of C-O, C=O and O-C=O groups, while C-C and C-H functional groups decreased, as currently observed for other polymer fibres **(Canal, 2007)**.

As shown in this work (Figure 4.30), the surface functionalisation recorded on the polymer surface is related to the improved wettability of the multifilaments. Research on PLA films evaluating a low pressure glow discharge, or an atmospheric pressure plasma jet found that air plasmas can be very efficient in increasing the wettability of PLA films: contact angles were found to decrease from approximately 80° to 40–45°, depending on the exact operating conditions **(Nakagawa, 2006; Safinia, 2005; Teraoka, 2006)**.

In the present work around 10° decrease in the contact angle values were recorded after the oxygen low pressure plasma treatment, which is not far from the values reported by other authors in literature. For instance, in Morent *et al.* **(Morent, 2010)**, PLA films displayed contact angle reductions of around 15° (from 75° to approximately 59–60°) after air and argon plasma treatment which can be considered to generate comparable surface functionalities as the oxygen plasma treatment performed here.

This value, apart from its intrinsic relationship with the surface chemistry of the PLLA fibres, is relevant with regard to the calcium phosphate cement preparation, as

the multifilaments will come in contact with the liquid phase of the cement, and may then absorb water differently after the plasma treatment, slightly modifying the effective L/P ratio of the CPC. In fact, as shown in Table 4.8, the initial and final setting times of the CPCs were modified both by the presence of the untreated PLLA multifilaments, as well as by the plasma treatment performed on the multifilaments. The setting time of a CPC is the time upon which the cement starts to harden, and cannot be moulded anymore. When the powder is mixed with the liquid, a plastic and mouldable paste is obtained. As time evolves, the paste loses its plasticity and mouldability, but increases its strength. The introduction of untreated staple multifilaments in the CPC matrix led to a water uptake which resulted in a lower effective L/P ratio, related to shorter initial setting time but keeping the final setting time unaltered with respect to the pristine CPC matrix. The CPC-PLLA composites prepared from low pressure plasma-treated PLLA fibres showed even shorter final setting times. Many other works found similar effects after addition of different kinds of fibres in CPC matrices where the faster setting times were attributed to the decrease in the effective L/P ratio due to the penetration of the liquid phase in the interspace between fibres (O'Hara, 2012; Zuo, 2010). As far as the clinical application is concerned, Driessens *et al.* (Driessens, 1998) proposed that adequate initial and final setting times of CPCs were in the range of: $4\text{min} < t_{\text{setting_initial}} < 8\text{min}$ and $10\text{min} < t_{\text{setting_final}} < 15\text{min}$. The plasma treated CPC-PLLA composites prepared here displayed initial setting times of 4 min and final setting times of 10 min, falling in the lower range mentioned, so in this sense they can be considered relevant for clinical use.

As confirmed by SEM images of the CPCs, the matrix structure clearly corresponds to the typical plate-like microstructure of CDHA crystals (Espanol, 2009) and the introduction of the PLLA fibres did not alter that. As shown in Figure 4.31 for CPC-PLLA composites where the fibres have been eliminated by burn-out, as well as in Figure 4.32a, the fibres from the multifilaments cut to 4 mm (Figure 4.28) did not keep together after blending with the cement paste, as such length was insufficient to maintain the torsion of the multifilament and thus keep its unity. Therefore, this led to a random distribution of the individual fibres in the CPC, which after

resorption would create pores in the range of 10 μm , corresponding to the diameter of a single PLLA fibre.

The total porosity remained mainly unchanged with blending of the fibres in the CPCs. After elimination of the fibres by burn-out at 250°C, the lower pore entrance size peak found at 0.02 μm , which corresponds to the intercrystallite distance (**Espanol, 2009**) displayed lower volume of pores and the total porosity only increased around 2 % (Figure 4.30). Taking into account that the volume % of fibres introduced in the cement is close to 10%, this indicates that part of the fused polymer remained in the CPC occupying the intercrystallite voids.

The effectiveness of polymer fibres as cement reinforcement depends upon many factors (**Krüger, 2012**) and one of the relevant parameters is the interface and thus the mechanical bond between the fibre and the matrix (**Zhang, 2000**). Some previous works regarding reinforcement of concretes showed that composites made with SiCl_4 plasma-treated polypropylene fibres (**Denes, 1996**) had better flexural strength and toughness than those made with untreated fibres, or (**Li, 1996**) that tensile and pull-out tests on plasma-treated polyethylene fibre concrete composites employing three different gases (NH_3 , CO_2 and Ar) showed optimal bonding strength improvement (35%) for NH_3 plasma treatments. In reinforcement of Portland concrete with polypropylene fibres and multifilaments, (**Zhang, 2000**) Ar and Air plasmas tended to increase the flexural strength of the composites (although no significant differences could be registered). From these earlier studies, it is clear that different plasma treatments may be appropriate for different types of polymeric fibres, and for their combinations with cement matrices. Despite these positive works on concrete, to the best of our knowledge, there have been no previous insights on plasma treatment of polymeric fibres to improve the mechanical properties of CPCs.

In our case, pristine CPCs subjected to flexural tests underwent critical fracture, corresponding to their brittle nature and yielding the same flexural strength as in previous works with very close CPC compositions (**Ginebra, 2001**) (Figure 4.34). The reinforcement by the PLLA fibres prevented the critical fracture of the PLLA-CPC composites, improving significantly the work of fracture (Figure 4.33c).

However, the untreated PLLA-CPC (C+UT PLLA) showed much lower values of flexural strength and elastic modulus than the pristine CPC (C), which can be attributed to the low adhesion at the interface between PLLA fibres and matrix. The improvement in the work of fracture can be attributed to two factors: first, the flexibility of polymer fibres allows the cements to consume more energy due to crack bridging by the fibres that dissipates the fracture energy; and second, the frictional sliding of fibres during pull-out consumes energy as well.

In literature, addition of resorbable fibres (PLLA) (Zuo, 2010) or yarns (PGA/PLA) to apatitic or brushitic cements (Xu, 2004; Gorst, 2006) led to a decrease in the Elastic modulus, as recorded here. As sought, in this work significant improvement was recorded in the mechanical properties of the O₂ low pressure plasma-treated PLLA-CPC composites in both of the conditions tested, as the bending strength values were recovered up to the level of the untreated CPC. Thus, the plasma treatment of the fibres resulted in an increase of the bending strength, compared to the untreated fibres of around 36%, which is comparable with the range of 15-35% obtained in (Tosun, 2012) with low pressure argon plasma treatment of polyester fibres for reinforcement of concrete. Moreover, the elastic modulus was significantly improved with respect to the composite with untreated PLLA (up to 4.5 times) and the work of fracture was improved with respect to the untreated PLLA-CPC composite. It has to be remarked that compared to the previous section (4.3), the values obtained here for the control cement with PLLA (C + UT PLLA) are much lower, possibly due to the lower L/P ratio, which may be related to more difficulties in homogeneous blending and worse wetting of the fibres, leading to worse mechanical properties due to the water absorption previously described. This absorption may be the cause of a weaker structure, thus leading to lower mechanical properties.

As recalled in a recent review (Zhang, 2014), one main challenge facing CPCs is that in general they have poor mechanical properties, not only in terms of strength, but especially in terms of toughness, brittleness limiting their application to non- or moderate- load bearing sites. When comparing to bone, the elastic modulus of cortical bone in bending has been reported to be around 13 ÷ 15 GPa (Ziopus & Currey, 1998), and thus, not far from the pristine and the CPC-plasma treated PLLA

composites produced here, but much higher than that of CPC-PLLA composites without plasma treatment.

On the contrary, the bending strength of cortical bone ranges between 50 and 200 MPa (**Currey, 1975; Barinov, 2010**), and thus an order of magnitude higher than that of CPCs. Although it could seem that the elastic modulus and bending strength were not significantly improved in the plasma treated composites when compared with the pristine CPCs, in fact the values increased with respect to the CPC with untreated fibers, indicating that the treatment had an effect on the interfacial strength. This was more clearly shown when analysing the fracture mechanisms as depicted in Figure 4.34. The reinforcement tended to a strain hardening mechanism, avoiding critical fracture and resulting in a significant increase in work of fracture, from 0.01 kJ/m² for the pristine CPC up to 0.2 kJ/m² for the CPC-PLLA, and tending to further increase to 0.4 kJ/m² in the CPC reinforced with plasma-treated PLLA. This value is closer to the work of fracture of adult cortical bone, which has been reported to range between 1.5 and 15 kJ/m² (**Currey, 1988**).

Additionally, although no significant differences were found in average between the different plasma treatment times, as observed in Figure 4.34, the morphology of the curves was clearly modified from the untreated PLLA-CPC composite to the plasma PLLA-CPC one. It was observed that a fragile fracture peak appeared randomly in some PLLA-CPC composites, both with UT PLLA or plasma-treated. As compared to the brittle nature of a pristine CPC, the composites with untreated PLLA-CPC showed a quasi-brittle behaviour, with a tension softening mechanism. Thus, the bridging of fibres across cracks provided a post-crack tensile strength as a result of gradual fibre pull-out, resulting in an increased work of fracture. In contrast, in the plasma-treated specimens the shape of the curve changed reflecting a strain hardening mechanism, characteristic of ductile composites (**Krüger, 2012**). The maximum load was comparable to the pristine CPC, and the load carrying capacity was maintained or even increased with increasing deflection, after first cracking of the matrix occurred. Taking into account that fibre pull-out is the main mechanism that avoids brittle fracture, this is a clear indication that plasma treatment results in enhanced bonding between the fibres and the cement matrix.

This improvement can be attributed to the improvement in the adhesive properties of the fibres thanks to their higher wettability after oxygen plasma treatment. By using other gases, such as nitrogen or helium plasma treatment, authors (**Morent, 2010**) found a much more pronounced contact angle decrease: a helium plasma treatment can decrease the contact angle to 36°, while a nitrogen treatment lead to an even lower contact angle (31°). This strategy could be evaluated in future for further enhancing the adhesion at the interface and maximising the benefits on the mechanical properties. Interestingly, although the surface roughness was considerably modified, no significant differences were found in the bending properties of the samples with different plasma treatment times. Thus, although one could have expected an improvement of the frictional bonding between fibres and matrix, the increased roughness produced in the long-time plasma treated PLLA fibres due to the etching of the fibre surface did not have a significant effect on the interfacial adhesion between fibres and cement matrix, indicating that the mechanical improvement in the CPC-plasma-treated PLLA composites is due to chemical bonds and not to frictional bonds between the fibres and the matrix.

4.4.5 Conclusions

This first study on oxygen plasma-treated fibres for preparation of fibre-CPC composites showed that the higher wettability of PLLA produced by the plasma treatment reverted in shorter setting times of PLLA-CPC composites. Moreover, oxygen plasma treatment of the PLLA fibres resulted in enhanced flexural properties, including a significantly higher elastic modulus, and higher work of fracture, and flexural strength and work of fracture tending to improve as compared to the untreated fibres. This can be attributed to the enhanced contact between the fibres and the hydraulic matrix, caused by the increased wettability of PLLA through surface functionalisation with oxygen-containing moieties. The higher roughness induced after long plasma treatment times due to surface etching did not result in additional frictional bonding between fibres and matrix.

4.5 Biological characterisation

This work was performed at the Ångström Laboratory of the Uppsala University in the Materials in Medicine group (MiM) of the Applied Materials Science, Department of Engineering Sciences. The collaboration was funded by the Swedish Foundation for International Cooperation in Research and Higher Education (STINT, project IG2011-2047) and supervised by Dr. Gemma Mestres and Prof. Cecilia Persson.

4.5.1 Introduction

During the years few *in vitro* studies have been carried out in regards to cell response to fibre reinforced calcium phosphate cements (FRCPCs).

Xu *et al.* studied MC3T3-E1 in contact calcium phosphate cements reinforced with woven fibres to ascertain the biocompatibility of the material, and found that there were no significant changes in either the adhesion after 1 day, or the proliferation after 14 days compared to material without reinforcing agents (**Xu & Simon, 2004**).

Recently Wu *et al.* (**Wu, 2014**) prepared FRCPCs based on TTCP:DCPA and reinforced them with chitosan fibres either plain (CF) or RGD-functionalised (RF) to improve cellular response. Murine cells C3H10T1/2 (C3), which are pluripotent cells, were seeded on the different types of cements. They found that for RF-FRCPCs both the cell proliferation and differentiation of C3 cells, as compared both to pure CPC and CF-CPC samples, were significantly enhanced.

Some of the CPCs and FRCPCs previously developed and characterised in this chapter have been selected for biological characterisation. The aim of this work was to perform *in vitro* cell culture studies of both CPCs with different additives (TriMethyl Chitosan or Lactic Acid) in the matrix and two different FRCPCs reinforced with PLLA fibres (C40-f2s and LA-f2s) in order to test the effects of the additives and/or the PLLA fibres on human osteosarcoma-derived cell line MG63. These studies are especially focused on cell proliferation and differentiation (measured through ALP expression) in direct contact with the material.

4.5.2 Materials and methods

a) Samples

Calcium phosphate cements were prepared, mixing a solid phase with different liquid phases (Table 4.9) moulded in discs (15 mm diameter x 2 mm height) and allowed to set in 100% Relative Humidity (RH) for 2 hours and then for 7 days in Ringer’s solution, at 37°C. PLLA yarns were cut to 4 mm long prior to inclusion to the cement (the length was selected due to practical aspects due to the moulds dimension).

Table 4.9- Calcium phosphate cements used for the in vitro cell culture

Reference	Liquid phase	Solid phase	Type of fibres	Fibres (wt %)	L/P (ml/g)
C40	water	98% α -TCP+ 2% pHA	-	-	0.40
TMC	1% TMC in water	98% α -TCP+ 2% pHA	--	-	0.40
LA	10% LA in water	98% α -TCP+ 2% pHA	-	-	0.40
C40-f2s	water	98% α -TCP+ 2% pHA	PLLA	2	0.40
LA-f2s	10% LA in water	98% α -TCP+ 2% pHA	PLLA	2	0.40

The samples were sterilised in 70% isopropanol solution (VWR International) for 2 hours with orbital shaking and then rinsed for 6 times x 10 minutes in sterilised distilled water. The rinsing was done through orbital shaking in order to enhance water penetration into the material. The material discs were placed in the 24-well plates and let dry for 2 hours in the hood.

b) pH monitoring

The behaviour of cells is influenced by all the factors in their environment. Among all, one important issue is the pH of the medium. Thus, it is important to monitor the potential pH changes, especially considering that some cements contained LA in their matrix. The pH was monitored every day in the same medium and conditions used for the cell culture in contact with the samples (1 ml of supplemented DMEM for each disc, daily changed).

c) **Experimental design**

MG63 cells are well known Osteoblastic line cells. Cells were cultured in Dulbecco's modified Eagle's medium (DMEM/F12, USA) supplemented with 10% fetal bovine serum (Hyclone, USA) and 2 mM L-glutamine, 100 U/mL penicillin, and 0.1 mg/mL streptomycin (Sigma- Aldrich, Germany) and kept at 37°C in a humidified atmosphere with 5% CO₂. A scheme of the experiment is shown in Figure 4.35. Cells were seeded on the specimens at a density of 50,000 cells/ cm² (100,000 cells/well) and cultured for 1, 3, and 7 days. Tissue culture Polystyrene (TCPS) was used as control. The experiment was performed twice and with n=4. The medium was changed on a daily base.

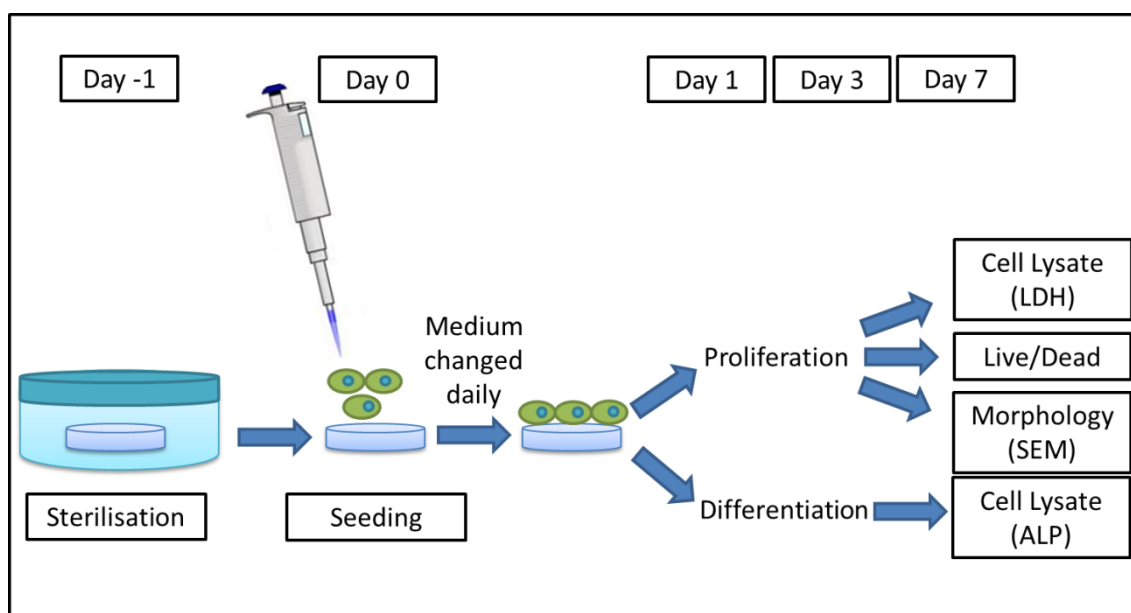


Figure 4.35 - Scheme of the experimental design

d) **Cell lysis**

At each time point the specimens were washed 3 times with sterile PBS to remove unattached cells, then 0.1% Triton (Triton X-100, Merck) in 500 µl of modified Eagle's medium (Hyclone, USA) was added to each well, and then the plate was incubated at 37°C for 50 minutes in order to lysate the cells.

e) Cell proliferation assay

LDH activity quantification

Lactate dehydrogenase (LDH) is a stable enzyme, present in all cell types, and rapidly released into the cell culture medium upon damage of the plasma membrane. LDH, therefore, is the most widely used marker in cytotoxicity study. The assay is based on an enzymatic coupling reaction: LDH oxidises lactate to generate NADH, which then reacts with a substrate to generate yellow colour. The intensity of the generated colour correlates directly with the number of lysed cells. In this work the total number of cells adhered to cement specimens was assessed by measuring the activity of LDH enzyme, using a TOX 7 kit (Sigma-Aldrich). 50 μ l of cell lysates were incubated in a 96 well plate with the LDH reagent mix, at a ratio 1:2, for 20 min, after which the reaction was stopped by the addition of 15 μ l of a solution of HCl 1M. The absorbance was measured, with a microplate reader (Tecan, Switzerland), at the primary wavelength of 490 nm and at background wavelength of 690 nm.

LDH activity of increasing concentrations of cells (from 0 to 1×10^6) was measured as calibration curve, and the results were expressed in cell number (n=4).

Live/dead staining

The principle of this technique is that membrane-permeant calcein is cleaved by esterases in living cells to yield cytoplasmic green fluorescence, and membrane-impermeant ethidium homodimer-1 labels nucleic acids of membrane-compromised cells with red fluorescence (**Life Technologies website**).

The number of viable cells was visualised after 1, 3 and 7 days using live/dead staining kit (Life Technologies, USA). Briefly, the specimens were rinsed in PBS twice followed by 15 min incubation in staining reagents according to the manufacturer's protocol. The cells were then visualised using an Eclipse TE2000-U Optical microscope coupled to a Super High Pressure Mercury Lamp Power Supply CSHG-1 (Nikon Corporation, Japan) and representative micrographs were acquired in which live cells fluoresced green and dead cells fluoresced red.

Cell morphology (SEM)

The morphology of the MG63 cells cultured on the cement specimens as well as the cement microstructures were visualised by Field Emission Scanning Electron Microscopy (FE-SEM, device: FIB Zeiss Neon40). After 3 and 7 days of culture, selected cement specimens from each group were rinsed twice in PBS and fixed with 2.5% glutaraldehyde (SERVA) in PBS solution for at least 60 min at 4°C. Samples were subsequently rinsed twice in PBS and dehydrated in several steps with graded ethanol followed by further dehydration in hexamethylsilazane (Sigma Aldrich).

The samples were mounted on the sample holder with carbon tape and aluminium tape was put on the side walls to allow conduction. Finally the samples were coated with Au/Pd by means of Emitech K950X metal evaporator and then investigated

f) ALP quantification in cell lysate

The osteogenic differentiation was determined by measuring the alkaline phosphatase (ALP) activity, which is an early osteogenic marker. Yellow (pNPP) Liquid Substrate Systems for enzyme-linked immunosorbent assay (ELISA; Sigma Aldrich) were added to 25 µl aliquots of the cell lysate at a ratio 2:1, and incubated for 10 min in the case of SaOS-2 and 30 min in the case of MG63. The reaction was stopped with 25 µl of a solution of NaOH 3M and the absorbance was measured at 405 nm with a microplate reader. The ALP values were normalised to the time of the reaction (there is a linear correlation between the time and the intensity of the signal) and to the total number of cells according to the LDH assay and expressed as p-nitrophenyl pmols/min/1000 cells. Standard ALP curves were made with different concentrations of p-nitrophenyl phosphate (Sigma Aldrich) in PBS.

g) Statistics

Statistical differences were determined using one-way ANOVA at 95% confidence with Tukey's post-tests using Minitab 16 software (Minitab, Inc., State College, PA). Statistical significance was noted when $p < 0.05$.

4.5.3 Results

a) Microstructure

Scanning electron micrographs of the surface of the samples is reported in Figure 4.36. The control C40 (Figure 4.36a) presented the typical plate-like structure, as well as C40-f2s (Figure 4.36e) and TMC sample (Figure 4.36b). LA sample (Figure 4.36c) had platelet-structure embedded in the matrix which seemed more dense compared to the other materials studied. The addition of PLLA fibres to the cement containing LA (Figure 4.36d) changed the structure to a more porous platelet-like structure with a fibre visible (indicated by an arrow).

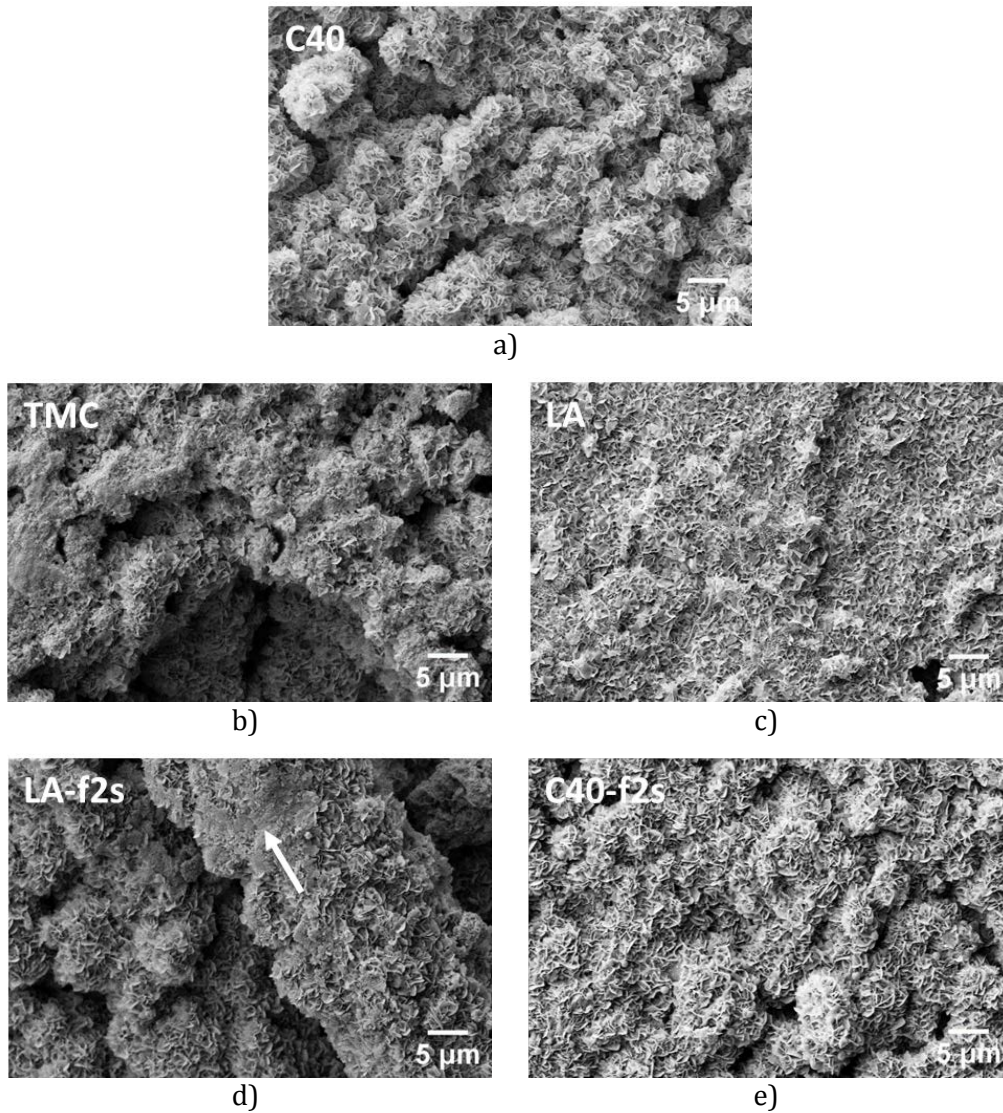


Figure 4.36- Scanning Electron Micrographs of the surface of materials: a) control CPC (C), b) with TMC in the matrix (TMC), c) with LA in the matrix, d) with LA in the matrix and PLLA fibres as reinforcement, e) without additives and with PLLA fibres.

b) pH monitoring

Monitoring pH changes of culture media in contact with different materials, and with daily medium replacement (Figure 4.37) allowed us to divide the pH behaviour into 3 categories up to day 5. The control (TCPS) pH without the material was between 7.2 and 7.4 for the whole experiment. Concerning the materials, on the one hand when LA was introduced in the matrix (LA and LA-f2s), pH dropped down to 6.7 for then reaching stability at neutral pH (pH = 7) after 3 days. On the other hand, the remaining materials laid in a range between 7 and 7.25.

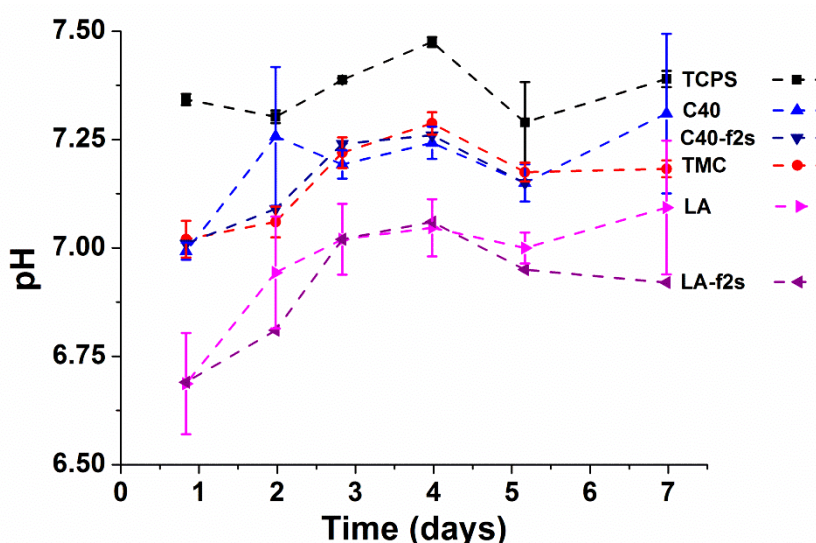


Figure 4.37 - pH monitoring in the first 7 days after samples immersion in DMEM medium changed daily.

c) Cell proliferation

Figure 4.38 shows the proliferation of MG63 cells on the materials. The trend showed a gradual cell number increase in C40, TMC and C40-f2s samples, while when LA was present in the matrix (LA or LA-f2s) a decrease at 3 days was registered, followed by a stabilisation.

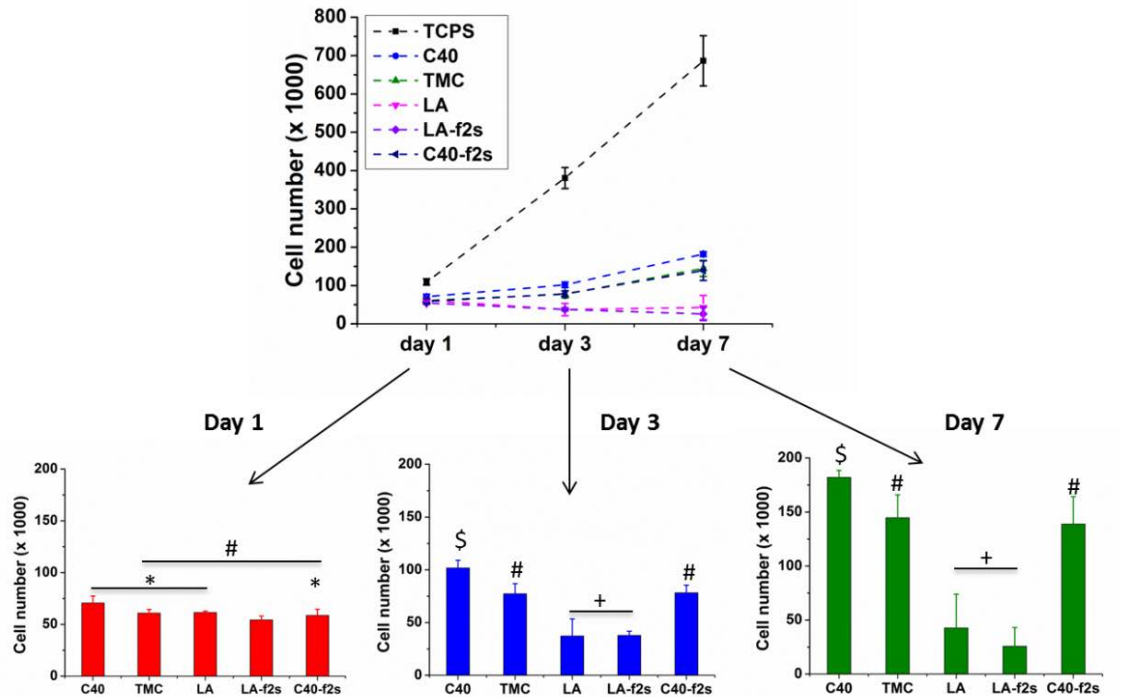


Figure 4.38- (top) Cell proliferation of MG63 for different periods up to 7 days, measured through LDH activity. TCPS was used to check normal cellular behaviour. (bottom) Zoom of the cell proliferation of the materials at day 1, 3 and 7; data are presented as average \pm SD; statistics is reported at each time point. Groups indicated with the same symbol do not have statistically significant differences ($p > 0.05$).

d) Live/dead staining

Figure 4.39 shows that fluorescent staining of live and dead MG63 cells on cement samples revealed some differences between groups. Mostly, the results agreed with the proliferation assay. However, some discrepancies could be noticed in LA-f2s where LDH revealed a decrease of cell count after 7 days while in the live/dead assay it seemed to keep constant.

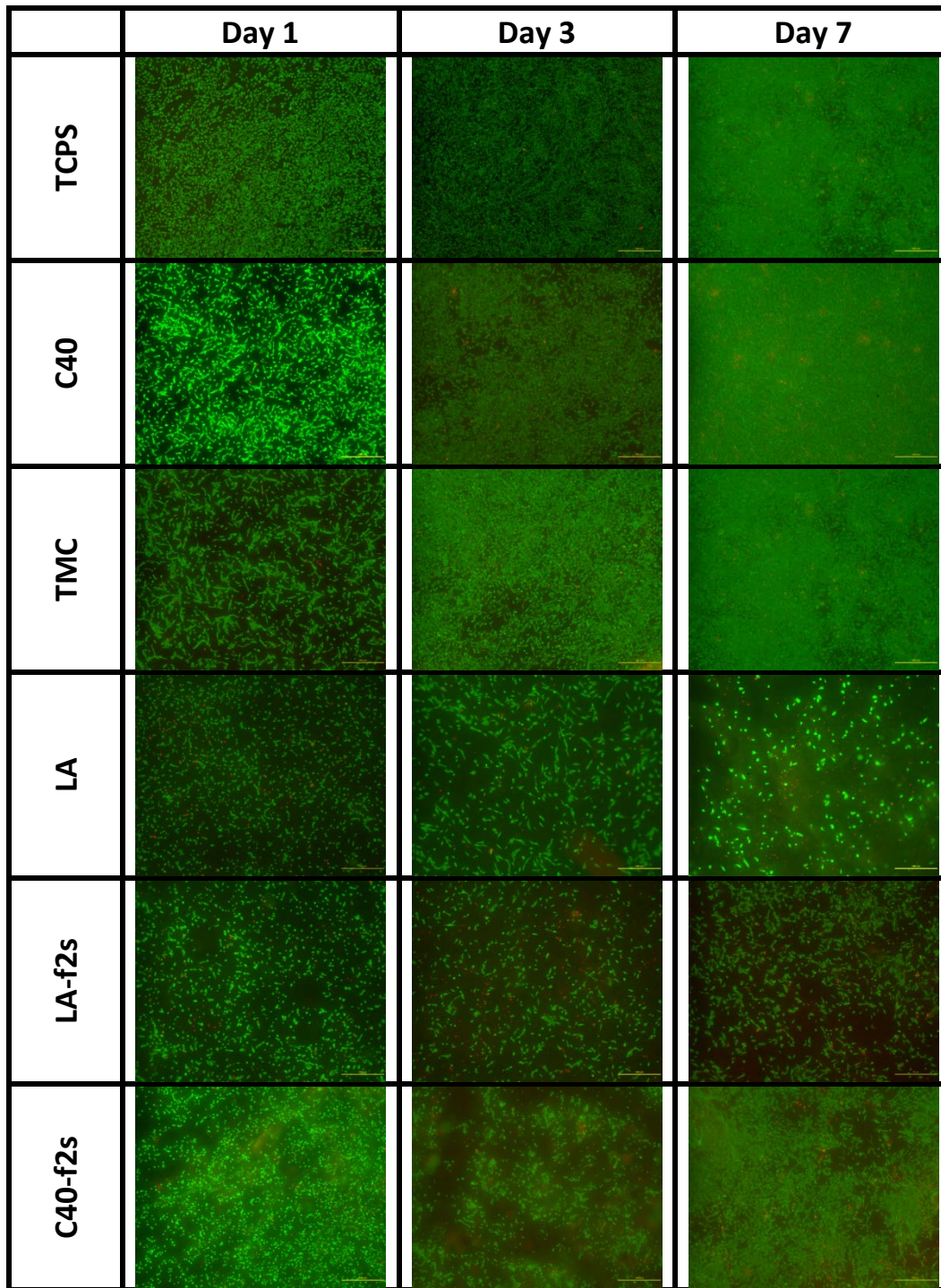


Figure 4.39-Live/dead staining of MG63 on different materials after 1, 3, 7 days. Bar = 500µm.

Figure 4.40 shows the live/dead assay at higher magnification of MG63 cells in order to ascertain their morphology. Generally, cells seemed to be spread on the cements, and they fully colonised the whole sample, as it can be observed at day 7 on most of the samples. Although the number of cells was lower in materials containing LA in the matrix, the cells were well spread.

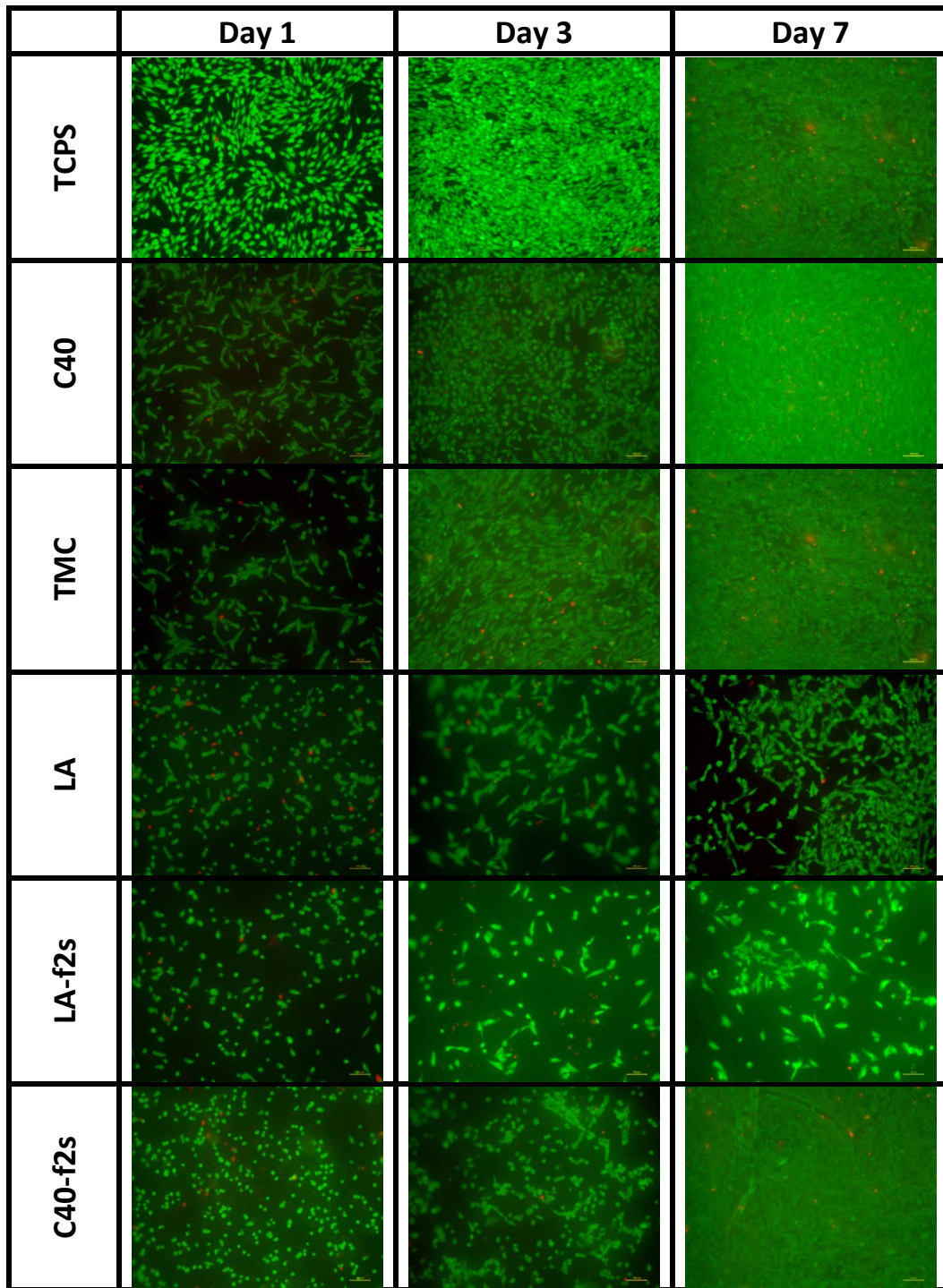


Figure 4.40 - Live dead staining of MG63 on different materials after 1, 3, 7 days. Bar = 100 μ m.

e) Cell morphology

Scanning electron micrographs of MG63 cells cultured on the different samples are shown in Figure 4.41. The cells cultured on different cement types exhibited spread morphology and mostly agreed to the proliferations results. Remarkably, MG63 distribution is quite non-uniform, above all in C40-f2s which would explain why the amount of cells on C40 is greater than the one on C40-f2s in LDH assays (Figure 4.38).

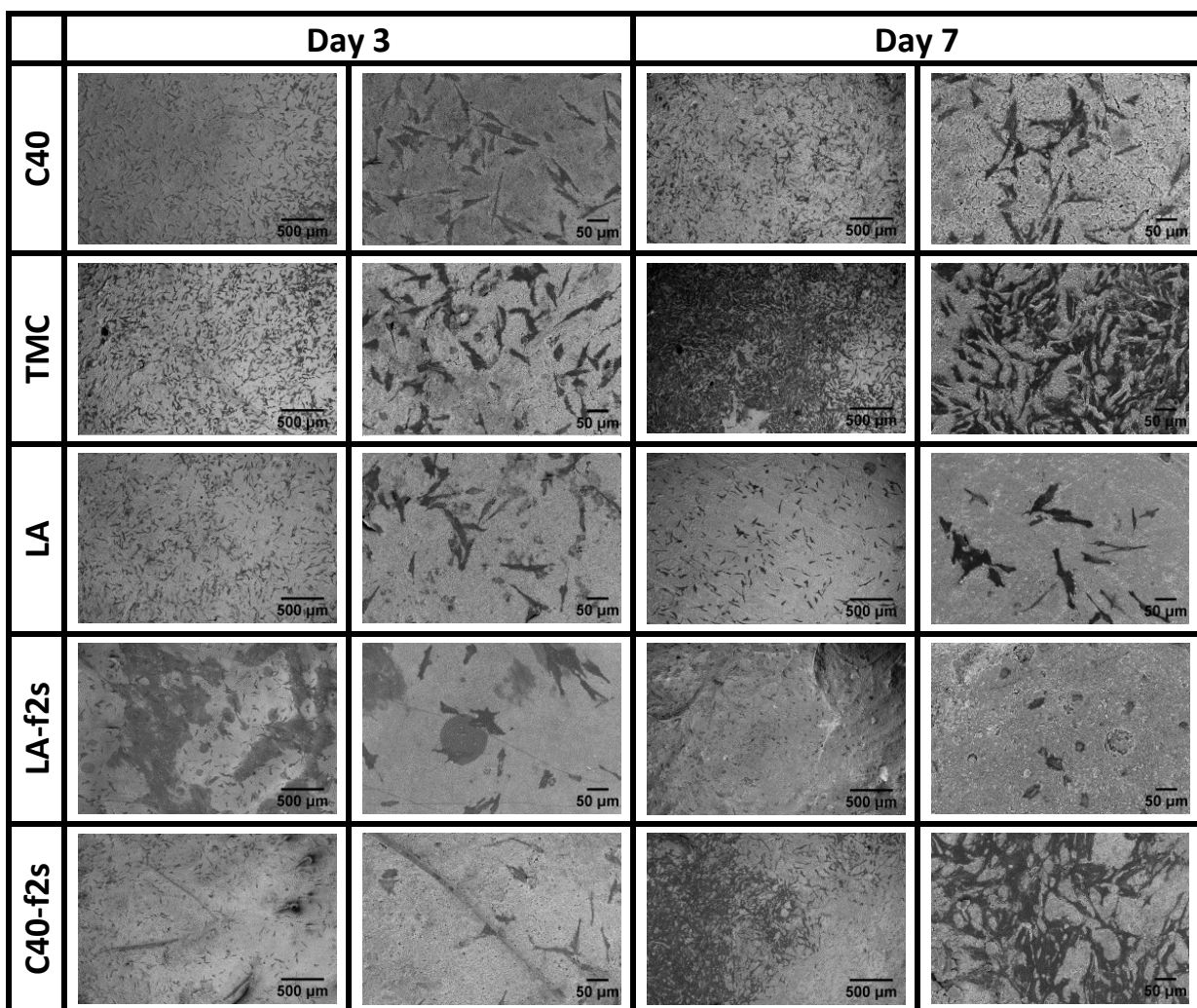


Figure 4.41- SEM images of MG63 on different materials after 3 and 7 days at two different magnifications.

f) ALP expression

Figure 4.42 shows MG63 ALP activity. Although the values are low, the maximum values were found after 3 days followed by a subsequent decrease after 7 days.

However, it seems that PLLA fibres had an effect as, in fact, the ALP activity was enhanced in the materials containing fibres with respect to their pristine counterparts (C40-f2s versus C and LA-f2s versus LA).

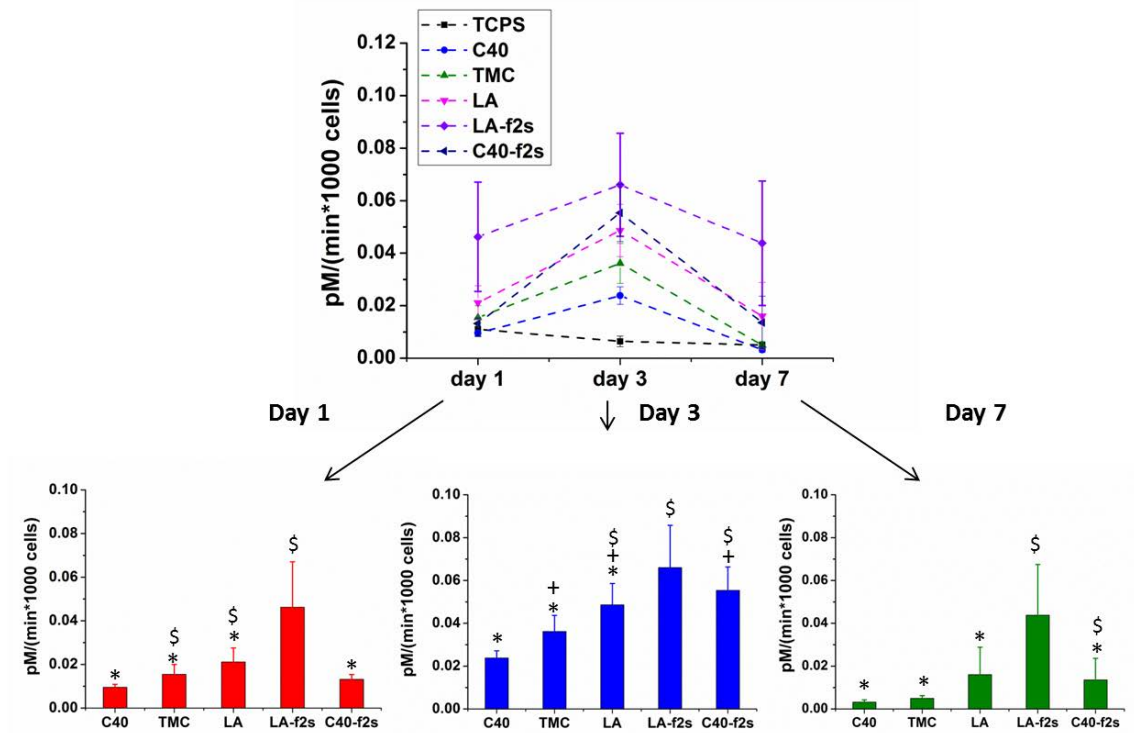


Figure 4.42- (Top) Alkaline phosphatase (ALP) expression level on the cements after different periods of culture of MG63 cells; (Bottom) ALP expression at day 1, 3 and 7; data are normalised to 1000 the number of cells; significant differences for the different materials at a given time point. Groups indicated with the same symbol do not have statistically significant differences ($p > 0.05$).

4.5.4 Discussion

The formulation of Fibre Reinforced Calcium Phosphate Cements (FRCPCs) has been a step forward towards widening the applications of calcium phosphate cements, by opening a window to load-bearing applications. Unfortunately, not so many FRCPCs have been characterised in cell culture studies. In literature there are some studies focusing on cytotoxicity of materials **(Xu & Simon, 2004)** while others evaluate the possibility of using FRCPCs as cell carriers **(Weir, 2010; Zhao, 2011a; Zhao, 2011b)**. In this work, the aim was to investigate how proliferation and differentiation of human osteosarcoma-derived cell lines MG63 are affected by direct contact with different formulations of calcium phosphate cements.

MG63 cells attached after day 1 and the proliferation were higher in the control TCPS than in all CPCs. These results have been previously observed in other studies concerning apatitic cements **(Engel, 2008; Yuasa, 2004)**. On the other hand the already low ALP expression had the lowest values for TCPCs compared to CPCs. It is known that cells which start differentiating show lower proliferation **(Engel, 2008)** and viceversa.

The number of MG63 gradually increased (Figure 4.38) in all samples up to 7 days, except for LA and LA-f2s samples. The lower pH values found in the medium of the LA and LA-f2s samples could be related to the lower cell number recorded (Figure 4.37). In fact, Han *et al.* **(Han, 2009)** found that at a pH around 6.8, MG63 cell viability dropped at around 40 %. El Ghannam *et al.* found that acidic pH reverts in a decrease of both cell proliferation and matrix formation in rat calvaria osteoblasts **(El Ghannam, 1997)**. However, Live/dead staining (Figure 4.39 and Figure 4.40) and cell morphology studies by SEM (Figure 4.41) showed that MG63 were spread on the cement.

Regarding the samples with TMC in the matrix, even though LDH assays showed lower proliferation on TMC than on C40, live/dead staining showed a similar number of cells on both materials (Figure 4.39 and Figure 4.40) while the SEM sample, after 7 days, displayed a higher number of cells than C40 (Figure 4.41). On the other hand in this case differentiation was low.

The presence of the fibres is possibly having an effect as well. Proliferation in the samples with fibres (C40-f2s and LA-f2s) was slightly lower. However, the results of C40-f2s with MG63 were a bit contradictory: scanning electron micrographs at 7 days seemed to reveal that the amount of cells was much greater than the control cement C, while LDH expression studies proved the opposite. The reason for this contradiction could be the fact that the cells were not uniformly distributed on the material (Figure 4.41), which could be misleading.

Although the ALP production is low in this kind of cells, the presence of PLLA fibres seemed to improve ALP production of MG63 cells (Figure 4.42). The mechanisms involved should be further investigated, possibly the studies should be done in a longer time frame (i.e. 21 or 28 days) and, at shorter time, studying differentiation through gene expression which might (compared to protein production) show earlier the activation due to the substrate. However, taking into account what previously said, one hypothesis of this enhancement could be that the presence of PLLA fibres slightly changed the microstructure and/or the surface topography. In fact, the fibres could have been acting as additional nucleation points in the process of dissolution/precipitation and this could revert into a slight change of the microstructure which has been shown to be very relevant for cell behaviour (**Engel, 2008**), as well as the fact that the surface, when fibres were embedded in the matrix, was visibly not completely flat.

4.5.5 Conclusions

The use of osteoblastic-like MG63 cells highlighted different behaviours by the different materials tested. On one hand this study showed a marked effect of apatitic cements compared to TCPS and that proliferation could be affected by the additives in the FRCPCs, especially by the addition of LA which resulted to be harmful towards MG63 cells due to the slightly acidic pH reached. On the other hand it was found that PLLA fibres might have an effect on ALP expression of human osteoblastic type MG63. If this was confirmed, it would mean that FRCPCs could not only improve mechanical properties but they might enhance differentiation at early stages. In the future, polymerase chain reaction (PCR)

methods could be carried out to determine how the gene expression for osteogenic specific markers is altered, and more studies with MG63 in a longer time frame to confirm the results should be performed.

References

Alves CM, Yang Y, Marton D, Carnes DL, Ong JL, Sylvia VL, Dean DD, Reis RL, Agrawal CM. Plasma surface modification of poly(D,L-lactic acid) as a tool to enhance protein adsorption and the attachment of different cell types. *J. Biomed. Mater. Res. B.* 2008; 87(1): 59-66.

ASTM C1161 - 02c (reapproved 2008) Standard Test Method for Flexural Strength of Advanced Ceramics at Ambient Temperature.

Aveston J, Cooper GA, Kelly A. Single and multiple fracture. IPC Science and Technology Press Ltd; 1971.

Badawy MEI, Rabea EI. A biopolymer chitosan and its derivatives as promising antimicrobial agents against plant pathogens and their applications in crop protection. *International Journal of Carbohydrate Chemistry*, vol. 2011, Article ID 460381, 29 pages, 2011. doi:10.1155/2011/460381.

Barinov SM. Calcium phosphate-based ceramic and composite materials for medicine. *Russ. Chem. Rev.* 2010; 79 (1): 13-29.

Beaudoin JJ, 1990. Handbook of fibre-reinforced concrete, Noyes Publications, New Jersey.

Behiri JC & Bonfield W. Orientation dependence of the fracture-mechanics of cortical bone. *J. Biomech.* 1989; 22 (8-9): 863–867, 869-872.

Benicewicz BC, Hopper PK. Review: Polymers for Absorbable Surgical Sutures–Part I. *J. Bioact. Compat. Polym.* 1990; 5(4): 453-472.

Bergsma JE, Rozema FR, Bos RR, Boering G, de Bruijn WC, Pennings AJ. In vivo degradation and biocompatibility study of in vitro pre-degraded as-polymerized polyactide particles. *Biomaterials* 1995; 16(4): 267-274.

Bonfield W. Mechanism of deformation and fracture in bone. *Composites.* 1971; 2 (3): 173-175

Braconnot H. “Sur la nature des champignons,” *Annual Chemistry*, vol. 79, pp. 265–304, 1811.

Bumgardner JD, Wisner R, Elder SH, Jouett R, Yang Y, Ong JL. Contact angle, protein adsorption and osteoblast precursor cell attachment to chitosan coatings bonded to titanium. *J. Biomater. Sci. Polym. Ed.* 2003; 14(12):1401-1409.

Burguera EF, Xu HHK, Takagi S, Chow LC. High early-strength calcium phosphate bone cement: Effects of dicalcium phosphate dehydrate and absorbable fibres. *J. Biomed. Mater. Res.* 2005; 75(4): 966-975.

Callister Jr WD, Rethwisch DG. *Materials science and engineering: an introduction.* John Wiley Sons Inc., Hoboken (2009)

Canal C, Gaboriau F, Molina R, Erra P, Ricard A. Role of the Active Species of Plasmas Involved in the Modification of Textile Materials Plasma Processes *Polym.* 2007; 4(4): 439-445.

Canal C, Ginebra MP. Fibre-reinforced calcium phosphate cements: A review. *J. Mech. Behav. Biomed. Mat.* 2011, 4 (8): 1658-1671.

Canal C, Molina R, Bertran E, Erra P. Wettability, ageing and recovery process of plasma-treated polyamide 6. *J. Adhesion Sci. Technol.* 2004, 18 (9): 1077-1089.

Canal C. Estudio de las propiedades superficiales y del post-suavizado de tejidos de lana y poliamida 6 tratados con plasma. PhD Thesis. UPC, 2005.

Chenite A, Buschmann M, Wang D, Chaput C, Kandani N. Rheological characterisation of thermogelling chitosan/glycerol-phosphate solutions. *Carbohyd. Polym.* 2001; 46(1), 39-47.

Chew KK, Low KL, Zein SHS, McPhail DS, Gerhardt LC, Roether JA, Boccaccini AR. Reinforcement of calcium phosphate cement with multi-walled carbon nanotubes and bovine serum albumin for injectable bone substitute applications. *J. Mech. Behavior Biomed. Mat.* 2011; 4(3): 331-339.

Chung FH. Quantitative interpretation of x-ray diffraction patterns mixtures. II. Adiabatic Principle of X-ray Diffraction Analysis of Mixtures. *J. Appl. Cryst* 1974; 7(6): 526-531.

Costa-Pinto AR1, Salgado AJ, Correlo VM, Sol P, Bhattacharya M, Charbord P, Reis RL, Neves NM. Adhesion, proliferation, and osteogenic differentiation of a mouse mesenchymal stem cell line (BMC9) seeded on novel melt-based chitosan/polyester 3D porous scaffolds. *Tissue Eng. Part A.* 2008; 14(6): 1049-1057.

Currey JD, Butler G. The mechanical properties of bone tissue in children, *J. Bone Joint Surg.* 1975, 57 (6): 810-814.

Currey JD. Ontogenetic Changes in Compact Bone Material Properties, in *Bone Mechanics*, Cowin, S.C., Ed., CRC Press, Boca Raton, FL, 1988.

Da Silva LP, de Britto D, Selegim MHR, Assis OB. In vitro activity of water-soluble quaternary chitosan chloride salt against E. Coli. *World J. Microb. Biot.* 2010; 26(11): 2089-2092.

Dash M, Chiellini F, Ottenbrite RM, Chiellini E. Chitosan-A versatile semi-synthetic polymer in biomedical applications Prog. Polym. Sci. 2011; 36(8): 981-1014.

Davis SS, Illum L, Stolnik S. Polymers in drug delivery. Curr. Opin. Colloid Interf. Sci. 1996 1(5), 660-666.

De Geyter N, Morent R, Desmet T, Trentesaux M, Gengembre L, Dubruel P, Leys C, Payen E. Plasma modification of polylactic acid in a medium pressure DBD. Surf. Coat. Technol. 2010 204(20): 3272-3279.

Denes F, Feldman D, Hua ZQ, Zheng Z, Young RA. J. Cementitious-matrix composites from SiCl₄-plasma-activated polypropylene fibres. Adhes. Sci. Technol. 1996; 10(1):61-77.

Domard A, Rinaudo M, Terrasin C. New method for the quaternization of chitosan. Int J. Biol. Macromol. 1986; 8(2): 105-107.

Dorozhkin SV. Calcium orthophosphate-based biocomposites and hybrid biomaterials. J Mater Sci 2009; 44: 2343-2387.

dos Santos LA, de Oliveira LC, da Silva Rigo EC, Carrodéguas RG, Ortega Boschi A, Fonseca de Arruda AC. Fiber reinforced calcium phosphate cement. Artif. Organs 2000; 24(3): 212-216

Driessens FCM, Planell JA, Boltong MG, Khairoun I, Ginebra MP. Osteotransductive bone cements. Proc. Inst. Mech. Eng. H. 1998; 212 (6): 427-435.

El-Ghannam A, Ducheyne P, Shapiro IM. Formation of surface reaction products on bioactive glass and their effects on the expression of the osteoblastic phenotype and the deposition of mineralized extracellular matrix. Biomaterials. 1997; 18(4):295-303.

Engel E, Del Valle S, Aparicio C, Altankov G, Asin L, Planell JA, Ginebra MP. Discerning the Role of Topography and Ion Exchange in Cell Response of Bioactive Tissue Engineering Scaffolds. *Tissue Eng Part A* 2008; 14(8): 1341-1351.

Espanol M, Perez RA, Montufar EB, Marichal C, Sacco A, Ginebra MP. Intrinsic porosity of calcium phosphate cements and its significance for drug delivery and tissue engineering applications. *Acta Biomater.* 2009; 5(7): 2752-2762.

Frankenburg EP, Goldstein SA, Bauer TW, Harris SA, Poser RD., Biomechanical and histological evaluation of a calcium phosphate cement. *J. Bone Joint. Surg. Am.* 1998; 80(8):1112-1124.

Ginebra MP, Espanol M, Montufar EB, Perez RA, Mestres G. New processing approaches in calcium phosphate cements and their applications in regenerative medicine. *Acta Biomater.* 2010; 6(8): 2863-2873.

Ginebra MP, Rilliard A, Fernandez E, Elvira C, San Roman J, Planell JA. Mechanical and rheological improvement of a calcium phosphate cement by the addition of a polymeric drug. *J. Biomed. Mater. Res.* 2001; 57(1): 113–118.

Ginebra MP. Desarrollo y caracterización de un cement óseo basado en fosfato tricálcico- α para aplicaciones quirúrgicas , PhD thesis, UPC, 1996.

Gorst NJ, Perrie Y, Gbureck U, Hutton AL, Hofmann MP, Grover LM, Barralet JE. Effects of fibre reinforcement on the mechanical properties of brushite cement. *Acta Biomater.* 2006; 2(1): 95-102.

Guinea GV, Planas J, Elices M. Measurement of the fracture energy using three-point bend tests part 1: influence of experimental procedures. *Mater. Struct.* 1992; 25(4): 212-218.

Gupta B, Revagade N, Hilborn J. Poly(lactic acid) fibre: An overview. *Prog. Polym. Sci.* 2007; 32(4): 455-482.

Gupta HS, Wagermaier W, Zickler GA, Aroush DR-B, Roschger P, Wagner HD, Fratzl P. Nanoscale deformation mechanisms in bone. *Nano Lett.* 2005; 5 (10): 2108–2111.

Han SH, Chae SW, Choi JY, Kim EC, Chae HJ, Kim HR. Acidic pH environments increase the expression of cathepsin B in osteoblasts: the significance of ER stress in bone physiology. *Immunopharmacol Immunotoxicol.* 2009; 31(3):428-431.

Handbook of chitosan research and applications. Editor: Richard G. Mackay and Jennifer M. Tait. ©2012 Nova Science Publisher, Inc. ISBN 978-1-61324-455-5.

Hirotsu T, Masuda T, Matumura Y, Takahashi M. Surface effects of plasma on some biodegradable polymers. *J. Photopolym. Sci. Technol.* 1997; 10: 123-128.

<http://www.lifetechnologies.com> , April 2014

Jain LK, Wetherhold RC. Effect of fiber orientation on the fracture toughness of brittle matrix composites. *Acta Metal. Mater.* 1992; 40 (6): 1135-1143.

Joint Committee for Powder Diffraction Studies [JCPDS] –International Center for Diffraction Data, and American Society for Testing and Materials. Powder Diffraction File. Swarthmore, PA: Joint Committee for Powder Diffraction Studies; 1991.

Kelly A. Interface effects and the work of fracture of a fibrous composite, *Proc Roy Soc. Lond. A.* 1970; 319: 95-116

Krüger R, Groll J. “Fiber reinforced calcium phosphate cements -- on the way to degradable load bearing bone substitutes?” *Biomaterials* 2012; 33(25): 5887-5900.

Leroux L, Hatim Z, Frèche M, Lacout JL. Effects of various adjuvants (lactic acid, glycerol, and chitosan) on the injectability of a calcium phosphate cement. *Bone*. 1999; 25(2 Suppl): 31S-34S.

Li VC, Maalej M. Toughening in cement based composites part II: fiber reinforced cementitious composites. *Cem Concr Compos* 1996; 18 (4): 239–249.

Li VC, Mishra DK, Wu HC. Matrix design for pseudo strain-hardening fiber reinforced cementitious composites. *Mater. Structures* 1995; 28 (10): 586-595.

Li VC, Stang H. Interface property characterization and strengthening mechanisms in fiber reinforced cement based composites. *Adv. Cem. Bas. Mater.* 1997; 6(1): 1-20.

Li VC, Wang Y, Backer S. A micromechanical model of tension-softening and bridging toughening of short random fiber reinforced brittle matrix composites. *J. Mech. Phys. Solids*. 1991; 39(5): 607-625.

Li VC. On engineered cementitious composites (ECC): a review of the material and its applications. *J. Adv. Concr. Technol.* 2003; 1 (3):215-230.

Lian Q, Li D, Jin Z, Wang J, Li A, Wang Z, Jin Z. Fabrication and *In Vitro* Evaluation of Calcium Phosphate Combined with Chitosan Fibers for Scaffold Structures. *J. Bioactive Compatible Polym.* 2009; 24(1): 113-124.

Lian Q, Li DC, He JK, Wang Z. Mechanical properties and in-vivo performance of calcium phosphate cement-chitosan fibre composite. *Proc. Inst. Mech. Eng. H*. 2008; 222(3): 347-353.

Liu D, Weiner S, Wagner HD. Anisotropic mechanical properties of lamellar bone using miniature cantilever bending specimens. *J. Biomech.* 1999; 32 (7): 647–654.

Low KL, Tan SH, Zein SHS, McPhail DS, Boccaccini AR. Optimization of the mechanical properties of calcium phosphate/multi-walled carbon nanotubes/bovine serum albumin composites using response surface methodology. *J. Mater. Design.* 2011; 32(6): 3312–3319.

Low KL, Tan SH, Zein SHS, Roether JA, Mourino V, Boccaccini AR. Calcium phosphate based composites as injectable bone substitute materials: a review. *J. Biomed. Mater. Res. B. Appl. Biomater.* 2010; 94B(1): 273-286.

Manich AM, Carilla J, Miguel RAL, Baena B, Lucas JM, Marti M, Cayuela D. Differential Scanning Calorimetry and elasticity of textured, heat set and mechanical strained polylactide multifilaments. *Fibres and Textiles East. Eur.* 2011 19(6): 22-27.

Manich AM, Carilla J, Miguel RAL, Lucas JM, Franco FGF, Montero LA, Cayuela D. Thermal transitions of polylactide false-twist textured multifilaments determined by DSC and TMA. *J. Therm. Anal. Calorim.* 2010; 99(3): 723-731.

Martin RB and Ishida J. The relative effects of collagen fiber orientation, porosity, density, and mineralization on bone strength. *J. Biomech.* 1989; 22 (5): 419–426.

Martin RI, Brown PW. Mechanical properties of hydroxyapatite formed at physiological temperature. *J. Mater. Sci.: Mater. Med.* 1995; 6(3): 138-143.

Meyers MA, McKittrick J, Chen P-Y. Structural biological materials: Critical mechanics-materials connections. *Science.* 2013; 339: 773–779.

Middleton J, Tipton A. Synthetic biodegradable polymers as orthopedic devices. *Biomaterials* 2000; 21(23): 2335-2346.

Morent R, De Geyter N, Trentesaux M, Gengembre L, Dubruel P, Leys C, Payen E. Influence of discharge atmosphere on the ageing behaviour of plasma-treated polylactic acid. *Plasma Chem. Plasma Process* 2010; 30(4): 525-536.

Nakagawa M, Teraoka F, Fujimoto S, Hamada Y, Kibayashi H, Takahashi J. Improvement of cell adhesion on poly(L-lactide) by atmospheric plasma treatment. *J. Biomed. Mater. Res. A* 2006, 77A(1), 108-112.

Nalla RK, Kruzic JJ, Ritchie RO. On the origin of the toughness of mineralized tissue: microcracking or crack bridging? *Bone*. 2004; 34(5): 790-798.

Nelson PK, Li VC, Kamada T. Fracture toughness of microfiber reinforced cement composites. *J. Mater. Civil Eng.* 2002; 14 (5): 384–391.

Neumann M, Epple M. Composites of calcium phosphate and polymers as bone substitution materials. *Eur. J. Trauma* 2006; 32(2): 125-131.

Nezafati N, Moztarzadeh F, Hesaraki S, Mozafar M. Synergistically reinforcement of a self-setting calcium phosphate cement with bioactive glass fibres, *Ceramics int.* 2010; 37(3): 927-934.

No HK, Meyers SP. Preparation of chitin and chitosan, in *Chitin Handbook*, R. A. A. Muzzarelli and M. G. Peter, Eds., pp. 475–489, European Chitin Society, Grottammare, Italy, 1997.

O'Hara RM, Orr JF, Buchanan FJ, Wilcox RK, Barton DC, Dunne NJ. Development of a bovine collagen-apatitic calcium phosphate cement for potential fracture treatment through vertebroplasty. *Acta Biomater.* 2012; 8(11): 4043-4052.

Pan Z, Jiang P, Fan Q, Ma B, Cai H. Mechanical and Biocompatible Influences of Chitosan Fiber and Gelatin on Calcium Phosphate Cement. *J Biomed Mater Res B Appl Biomater.* 2007; 82(1): 246-252.

Perez RA, Altankov G, Jorge-Herrero E, Ginebra MP. Micro-and nanostructured hydroxyapatite–collagen microcarriers for bone tissue-engineering applications. *J. Tissue Eng. Regen. Med.* 2013a; 7(5): 353–361.

Perez RA, Kim HW, Ginebra MP. Polymeric additives to enhance the functional properties of calcium phosphate cements. *J. Tissue Eng.* 2012; 3(1): 2041731412439555

Peterlik H, Roschger P, Klaushofer K, Peter Fratzl P. From brittle to ductile fracture of bone. *Nature Mat.* 2006; 5: 52 – 55.

Rösler J, Harders H, Bäker M. *Mechanisches Verhalten der Werkstoffe.* Wiesbaden: Teubner Verlag; 2006.

Sabir MI, Xu X, Li L. A review on biodegradable polymeric materials for bone tissue engineering applications. *Mater. Sci.* 2009; 44(21): 5713–5724.

Safinia L, Datan N, Hohse M, Mantalaris A, Bismarck A. Towards a methodology for the effective surface modification of porous polymer scaffolds. *Biomaterials* 2005; 26(36): 7537-7547.

Tattersall HG, Tappin G. The work of fracture and its measurement in metals, ceramics and other materials. *J. Mater. Sci.* 1966; 1(3): 296-301.

Teraoka F, Nakagawa M, Hara M. Surface modification of poly (L-lactide) by atmospheric pressure plasma treatment and cell response. *Dent. Mater. J.* 2006, 25(3): 560-565.

Thanou M, Verhoef JC, Junginger HE. Chitosan and its derivatives as intestinal absorption enhancers. *Adv. Drug Delivery Reviews* 2001; 50 (Supplement 1): S91-S101.

Thomas S, Durand D, Chassenieux C, Jyotishkumar P. *Handbook of Biopolymer-Based Materials: From Blends and Composites to Gels and Complex Networks* Wiley-VCH Verlag GmbH & Co. KGaA, p. 813.

Tosun K, Felekoglu B, Baradan B. Multiple cracking response of plasma treated polyethylene fiber reinforced cementitious composites under flexural loading. *Cement Concrete Comp.* 2012; 34(4): 508-520.

Vainionpaa S, Rokkanen P, Tormala P. Surgical applications of biodegradable polymers in human tissues. *Progr. Polym. Sci.* 1989 14(5): 669-716.

Vashishth D, Tanner KE, Bonfield W. Experimental validation of a microcracking-based toughening mechanism for cortical bone. *J. Biomech.* 2003; 36 (1): 121–124.

Von Gonten AS, Kelly JR, Antonucci JM. Load-bearing behavior of a simulated craniofacial structure fabricated from a hydroxyapatite cement and bioresorbable fibre-mesh. *J. Mat. Sci.: Mat. in Medicine* 2000; 11(2): 95-100.

Wang X, Ye J, Wang Y. Reinforcement of Calcium Phosphate Cement by Bio-Mineralized Carbon nanotube. *J. Am. Ceram. Soc.* 2007; 90(3): 962-964.

Weir MD, Xu HHK. Human bone marrow stem cell-encapsulating calcium phosphate scaffolds for bone repair. *Acta Biomater* 2010; 6(10): 4118-4126.

Weir MD, Xu HKK, Simon Jr., CG. Strong calcium phosphate cement-chitosan-mesh construct containing cell-encapsulating hydrogel beads for bone tissue engineering. *J. Biomed. Mater. Res* 2006; 77(3): 487-496.

Wenisch S, Stahl JP, Horas U, Heiss C, Kilian O, Trinkaus K, Hild A, Schnettler R. In vivo mechanisms of hydroxyapatite ceramic degradation by osteoclasts: fine structural microscopy. *J. Biomed. Mater. Res. A.* 2003; 67(3):713-718.

Wu T-Y, Zhou Z-B, He Z-W, Ren W-P, Yu X-W, Huang Y. Reinforcement of a new calcium phosphate cement with RGD-chitosan-fiber. *J. Biomed. Mater. Res. Part A.* 2014; 102A: 68–75.

Xu HHK, Carey LE, Burguera EF. Strong, macroporous, and in situ-setting calcium phosphate cement layered structures. *Biomaterials* 2007b; 28(26): 3786-3796.

Xu HHK, Carey LE, Simon CG. Premixed macroporous calcium phosphate cement scaffold. *J. Mater. Sci.: Mater. Med.* 2007a; 18(7): 1345-1353.

Xu HHK, Eichmiller FC, Barndt PR. Effects of fiber length and volume fraction on the reinforcement of calcium phosphate cement. *J. Mater. Sci. Mater. Med.* 2001a; 12 (1): 57-65.

Xu HHK, Eichmiller FC, Giuseppetti AA. Reinforcement of a self-setting calcium phosphate cement with different fibers. *J. Biomed. Mater. Res.* 2000; 52(1): 107-114.

Xu HHK, Quinn JB, Takagi S, Chow LC, Eichmiller FC. Strong and macroporous calcium phosphate cement: effects of porosity and fiber reinforcement on mechanical properties. *J. Biomed. Mater. Res.* 2001b; 57(3): 457-466.

Xu HHK, Quinn JB, Takagi S, Chow LC. Synergistic reinforcement of in situ hardening calcium phosphate composite scaffold for bone tissue engineering. *Biomaterials* 2004; 25(6): 1029-1037.

Xu HHK, Quinn JB, Takagi S, Chow LC. Synergistic reinforcement of in situ hardening calcium phosphate composite scaffold for bone tissue engineering. *Biomaterials.* 2004 25(6): 1029-1037.

Xu HHK, Quinn JB. Calcium phosphate cement containing resorbable fibers for short-term reinforcement and macroporosity. *Biomaterials.* 2002; 23(1): 193-202.

Xu HHK, Quinn JB. Calcium phosphate cement containing resorbable fibres for short-term reinforcement and macroporosity. *Biomaterials.* 2002; 23(1): 193-202.

Xu HHK, Simon CG. Self-hardening calcium phosphate composite scaffold for bone tissue engineering. *J. Orthopaedic Res.* 2004; 22(3): 535-543.

Xu HHK, Weir MD, Burguera EF, Fraser AM. Injectable and macroporous calcium phosphate cement scaffold. *Biomaterials.* 2006; 27(24): 4279-4287.

Yuasa T, Miyamoto Y, Ishikawa K, Takechi M, Momota Y, Tatehara S, Nagayama M. Effects of apatite cements on proliferation and differentiation of human osteoblasts in vitro. *Biomaterials.* 2004; 25(7-8): 1159-1166.

Zhang C, Gopalaratnam VS, Yasuda HK. Plasma treatment of polymeric fibers for improved performance in cement matrices. *J. Appl. Polym. Sci.* 2000; 76(14): 1985-1996.

Zhang J, Liua W, Schnitzler V, Tancret F, Bouler JM. Calcium phosphate cements for bone substitution: Chemistry, handling and mechanical properties *Acta Biomater.* 2014; 10(3): 1035-1049.

Zhang Y, Xu HHK. Effects of synergistic reinforcement and absorbable fibre strength on hydroxyapatite bone cement. *J. Biomed. Mater. Res.* 2005; 75(4): 832-840.

Zhao L, Burguera EF, Xu HHK, Amin N, Ryou H, Arola DD. Fatigue and human umbilical cord stem cell seeding characteristics of calcium phosphate-chitosan-biodegradable fibre scaffolds. *Biomaterials.* 2010a; 31(5): 840-847.

Zhao L, Weir MD, Xu HHK. Human umbilical cord stem cell encapsulation in calcium phosphate scaffolds for bone engineering. *Biomaterials.* 2010b; 31(14): 3848-3857.

Zhou H, Weir MD, Xu HH. Effect of cell seeding density on proliferation and osteodifferentiation of umbilical cord stem cells on calcium phosphate cement-fiber scaffold. *Tissue Eng. Part A.* 2011; 17(21-22): 2603-2613.

Zioupos P, Currey JD. Changes in the stiffness, strength, and toughness of human cortical bone with age. *Bone*. 1998; 22(1): 57-66.

Zuo Y, Yang F, Wolke JGC, Li Y, Jansen JA. Incorporation of biodegradable electrospun fibres into calcium phosphate cement for bone regeneration. *Acta Biomater*. 2010; 6(4): 1238-1247.

Chapter 5

Macroporous calcium phosphate scaffolds for the delivery of simvastatin acid

In this chapter, calcium phosphate (CaP) foams with different compositions and microstructure are developed and characterised. CDHA foams (hereinafter CPF) are obtained through cementitious reaction after a foaming process and, part of them, are sintered in order to obtain β -TCP foams (hereinafter β -CPF). Both types of scaffolds are then used to study the incorporation of simvastatin acid (SVA), an angiogenic promoter. Plasma polymerisation on the drug loaded scaffold is used as a strategy to delay the drug release. Finally, drug release is studied.

5.1 Introduction

5.1.1 Calcium phosphate for drug delivery

During the past years calcium phosphates have been studied as carriers to deliver molecules in situ (**Ginebra, 2012; Bose & Tarafder, 2012**) and seem to be the most suitable option when skeletal tissue is the target. There are several parameters affecting the release, the most relevant being: i) the microstructure and ii) the interaction of the drug with the carrier material.

Macroporosity is one of the key requirements for the materials designed to act as substrates for tissue engineering and regenerative medicine. In fact, macroporosity has the role to guide and support tissue ingrowth within the material so that cell and vessel colonisation events can take place during the progressive bioresorption of the

scaffold (**Ginebra, 2010**). There are several methods to fabricate macroporous scaffolds (**Ginebra, 2010**); one of the most interesting due to the easy process and the interconnected macroporosity obtained was developed by Montufar *et al.* and consists in using surface active foaming agents in the liquid phase, where the foam obtained was successfully mixed with the cement powder and CDHA foams were obtained after setting (**Montufar, 2010**). Due to the low mechanical properties of CDHA foams, the same scaffolds can be sintered in order to obtain β -TCP which are stronger, and have the same macrostructure with different microstructure and chemical composition (**Montufar, 2008**).

In regards to the loading of the drug on the set or sintered foams, two potential ways can be considered: i) loading by droplet addition and ii) loading by immersion in a drug solution. In this thesis, loading by immersion has been chosen for two reasons: i) to obtain a more homogeneous distribution of the drug and ii) in order to be able to study the difference in drug loading between scaffolds obtained by low-temperature (cementitious reaction) and high-temperature (sintering) processes.

Several features of CPCs as the nano/micrometric pore size (**Espanol, 2009**), the interconnected macroporosity, the dimension of the pores and the specific surface area (SSA) are relevant both in drug loading and in the control of drug release (**Ginebra, 2008**). By sintering the scaffolds, some properties such as i.e. nano/micrometric pore size and specific surface area are modified, so these modifications are studied in this chapter in regard to the loading and the release of the drug.

5.1.2 Potential of plasma polymerisation on controlled drug release from calcium phosphates

As previously mentioned CaPs have been shown to be excellent candidates as drug carriers. The release of the drug is generally controlled by the microstructure of the scaffold and the interactions of the scaffold with the drug (**Ginebra, 2012**).

An additional way to tune the release kinetics can be found in low temperature plasma technologies. Plasma has already, been defined in section 4.1.5 but for the

sake of clarity the three main effects of plasmas on the surface of a material are following reported: i) functionalisation or grafting; ii) etching (removal of surface material); and iii) thin film deposition (deposition of thin layers).

The film deposition of polymer layers is investigated in this chapter. Coating by plasma polymerisation refers to the deposition of polymer films due to the excitation of an organic monomer in the gas state and subsequent deposition and polymerisation of the excited species on the surface of a substrate. The latter is exposed to the plasma which gives rise to the creation of free radicals and therefore leading to a good adhesion of the plasma coating on the surface. Polymers formed by plasma polymerisation are, in most cases, highly branched and highly cross-linked. The deposition of solid polymer coatings under plasma conditions has been well studied since the 1960s, with a very wide range of materials now accessible **(Yasuda, 1985)**.

Application of different kinds of coatings for drug delivery has been used both with ceramics and polymers. In either case, the stability of the coating is of paramount importance. The coating can be used either to regulate the incorporation of the active principle, or to act as a shield to delay its release. Stability of a polymeric coating (as in this case) is controlled by the physico-chemical properties of the polymer such as composition, crosslinking and coating thickness. All these variables can be tuned through the initial composition of the gas and plasma parameters such power and time of the treatment.

Low pressure plasma polymerisation (hereinafter plasma polymerisation) has been used in two ways: i) in soft conditions (Pulsed Wave (PW) polymerisation) in order to retain the functionalities of the precursor or ii) in a Continuous Wave (CW mode) to deposit crosslinked thicker layers **(Bhatt, 2012a)**. Bhatt *et al.* used PW plasma polymerisation for biomedical application. They developed multilayer biodegradable PCL-co-PEG (poly (ϵ -caprolactone)-poly (ethylene glycol) copolymer) coatings on model glass surfaces, for the controlled delivery of Cisplatin, an anticancer drug, which was embedded between two of the polymeric layers of the coating **(Bhatt, 2013)**. It was shown that by gradually increasing the layer thickness with plasma polymerisation deposition time, the amount of drug released

diminished. To the best of our knowledge, in the field of CaP materials for drug delivery applications, plasma polymerisation has not been investigated yet.

5.1.3 Statins in bone regeneration

Statins are drugs commercially used in cholesterol-lowering activity. However, in addition to the cholesterol-lowering effect, statins have a series of pleiotropic effects, including bone anabolic, vasodilative, antithrombotic, antioxidant, anti-inflammatory, and immunosuppressive actions (**Mundy, 2001**). Since Mundy *et al.* (**Mundy, 1999**) first described the bone anabolic properties of statins almost 15 years ago, the research for using them in applications for bone catabolic diseases, such as osteoporosis, has been pursued. *In vitro* investigations have explored the mechanisms of statin effects on the mevalonate pathway, as well as osteoblast and osteoclast function. *In vivo* animal studies confirmed that ovariectomy- and inflammation-induced bone loss could be reduced by systemic statins. Additionally, human clinical studies showed promise that systemic statins could reduce osteoporotic fracture risk and increase bone mineral density (**Zhang, 2014**).

As reported in Figure 5.1, the action of statins is from different frontlines (**Zhang, 2014**): first of all statins inhibit the rate-limiting enzyme 3-hydroxy-3-methylglutarylcoenzyme A (HMG-CoA) reductase in the cholesterol metabolism pathway which leads to a chain reaction that has as ultimate effect the increase of both BMP-2 and VEGF and, thus, osteoblastic differentiation. In the late 2000 some groups showed that statins could promote osteoblast viability through decreasing apoptosis (**Kaji, 2008**), and differentiation via BMP-2 mediated pathways (**Chen, 2010**). Furthermore, the enhancement of osteoblast mitochondrial function attributed to simvastatin (**Chuang, 2013**) has been applied to implant surfaces to promote osteoblast differentiation *ex vivo* (**Yang, 2011**) and *in vivo* (**Walter, 2013**). Moreover, it seems that osteoclast differentiation is reduced by statins action in a dose-dependent manner (**Kaji, 2005**).

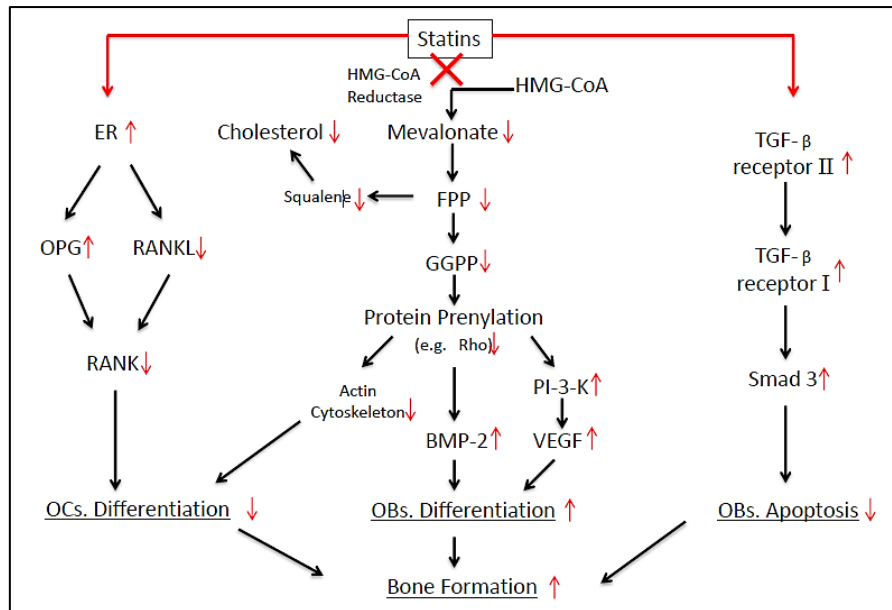


Figure 5.1 - Statins impact on multiple pathways which results in enhanced bone formation. Abbreviations: BMP, bone morphogenetic protein; ER α , estrogen receptor-alpha; FPP, farnesyl pyrophosphate; GGPP, geranylgeranyl pyrophosphate; GGPPs, GGPP synthase; HMG-CoA, 3-hydroxy-3-methylglutaryl-coenzyme A; mPEG, methoxy polyethylene glycol; OBS, osteoblasts; OCs, osteoclasts; OPG, osteoprotegerin; PI3-K, phosphatidylinositol 3 kinase; RANKL, receptor activator of nuclear factor kappa-B ligand; RCT, randomised controlled trials; Smad3, small mothers against decapentaplegic homolog 3; TGF- β , transforming growth factor-beta; VEGF, vascular endothelial growth factor. (Zhang, 2014).

Several reports have indicated a therapeutic benefit of statins for neovascularisation and bone formation; however systemic administration of statins is compromised by metabolism in the liver (only 7% reaches the general circulation intact (Mauro, 1993)) and clearance in the digestive system (Tiwari, 2011), whereas high-dose treatment can introduce adverse side effects (Golomb, 2008). Therefore, to avoid low efficiency and side effects, local drug delivery of simvastatin to promote fracture healing, as proposed in this PhD thesis, may be particularly advantageous.

In the last years several studies have been performed using local delivery of these molecules with aim of triggering of vascularisation and osteogenesis.

Zhang *et al.* found that the combined use of simvastatin with bone marrow derived mesenchymal stem cells enhanced angiogenesis, resulting in higher capillary densities compared to cell or drug therapy alone in a murine model of hind limb ischemia (Zhang, 2012).

Wadagaki *et al.* tested simvastatin in combination with biodegradable polymers, generating simvastatin-releasing nano and microscale fibre scaffolds that promoted

osteoblastic differentiation and bone formation in ectopically implanted murine bone marrow stromal cells (**Wadagaki, 2011**). Similarly, low-dose simvastatin coating of osteosynthetic stabilisation wires in a closed tibia fracture model in rats was shown to have improved fracture healing as well as biomechanical, radiographic, and histomorphometric properties comparable to high-dose BMP-2 coated stabilisation wires (**Pauly, 2009**). Furthermore, the local administration of low-dose simvastatin with gelatine hydrogel successfully induced fracture union in a rat unhealing fracture model due to its effect on both angiogenesis- and osteogenesis-related growth factor expressions (**Fukui, 2012**). Similar studies on rabbits were performed by Wong and Rabie in 2005 (**Wong & Rabie, 2005**), where simvastatin collagen grafts were implanted in parietal bone defects and showed 380% more new bone compared to the control. The quantity loaded was 0.5 mg/sponge.

Nyan et. al (**Nyan, 2007**) found that in critical-size defects in rats, the combination of 1 mg Simvastatin with calcium silicate gave the best result at 8 weeks compared with other doses, after 5 weeks of significant soft tissue inflammation. The same group (**Nyan, 2009**) evaluated different amounts of simvastatin (0.01, 0.1, 0.25 and 0.5 mg) combined with α -TCP particles and found that the best amount in rat 5 mm-diametral-calvarial defects the optimum was given by 0.1 mg since it was effective but with limited inflammation. In another study, the same group explored the mechanisms related with bone regeneration: rat calvarial defects grafted with α -tricalcium phosphate and simvastatin showed that both new bone formation and BMP-2 expression were significantly increased in the simvastatin group, along with an increased up-regulation of TGF- β (**Nyan, 2010**). Different calcium phosphate materials were also evaluated (α -TCP, β -TCP and HA) and found that there was an increased bone formation and the highest amount of new bone was found for both α -TCP combined with simvastatin, even if not significantly different, higher than the one observed for β -TCP combined with simvastatin (**Rojbani, 2010**). In all studies involving calcium phosphates, loading was performed through a droplet of simvastatin dissolved in ethanol and allowed to evaporate. Since simvastatin is highly lipophilic, there have been studies where the molecule was hydrolysed to β -hydroxy acid (Simvastatin acid, SVA), the active form of this drug

(Montazerolghaem, 2014). This molecule is more water soluble than its precursor and can be dissolved more easily. Montazerolghaem *et al.* introduced SVA (0, 0.25, 0.5 and 1 mg_{sva}/g_{cement}) in pre-mixed brushitic cements and evaluated SVA release and the *in vitro* behaviour of osteosarcoma-derived SaOS-2 cells in contact with the cement extract. They found the highest mineralisation for extracts of cement containing 0.25 or 0.5 mg_{sva}/g_{cement}. This is an indication of the importance of the right dosage in order to obtain the desired response from the body.

5.2 Objectives

The aim of this research is to design calcium phosphate foams (macroporous scaffolds) with similar macrostructure but different compositions and microstructures, obtained by low temperature processes or by sintering. The physico-chemical features of the scaffolds are characterised with special attention on the effects on simvastatin acid loading and release. Furthermore, the effects of plasma polymerisation coatings on the drug-loaded scaffolds are evaluated as a possible way to control the release of the drug.

5.3 Experimental design

In order to help the reader to understand the sequence of this chapter, Figure 5.2 shows the structure of this chapter. Firstly, the low temperature scaffolds are obtained through cementitious reaction (CDHA foams, herein CPF), part of which is sintered in order to obtain β -TCP foams (β -CPF). Both materials are characterised and loaded with SVA. Furthermore, part of the drug-loaded foams are coated through plasma polymerisation (CPF-p and β -CPF-p). Finally yet importantly, drug release is evaluated.

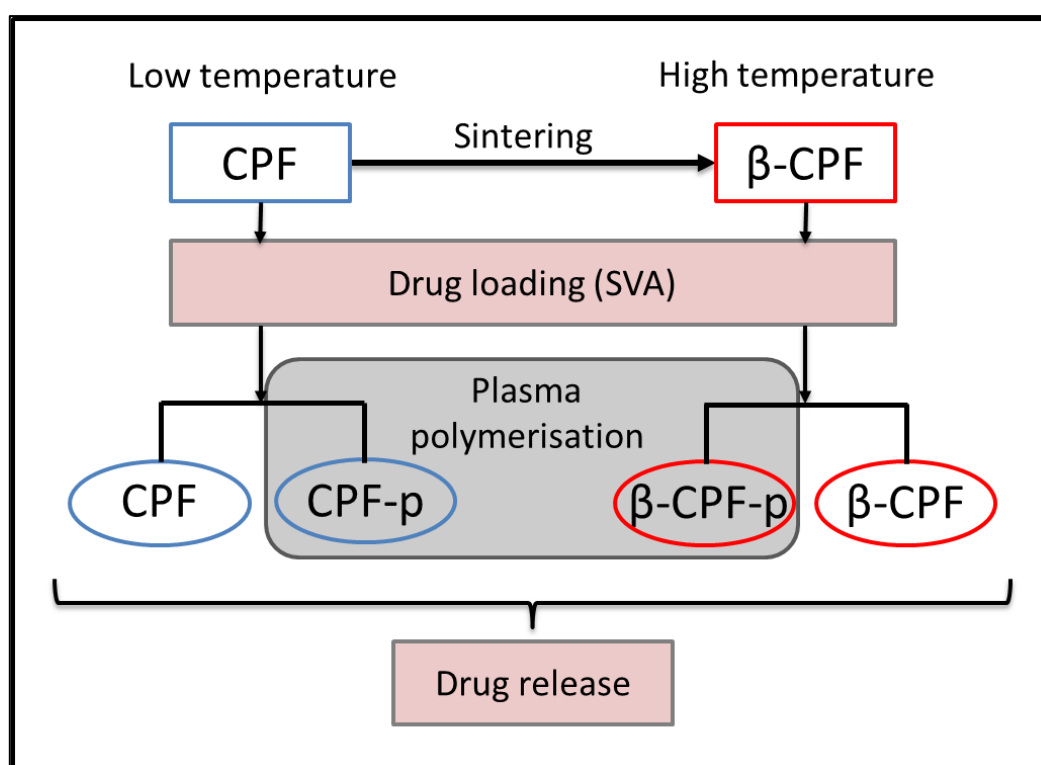


Figure 5.2- Scheme of the chapter.

5.4 Materials and Methods

5.4.1 Calcium phosphate solid and liquid phases

α -TCP was used as starting material for the preparation of the cement's solid phase mixed with 2 wt% precipitated hydroxyapatite (pHA, Alco) as previously described in section 4.3.1.a). Pluronic F-127 (PLU, Sigma-Aldrich) was milled 15 minutes at 150 rpm using 10 balls ($d = 30\text{mm}$). The final solid phase of CaP foams was

composed by 90 wt% α -TCP with pHA and 10 wt% PLU and the liquid phase used was 1wt% of Polysorbate 80 (Tween 80, Sigma-Aldrich) in distilled water. The solution was prepared fresh on daily base. A control foam without PLU was produced mixing 98 wt% α -TCP with 2% pHA with the Tween 80 solution.

5.4.2 Co-polymer precursors

ϵ -caprolactone (ϵ -CL, Purity: 97%, MW: 114 mol/g, Empirical formula: $C_6H_{10}O_2$), and DEGME (Purity: 99.5%, MW: 134.17 mol/g, linear formula: $(CH_3OCH_2CH_2)_2O$) were purchased from Sigma Aldrich, France and used in this study without further purification.

5.4.3 Calcium phosphate foams and cements preparation

Solid and liquid phase were mixed at $L/P = 0.65$ ml/g and cement foams were obtained using a direct foaming method (**Pastorino, 2014a**). The material was shaped in different moulds depending on the final use, two types of cylindrical specimens were produced: i) 12 mm height x 6 mm diameter for mechanical testing and ii) 6 mm height x 6 mm diameter (which became 4 mm height x 6 mm diameter after an accurate removal of the top and bottom by means of a needle, in order to ensure an open porosity of the scaffold) for *in vitro* testing, SSA measurement, drug release studies.

Scaffolds were allowed to set for 24h in 100% RH at 37°C, followed by 9 days in water at 37°C to obtain CDHA calcium phosphate foams.

Unfoamed specimens were prepared at $L/P = 0.35$ ml/g in order to have a model CaP surfaces to study the effects of plasma polymerisation. The powder phase composed by α -TCP with 2% pHA was mixed with the liquid phase in a mortar for about 1 min and then transferred into disc moulds of 15 mm diameter x 2 mm height. Samples were allowed to set in 100% RH for 1h and then Ringer's solution for 7 days at 37 °C to obtain Calcium-Deficient Hydroxyapatite (CDHA) discs.

To obtain β -Tricalcium Phosphate (β -TCP) ceramic discs and foams, the CDHA samples were sintered in an oven (Hobersal), in air, by heating for 2.5 h up to 400°C, and then for 2.20 h up to 1100°C where samples were maintained for 9h. The material was allowed to cool down in the furnace till room temperature.

5.4.4 Simvastatin acid preparation

The simvastatin molecule is very hydrophobic and thus insoluble; to make it more water-soluble and enable the release kinetics to be less affected by solubility issues, it was hydrolysed to β -hydroxy acid (SVA, Simvastatin acid). Hydrolysis was obtained following the same procedure as Kaesemeyer *et al.* (Kaesemeyer, 1999), by dissolving 42 mg of simvastatin (Sigma-Aldrich, S6196) in 1 mL 95% ethanol, adding 1.5 mL of NaOH 0.1 M and heating for 2 h at 50°C (Figure 5.3). The solution was then neutralised to pH 7.4 by adding a HCl solution 0.1 M. Finally, the solution was freeze-dried to obtain SVA powder in the freeze-drier (Cryodos, Telestar) and stored at -20°C in the freezer and protected from light until use.

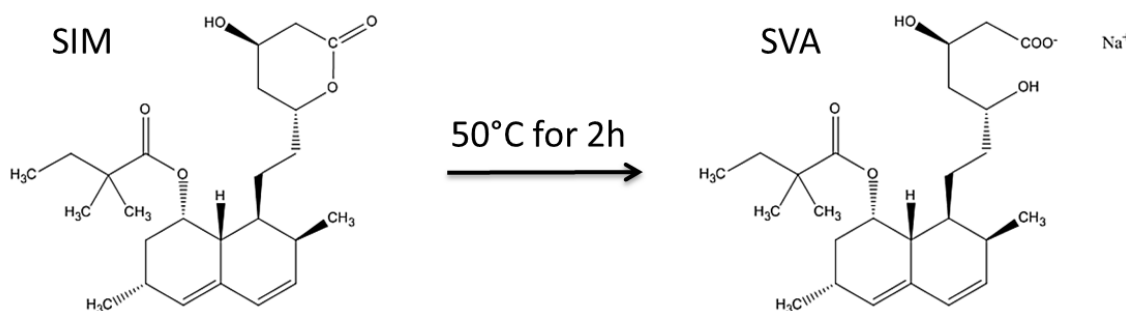


Figure 5.3-Reaction from simvastatin (SIM) to β -hydroxy acid (SVA)

5.4.5 Plasma polymerisation of PCL-co-PEG coatings^{5.1}

Plasma polymerisation coatings of PCL-co-PEG were produced in a low pressure inductively excited radio frequency-tubular quartz plasma reactor system (5 cm

^{5.1} This work was performed at the "Laboratoire de genie des procedes plasma et traitement de surface" (LGPPTS), at the "Université Pierre et Marie Curie", ENSCP, Paris, France during a short term scientific mission (STSM) within the COST ACTION MP1101-(Bioplasma) "Biomedical Applications of Atmospheric Pressure Plasma Technology", funded by the European Union. The work has been supervised by Prof. Farzaneh-Arefi Khonsari and performed with the help of Dr. Sudhir Bhatt.

diameter, 40 cm length, base pressure of 3×10^{-2} mbar). The plasma deposition set-up, its schematics and technical details of the process are summarised in Figure 5.4.

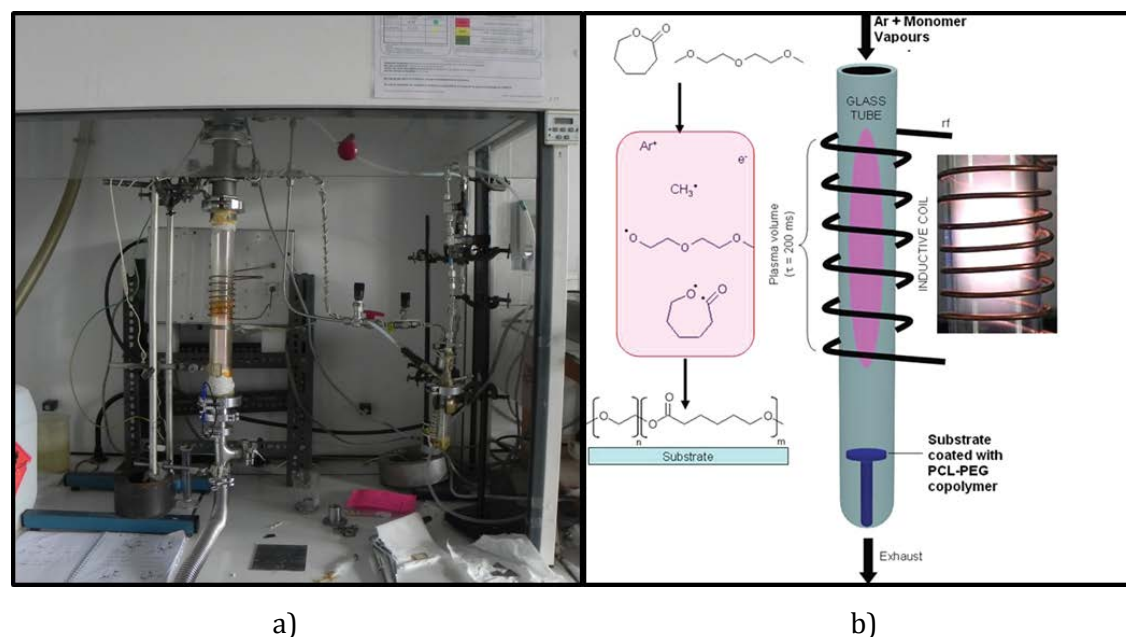


Figure 5.4- a) Plasma polymerisation set-up and b) schematic view of the experimental setup consisting of a low pressure Inductive Coupled Plasma glass reactor used to synthesise PCL-PEG copolymers from precursor vapours. Precursors are activated in the plasma volume and a thin copolymer film is obtained downstream on the substrate. A hypothesised simple mechanism for the formation of PCL-PEG copolymer is also shown and a snapshot of plasma polymerisation process (figure b) is modified from Bhatt, 2012b).

The partial pressure ratio of the two monomers fed in the reactor was controlled by the flow rate of carrier gas (i.e. Ar), which was regulated and measured by electronic mass flow controllers (MKS instruments). The partial pressure of ϵ -CL and DEGME exhibited linear correlations with the flow rate of argon gas and were comparable with each other. Plasma co-polymerisation of organic monomers was carried out on CDHA and β -TCP discs as well as on macroporous CDHA and β -TCP foamed scaffolds, on both sides. For the current study, the total flow rate was varied from 20 to 25 sccm^{5.2} by keeping the operating pressure constant.

In the present work, the treatment used to coat the cements was previously optimised by the hosting group (Bhatt, 2012b). Specifically a PCL-co-PEG copolymer at a ratio 4:1 was used. The copolymerisation was a two-step process. Firstly a layer of PEG was deposited at 1 W Pulse Wave (PW) for 5 minutes in order to obtain a hydrophilic layer where the copolymer could adhere. Subsequently, a

^{5.2} sccm is an abbreviation of standard cubic centimetres per minute indicating cc/min at a standard temperature ($T = 0^\circ\text{C}$) and pressure ($P = 1 \text{ atm}$). It is a common flow measurement term.

20W Continuous Wave (CW) plasma polymerisation was performed for 90 min in order to deposit a thicker layer of copolymer (PCL-co-PEG at a ratio 4:1).

CW plasma polymerisation produces high energy ions which permit to obtain more crosslinked copolymers compared to PW plasma polymerisation. For the PW plasma discharge, the peak power (P_{pk}) of the wave was 25 W and the duty cycle^{5.3} (DC) was 4 %; which allowed to obtain the effective plasma power (P_{eff}) of 1W PW. During the plasma “ON” time, bond dissociation of the molecules occurs as well as the formation of active species and ions. In PW plasma polymerisation during the plasma “OFF” time, the copolymer chain grows. After polymer deposition, the reactor was again evacuated to base pressure before the plasma polymerisation system was vented to atmospheric pressure with air

5.4.6 Calcium phosphate foam characterisation

Phase composition of the foams was assessed by X-ray diffraction as described in section 4.3.1.c).

The compressive strength was evaluated in cylindrical specimens (CPF: 12 mm height x 6 mm diameter; β -CPF: 10.5 mm height x 5.1 mm diameter) at a cross-head speed of 1 mm/min using an Electromechanical Testing Adamel Lhomargy (model DY 32/34) with a load cell of 100 N. At least ten CPF or β -CPF replicates were prepared. The material was tested wet and the top and bottom surfaces of the specimens were previously flattened through manual polishing^{5.4} in order to obtain parallel surfaces and ensure a full contact of the specimen surface with the piston surface.

To ascertain the surface macro- and micro- structure of CPFs and β -CPF, the materials were investigated by Field Emission Scanning Electron Microscopy (FIB, Zeiss Neon40). Samples were prepared as described in 3.3.3.e.

The porosity and pore entrance size distribution were measured by Mercury Intrusion Porosimetry as described in section 3.3.3.h.

^{5.3} DC = $(t_{on} / (t_{on} + t_{off}))$, where t_{on} and t_{off} were the plasma is “switched ON” and plasma is “switched OFF” times respectively, so DC is the fraction of time the plasma is switched on over the total time frame.

^{5.4} In the case of β -TCP foams the foams were polished prior to sintering.

The SSA of CPF and β -CPF was measured by Nitrogen adsorption at 77 K according to the BET method as described in section 4.3.1.c.

5.4.7 Drug incorporation

Calcium Phosphate Foams were loaded with SVA by immersion of 10 CaP cylinders in 4 ml of nominal concentration 200 $\mu\text{g/ml}$ of SVA solution at ambient temperature, with orbital shaking and protected from light. CPFs were loaded by immersion for 2h, while β -CPF loading was optimised (at 2h, 4h or 24h). Foams were subsequently freeze-dried. The quantity of SVA loaded was calculated by difference in concentration of the solution before and after loading, following the equation:

$$Q_{SVA} = Q_{absorbed} + Q_{trapped} = (C_f - C_i) * V_{solution} + C_f * (V_{trapped}) \quad (6.1)$$

Where:

Q_{SVA} : SVA quantity loaded;

$Q_{absorbed}$: SVA quantity loaded by absorption;

$Q_{trapped}$: SVA quantity trapped in the scaffold with the liquid;

C_i : Initial concentration;

C_f : Final concentration;

$V_{solution}$: Volume of the solution (4 ml)

$V_{trapped}$: Volume trapped in the scaffold, calculated as $(M_f - M_i) * \delta_{sol}$, with M_f : final wet mass, M_i : initial mass, $\delta_{sol} \cong 1$ (aqueous solution).

The drug concentration was evaluated by UV-VIS spectroscopy (UV-visible-NIR Spectrometer (Shimadzu 3600)) at $\lambda_{max} = 238$ nm. A blank was subtracted to the values recorded.

5.4.8 Characterisation of Plasma Polymerised Coatings

The chemical properties of plasma copolymerised coatings were analysed by recording FT-IR spectra of PCL-co-PEG coatings using a Nicolette 3700

Thermoscientific spectrophotometer. The FT-IR spectra were recorded with the resolution of 4 cm^{-1} by scratching the surface of the samples to obtain material from the surface layers, and blending with KBr to prepare a tablet. Baseline correction was performed by OMNIC software after 64 scans of each sample.

The chemical composition was analysed by XPS with a SPECS (Germany) using an Al non monochromated source XR50 (200W and 14 kV) with an analyser Phoibos 150 MCD-9 with pass energy of 25 eV, high resolution steps of 0.1 eV, chamber pressure of 5.10^9 mbar and using a Flood gun FG15/40. Peak deconvolution was performed with CasaXPS software. The cumulative error associated to XPS measurement was around 10%.

Sessile drop contact angle values were measured using a video capture apparatus (Digidrop GBX-3S system, France). For each measurement, 6 μL of deionised water droplets were dispensed onto the coated surfaces. Four measurements were carried out on each coating and resulting values were averaged.

Surface topography changes after plasma polymerisation of CDHA and β -TCP discs as well as the copolymer penetration inside CPF and β -CPF were investigated by Field-Emission Scanning Electron Microscopy. The samples were studied and prepared as described in section 3.3.3.e.

To ascertain the thickness of the plasma polymer layer deposited on the CDHA and β -TCP surface of the CPC discs, Focus Ion Beam tomography (FIB, Zeiss Neon40) was performed on a sample coated with Au-Pd. A cross-section from the surface was cut. The thickness of the deposited layer was calculated as the average of ten measurements of the coating.

5.4.9 Drug release experiment

CDHA and β -TCP foams loaded with SVA both plasma treated (CPF-p and β -CPF-p) or native (CPF and β -CPF) were immersed in 2 ml of Dulbecco Phosphate Buffer Saline (DPBS, Sigma Aldrich) at 37°C with continuous shaking. 1 ml of sample was

extracted at different time points and reintroduced right after the measurement in the release vessel.

The amount of drug released was obtained by measuring the release media collected at each time point by UV-VIS spectroscopy at the maximum absorption wavelength of SVA which is located at $\lambda_{\max} = 238$ nm for SVA in a M550 DoubleBeam UV-VIS spectrometer (Camspec, Leeds, UK).

5.4.10 Statistics

Statistical differences were determined using one-way ANOVA with Tukey's post-hoc test (95%) using Minitab software (Minitab Inc, US). Statistical significance was noted when $p < 0.05$.


5.5 Results

5.5.1 Calcium phosphate foam optimisation

To develop new CaP foams by low temperature processes with adequate rheological properties and improved mechanical properties, but without losing porosity of the scaffold, Pluronic-127 (PLU, Sigma) was added to formulations based on α -TCP, previously described in (Montufar, 2010). After optimisation, the combination chosen in this Thesis was 10 % PLU and L/P = 0.65 ml/g.

This method is very versatile since the foamed CaP paste can be injected in moulds with different shapes and sizes. In particular, Table 5.1 shows the dimensions of the cylinders used for this study after the setting reaction (CPF) or the sintering protocol (β -CPF). The scaffolds shrank between 10-15 % after sintering.

Table 5.1- Dimensions of the cylinders for drug release.

Material		Dimensions	CPF	β -CPF
	Diameter(mm):		6.0 \pm 0.1	5.2 \pm 0.1
	Height(mm)		4.2 \pm 0.3	3.6 \pm 0.5

Moreover, the injectability of the CaP foam allowed obtaining complicated geometries, such as “Pacman-shaped” scaffolds that were used for *in vivo* testing (shown in Figure 5.5). The *in vivo* tests were foreseen in a rabbit arterial pedicle model. The shape of the scaffold was optimised to fit the anatomical site, resulting in a channelled structure designed to cradle the blood vessel.

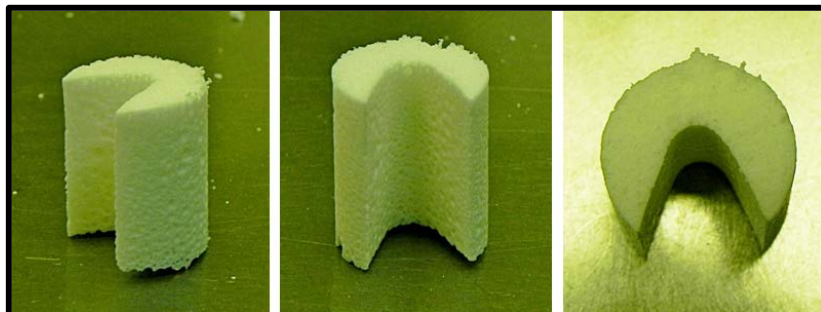


Figure 5.5 – Scaffold shapes for *in vivo* tests (“Pacman-shaped” scaffolds).

5.5.2 Phase quantification

As it can be observed in Figure 5.6a, CDHA was the main phase obtained in CPFs after 10 days setting at 37°C (92 %) but some α -TCP remained still unreacted (8 %) after the setting in water, possibly due to the presence of 10% PLU in the formulation. Figure 5.6b shows the XRD pattern of β -CPF. Although after sintering most CDHA transformed into β -TCP (94 %), there were traces of untransformed HA (6 %); in this case HA was much more crystalline (due to sintering) as denoted by the narrower peaks.

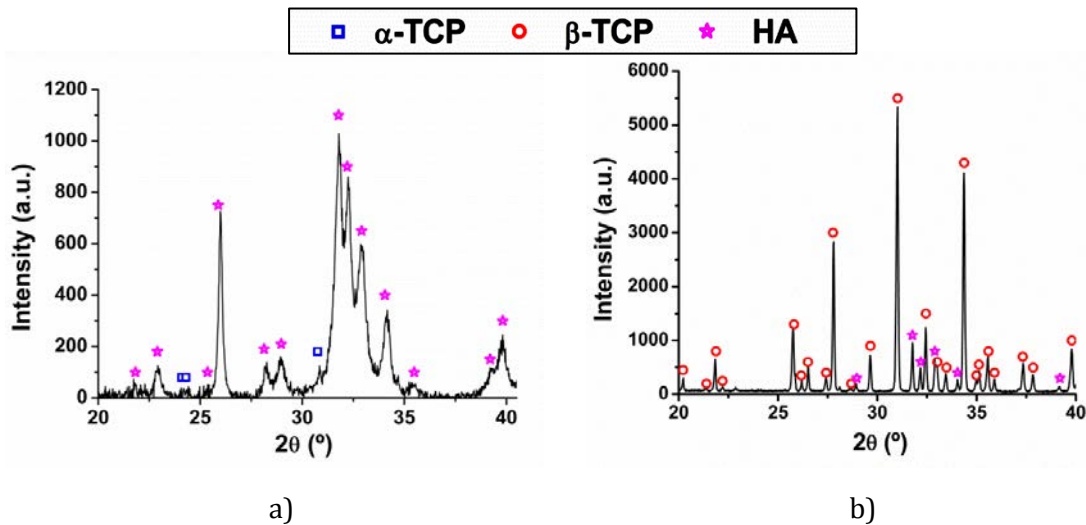


Figure 5.6- DRX pattern of a) CPFs at L/P=0.65, set in water for 10 days and b) of β -CPF, obtained after sintering CPF at 1100°C for 9 hours.

5.5.3 Compressive strength

The compressive strength of CPFs was significantly higher compared to the one of the material without PLU (CPF-0% PLU). β -CPF presented a compressive strength about 3.5 fold of the counterpart before sintering.

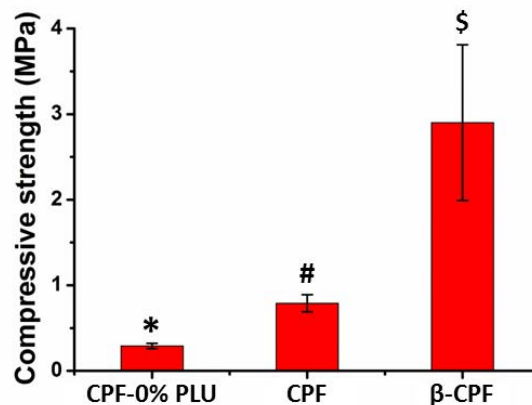


Figure 5.7-Compressive strength of the control cement without PLU (CPF-0% PLU), with 10% PLU (CPF) and of β -CPF. Groups indicated with the same symbol do not have statistically significant differences ($p > 0.05$).

5.5.4 Macro- and micro- structure

Macrostructure of CPF and β -CPF showed a quite uniform distribution of the pores (Figure 5.8a and b, respectively); the porosity was interconnected in both materials (Figure 5.8c and d); and microporosity was similar in both materials (Figure 5.8e and f). The microstructure of CPF consisted of combined crystal structures of needles and plates (Figure 5.8g), while β -CPF displayed the typical sintering necks and polyhedral crystal grains (Figure 5.8h).

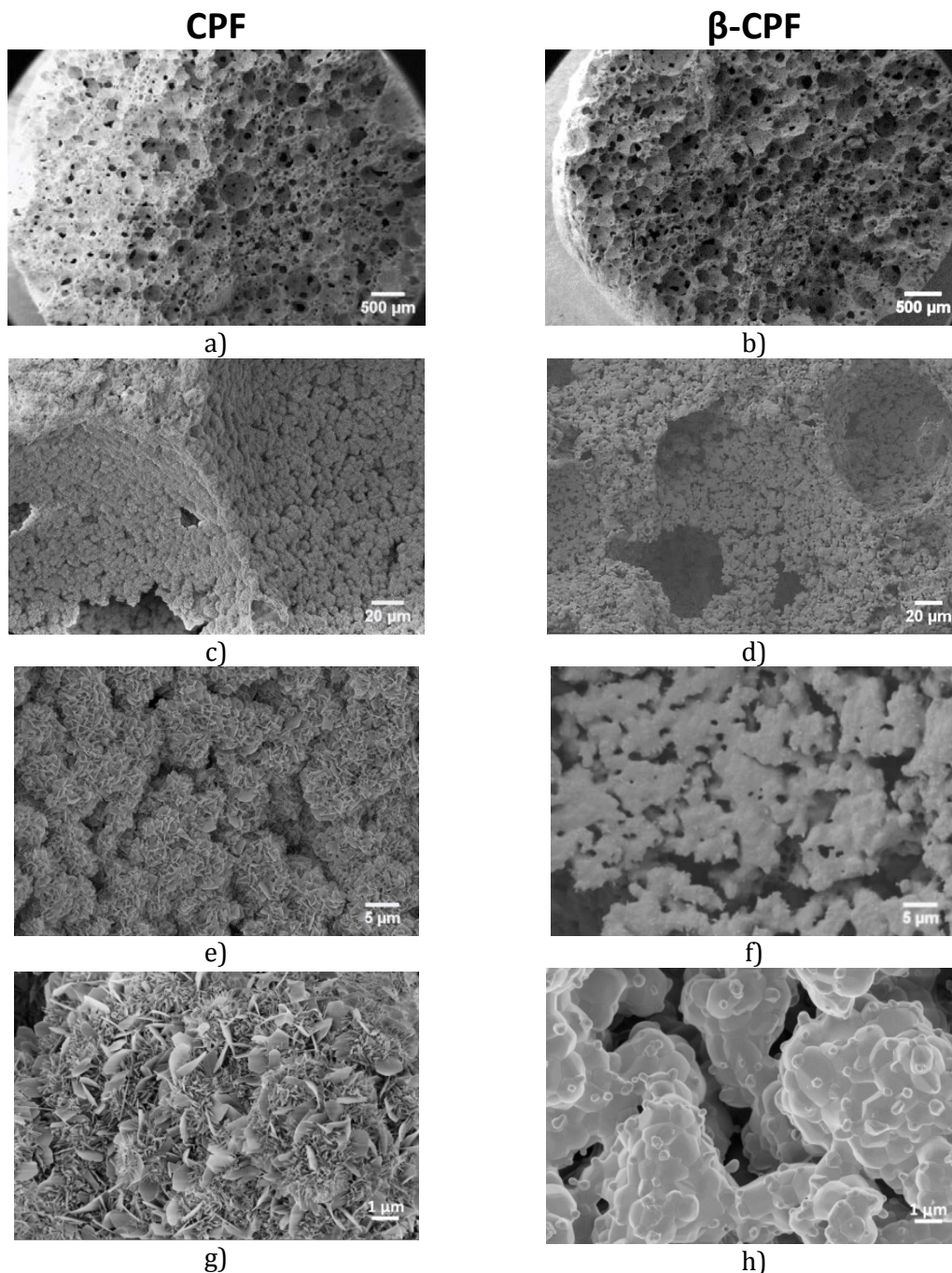


Figure 5.8 - Scanning electron micrographs of CPF (a, c, e, g) and β -CPF (b, d, f, h) at different magnification.

The specific surface area (SSA) of CPFs was 17.2 m²/g while that of β -CPF was 0.60 m²/g. The decrease of SSA was due to the sintering and it is in accordance to the microstructure showed in the scanning electron micrographs (Figure 5.8).

5.5.5 Total porosity and pore entrance size distribution

The total porosity and the pore entrance size distribution of CPFs and β -CPF were measured by mercury intrusion porosimetry. The total porosity was approximately the same for both materials developed and the control without PLU: 82.2 % for CPF, 77.7 % for CPF-0% PLU and 81.5 % for β -CPF. In Figure 5.9 the pore entrance size distribution measured by MIP is shown. The maximum peak of both CPF and β -CPF is at around 80 μ m as indicated in Figure 5.9 corresponding to the entrance size of the macropores, lower than that of the control which was around 110 μ m. There is another peak at around 2 μ m which corresponds to the distance between crystals/sintering-necks aggregates; this peak is visible both in β -CPF and CPF-0% PLU. The peak at the nanoscale was visible only in the low-temperature materials (CPF and CPF-0% PLU) and it is attributed to the distance between crystal platelets observed in these materials, which are not present in β -CPF.

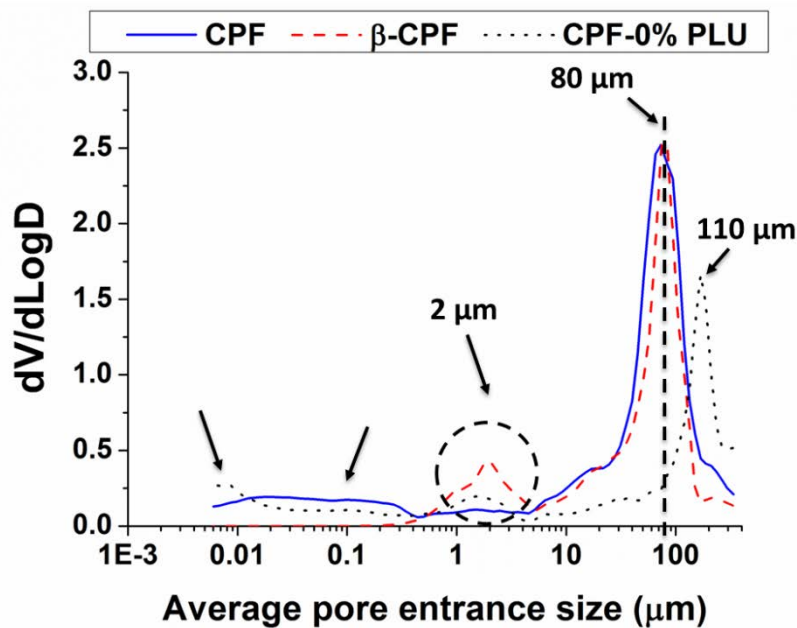


Figure 5.9-Pore entrance size of CPF (continuous line), β -CPF (dashed line) and of CPF-0% PLU (dot line).

5.5.6 Characterisation of the plasma polymer layer on flat models

In the first place it was of interest to evaluate the possibility of producing plasma polymer layers on the CaP materials, and to characterise the plasma polymer layer (PCL-co-PEG 1:4, indicated with p in the material) deposited on the CDHA and β -TCP. To this aim CaP discs with a L/P = 0.35 ml/g (herein named CDHA and β -TCP), without additives in the solid phase and with 2.5 wt% of Na_2HPO_4 as liquid phase, were employed.

a) FTIR-ATR spectroscopy

FTIR measurements were performed on material obtained from the top surface of the CaPs. As shown in Figure 5.10, all materials tested displayed phosphate vibrations, where the wide, strong bands correspond to ν_3 stretching (944–1122 cm^{-1}) and ν_4 bending (545–640 cm^{-1}) typical of calcium phosphates or apatites (**Radin, 1993; Mestres, 2011**). On the plasma coated materials (CDHA-p and β -TCP-p) different bands indicated the presence of the coating, which were more evident in β -TCP-p suggesting that a thicker coating was obtained. In particular, bands were recorded at 1716 cm^{-1} , which were attributed to the C=O stretching vibrations of the ester carbonyl group from PCL; C-H stretching bonds were centred at 2950 and 2870 cm^{-1} . The C-H bending was observed at 1380 and 1460 cm^{-1} . The weak absorption band at 3430 cm^{-1} was assigned to terminal -OH groups in the coatings which indicated the presence of polar groups incorporated into the copolymer structures (**Bhatt, 2012a**) (-OH groups from hydroxyapatite usually appear at higher bending energies 3567 cm^{-1} , according to (**Antonakos, 2007**)).

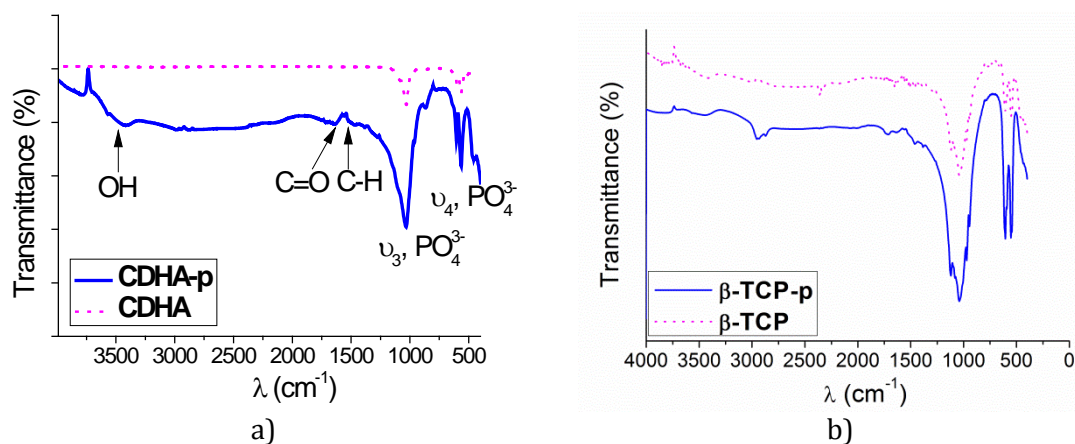


Figure 5.10 - IR-ATR spectra of the CaP materials without and with polymer layer a) CDHA and b) β -TCP.

b) X-ray Photoelectron Spectroscopy and wettability

Modifications on the surface chemistry were recorded by means of static contact angle and XPS measurements (Table 5.2). While both untreated materials were very hydrophilic and, due to their inherent porosity absorbed water very fast, and did not allow contact angle measurement, after the plasma polymerisation water was no longer absorbed and the contact angle raised to hydrophobic values above 110° in both materials, showing the highest values for β-TCP-p.

Table 5.2- Static contact angle and X-ray photoelectron spectroscopy (atomic concentration and atomic ratio) of the different CaP discs either untreated or after plasma polymerisation.

	θ_s (°)	Atomic concentration %				Atomic ratio	
		C1s	O1s	Ca2p	P2p	O/C	Ca/P
CDHA	*	10.51	57.81	19.05	12.62	5.50	1.51
CDHA-p	115 ± 1	76.09	23.75	0.12**	0.04**	0.30	--**
β-TCP	*	14.83	53.61	19.54	11.98	3.61	1.63
β-TCP-p	121 ± 2	76.99	23.01	--	--	0.29	--

* Not possible to measure contact angle due to too fast water absorption.

** Too small quantities to be taken with precaution.

The surface chemistry of the untreated CaPs correlated adequately with their chemical structure. The chemical formula of β-TCP is Ca₃(PO₄)₂, with a theoretical Ca/P ratio of 1.5 and for CDHA, the chemical formula is Ca₉(HPO₄)(PO₄)₅(OH)₂. None of the materials itself contains carbon, so its presence on the surface of the samples indicates either contamination by adsorbed hydrocarbons or to surface carbonation. The polymerisation treatment with PCL-PEG led to a decrease in the O/C ratio, showing the presence of polymer on the surface. The layer deposited in the case of β-TCP-p was thicker than the detection limit of the XPS (10 nm), as Ca and P species were no longer detected by the technique. In the case of CDHA-p both Ca and P were detected but in very small quantities which could be also ascribed to background noise, so they should be taken with precaution.

Table 5.3- C1s peak deconvolution.

Peak Material	Atomic percentage		
	C1s		
	284.77 C-C,C-H	286.40 C-O	288.41 C=O
CDHA-p	51.496	42.440	6.065
β-TCP-p	55.695	37.907	6.398

Table 5.3 presents the deconvolution of C1s peaks of the polymerised materials, and the deconvoluted peaks are shown in Figure 5.11. C1s core level spectra of the plasma polymerised samples showed a profile clearly including 3 peaks corresponding to: C-C C-H 284.77 eV, which were the most abundant groups, followed by C-O at 286.40 eV (in ether groups) and C=O 288.41 eV (probably carboxylic groups). The presence of these bonds is compatible with the presence of the copolymer PCL:PEG 1:4. The contribution of the C=O peaks was up to around 6% in both β -TCP-p and in CDHA-p.

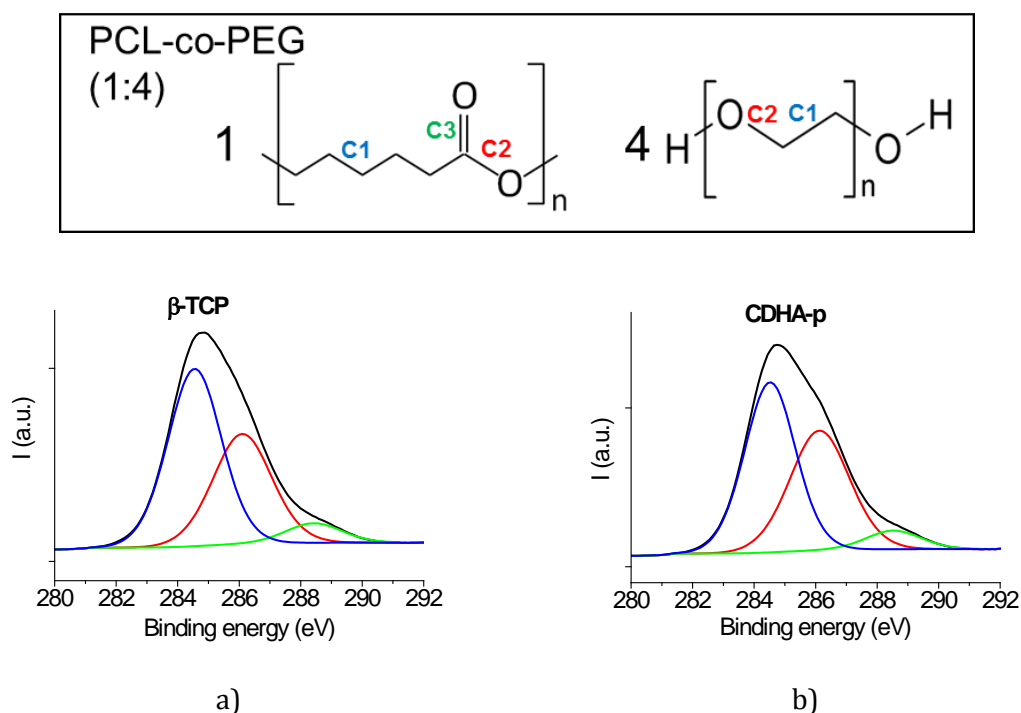


Figure 5.11 - X-ray Photoelectron Spectroscopy C1s peak deconvolution, of a) β -TCP and b) CDHA with PCL-co-PEG (1:4) plasma coating.

c) Micro- and macrostructure

The scanning electron micrographs obtained on the surface of the flat materials (Figure 5.12) reveal a mix of needle- and plate-like crystalline structures of CDHA and the sintering neck and grains of β -TCP (as described in 5.5.4). After plasma polymerisation with PCL-PEG the structure of the CaPs was covered by a layer following the original patterns of the materials, on the CDHA-p worm-like structures are visible, while on β -TCP-p the structures are more bush-like.

Transversal sections obtained by FIB (Figure 5.12e and f) revealed that the polymer layer was thick in both CaP materials, and confirmed the observations made by XPS regarding the plasma polymer deposited on β -TCP-p ($1.53 \pm 0.16 \mu\text{m}$) being thicker than that deposited on CDHA-p ($0.66 \pm 0.06 \mu\text{m}$) in the same experimental conditions.

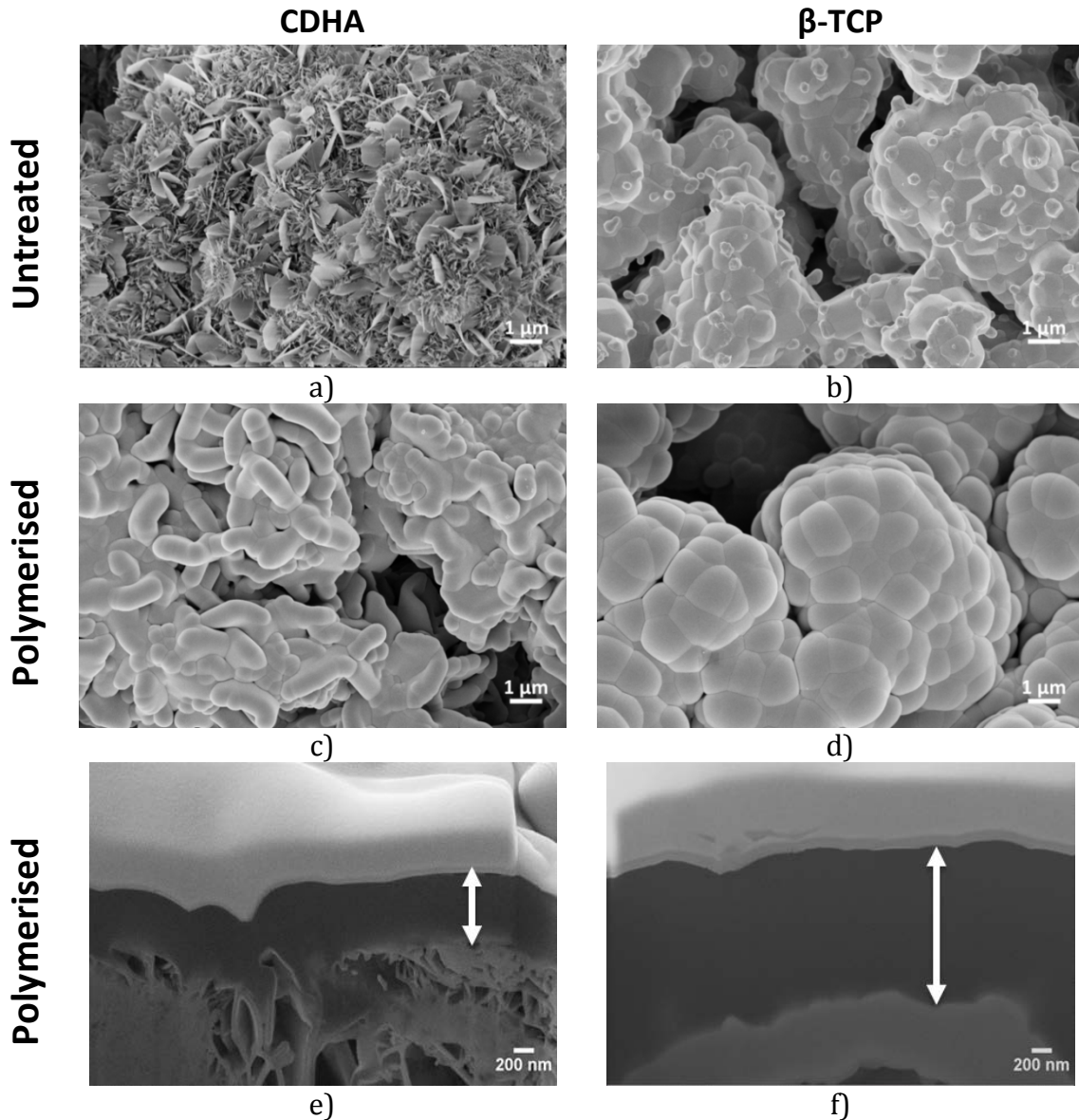


Figure 5.12- Scanning electron micrographs of the different materials before (top images) and after plasma polymerisation with PCL-PEG (4:1). a) CDHA, b) β -TCP, c) CDHA-p, d) β -TCP-p, and FIB-SEM cross-section of the surface of both polymerised materials e) CDHA-p and f) β -TCP-p.

5.5.7 Plasma polymerisation on 3D scaffolds

Once demonstrated that it was possible to produce PCL-co-PEG coatings on the surface of CDHA and β -TCP discs, treatment of 3D macroporous samples (Calcium Phosphate Foams, CPFs and β -CPFs) was evaluated. The scaffold was transversally sectioned in order to study the depth of penetration of the polymer.

As shown in the transversal section of a CaP foam (Figure 5.13 left), the sample contained macropores through all the structure, and plasma polymerisation showed the same bush-like and worm-like structures on the pores located on the top surface of the samples. In addition, for β -CPF, the plasma copolymers PCL-co-PEG were capable of penetrating up to a depth of 550 μm by diffusion through the interconnected macropores of the material. This was not observed for CPF samples, where the coating was restricted to the outer surface.

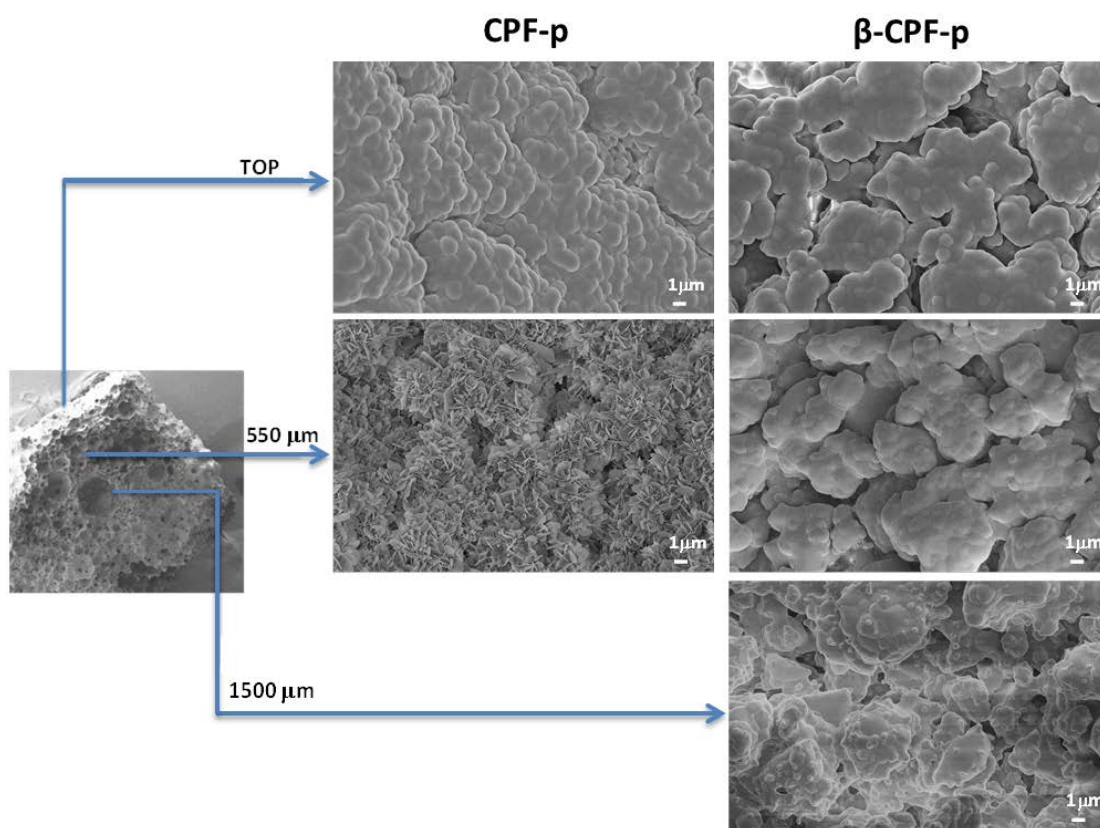


Figure 5.13- Scanning electron micrographs of transversal sections of CPF and β -CPF after polymerisation at different depths. Views of the surface of pores found on the top surface layer (top image), at a depth of 550 μm , and at 1500 μm (lower image).

5.5.8 SVA loading and release from 3D scaffolds

CaP scaffolds were drug-loaded by immersion in a solution containing SVA and subsequently freeze dried. High amounts of SVA were loaded on CPF (87 %) in only 2 h. As the SVA loading of β -CPF was much lower in the same timeframe, loading was evaluated at different timepoints (between 2 and 24 h), leading to loadings between 20% and 38 % of SVA, respectively. Accordingly, the longest loading time (24h) was selected for loading of β -CPF. Table 5.4 shows the data for the loading of the CPF and β -CPF.

Table 5.4- Simvastatin acid loaded on CPFs and β -CPFs.

Material	Q _{loaded} (μ g)	% Loaded
CPF	66 \pm 3	87.2 \pm 1.0*
β -CPF	35 \pm 2	38.1 \pm 1.7**

* Loading by immersion of the sample for 2 h. ** Loading by immersion of the sample for 24 h.

5.5.9 SVA release from 3D scaffolds

The release profile of SVA in PBS during 48 h from the different scaffolds is represented in Figure 5.14. The low release from CPF-SVA was fast in the first hour, reaching a plateau corresponding to \sim 10% of release after 2 h (Figure 5.14a). After polymerisation, significant differences were observed (Figure 5.14a) due to the polymer layer covering the drug. It is important to note that in CPF-SVA-p the release started after 2 h (delay) and then it was sustained reaching up to 15% in 48 h (Figure 5.14a). However, it has to be underlined that the amount of drug released was low in both cases and close to the lower limit of detection with this technique (which is around 2-3 μ g/ml) as well as the interferences of PLU (described in annex II) which might have been relevant.

Table 5.5- Simvastatin acid loaded and released from CPFs and β -CPFs.

Material	Q _{loaded/sample} (μ g)	% Loaded	Q _{released/sample} (μ g)	% Released 48h
CPF-SVA	66 \pm 3	87.2 \pm 1.0*	5.4 \pm 1.6	8.2 \pm 2.4
CPF-SVA-p	66 \pm 3	87.2 \pm 1.0*	10.0 \pm 0.6	15.1 \pm 0.9
β -CPF-SVA	35 \pm 2	38.1 \pm 1.7**	21.1 \pm 1.3	60.2 \pm 3.7
β -CPF-SVA-p	35 \pm 2	38.1 \pm 1.7**	0.7 \pm 0.3	1.9 \pm 0.9

* Loading by immersion of the sample for 2 h. ** Loading by immersion of the sample for 24 h.

In β -CPF a significantly different behaviour was observed. The quantity of drug loaded was much smaller (Table 5.5), but the amount and percentage of drug released was significantly higher, up to 60 % after 48h (Figure 5.14a). The release profile of SVA from β -CPFs was considerably altered after the plasma polymerisation. In fact, the untreated β -CPFs showed a progressive release, with a burst up to 45 % in the first 6 h of the experiment. On the contrary, in β -CPF-p, the PEG-PCL polymer layer deposited on the surface acted as a very effective barrier for the release of SVA, as no drug was released within the first 48 h. This might be interesting in the applications where a delayed release is needed.

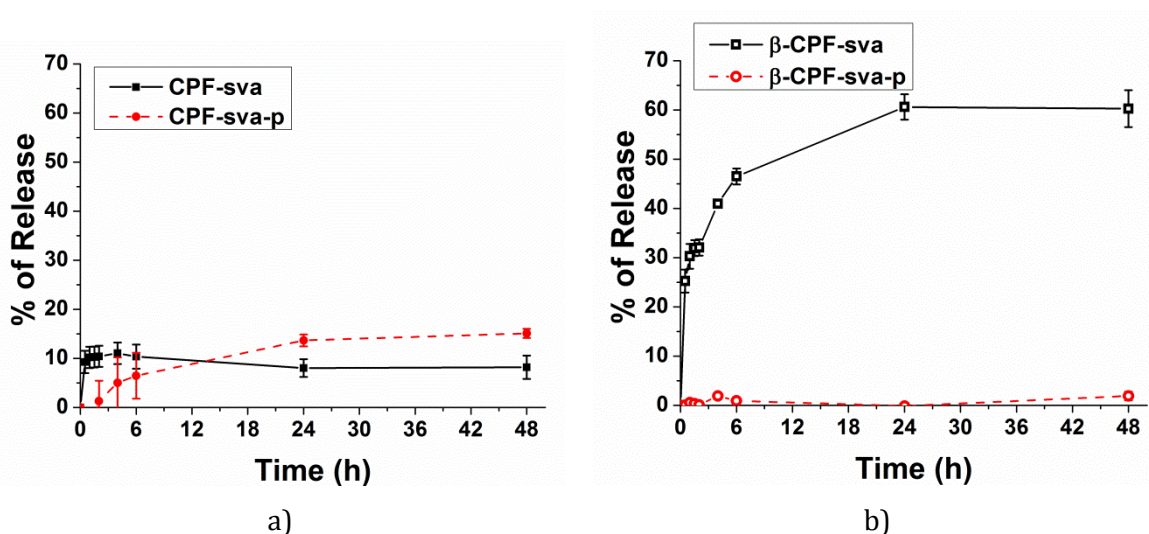


Figure 5.14- Cumulative release of SVA in (%) from a) CPFs or b) β -CPFs with hypothesis on the possible phenomena taking place (right).

5.6 Discussion

This work is based on the characterisation study of two different calcium phosphate (CaP) foams and their combination with simvastatin acid (SVA), in order to see the interactions of these materials with the drug and quantify loading and release with views on *in vitro* and *in vivo* studies. Drug release from CaPs greatly depends on properties such as specific surface area (**Canal, 2013; Ginebra, 2012**) or microporosity. To overcome some of the intrinsic limitations of CaPs to regulate drug release, this work has also focused on using an innovative treatment with cold plasma to create a polymer layer on the surface of drug loaded calcium phosphate scaffolds and being thus able to control drug release by a dry method.

Macroporosity is really important in bone regeneration. The lack of bone ingrowth due to absence of macroporosity led to failure of many bone substitutes (**Nguyen, 2012**). The advantage of introducing macroporosity in CaPs is envisaged as a method to facilitate bone ingrowth not only from the external surface but throughout the whole bulk of the material (**Montufar, 2011**) and it is also relevant in views of drug delivery (**Pastorino, 2014b Submitted**). Furthermore, macroporosity would accelerate scaffold resorption and transformation in newly formed bone tissue (**Karageorgiou, 2005**). The debate about the right dimensions of macroporosity is still an open dialogue but for sure it is known to influence cell behaviour (**Karageorgiou, 2005; Bchner, 2011**). There is a consensus about the importance of having an open porosity in order to allow fluids and cells penetration through the whole scaffold. The materials investigated in this work had a total porosity of about 80%, in the range of that of trabecular bone (75%-90%) (**Dorozhin, 2009**). The porosity was interconnected through an average pore entrance around 80 μm (also confirmed by scanning electron micrographs, Figure 5.8), which is a dimension adequate for cell colonisation. Nevertheless, materials with such a high porosity have a lack of mechanical properties; in fact it is well known that mechanical properties decrease with the increase of porosity (**Ishikawa, 1995; Takahashi, 1997; Barralet, 2002, Montufar, 2010**). The addition of Pluronic-127 (PLU) in the solid phase of the CPF increased mechanical properties in compression of about 2-3 times compared to the same material

without the polymer, probably due to the decrease of the micro-/nano- porosity observed in Figure 5.9. Sintering led to a further 3.5-fold increase (2.91 ± 0.91 MPa) compared to the CDHA scaffolds which can be attributed to the loss of the nanoporosity during sintering (Figure 5.9). Thus the compressive strength was still low but closer to that of trabecular bone (2-12 MPa (**Barinov, 2010**)) for CPFs, and in its range in the case of β -CPF.

As aforementioned, the addition of PLU in the solid phase increased the mechanical properties of CPFs, but it is important to underline that it did not hinder the cementitious reaction. In fact, one of the most important advantages of these materials is that they transform into CDHA, which is very close to the inorganic part of the bone (**Ginebra, 2008**). As shown in Figure 5.6, α -TCP hydrolysed into CDHA except for 8 % and, the thermal treatment led to calcium phosphate scaffolds made of β -TCP (Figure 5.6).

The macrostructure, porosity and interconnection diameter of the scaffolds did not change significantly after thermal treatment, while the microstructure with the associated properties (SSA) did. CPFs have a plate-like mixed with a needle-like crystalline structure (Figure 5.8e and g) while β -CPF presented the typical necks and polyhedral crystal grains consequent to sintering (Figure 5.8f and h). SSA decreased (around 30-fold) from $17.2 \text{ m}^2/\text{g}$ for CPF to $0.60 \text{ m}^2/\text{g}$ for β -CPF.

The differences in microstructure and thus in SSA reverted in a different drug loading. The behaviour followed here is in accordance with the fact that CaP microstructure is really relevant for the interactions with molecules. As shown in Table 5.4, the adsorption of SVA was much higher in CPF than in β -CPFs, as drug loading was more than doubled after only 2 h of soaking in front of 24 h employed for loading β -TCP scaffolds. This can probably be attributed to the higher SSA of CDHA, the different microstructure of the material and the chemical interactions between the drug and the substrate.

In order to delay and obtain a more controlled release, a polymer layer was deposited on the material through plasma polymerisation on the drug-loaded CaP foams. One advantage of using a dry method such as plasma for controlling the release lies in avoiding, for instance, any ion dissolution of the calcium phosphates and thus conserving intact their initial properties. Furthermore, if the material has

already been loaded with drugs as in this case, coating them is a complicated issue, as any contact with processing solutions would lead to dissolution/diffusion of the drugs and thus loss of the active principle from the biomaterial. Since plasma coating could have a great potential in this field, in order to investigate the feasibility of this type of coatings, flat specimens were used for the characterisation.

It has been shown that plasma polymers can be deposited on the surface of CaP materials. As shown by the IR spectra (Figure 5.10), the bands corresponding to C-H, C-O and OH confirm the formation of a polymer layer on the surface of the ceramics. The thickness of this polymeric layer is variable depending on the material used, i.e. the thickness was different in β -TCP ceramics or Hydroxyapatite CPCs since they have different microstructures and specific Surface Area (SSA). This was confirmed both by XPS, in which the Ca and P species were not detectable after the polymerisation treatment, and also by FIB cross-sectioning, which allowed measuring the thickness of the layers. Thus, β -TCP showed a layer which was two times thicker than the one deposited on CDHA in the same conditions. This can be attributed to the great differences in SSA between both materials. The thickness of the layer obtained was much higher than that recorded in previous works using the same techniques (**Bhatt, 2013**), mainly due to the longer treatment times employed (90 minutes in this study versus 20 minutes in the study of Bhatt *et al.*). The coating thickness (0.66 μm and 1.5 μm on CDHA and β -TCP, respectively) led to important changes in the surface topography of the CaP materials, leading to the formation of worm-like or bush-like structures (Figure 5.12). From the biological point of view this result can be of high relevance, as it is known (**Boyan, 1996; Deligianni, 2001**) that the cell response to biomaterials depends, among many other factors, on the topography, and the significant changes produced by the plasma copolymers deposited on CDHA and on β -TCP will for sure have an influence on their biological behaviour, which will have to be further investigated.

In this sense, the surface chemistry was also significantly modified, as shown by XPS results (Table 5.2) and the modified wettability of the materials. The thickness of the plasma polymer coatings was confirmed by the fact that Ca2p and P2p were

no longer detected by XPS. The 0.3 O/C ratio obtained in β -TCP and CDHA is lower than that of **(Bhatt, 2013)**, possibly related to differences in deposition conditions (mainly treatment time) and lower than the theoretical ratio of the copolymer which is around 0.42.

The PCL:PEG 1:4 plasma coatings deposited on the surface led to a significant changes in the wetting properties of the materials; both CaPs were initially hydrophilic, with fast water absorption, while after plasma polymerisation they were found to be hydrophobic, with contact angles between 115° and 121° . These high values contrast with the 8° obtained for a plasma polymer PCL-co-PEG (1:4) coating deposited at 1 W on a flat surfaces. **(Bhatt, 2012b)**. Although a short treatment was performed on top of the barrier layer at 1W PW, given the high specific surface area of the materials, they might not be completely covered by it. Thus, while it has been shown **(Bhatt, 2013)** that polymers deposited at 1W PW have C-O/C-C ratios of 2.2, in agreement to the low contact angles obtained, copolymers prepared in the same conditions as the thick layer of our work (20W CW) display C-O/C-C ratios of 0.35. Although we do not have data for contact angles deposited on flat surfaces at 20W CW, considering the C-O/C-C ratio it can be expected that contact angles for such copolymer are much higher. In future works, the parameters of the plasma polymerised coatings could be optimised in order to obtain a layer with a more hydrophilic behaviour.

Once corroborated the possibility to obtain plasma polymerised coatings on 2D CaPs, the attention shifted to the macroporous 3D scaffolds (CPFs and β -CPFs). Also, in this case it was demonstrated that the plasma polymer coating can be performed successfully on the materials, and that the interconnections between the macropores of the CaP foams allowed the penetration of the plasma polymer inside the scaffold (Figure 5.13). This was particularly evident in the case of β -CPF, where the characteristic bush-like structures can be observed both on the surface, and inside pores of the scaffold up to a depth of $550\ \mu\text{m}$. The higher SSA of CDHA was probably related to the fact that the coating layer was restricted to the top surface of the CPFs, and no penetration was observed, as possibly most available monomer was already consumed in the coating of the wide surface.

In the subsequent steps, the release behaviour of the different samples (native or plasma-coated) was evaluated.

Drug release patterns were significantly modified by the PCL-co-PEG plasma coating (Table 5.5) on top of the drug-loaded scaffold. On one hand, untreated β -CPF scaffolds showed an initial burst release leading to a release above 60 % in 48h. Contrarily, the β -CPF scaffolds plasma coated with the PCL-co-PEG (β -CPF-p) did not show any SVA release in the timeframe evaluated (Scheme on Figure 5.15b).

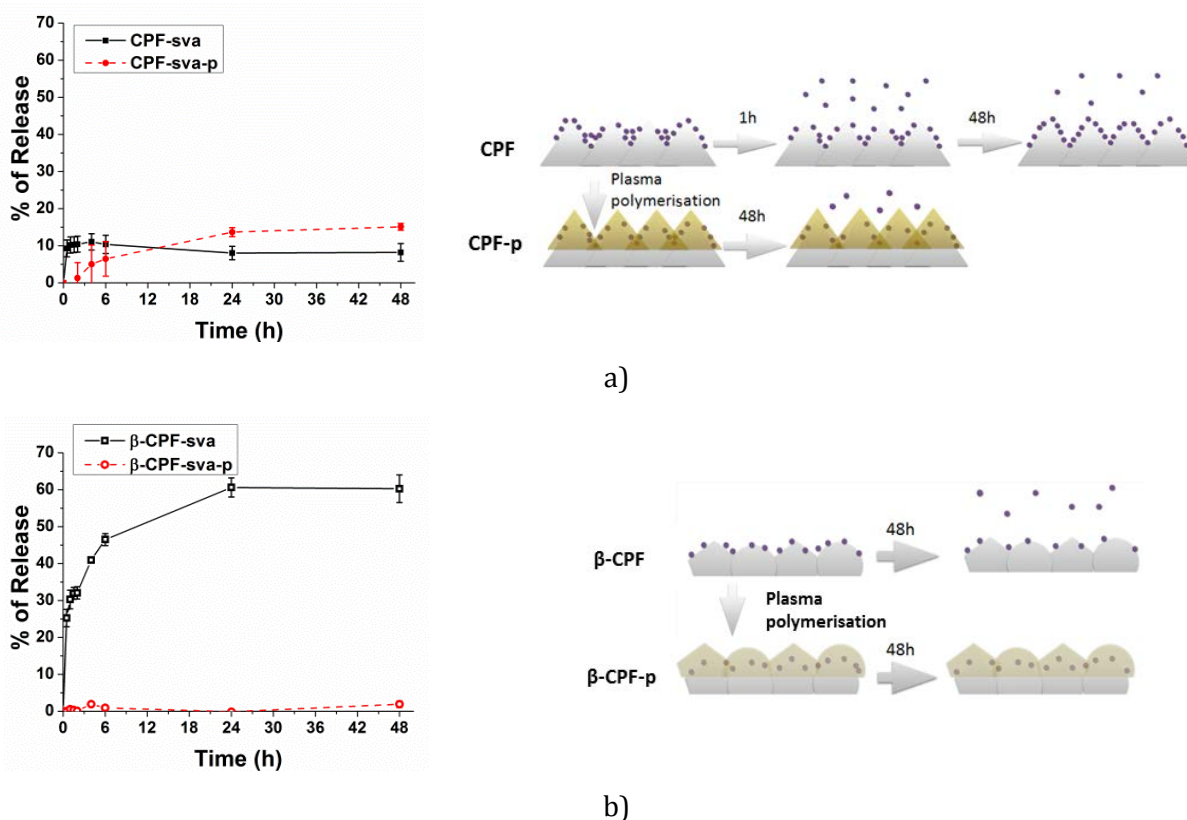


Figure 5.15- Cumulative release of SVA in (%) from a) CPFs or b) β -CPFs with hypothesis on the possible phenomena taking place (right).

This is indicative of the lack of diffusion through the thick layer deposited on the β -TCP, so possibly it will be required that the layer would degrade, at least partly, before any drug release can be detected. This result is relevant since it allows both avoiding the burst release in β -CPF and obtaining a late release when desired, dependent on the degradation of the polymer.

On the other hand, the different features of CPF, such as the more intricate microstructure, high SSA and probably a high affinity of the drug with the

substrate impaired SVA release from the untreated CPF, and only $\approx 10\%$ was released in the same timeframe. In the case of the drug-loaded CPF which was coated with the PCL-co-PEG copolymers, the thinner layer on CPF-p (with respect to β -CPF-p) reverted in a different drug release kinetics (Figure 5.15a): i) the release was delayed of 2 h, ii) there was no burst release but a slow diffusion of SVA through the polymer layer and iii) the release rate was lower, sign of a more sustained release. It is possible that the interactions of SVA with the external surface of the scaffold (the one in contact with the media) were modified by the polymeric layer; the probable lower affinity of the drug to the polymer might have displaced the equilibrium and allowed a higher extent of drug (15 %) to be released to the media. Longer time-frame *in vitro* studies are needed in future to better understand the release mechanisms and the degradation rate of the plasma polymer layer.

5.7 Conclusions

In this work it has been shown that calcium phosphate scaffolds can successfully be loaded with simvastatin acid, an angiogenic promoter. Their mechanical properties are high enough to bear implantation even if the porosity is really high and well interconnected. Different microstructures with a similar macrostructure have been successfully obtained by thermal treatment. Furthermore, it has been shown that plasma polymerisation of PCL-co-PEG (1:4) is possible on calcium phosphate biomaterials (β -TCP and CDHA), and that the thickness and structure of the polymer layer obtained is highly dependent on the texture of the materials, in particular on its SSA. Thicknesses of up to 1.5 μm were obtained on β -TCP, and the plasma polymers were able to penetrate the macroporous structure of 3D calcium phosphate foams, up to a certain depth. The topography and chemistry of the materials were significantly modified by the coatings which led to nanorough structures which could partly explain the low wettability measured on the materials.

The amount of drug released from CPF was really low, due to the intricate microstructure, the high SSA and possibly the drug interactions with the scaffold.

On the contrary, fast release was obtained by β -CPF. The thicker PCL-co-PEG layer acted as barrier on β -CPF delaying SVA release above 48 h, while on CDHA the presence of the thinner polymer layer allowed for the diffusion of the drug leading to progressive and enhanced drug release with respect to the uncoated biomaterial. Thus, the plasma coatings evaluated can be useful tools for the tuning of drug release from bone biomaterials. Longer time-frame studies should be conducted to better understand the release.

However, since the debate on the proper dose is still open, to corroborate the effects of these materials, *in vitro* and, above all, *in vivo* studies should be performed.

5.8 Biological characterisation of the foams

Preliminary results of the *in vitro* biological characterisation of the β -CPFs performed by some partners of the European project REBORNE are briefly introduced in this section. β -CPFs were selected for these studies due to their higher mechanical properties and higher SVA release.

5.8.1 Evaluation of β -CPF and human mesenchymal stem cells.

The *in vitro* studies in this section were obtained at the Max Plank Institute of Polymer Research (MPIP) of Mainz (Germany) by Dr. Sandra Ritz.

The objective of this work was the evaluation of the interaction between the novel scaffold, based on β -CPF developed and characterised in the previous section and human Mesenchymal Stem Cell (hMSC) seeded either statically or dynamically.

Different amounts of hMSCs ranging between 0.25×10^6 and 2×10^6 were successfully seeded on β -TCP both statically and dynamically. No difference between the two types of seeding was recorded. Furthermore, the highest efficiency of the seeding (ratio viable cells/seeded cells) was obtained for 0.25×10^6 cells per scaffold, possibly due to the fact that in the other cases the number of cells was so high that confluence was already reached in the beginning. Moreover, it is remarkable the fact that after 21 days hMSCs could be observed well spread all over the scaffolds.

5.8.2 Rabbit Mesenchymal Stem Cell and Endothelial Cell Response to β -TCP Scaffolds with Simvastatin Acid

This work was performed at the University of Modena and Reggio Emilia (UNIMORE), in Modena (Italy) by the group of Prof. Massimo Dominici. In the second part of the work, the partner also collaborated with the laboratory of Prof. Giulio Alessandri (University of Milan).

The aim of the study was to preliminary test *ex vivo* the behaviour of β -CPF loaded with simvastatin acid (SVA), in views of *in vivo* tests in a rabbit arterial pedicle model. For testing the initial cell responses to the new β -CPF, rabbit mesenchymal stem cells (rMSCs) transfected with green fluorescent protein were used. In the second part, the work aimed at determining whether the scaffolds with SVA, could exert an *ex vivo* cellular response consistent with an enhancement of angiogenic activity.

The preliminary *ex vivo* characterisation of the scaffolds was performed to see whether the scaffolds could be combined with bioactive compounds to enhance vascular growth. It was observed prompt adhesion of rMSC onto the scaffolds, achieved within a clinically relevant time frame of one hour. The scaffolds maintained the viability of rMSCs over an extended period of *ex vivo* culture and after 14 days it was observed that the cells had migrated well within the cylindrical scaffold.

SVA addition did not seem to greatly influence the adhesion or migration potential of the MSC (neither positively nor negatively), but a significant endothelial cell mitogenic response was seen using conditioned medium from human MSC (hMSC) grown on β -CPF previously loaded with SVA. Although when testing the conditioned medium obtained from hMSC grown on SVA loaded β -CPF scaffolds, there was a marked induction of endothelial proliferation and morphological change to more fusiform cells consistent with endothelial activation, this effect was not seen in conditioned medium from hMSC grown on β -CPF scaffolds alone, or with medium conditioned by β -CPF loaded with SVA but without hMSC. This result would suggest that SVA on the β -TCP scaffold was bioactive on the hMSC, inducing them to secrete a factor into the conditioned medium that could enhance endothelial proliferation. However what this factor or factors might be was not explored.

In vivo experiments are underway to provide further verification of these positive *ex vivo* observations and explore the biodegradability of the scaffold.

References

Antonakos A, Liarokapis E, Leventouri T. Micro-Raman and FTIR studies of synthetic and natural apatites. *Biomaterials*. 2007; 28(19): 3043-3054.

Barinov SM. Calcium phosphate-based ceramic and composite materials for medicine. *Russ. Chem. Rev.* 2010; 79 (1): 13-29.

Barralet JE, Grover L, Gaunt T, Wright AJ, Gibson IR. Preparation of macroporous calcium phosphate cement tissue engineering scaffold. *Biomaterials* 2002; 23(15): 3063-3072.

Bhatt S, Pulpytel J, Mirshahi M, Arefi-Khonsari F. Catalyst-Free Plasma-Assisted Copolymerization of Poly(ϵ -caprolactone)-poly(ethylene glycol) for Biomedical Applications. *ACS Macro Lett.*, 2012a; 1 (6): 764–767.

Bhatt S, Pulpytel J, Mirshahi M, Arefi-Khonsari F. Catalyst-Free Plasma-Assisted Copolymerization of Poly(ϵ -caprolactone)-poly(ethylene glycol) for Biomedical Applications. *ACS Macro Lett.* 2012b; 1 (6): 764–767.

Bhatt S, Pulpytel J, Mirshahi M, Arefi-Khonsari F. Plasma Co-polymerized Nano Coatings – As a Biodegradable Solid Carrier for Controlled Drug Delivery Applications. *Polymer*. 2013; 54 (18): 4820-4829.

Bohner M, Loosli Y, Baroud G, Lacroix D. Commentary: Deciphering the link between architecture and biological response of a bone graft substitute. *Acta Biomater.* 2011; 7(2): 478-484.

Bose S, Tarafder S. Calcium phosphate ceramic systems in growth factor and drug delivery for bone tissue engineering: a review. *Acta Biomater.* 2012; 8(4): 1401-1421.

Boyan BD, Hummert TW, Dean DD, Schwartz Z. Role of material surfaces in regulating bone and cartilage cell response. *Biomaterials.* 1996; 17(2): 137-146.

Canal C, Pastorino D, Mestres G, Schuler P, Ginebra MP. Relevance of microstructure for the early antibiotic release of fresh and pre-set calcium phosphate cements. *Acta Biomater.* 2013; 9(9): 8403-8412.

Chen PY, Sun JS, Tsuang YH, Chen MH, Weng PW, Lin FH. Simvastatin promotes osteoblast viability and differentiation via Ras/Smad/Erk/BMP-2 signaling pathway. *Nutr. Res.* 2010; 30(3): 191-199.

Chuang SC, Liao HJ, Li CJ, Wang GJ, Chang JK, Ho ML. Simvastatin enhances human osteoblast proliferation involved in mitochondrial energy generation. *Eur. J. Pharmacol.* 2013; 714(1-3): 74-82.

Deligianni DD, Katsala ND, Koutsoukos PG, Missirlis YF. Effect of surface roughness of hydroxyapatite on human bone marrow cell adhesion, proliferation, differentiation and detachment strength. *Biomaterials.* 2001; 22(1): 87-96.

Dorozhin SV. Calcium orthophosphates in Nature, Biology and Medicine. *Materials* 2009; 2(2): 399-498.

Espanol M, Perez RA, Montufar EB, Marichal C, Sacco A, Ginebra MP. Intrinsic porosity of calcium phosphate cements and its significance for drug delivery and tissue engineering applications. *Acta Biomater.* 2009; 5(7): 2752-2762.

Fukui T, Ii M, Shoji T, Matsumoto T, Mifune Y, Kawakami Y, Akimaru H, Kawamoto A, Kuroda T, Saito T, Tabata Y, Kuroda R, Kurosaka M, Asahara T.

Therapeutic effect of local administration of low-dose simvastatin-conjugated gelatin hydrogel for fracture healing. *J. Bone Miner. Res.* 2012; 27(5): 1118-1131.

Ginebra MP, Espanol M, Montufar EB, Perez RA, Mestres G. New processing approaches in calcium phosphate cements and their applications in regenerative medicine. *Acta Biomater.* 2010; 6(8): 2863 - 2873.

Ginebra MP. Calcium phosphate bone cements, in: Deb S, ed. *Orthopaedic bone cements*. Woodhead Publishing Ltd., Cambridge, 206-230 (2008).

Ginebra, MP, Canal C, Espanol M, Pastorino D, Montufar EB. Calcium phosphate cements as drug delivery materials. *Adv. Drug Deliver. Rev.* 2012; 64(12): 1090-1110.

Golomb BA, Evans MA. Statin adverse effects : a review of the literature and evidence for a mitochondrial mechanism. *Am J Cardiovasc Drugs.* 2008; 8(6): 373-418.

Ishikawa K, Asaoka K. Estimation of ideal mechanical strength and critical porosity of calcium phosphate cement. *J Biomed Mater Res.* 1995; 29(12): 1537-1543.

Kaesemeyer WH, Caldwell RB, Huang J, Caldwell RW. Pravastatin sodium activates endothelial nitric oxide synthase independent of its cholesterol-lowering actions. *J Am Coll Cardiol.* 1999; 33(1): 234-241.

Kaji H, Kanatani M, Sugimoto T, Chihara K. Statins modulate the levels of osteoprotegerin/receptor activator of NFkappaB ligand mRNA in mouse bone-cell cultures. *Horm Metab Res* 2005; 37(10): 589-592.

Kaji H, Naito J, Inoue Y, Sowa H, Sugimoto T, Chihara K. Statin suppresses apoptosis in osteoblastic cells: role of transforming growth factor-beta Smad3 pathway. *Horm Metab Res* 2008; 40(11): 746-751.

Karageorgiou V, Kaplan D. Porosity of 3D biomaterial scaffolds and osteogenesis. *Biomaterials*. 2005; 26(27): 5474-5491.

Mauro VF. Clinical pharmacokinetics and practical applications of simvastatin. *Clin Pharmacokinet*. 1993; 24(3):195-202.

Mestres G, Le Van C, Ginebra MP. Silicon-stabilized α -tricalcium phosphate and its use in a calcium phosphate cement: characterization and cell response. *Acta Biomater*. 2012; 8(3): 1169-1179.

Montazerolghaem M, Engqvist H, Karlsson Ott M. Sustained release of simvastatin from premixed injectable calcium phosphate cement. *J. Biomed. Mater. Res. A*. 2014; 102(2): 340-347.

Montufar EB, Gil C, Traykova T, Ginebra MP, Planell JA. Foamed beta-Tricalcium phosphate scaffolds. *Key Eng. Mater*. 2008; 361-363: 323-326.

Montufar EB, Traykova T, Gil C, Harr I, Almirall A, Aguirre A, Engel E, Planell JA, Ginebra MP. Foamed surfactant solution as a template for self-setting injectable hydroxyapatite scaffolds for bone regeneration *Acta Biomater*. 2010; 6 (3): 876-885.

Montufar EB, Traykova T, Planell JA, Ginebra MP. Comparison of a low molecular weight and a macromolecular surfactant as foaming agents for injectable self setting hydroxyapatite foams: Polysorbate 80 versus gelatine. *Mat. Sci. Eng. C*. 2011; 31: 1498–1504.

Mundy G, Garrett R, Harris S, Chan J, Chen D, Rossini G, et al. Stimulation of bone formation in vitro and in rodents by statins. *Science*. 1999; 286: 946-949.

Mundy GR. Statins and their potential for osteoporosis. *Bone* 2001; 29 (6): 495-497

Nguyen LH, Annabi N, Nikkhah M, Bae H, Binan L, Park S, Kang Y, Yang Y, Khademhosseini A. Vascularized bone tissue engineering: approaches for potential improvement. *Tissue Eng. Part. B Rev.* 2012; 18(5): 363-382.

Nyan M, Miyahara T, Noritake K, Hao J, Rodriguez R, Kuroda S, Kasugai S. Molecular and tissue responses in the healing of rat calvarial defects after local application of simvastatin combined with alpha tricalcium phosphate. *J. Biomed. Mater. Res. B. Appl. Biomater.* 2010; 93(1): 65-73.

Nyan M, Sato D, Kihara H, Machida T, Ohya K, Kasugai S. Effects of the combination with alpha-tricalcium phosphate and simvastatin on bone regeneration. *Clin. Oral. Implants. Res.* 2009; 20(3): 280-187.

Nyan M, Sato D, Oda M, Machida T, Kobayashi H, Nakamura T, Kasugai S. Bone formation with the combination of simvastatin and calcium sulfate in critical-sized rat calvarial defect. *J. Pharmacol. Sci.* 2007; 104(4): 384-386.

Pastorino D, Canal, C, Ginebra MP. New single-step manufacturing process for foamed biomaterials. 2014a. Patent number: P201430964.

Pastorino D, Canal, C, Ginebra MP. Macropores, antibiotic and calcium phosphate, the winning cocktail? *Acta Biomater.* (Submitted 2014b)

Pauly S, Luttosch F, Morawski M, Haas NP, Schmidmaier G, Wildermann B. Simvastatin locally applied from a biodegradable coating of osteosynthetic implants improves fracture healing comparable to BMP-2 application. *Bone.* 2009; 45(3): 505-511.

Radin SR, Ducheyne P. The effect of calcium phosphate ceramic composition and structure on in vitro behavior. II. Precipitation. *J. Biomed. Mater. Res.* 1993; 27(1): 35-45.

Rojbani H, Nyan M, Ohya K, Kasugai S. Evaluation of the osteoconductivity of α -tricalcium phosphate, β -tricalcium phosphate, and hydroxyapatite combined

with or without simvastatin in rat calvarial defect. *J. Biomed. Mater. Res. A.* 2011; 98(4): 488-498.

Takahashi T, Yamamoto M, Ioku K, Goto S. Relationship between compressive strength and pore structure of hardened cement pastes. *Adv. Cem. Res.* 1997; 9(30): 25-30.

Tiwari R, Pathak K. Statins therapy: a review on conventional and novel formulation approaches. *J. Pharm. Pharmacol.* 2011; 63(8): 983-998.

Wadagaki, R, Mizuno, D, Yamawaki-Ogata, A, Satake, M, Kaneko, H, Hagiwara, S, Yamamoto, N, Narita, Y, Hibi, H, Ueda, M. Osteogenic induction of bone marrow-derived stromal cells on simvastatin-releasing, biodegradable, nano- to microscale fiber scaffolds. *Ann. Biomed. Eng.* 2011, 39(7): 1872-1881.

Walter MS, Frank MJ, Rubert M, Monjo M, Lyngstadaas SP, Haugen HJ. Simvastatin-activated implant surface promotes osteoblast differentiation in vitro. *J. Biomater. Appl.* 2014; 28(6): 897-908.

Wong RW, Rabie AB. Histologic and ultrastructural study on statin graft in rabbit skulls. *J. Oral. Maxillofac. Surg.* 2005; 63(10): 1515-1521.

Yang F, Zhao SF, Zhang F, He FM, Yang GL. Simvastatin-loaded porous implant surfaces stimulate preosteoblasts differentiation: an in vitro study. *Oral. Surg. Oral. Med. Oral. Pathol. Oral. Radiol. Endod.* 2011; 111(5): 551-556.

Yasuda H. Plasma polymerization, Academic Press Inc., Orlando, FL, 1985.

Zhang Y, Bradley AD, Wang D, Reinhardt RA, Statins, Bone Metabolism and Treatment of Bone Catabolic Diseases, *Pharmacological Research* (2014), <http://dx.doi.org/10.1016/j.phrs.2013.12.009>

Zhang Y, Zhang R, Li Y, He G, Zhang D, Zhang F. Simvastatin augments the efficacy of therapeutic angiogenesis induced by bone marrow-derived

mesenchymal stem cells in a murine model of hindlimb ischemia. *Mol. Biol. Rep.* 2012, 39(1): 285-293.

Chapter 6

General conclusions and future perspectives

6.1. Conclusions

Biphasic calcium phosphates cements

1. Biphasic calcium deficient hydroxyapatite/ β -Tricalcium phosphate (CDHA/ β -TCP) with a precise control of phase composition were obtained by hydrolysis of a combination of α -TCP and β -TCP. Setting times increased by the addition of β -TCP, which was associated to the fact that the setting of the cement was caused by the transformation of α -TCP to CDHA, whereas β -TCP remained unaltered. The smaller amount of CDHA crystals caused a less efficient interlocking, which affected the mechanical properties.
2. The final microstructure consisted of β -TCP particles embedded in the CDHA matrix. . This complex microstructure, together with the decreasing SSA with increasing β -TCP content explains the fact that Ca^{2+} release and weight loss were unaffected by the increasing amounts of β -TCP in the timeframe evaluated. However, higher dissolution and Ca^{2+} release should not be ruled out in longer-term studies, once the more soluble phase β -TCP is exposed to the surrounding media.

Fibre-reinforced calcium phosphate cements

1. Fibre-reinforced calcium phosphate cements (FRCPCs) with improved fibre-matrix adhesion were obtained by introducing a polymer in the liquid phase of the cement with high affinity to the fibres used as reinforcing agents. A marked effect was observed in Trimethyl chitosan (TMC)-containing CPCs reinforced with chitosan fibres, with significantly improved elastic modulus, flexural strength and work of fracture compared to the fibre-containing cements without TMC. Contrarily, lactic acid-containing CPCs mixed with polylactic acid (PLLA) fibres did not show any enhancement of the mechanical properties when compared with the FRCPCs without lactic acid.
2. Oxygen plasma treatment of the fibres was shown to be an efficient method to increase wettability and subsequently enhancing the compatibility between fibres and matrix of FRCPCs. Specifically, surface functionalisation of PLLA yarns with oxygen-containing moieties improved the adhesion between the fibres and the hydraulic matrix, as demonstrated by the enhanced flexural properties, including elastic modulus, flexural strength and work of fracture compared to the untreated fibres.
3. MG63 cell behaviour was affected both by the additives in the matrix and the presence of the fibres. The acidic pH generated by the presence of LA in the matrix impaired and/or slowed down the MG63 cell growth. PLLA fibres improved ALP expression by MG63.

Macroporous calcium phosphate scaffolds for the delivery of simvastatin acid

1. Macroporous calcium phosphate foams with different compositions (either CDHA or β -TCP) and microstructures, and a similar macrostructure can be obtained by foaming of a calcium phosphate cement (CDHA), followed by a thermal treatment (β -TCP).

2. Simvastatin acid (SVA) loading and release from macroporous calcium phosphate scaffolds was strongly affected by the microstructure and its associated properties as SSA and microporosity. A higher amount of SVA and faster loading was found for the CDHA foams than for β -TCP foams, possibly due to the higher SSA. Fast release was obtained from both materials. The amount of drug released in 48 hours from CDHA foams was low (around 10%) due to the intricate microstructure, high SSA and possibly the drug interactions with the scaffold, whereas it was around 60 % for β -TCP foams.
3. Biocompatible polymeric coatings on the calcium phosphate scaffolds can be obtained by plasma polymerisation. Specifically, Polycaprolactone-co-Polyethylene glycol (PCL-co-PEG) coatings were successfully obtained, the thickness and structure of the polymer layer being highly dependent on the texture of the substrate. The presence of the coating was shown to modulate the drug release from these biomaterials; the thicker PCL-co-PEG layer acted as barrier on β -TCP foams, avoiding any SVA release in the first 48 h, while the presence of the thinner polymer layer on the CDHA foams allowed for the diffusion of the drug, leading to a delayed and slower drug release with respect to the uncoated biomaterial.

6.2. Future Perspectives

The results obtained in this Thesis are promising in the field of bone substitute development. In order to increase their potential further studies should be performed.

Long-term degradation studies of BCPCs should be performed, since higher dissolution and Ca^{2+} release should not be excluded once the more soluble phase is exposed to the surrounding media. This change in the ion concentration could trigger bone cell activity. Furthermore, BCPCs could also be prepared as macroporous foams in order to increase the dissolution rate and eventually allow cells and vessel penetration.

Regarding the work on FRCPCs further investigation should be performed as well. First of all pull-out testing should be performed since they could be useful to further evaluate the adhesion between matrix and fibres. Moreover, degradation studies should be undertaken in order to verify how long the mechanical properties improvement lasts. Regarding the work using chitosan fibres, it could be possible to graft some molecules (i.e. drugs or growth factors) on them in order to further improve the adhesion fibre matrix or to allow their release. Furthermore different longitudes of the fibres could be also tested, as well as, different fibres shapes (in order to increase the fraction during the pull-out). Concerning the materials containing PLLA fibres, probably it would worth to use PLGA fibres instead of PLLA, in order to tune the degradability and obtain a faster resorbability. Moreover, the use of plasma for improving fibre/matrix adhesion should be further investigated, i.e. using Ar or N₂ at different treatment times. Furthermore the effect of the ageing of the plasma treatment on the fibres should be tested for eventual clinical purposes (shelf-life).

In regard to macroporous scaffolds for SVA release, since the amount of drug released is crucial, the efficiency of the release should be optimised. One approach could be changing the initial amount loaded, possible to obtain modifying the concentration of the initial solution. Another approach could be pursuing the controlled-release through the modulation by plasma co-polymerisation coatings. The hydrophobic properties of the co-polymer should be changed to more hydrophilic properties, possible to obtain through the modification of the copolymer composition together with the setting of the treatment (e.g. power and time). Furthermore, long term degradation studies of the polymer layer should be undertaken, as well as longer time-frame for the release studies, in order to verify the delay of the drug release from β -TCP scaffolds. Since the debate on the proper SVA dose to obtain angiogenesis is still open, more *in vitro* and, above all, *in vivo* studies (some *in vivo* experiments are already underway) should be performed with different SVA amounts.

Annexes

Annex I

X-ray diffraction (Phase quantification)

X-ray diffraction (XRD) is used in order to quantify either the relative amount of crystalline phases in mixtures, or simply the powder composition, by referencing the relative peak intensities. Diffraction occurs when light is scattered by a periodic array with long-range order, producing constructive interference at specific angles. Therefore, depending on the crystalline structure the constructive interference will be at different angles.

The scattering of the X-rays from the atoms produces a diffraction pattern, which contains information about the atomic arrangement within the crystal. The intensity of the diffraction peaks are determined by the arrangement of atoms in the entire crystal.

The position of the diffraction peaks are determined by the distance between parallel planes of the atoms. Bragg's law (Equation below) allows calculating the angle where constructive interference from X-ray scatter by parallel planes of atoms takes place:

$$\lambda = 2d_{hkl} \sin\theta \quad (\text{A.1})$$

Where:

λ is the x-ray wavelength which is often fixed with the device.

d_{hkl} is the vector drawn from the origin of the unit cell to intersect the crystallographic plane (hkl) at a 90° angle and it is a geometric function of the size and shape of the unit cell.

θ is the angle which is varied by time.

A scheme of the apparatus is reported in Figure 1 where the X-ray tube, the sample and the detector are drawn together with the different parameters.

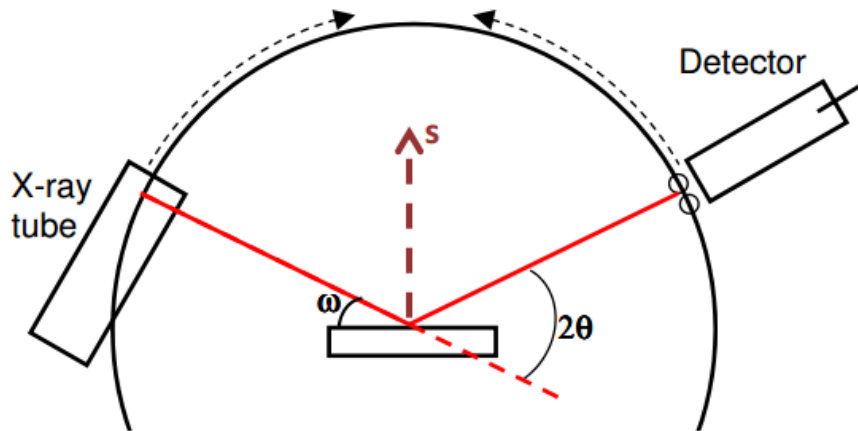


Figure 1- Scheme of the X-ray diffraction device.

As shown in Figure 1:

- The incident angle, ω , is defined between the x-ray source and the sample.
- The diffraction angle, 2θ , is defined between the incident beam and the detector.
- The incident angle ω is always $\frac{1}{2}$ of the detector angle 2θ .

It is known that amorphous materials do not have a periodic array with long-range order, so they do not produce a diffraction pattern. Thus the signal decreases from perfectly crystalline to amorphous materials.

In calcium phosphates composed by more than one phase (due to incomplete transformation or to desired multiphasic composition), the difference in absorption of the x-rays by the different phases has to be taken into account. In 1974 Chung (**Chung, 1974**) developed a simple method to quantify the different phases. The complexity of the analysis of multiple phases in a mixture can be greatly reduced if all of the pure phase peak intensities are referenced to a single standard (I_c is the intensity of corundum or α -alumina). The reference intensity for a phase i is defined as:

$$k_i = I_i/I_c \quad (A.2)$$

The following equation shows how to calculate the weight fraction (X) of a *i*-component in a multiple-phase mixture with n elements:

$$X_i = \frac{1}{\frac{k_i}{I_i} \sum_{i=1}^n \frac{I_i}{k_i}} \quad (\text{A. 3})$$

In the materials analysed in this thesis n=2 or 3, depending on the case. The equation becomes, in the case of n=3:

$$X_1 = \frac{1}{\frac{k_1}{I_1} \left(\frac{I_2}{k_2} + \frac{I_3}{k_3} \right)} \quad (\text{A. 4})$$

Specifically for β -TCP:

$$X_{\beta TCP} = \frac{1}{\frac{k_{\beta TCP}}{I_{\beta TCP}} \left(\frac{I_{\alpha TCP}}{k_{\alpha TCP}} + \frac{I_{CDHA}}{k_{CDHA}} \right)} \quad (\text{A. 5})$$

For α -TCP:

$$X_{\alpha TCP} = \frac{1}{\frac{k_{\alpha TCP}}{I_{\alpha TCP}} \left(\frac{I_{\beta TCP}}{k_{\beta TCP}} + \frac{I_{CDHA}}{k_{CDHA}} \right)} \quad (\text{A. 6})$$

And for CDHA:

$$X_{CDHA} = \frac{1}{\frac{k_{CDHA}}{I_{CDHA}} \left(\frac{I_{\beta TCP}}{k_{\beta TCP}} + \frac{I_{\alpha TCP}}{k_{\alpha TCP}} \right)} \quad (\text{A. 7})$$

Annex II

Simvastatin acid stability studies and cements interference.

The stability of Simvastatin acid (SVA) in dissolution was investigated at different temperatures in order to explore the possibility to store a SVA solution (4 °C) and to take into account possible degradation of the drug at release temperature (37 °C). Studies were performed in PBS (the release media, pH=7.4) at different time-steps (up to 144 h). Furthermore possible interference of the cement at the maximum wavelength of SVA ($\lambda_{\max} = 238 \text{ nm}$) was explored.

II.1 Simvastatin acid stability studies

A known quantity of SVA was dissolved in PBS and quantification was done by sampling at different time-points and re-introducing the liquid right after the measurement. The degradation of the drug was obtained by measuring the concentration at each time-point at $\lambda_{\max} = 238 \text{ nm}$ by UV-VIS spectroscopy (UV-visible-NIR Spectrometer (Shimadzu 3600)).

SVA was tested at physiological pH (7.4), both at storage temperature (4 °C) and at release temperature (37 °C). Figure II.1 shows that SVA was stable in PBS (pH=7.4) for about 24h at both temperature tested, followed by a progressive decrease afterwards. SVA was stored freeze dried and the decrease has been taken into account with proper corrections.

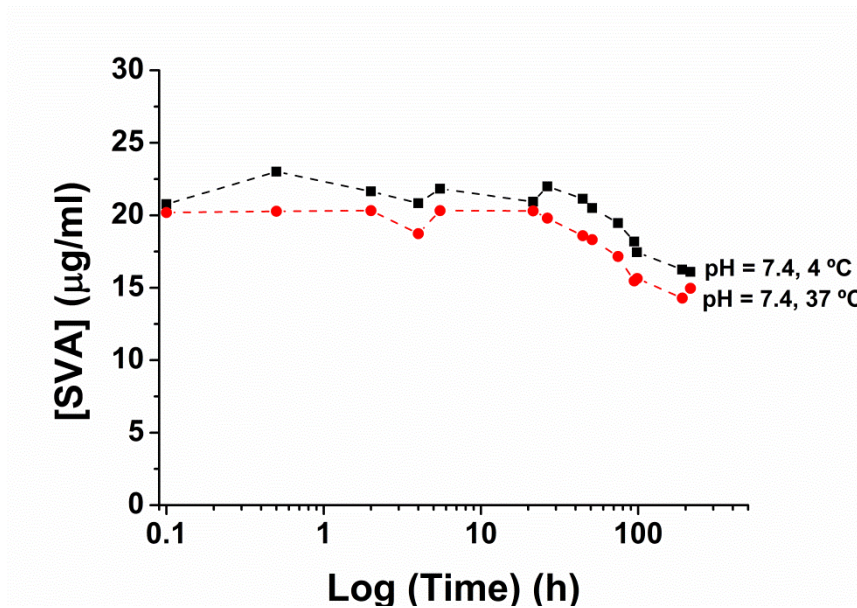


Figure II.1- Degradation of simvastatin acid in PBS (pH =7.4) at storage temperature (4°C) or release temperature (37°C).

II.2 Cement interference with SVA signal

Figure II.2 shows UV-visible spectra of different materials after immersion in water for 2 h, in a range between 200 and 300 nm of a Pacman-shaped scaffold or equivalent¹ immersed in 5 ml medium.

The samples analysed were: a CPF without PLU (control, CPF-0% PLU), a CPF with 10% PLU (CPF-10% PLU), a β -CPF (which were CPF with 10% PLU before sinterisation, β -CPF-10% PLU) and a SVA solution at a concentration of 20 $\mu\text{g/ml}$. It can be observed that at $\lambda_{\text{max}} = 238 \text{ nm}$, SVA shows the maximum absorption. At the same λ , both CPF-0% PLU and β -CPF-10% PLU gave no signal. Differently from the other cements, at this λ , CPF-10% PLU showed a hump due to the presence of PLU. This interference has to be taken into account for measuring SVA concentrations from CPFs and could be a problem when measuring low SVA concentrations in the presence of PLU. Indeed, the amplitude of the hump is supposed to be proportional to the dimension of the scaffold.

¹In the case of CPF without pluronic in the matrix, it was used an equivalent mass of the material.

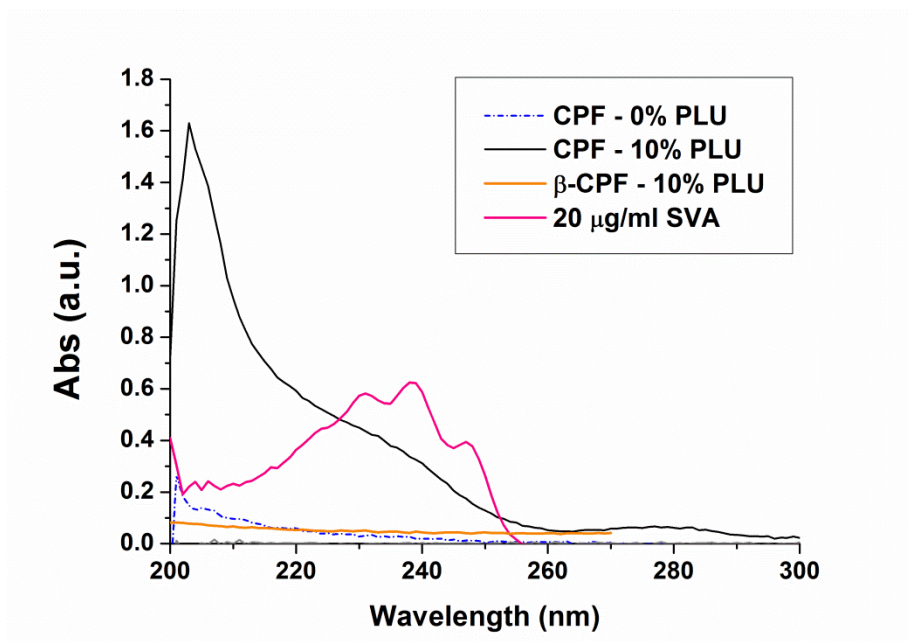


Figure II.2- UV-Visible spectra of aqueous extracts in contact with CPF (0% and 10% PLU), β -CPF and a aqueous solution of SVA at a concentration of 20 μ g/ml.